BULLETIN of GEOSCIENCES

Volume 80 • 2005 • No. 4

Contents

Česká geologická služba
Czech Geological Survey

Bulletin of Geosciences, Vol. 80, No. 4, 239–243, 2005
© Czech Geological Survey, ISSN 1214-1119

Eighty years of the Bulletin of Geosciences

Lilian Švábenická [1] – Zdeněk Kukal [1] – Daniel Nývlt [2]

[1] Czech Geological Survey, Klárov 3, 118 21 Praha 1, Czech Republic. E-mail: svab@cgu.cz, kukal@cgu.cz
[2] Czech Geological Survey, Leitnerova 22, 602 00 Brno, Czech Republic. E-mail: nyvlt@cgu.cz

Abstract: The eightieth anniversary of the Bulletin of Geosciences, the periodical edited by the Czech Geological Survey, is documented and evaluated. The milestones in the development of this Bulletin, which have mirrored the evolution of the activities of the Czech Geological Survey, as well as political and social changes, are described.

Key words: Bulletin of Geosciences, editorial policy, Czech Geological Survey

Introduction

With this issue, the Bulletin of Geosciences has reached the end of its 80th volume, and a practically unbroken eighty-year record of publication. During these years of continued coverage of the geosciences, the Bulletin has witnessed many changes and reorganisations of state structure as well as of the Czech Geological Survey. Important geological events have been anchored in the contents of the Bulletin, such as the stratigraphic events of the Earth's history, the onset of plate tectonics, impact cratering, and international geological congresses.

The Bulletin has undergone several changes throughout its history, as its title, its chief editors, its layout, and its distribution policy have all changed several times. Nevertheless, its main objective has remained unchanged. Even at the time of the establishment of the Geological Survey of Czechoslovakia, the problem of publishing the results of our geological investigations was already urgent. This is why the Geological Survey's responsibility for publishing geoscience literature was stated in its foundation charter.

The Bulletin of Geosciences was not the first journal of the Survey, but it was the first one to appear regularly on a quarterly, bimonthly, or annual basis. The Bulletin was overtaken by the Sborník (Journal of the Geological Survey) and the Knihovna (Library of the Geological Survey). Whereas the Sborník started to appear regularly each year, the Knihovna was only published occasionally.

The first issue of the Bulletin in 1925 and its successors

The appearance of the first issue of the Bulletin can be considered as a significant editorial act because of its importance and its subsequently unbroken record. The State Geological Survey of the Republic of Czechoslovakia was a successor of the Austrian "Reichsanstalt", the Geological Survey responsible for geological activities in all of the countries belonging to the Austrian-Hungarian Empire until the end of the First World War. In the same way, the Bulletin can be considered as the successor of the geological periodical that was edited by this Institute.

In the editorial of the first issue (see Fig. 1), the Survey's director emphasized that detailed reports on mapping and research are to be published there. He also expressed his hope that the Bulletin would be a high-quality periodi-


VĚSTNÍK
Státního geologického ústavu Česko-slovenské republiky.

Figure 1. First issue of the Bulletin of Geosciences – former Věstník Státního geologického ústavu Československé republiky (Bulletin of the State Geological Survey of the Republic of Czechoslovakia).

cal, based on the importance of geological literature for science and practice, as well as for culture and education. Esteemed professors of geology, such as Cyril Purkyně (the first director of the Survey), František Slavík, and Radim Kettner stood at the cradle of the Survey and the Bulletin. A French résumé was attached to each publication "in order to make the reports understandable also in foreign countries". It is of interest that within the 158 pages of the first issue, short papers on Czech geology were published together with one paper on the geology of the Carpathian Ruthenia (at that time part of Czechoslovakia). The latter article, curiously enough, was written in English, with another in German, while the remaining papers were in Czech with short French abstracts. Reports on research activities have been an integral part of the Bulletin since its very beginning; not only general reports on the Survey's activities written by its directors, but also reports on the activities of the chemical laboratories, and, starting from 1927, reports from the Czechoslovak Society of Mineralogy and Geology. The structure of the Bulletin crystallized step by step, and by 1928 the contents were subdivided into five main sections: A – original publications concerning geology, petrology, mineralogy, and paleontology, B – reports from the State Geological Survey, C – reports from the chemical laboratory, D – reports from the Czechoslovak Society for Mineralogy and Geology, E – chronicles, reviews, and reports from the library. By 1935 the sections for chronicles, personal columns, and reviews had been enlarged. Mineralogical and geological bibliographies also started to appear in several issues.

Up to 1938 Czech articles with French abstracts strongly prevailed, even though some German papers and occasional abstracts in English also appeared. From 1928 the French subtitle "Věstník du Service Géologique de la République Tchécoslovaque" was printed on the front page.

Articles of local geological character dominated the topics of the first ten issues, followed by paleontological papers. Many of the titles included adjectives like "preliminary" or substantives such as "remarks" or "notes". Major papers of general interest were relatively rare, even though some of the smaller paleontological and petrological papers were of significant interest and are still being referred to in the literature.

The 1937 Bulletin was opened by the obituary notice announcing the death of the first president of Czechoslovakia, T. G. Masaryk, by the following words in French:

"C'est avec une profonde douleur que la Service géologique de la République Tchécoslovaque joint au deuil de toute la nation qui pleure la mort de celui qui fut son Libérateur." This is followed by another notice concerning the passing away of the first director of the Survey, Prof. Cyril Purkyně.

With this and the subsequent 1938 volume, the first era of the Bulletin had come to an end. Beginning in 1939 the Bulletin and the entire Survey had to change not only its title, but also its contents and language while under Nazi occupation. The German title "Věstník der Geologischen Anstalt für Böhmen und Mähren", which was changed in 1940 to "Mitteilungen der Geologischen Anstalt für Böhmen und Mähren", was printed at the top of the front page. Articles written in Czech had full-length German translations, and many papers were written in German.

A complete overview of the Bulletin's names is listed in Table l.

The post-war development

Immediately after the Second World War, the Bulletin readopted its pre-war title. However, its structure and volume changed drastically. Russian abstracts started to appear together with English ones, whereas French abstracts and German articles hardly survived. In comparison with the 1946 volume, that of 1947 was doubled in volume as the post-war boom in geology and the need for mineral resources became evident. Folders, maps, and photographic plates grew in number, and many English and Russian articles appeared. This evolution culminated in the 1949 volume, after the communist takeover and a political reversal. This manifested itself mainly in political editorials and proclamations on the role of geology in a socialist economy.

A new layout for the Bulletin was adopted in 1952. Changes in the organisation of geological work were in

Table 1. The history of the titles of the current Bullein of Geosciences

Year	Title in original language	English analogy
1925–1938	Věstník Státního geologického Ústavu Československé republiky	Bulletin of the State Geological Survey of the Republic of Czechoslovakia
1939	Věstník Geologického ústavu pro Čechy a Moravu	Bulletin of the Geological Survey of Bohemia and Moravia
1940–1942	Zprávy Geologického ústavu pro Čechy a Moravu	Reports of the Geological Survey of Bohemia and Moravia
1943–1944	Zprávy Úřadu pro výzkum půdy v Čechách a na Moravě	Reports of the Office for the soil investigation in Bohemia and Moravia
1945–1950	Věstník Státního geologického Ústavu Republiky Československé	Bulletin of the State Geological Survey of the Republic of Czechoslovakia
1951–1973	Věstník Ústředního Ústavu Geologického	Bulletin of the Central Geological Survey
1974–1991	Věstník Ústředního ústavu geologického	Bulletin of the Geological Survey, Prague
1992–2002	Věstník Českého geologického ústavu	Bulletin of the Czech Geological Survey
2002 onwards	Bulletin of Geosciences	Bulletin of Geosciences

progress during that year, and this is apparent in the Bulletin's content. Its structure started to be as follows: A – personal column, B – original articles, C – mapping reports, D – general reviews, E – reviews of literature, F – chronicles. Only short papers were published, mostly without abstracts, or with Russian and English annotations. An overview of the Survey's activities was published in almost every volume. Great emphasis was laid on the positive evaluation of geological science in the countries of the Eastern Block. Nevertheless, many important papers appeared from various fields of the Earth sciences. Some English papers were also published. Moreover, English translations of the table of contents began to be printed in 1968. The sections of discussions and chronicles were extended. In 1973 much space was devoted to the report on the International Geological Congress in Montreal. In 1989, an entire issue was dedicated to the International Geological Congress in Washington.

These developments demonstrate the gradual approach toward the modern Bulletin of Geosciences.

From institutional newsletter to scientific periodical

In its very beginnings the Bulletin also fulfilled the function of a "gazette", as it was the official journal of a formal institution that published reports on activities, chronicles, obituaries, awards, and biographies with lists of publications. Twenty years ago the Survey's directorate posed the question of whether the Bulletin should have the internal character of a newsletter, or if it should be transformed into a purely scientific periodical. Fortunately, the second option won, being backed not only by progressive members of the management but also by a great majority of Czech geologists.

Towards publications of general interest

The so-called "preliminary reports" and "notes and reports" appeared very often in the former Bulletin. This system of publications was very popular among Czech geologists who were concerned with establishing priority for new discoveries. This practice had already been strictly abandoned during the late 1980s.

Towards the international scientific language

In this respect the Bulletin passed through developments that were similar to those experienced by many European geoscientific periodicals, though with some delay. Czech papers, although with French, English, German, and Russian abstracts, gave place to articles written in English. Only English manuscripts have been accepted since 1998.

Towards an international perspective

As seen in Fig. 2, foreign contributions comprise a significant proportion of the Bulletin's contents. In recent years, the percentage of foreign authors is getting up. The publications of international research teams are far from being an exception nowadays.

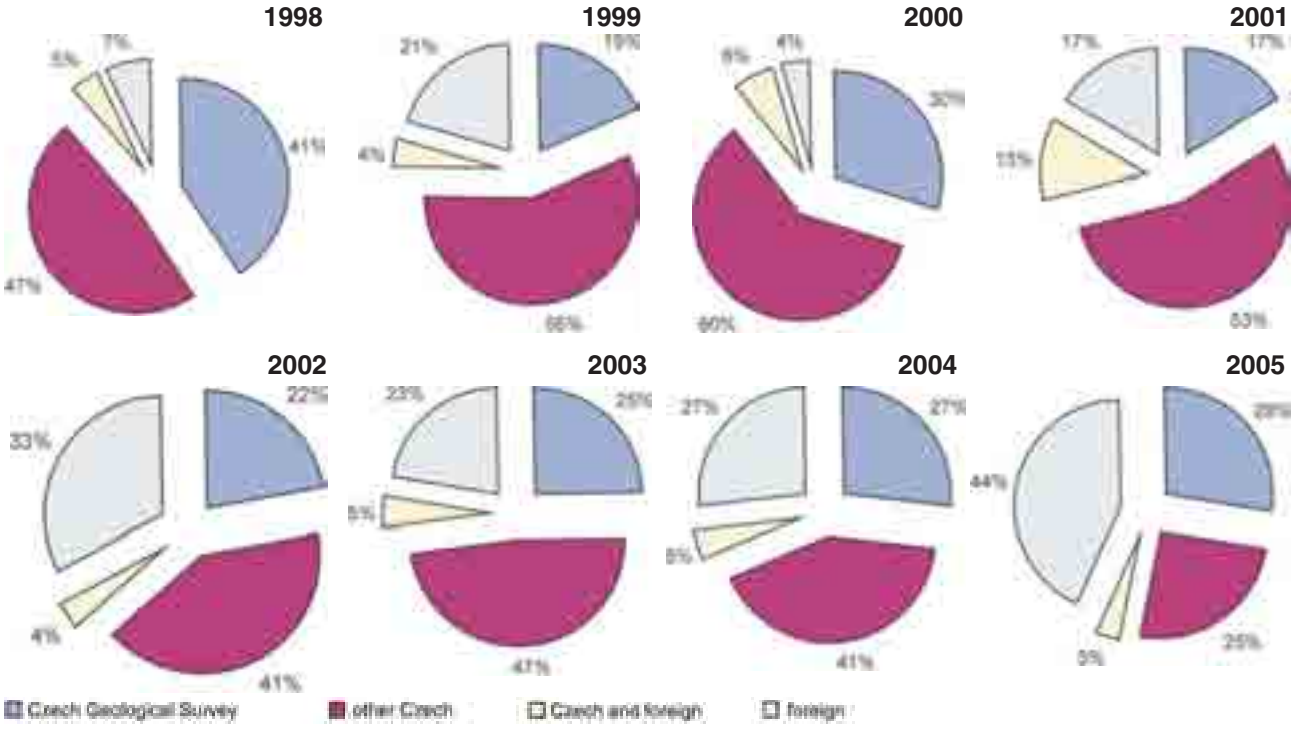

Figure 2. The proportion of papers published by Czech and foreign geoscientists and/or research teams.

The Bulletin offers room for proceedings

Some issues of the Bulletin are devoted to important geoscientific problems. From 1999 onwards nine special issues have been published (Table 2).

Towards an international Editorial Board

Since 1990 the Editorial Board has been extended by members from foreign countries. The present Board, nominated by the Survey's Director, has five non-Czech Members from the United Kingdom, Germany, France, and Slovakia.

Towards progressive manuscript processing

Since 2000 all the manuscripts are evaluated first by a handling editor who suggests two reviewers, preferably from abroad. Their reviews are evaluated by the Chief Editor for further processing.

Table 2. Overview of monothematic issues in years 1999–2005

Year	Title of the special number
1999	Eighty years of the Czech Geological Survey
	Proceeding of the 8th Coal Geology Conference held in Prague in 1998
2000	Neoproterozoic of the Barrandian (Czech Republic)
2002	Proceedings of the conference: Petrology, geochemistry, and structural geology of phosphorus and fluorine rich granites
	Proceedings of the conference: Asteroids, impact cratering and shock metamorphism
2003	The Middle Ordovician in the temporary outcrops of Prague
	Complex geochemical research on interaction and migration of organic and inorganic compounds in rocks and soils
	Memorial volume in honour of Prof. Ivo Chlupáč (Early Paleozoic stratigraphy and paleontology, bibliography of works of Prof. Chlupáč)
2005	Proceedings of the 10th Coal Geology Conference held in Prague in 2004

Towards an international layout

Since 1989 the Bulletin has been published in a large format and printed on high-quality paper. A table of contents is printed on the front page, which is illustrated by colour photographs with geological themes that represent various geoscientific disciplines.

The first coloured geological map was printed in the Bulletin in 1966. Colour photographic plates and text photos started to appear in the 1980s, while the current issues are completely multicoloured.

Towards an informational society

The Bulletin website is http://www.geology.cz/app/bulletin.htm. Full papers in PDF format are available there, starting from Volume 77/2002.

The Bulletin is indexed and/or abstracted in: Current contents (Physics, Chemical and Earth Sciences), GeoRef, GEOBASE, Zoological Record, EZB – Elektronische Zeitschriften Bibliothek (full version of papers), and DOAJ – Directory of Open Access Journals.

The esteemed editors-in-chief

The function of chief editors requires not only great geoscientific knowledge, but also professional and diplomatic capabilities. Among the Bulletin's chief editors there have been the Survey's directors and research directors, heads of departments, and/or reputable senior geologists. A list of them is given in Table 3.

The role of executive editors should also be mentioned. Several names deserve to be added to the list of good souls of the Bulletin's staff. Helena Neumannová

Table 3. Chief editors of the Bulletin

Years	Name	Fields of interest
1925–1930	Prof. Dr. Cyril Purkyně	stratigraphy, paleontology, Survey's director
1931–1934	Prof. Dr. Odolen Kodym	regional and structural geology
1934–1937	Prof. Dr. Josef Woldřich	applied geology, petrology, paleontology, Survey's director
1937–1941	Dr. Vojtěch Smetana	applied geology, mineralogy, paleontology, Survey's director
1941–1944	Prof. Dr. Odolen Kodym	regional and structural geology
1945–1965	Dr. Josef Svoboda	regional and economic geology, stratigraphy, Survey's director
1966–1970	Doc. Dr. Zdeněk Roth	Carpathian geology, petroleum geology
1970–1974	Dr. Vladimír Šibrava	Quaternary geology, Survey's director
1974–1983	Dr. Zdeněk Vejnar	petrology and structural geology of crystalline formations
1983–1989	Dr. Jan Hus Bernard	mineralogy, ore deposits
1989–2000	Dr. Mojmír Eliáš	Carpathian geology, lithology, stratigraphy
2000–2003	Dr. Jan Pašava	economic geology, geochemistry
2003 onwards	Dr. Lilian Švábenická	Carpathian stratigraphy, micropaleontology

was the Bulletin's executive editor until 1958. She was replaced by Marie Vejlupková, who served in this capacity until her retirement in 1985. Šárka Beránková took this office until her retirement in 1999. After a short period of rapid takeovers, Eva Pačesová took up the torch in 2001 followed by Petr Maděra in 2003, who finally handed the baton on to Šárka Doležalová in 2005.

Some statistics

The thematic structure of articles published in the Bulletin during the past nine years is documented in Fig. 3.

In the interest of IF (Impact Factor) calculation the proportions of articles representing individual disciplines, a diagram is also attached (Fig. 4).

The data on the proportions of Czech and foreign authors are also interesting. The Czech geoscientists are subdivided into two groups, the first one representing staff members of the Czech Geological Survey, the second being comprised of contributors from other institutions (see diagram on Fig. 2).

Attached diagram (Fig. 2) shows the more-or-less expected situation: the share of foreign contributions is slightly increasing, while that of international teams has remained stable.

The Bulletin's plans for the future

Since its foundation the Bulletin has experienced rapid growth in scientific scope, and has been transformed from a sort of newsletter into a real international scientific journal. As the Bulletin will try to mirror the evolution of the geosciences, the Editorial Board hopes that the ongoing development of the Bulletin has been noticeable and has positioned it well for continued progress in the forthcoming years.

At present, the Bulletin's Chief Editor, Associate Editors, and the entire Editorial Board is giving special consideration to several important measures, such as

- quality control in order to achieve a high standard submissions;
- calls for papers and the publishing of challenging contributions referred to in high-impact periodicals;
- advertising and the extension of contacts with domestic and foreign geological communities.

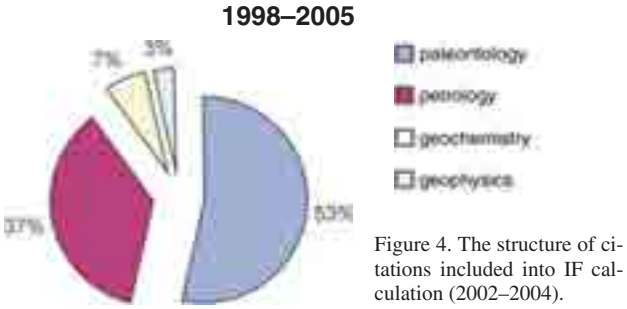

Figure 4. The structure of citations included into IF calculation (2002–2004).

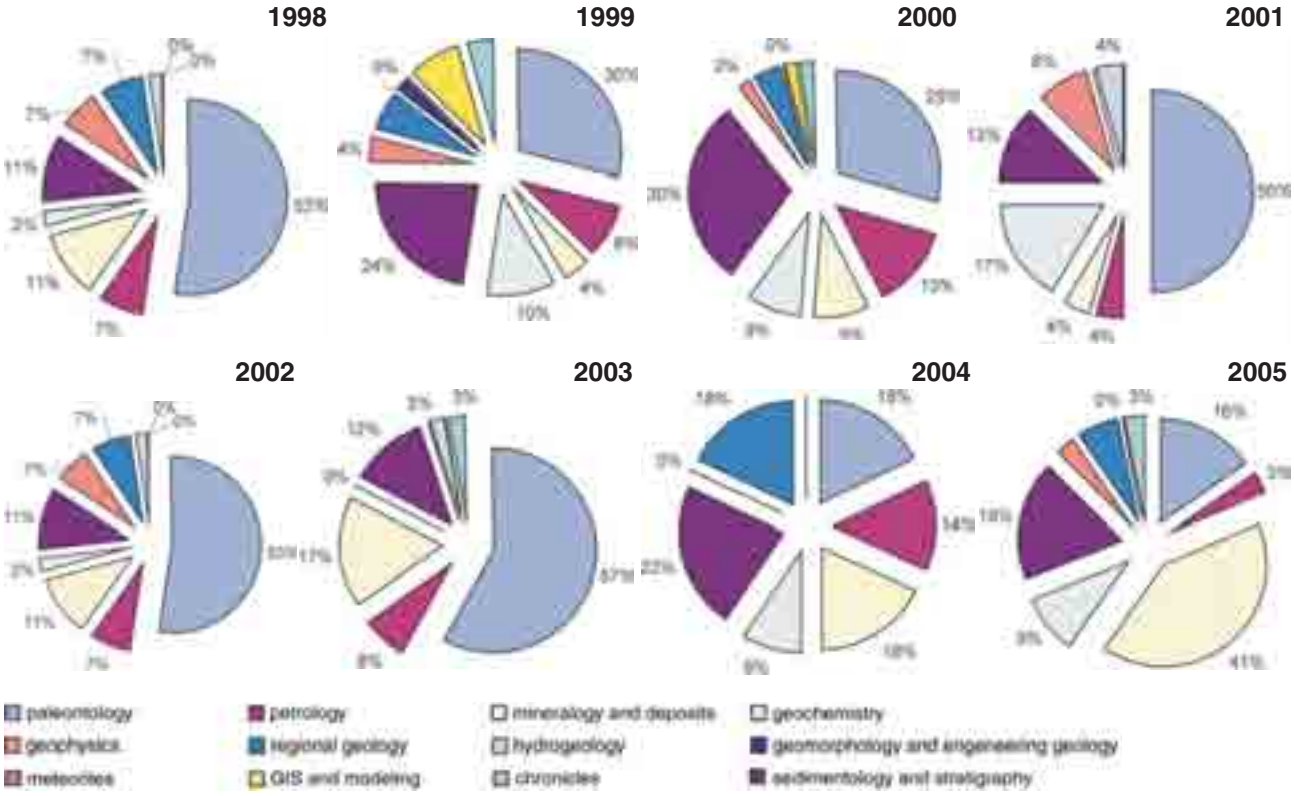

Figure 3. The proportion of published papers according to geoscientific discipline.

Bulletin of Geosciences, Vol. 80, No. 4, 245–276, 2005
© Czech Geological Survey, ISSN 1214-1119

Silurian and Lower Devonian chitinozoan taxonomy and biostratigraphy of the Trombetas Group, Amazonas Basin, northern Brazil

Yngve Grahn

Universidade do Estado do Rio de Janeiro, Faculdade de Geologia, Bloco A – Sala 4001, Rua São Francisco Xavier 524, 20550-013 Rio de Janeiro, RJ, Brazil. E-mail: yngvegrahn@hotmail.com

Abstract. Silurian and Devonian (Lower Lochkovian) chitinozoans from the Trombetas Group, and the basal Jatapu Member of the Maecuru Formation, have been studied in outcrops and shallow borings from the Amazonas Basin, northern Brazil. Outcrops were examined along the Trombetas River and its tributaries, the Cachorro and Mapuera rivers, situated on the northern margin of the Amazonas Basin, and from shallow borings in the Pitinga Formation along the Xingu River at Altamira and Belo Monte, together with outcrops along Igarapé da Rainha and Igarapé Ipiranga on the southern margin of the Amazonas Basin. In addition, nine deep borings in the central part of the Amazonas Basin were used as reference sections. The chitinozoans confirm a Llandovery (Late Rhuddanian–Late Telychian) to Early Wenlock (Sheinwoodian) age for the lower part of the Pitinga Formation, and a Ludlow to Early Pridoli age for the upper part of the Pitinga Formation. The overlying Manacapuru Formation is comprised of lower Pridoli rocks in the basal part, but middle and upper Pridoli strata are missing. The upper part of the formation and the basal part of the Jatapu Member of the Maecuru Formation consist of Lower Lochkovian rocks. Seven chitinozoan assemblages (designated in ascending stratigraphic order 1–7) can be distinguished. Of the 104 chitinozoan species encountered, 51 are left in open nomenclature, and three are newly described (*Ancyrochitina pitingaense*, *Belonechitina*? *plumula* and *Linochitina penequadrata*).

Key words: Silurian, Devonian, Trombetas Group, Chitinozoa, biostratigraphy, zonation, Amazonas Basin, Brazil

Introduction

During November 1986 geologists from Eletronorte and the Brazilian national oil company PETROBRAS sampled Paleozoic outcrops along the Trombetas River and its tributaries, the Cachorro and Mapuera rivers. Shallow borings drilled by Eletronorte in that area were also collected at that time (Fig. 1). Shallow drillings along the Xingu River (Fig. 2) at Altamira (Fig. 3A) and Belo Monte (Fig. 3B) were sampled in June 1989. Included in this study are outcrops of Silurian rocks along Igarapé da Rainha and Igarapé Ipiranga (Fig. 3C) on the southern margin of the Amazonas Basin (Costa 1970, 1971), and nine deep borings from the Northern Platform, Central Basin, and Southern Platform (Figs 1A, 2A) which were documented and used as reference sections (Grahn 1988a, b, 1990). The geological results were, in part, included in PETROBRAS internal reports (Grahn 1988a, b, 1990, Grahn and Melo 1990), and published by Azevedo-Soares and Grahn (2005). The Trombetas River has become a classic area for Brazilian Siluro-Devonian geology ever since the American Morgan-expeditions to the Amazonas Basin in 1870 and 1871. Trombetas megafossils collected from

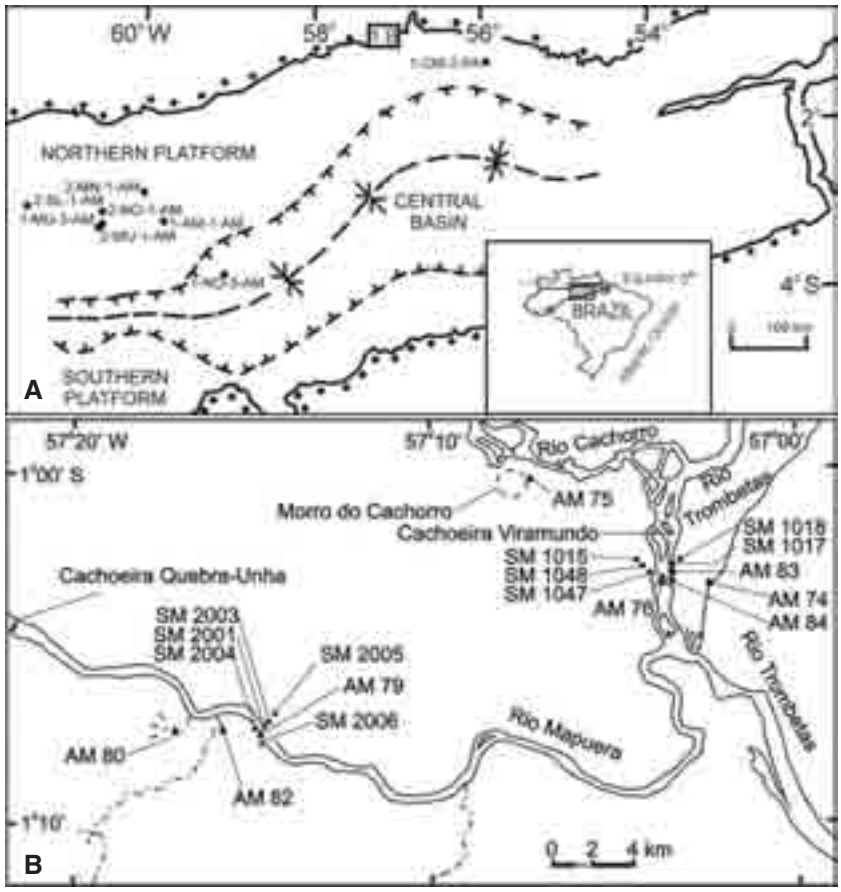

Figure 1. A – location map showing the geographic positions of investigated wells in the Amazonas Basin (Northern Platform and Central Basin) and the Trombetas area (inset 1B), ✚ – outline of the Amazonas Basin. B – location of the outcrop localities and shallow boreholes in the Trombetas area, ▲ – outcrop locality, ● – shallow boreholes.

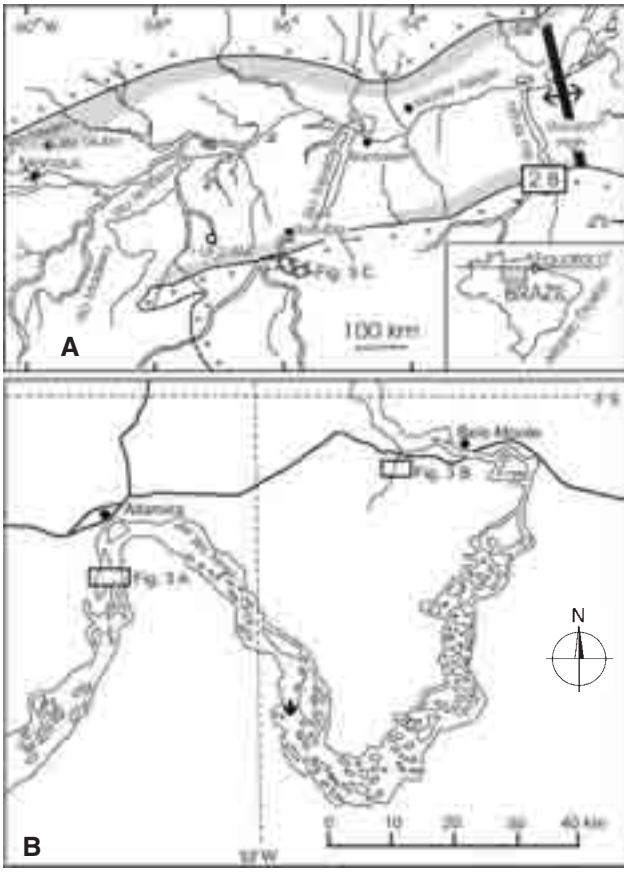

Figure 2. A – location map of the geographic position of the investigated wells on the southern margin of the Amazonas Basin, Igarapé da Rainha and Igarapé Ipiranga area (arrow 3C) and the Xingu River area (inset 2B). Grey area corresponds to the outcrop belts of the Trombetas Group. B –map showing the Altamira (inset 3A) and Belo Monte (inset 3B) areas at the Xingu River.

outcrops along the Cachorro and Trombetas Rivers by these expeditions were first described and published by Derby (1878). Shelly fossils are concentrated in the lower part of the Pitinga Formation (Melo 1988, Grahn 1992a), where they occur together with the Early Silurian graptolites *Climacograptus innotatus brasiliensis* and *Monograptus* cf. *M. gregarius* (Ruedemann 1929, Jaeger 1976). For many years the entire Trombetas Group was considered to be Lower Silurian (Lange 1967, 1972). The first paper documenting chitinozoans from the Trombetas Group was by F. W. Lange in 1967. He also established a biozonation utilizing chitinozoans and acritarchs. According to Lange's (1967) interpretation of the succession, a hiatus corresponding to Lower Llandovery through Emsian strata occurred at the top of the Trombetas Group (then defined in core 35 at a level 1506 m in well 1-AM-1-AM; see Figs 1A and 4). Later, Quadros (1985) found Late Silurian and Lochkovian microfossils below this supposed hiatus, and his observations were confirmed by Grahn (1988a, b, 1992a), Grahn and Paris (1992), and Azevedo-Soares and Grahn (2005). This paper updates the biostratigraphy along the above-mentioned rivers, and compares it with other Silurian and Lower Devonian successions from deep borings in the Amazonas Basin (Figs 1A, 2A). A review of the different Silurian and Lower Devonian formations in the Amazonas Basin was given by Grahn (1992b) and Grahn and Paris (1992).

Material and methods

The locations of the outcrops and borings investigated in this paper are shown in Figs1–3. In total 225 samples were studied from the Pitinga and Manacapuru formations of the Trombetas Group, and the Jatapu Member of the Maecuru Formation, in the Amazonas Basin. The residues were examined for chitinozoans using a binocular stereoscopic microscope, and representative chitinozoan specimens were picked for scanning electron microscope (SEM) studies at the former DIGER/SEGEX (CENPES, PETROBRAS) laboratory in Rio de Janeiro, and in Institute de Géologie at Université de Rennes, Rennes, France. Sample processing and SEM-preparations were done according to the techniques described by Laufeld (1974) and Paris (1981). Photographed chitinozoan specimens are stored at the Department of Stratigraphy and Paleontology at Universidade do Estado do Rio de Janeiro (UERJ/DEPA), and at Institute de Géologie, Université de Rennes (designated by IGR in the plate captions).

Geological setting

The localities in this study cover the northern and southern margins of the Amazonas Basin, and include the central basin where the most complete Siluro-Devonian succession is represented. The Trombetas Group is divided, in ascending order, into Autas-Mirim, Nhamundá, Pitinga (lower and upper), and Manacapuru (lower and upper) formations (Grahn 1992a, Grahn and Paris 1992, Azevedo-Soares and Grahn 2005). It is exposed along the northern margin of the Amazonas Basin from the Gurupa High in the east to Rio Negro in the west, and in two belts along the southern margin of the Amazonas Basin from an area between the Tapajos and Madeira rivers in the west to the Gurupa High (Fig. 2A).

Systematic inventory of chitinozoan species in alphabetical order by genus and species

Ancyrochitina ancyrea (Eisenack 1931). Plate I, fig. 1.
Ancyrochitina cantabrica Cramer and Díez 1978. Plate I, fig. 6.
Ancyrochitina fragilis Eisenack 1955a. Plate I, fig. 8.
Ancyrochitina ollivierae Boumendjel 2002. Plate I, fig. 9.
Ancyrochitina pitingaense n. sp. Plate I, figs 15–16; Plate II, fig. 1.
Ancyrochitina primitiva Eisenack 1964. Plate I, fig. 10; Plate V, fig. 1.
Ancyrochitina regularis Taugourdeau and Jekhowsky 1960. Plate I, figs 11–12.
Ancyrochitina cf. *A. brevis* Taugourdeau and Jekhowsky 1960. Plate I, figs 4–5.

Ancyrochitina aff. *A. asterigis* Paris 1981. Plate I, fig. 3.
Ancyrochitina aff. *A. regularis* Taugourdeau and Jekhowsky 1960. Plate VI, fig. 2.
Ancyrochitina aff. A. tomentosa Taugourdeau and Jekhowsky 1960. Plate I, fig. 13; Plate VI, fig. 1.
Ancyrochitina ex. gr. *ancyrea* (Eisenack 1931). Plate I, fig. 2.
Ancyrochitina ex. gr. *floris* Jaglin 1986. Plate I, fig. 7.
Ancyrochitina sp. A *sensu* Grahn and Paris 1992. Plate VI, fig. 3.
Ancyrochitina n. sp. A. Plate II, fig. 2.
Ancyrochitina n. sp. B. Plate II, fig. 3.
Ancyrochitina n. sp. C. Plate II, fig. 4.
Ancyrochitina n. sp. D. Plate II, fig. 5.
Ancyrochitina n. sp. E. Plate II, fig. 6.
Angochitina echinata Eisenack 1931. Plate II, fig. 8.
Angochitina elongata Eisenack 1931. Plate VI, fig. 4.
Angochitina filosa Eisenack 1955a. Plate II, fig. 10.
Angochitina longicollis Eisenack 1959. Plate II, fig. 11.
Angochitina strigosa Boumendjel 2002. Plate II, fig. 12.
Angochitina n. sp. aff. *A. cyrenaicensis sensu* Grahn and Paris 1992. Plate II, fig. 7.
Angochitina cf. *A. echinata* Eisenack 1931 *sensu* Grahn and Paris 1992. Plate VI, figs 6–7.
Angochitina cf. *A. elongata* Eisenack 1931. Plate VI, fig. 5.
Angochitina sp. aff. *A. mourai* non Lange 1952 *sensu* Schweineberg 1987. Plate V, fig. 2.
Angochitina sp. A *sensu* Grahn and Paris 1992. Plate II, figs 9, 13.
Angochitina sp. B. Plate II, fig. 15.
Angochitina sp. C. Plate II, fig. 16.
Angochitina sp. D. Plate II, fig. 17.
Angochitina cf. *Sphaerochitina densibaculata* Volkheimer et al. 1986. Plate II, fig. 14.
Angochitina? *thadeui* Paris 1981. Plate VII, fig. 11.
Angochitina? sp. *sensu* Grahn and Paris 1992. Plate II, figs 18–19.
Belonechitina? *plumula* n. sp. Plate VI, figs 8–11.
Belonechitina sp. A. Plate V, figs 3–4.
Belonechitina sp. B. Plate V, fig. 13.
Bursachitina wilhelmi (Costa 1970). Plate V, figs 5–6; Plate VII, fig. 2.
Cingulochitina convexa (Laufeld 1974). Plate II, fig. 20; Plate III, fig. 1.
Cingulochitina cylindrica (Taugourdeau and Jekhowsky 1960). Plate III, fig. 18.
Cingulochitina ervensis (Paris in Babin et al.1979). Plate III, fig. 2.
Cingulochitina serrata (Taugourdeau and Jekhowsky 1960). Plate III, fig. 4.
Cingulochitina wronai Paris 1984. Plate III, fig. 6.
Cingulochitina aff. *C. convexa* (Laufeld 1974). Plate II, fig. 21.
Cingulochitina aff. *C. ervensis* (Paris in Babin et al.1979). Plate III, fig. 3.
Cingulochitina aff. *C. serrata* (Taugourdeau and Jekhowsky 1960). Plate III, fig. 5.
Conochitina acuminata Eisenack 1959. Plate III, fig. 8.

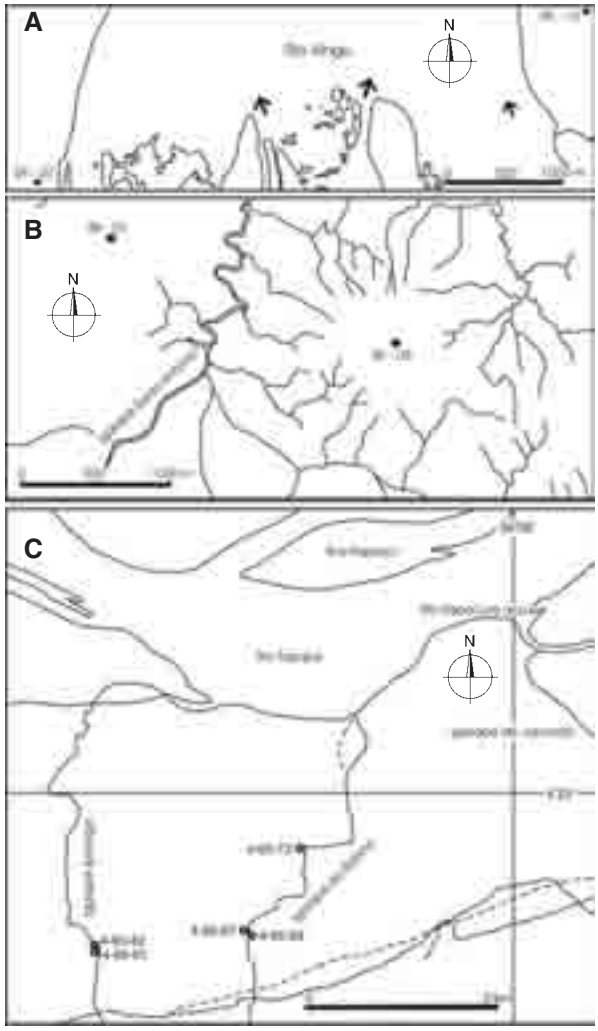

Figure 3. A – detailed locality map of shallow boreholes in the Altamira area. Arrows indicate direction of current. B – detailed locality map of shallow boreholes in the Belo Monte area. C – locality map showing the sampling sites for Silurian Trombetas Group outcrops along Igarapé da Rainha and Igarapé Ipiranga rivers.

Conochitina edjelensis (Taugourdeau and Jekhowsky 1960). Plate V, figs 9, 14.
Conochitina elongata (Taugourdeau and Jekhowsky 1960). Plate V, fig. 8.
Conochitina gordonensis Cramer 1964. Plate III, fig. 9.
Conochitina pachycephala Eisenack 1964. Plate III, figs 11–12.
Conochitina proboscifera Eisenack 1937. Plate III, fig. 13.
Conochitina tuba Eisenack 1932. Plate III, fig. 10.
Conochitina cf. *C. acuminata* Eisenack 1959. Plate VI, fig. 12.
Conochitina cf. *C. tuba* Eisenack 1932. Plate V, fig. 15.
Cyathochitina campanulaeformis (Eisenack 1931). Plate V, fig. 7.
Cyathochitina caputoi Costa 1971. Plate III, fig. 14.
Cyathochitina sp. B *sensu* Paris 1981. Plate III, fig. 15; Plate VI, fig. 13.
Desmochitina densa Eisenack 1962. Plate III, figs 16–17.
Eisenackitina granulata (Cramer 1964). Plate III, fig. 20.
Eisenackitina cf. *E. bohemica* (Eisenack 1934). Plate III, fig. 19.

Figure 4. Lithologic column and chitinozoan range chart for the reference well 1-AM-1-AM. Shaly intervals within the sandstones of the Nhamundá Formation represent interfingering shales of the lower part of the Pitinga Formation.

Euconochitina cruzi Costa 1970. Plate V, fig. 16.
Euconochitina iklaensis (Nestor 1984). Plate III, figs 21–22.
Euconochitina patula (Costa 1971). Plate III, fig. 23.
Euconochitina sulcata (Costa 1971). Plate III, fig. 24.
Euconochitina sp. A. Plate VI, figs 14–15.
Fungochitina kosovensis Paris 1981. Plate III, fig. 25.
Fungochitina sp. A. Plate III, fig. 26.
Lagenochitina aff. *L. navicula* Taugourdeau and Jekhowsky 1960. Plate VI, figs 16–17.
Linochitina penequadrata n. sp. Plate VI, fig. 18. Plate VII, fig. 1.

Linochitina ex. gr. *erratica* (Eisenack 1931). Plate III, fig. 27; Plate V, fig. 17.
Margachitina catenaria Obut 1973. Plate III, fig. 28.
Margachitina margaritana (Eisenack 1937). Plate IV, fig. 1.
Margachitina aff. *M. saretensis* Boumendjel 2002. Plate IV, fig. 2.
Margachitina? sp. Plate VII, fig. 3.
Plectochitina n. sp. A. Plate IV, fig. 3.
Pogonochitina djalmai (Sommer and van Boekel 1965). Plate IV, figs 4–5.
Pogonochitina inornata (Costa 1971). Plate IV, fig. 7.
Pogonochitina tianguaense Grahn et al. 2005. Plate IV, fig. 19.
Pogonochitina cf. *P. djalmai* (Sommer and van Boekel 1965) *sensu* Grahn and Paris 1992. Plate IV, fig. 6.
Pogonochitina n. sp. A. Plate VII, fig. 4.
Pterochitina deichaii Taugourdeau 1963. Plate VII, fig. 13.
Pterochitina megavelata Boumendjel 2002. Plate IV, fig. 8.
Pterochitina perivelata (Eisenack 1937). Plate IV, fig. 9.
Pterochitina sp. A. Plate V, figs 10–11.
Pterochitina sp. B. Plate VII, figs 5–6.
Ramochitina bjornsundquisti Grahn and Melo 2003. Plate IV, fig. 10
Ramochitina illiziensis Boumendjel 1985. Plate VII, fig. 12.
Ramochitina n. sp. cf. *R. devonica* (Eisenack 1955b). Plate IV, fig. 11.
Ramochitina sp. *sensu* Grahn and Paris 1992. Plate VII, figs 7–8.
Ramochitina n. sp. A. Plate I, fig. 14.
Rhabdochitina conocephala? Eisenack 1931 *sensu* Boumendjel 1987. Plate IV, fig. 12.
Sagenachitina sp. A. Plate VII, fig. 9.
Saharochitina gomphos Grahn and Melo 2003. Plate IV, fig. 13.
Salopochitina monterrosae (Cramer 1969). Plate IV, fig. 14.
Salopochitina aff. *S. monterrosae* (Cramer 1969). Plate IV, fig.15.
Sphaerochitina palestinaense Grahn et al. 2005. Plate IV, figs 17–18.
Spinachitina n. sp. A. Plate IV, fig. 16; Plate V, fig. 12.
Tanuchitina elenitae (Cramer 1964). Plate IV, fig. 21.
Tanuchitina aff. *T. cylindrica* (Taugourdeau and Jekhowsky 1960) *sensu* Boumendjel 1987. Plate IV, fig. 20.
Tanuchitina sp. A. Plate VII, fig. 10.
Urochitina n. sp. A. Plate IV, figs 22–23.
Vinnalochitina corinnae (Jaglin 1986). Plate IV, fig. 24.

Systematic paleontology

One hundred and four chitinozoan species have been identified, three of which are newly described, and fifty-one are left in open nomenclature. Their regional stratigraphic ranges for the Amazonas Basin are given in the chapter Chitinozoan biostratigraphy on page 265 and Figs 12, 13, this paper, which includes also seven recently distinguished chitinozoan assemblages. Most of the recovered specimens are compressed, and a correction factor of 0.8 (Paris 1981, Jaglin 1986) was used to calculate the uncompressed dimensions of the specimens (corrected values are given within brackets). The taxonomy follows the scheme proposed by Paris et al. (1999). Only the new species and those left in open nomenclature are described below.

Group Chitinozoa Eisenack 1931
Order Operculatifera Eisenack 1931
Family Desmochitinidae Eisenack 1931 emend. Paris 1981
Subfamily Pterochitininae Paris 1981

Genus *Pterochitina* Eisenack 1955a

Pterochitina sp. A
Plate V, figs 10, 11

Discussion: The velum of this species of *Pterochitina* is situated above the equatorial plane of the vesicle, which is characteristic of *P. perivelata*. Specimens of *P.* sp. A differ in having a smaller velum and comparatively wider body. The contemporaneous species *P. deichaii* Taugourdeau 1963 has a velum below the equatorial plane.

Dimensions (five specimens measured): Total length 59–104 µm, maximum width 113 (90)–212 (170) µm, width of aperture 59–125 µm, maximum width of velum ca 15 µm.

Occurrence: Amazonas Basin, shallow boreholes SM 1015, SM 1017, SM 1018, and SM 1047 (Figs 1B, 5). Lower part of the Pitinga Formation. Assemblage 3, see Fig. 12.

Pterochitina sp. B
Plate VII, figs 5, 6

Discussion: The velum of *Pterochitina* sp. B is situated at the equatorial plane, and consists of four thin annular structures. These are a characteristic feature of *Pterochitina* sp. B, and separates this species from other *Pterochitina* species in the Trombetas Group.

Dimensions (16 specimens measured): Total length 38–58 µm, maximum width 84 (67)–105 (84) µm, width of aperture 46 (37)–50 (40) µm, maximum width of annular structure ≤ 4 µm.

Occurrence: Amazonas Basin, shallow boreholes SR 01, SR 03, and SR 07 (Figs 2B, 3A–B, 6–8). Lower part of the Pitinga Formation. Assemblage 3, see Fig. 12.

Genus *Cingulochitina* Paris 1981

Cingulochitina aff. *C. convexa* Laufeld 1974
Plate II, fig. 21

2005 *Cingulochitina* cf. *C. convexa* – Azevedo-Soares and Grahn, Fig. 4:13

Discussion: *Cingulochitina* aff. *C. convexa* differs from *C. convexa* Laufeld 1974 by being smaller in size and having less convex flanks.

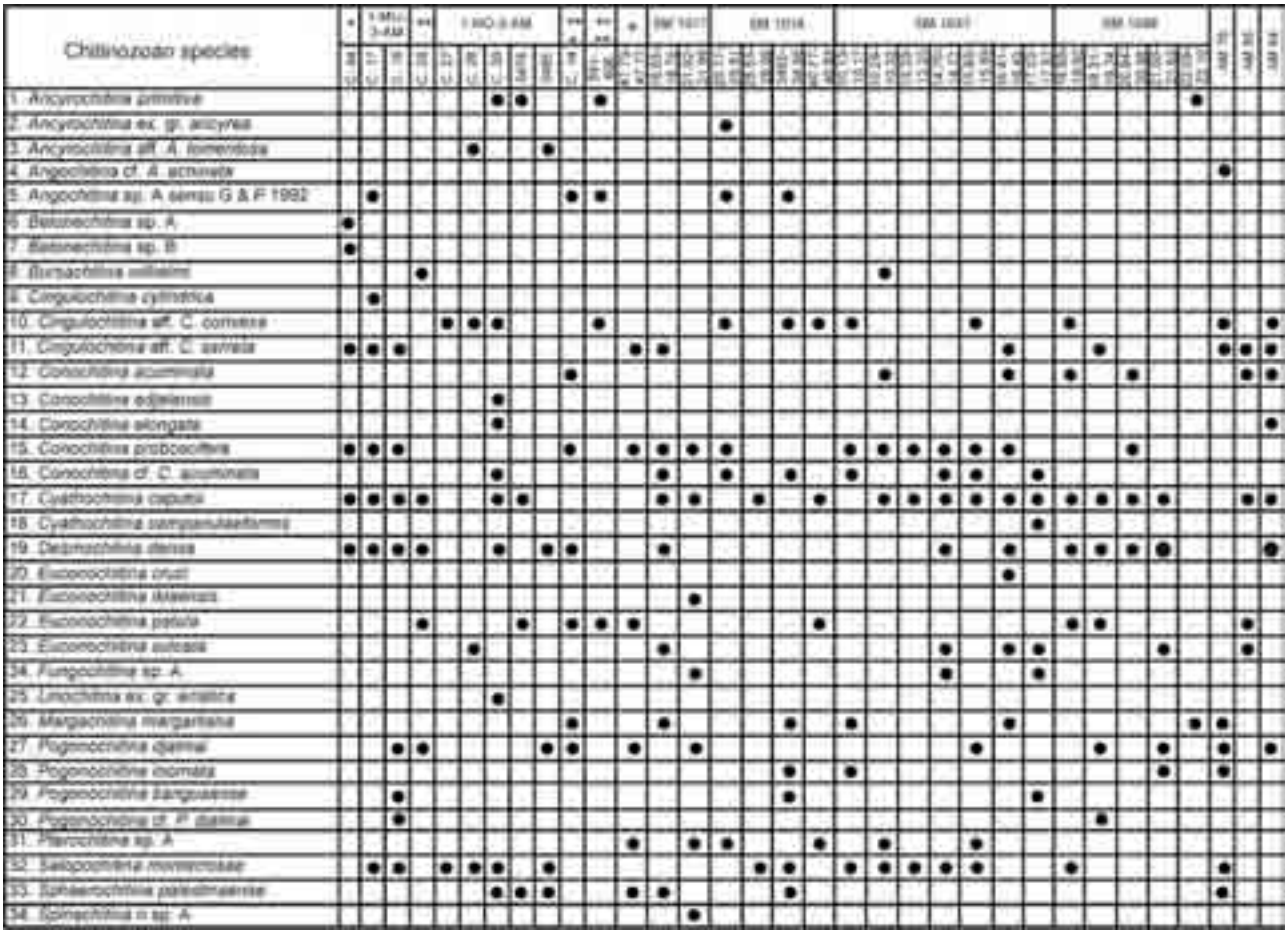

Figure 5. Chitinozoan distribution chart for various wells and outcrops containing assemblages 1–3 on the northern margin and central part of the Amazonas Basin. * = 1-CM-2-PA. ** = 2-MU-1-AM. *** = 2-NO-1-AM. **** = 2-SL-1-AM. + = SM 1015. C = core. For localities see Fig. 1.

Dimensions (62 specimens measured): Total length 103–183 µm, maximum width 50 (40)–80 (64) µm, width of aperture 33 (26)–56 (45) µm, length of neck 1/3–1/2 of the total length.

Occurrence: Amazonas Basin, PETROBRAS 1-AM-1-AM, 1-NO-3-AM and 2-SL-1-AM wells (Figs 1A, 4, 5), shallow boreholes SM 1015, SM 1018, SM 1047, and SM 1048 (Figs 1B, 5), outcrop localities AM 76 and AM 78 (Figs 1B, 5). Lower part of the Pitinga Formation (Azevedo-Soares and Grahn 2005). Assemblages 2 and 3, see Fig. 12.

Cingulochitina aff. *C. ervensis* Paris (in Babin et al. 1979)
Plate III, fig. 3

2003 *Cingulochitina* aff. *C. ervensis* – Grahn and Melo, p. 375, 377, Plate 4, figs 8–9 (see for additional references)
2005 *Cingulochitina* aff. *C. ervensis* – Azevedo-Soares and Grahn, Fig. 4:14

Discussion: The specimens of *Cingulochitina* aff. *C. ervensis* from the Trombetas area are larger than those from the Urubu area, described by Grahn and Melo (2003). *Cingulochitina* aff. *C. ervensis* differs from *C. serrata* by having more convex flanks.

Dimensions (16 specimens measured): Total length 115–200 µm, maximum width 63 (50)–81 (65) µm, width of aperture 46 (37)–56 (45) µm, length of neck 1/4–1/3 of the total length.

Occurrence: Amazonas Basin, PETROBRAS 1-AM-1-AM well (Figs 1A, 4), shallow borehole SM 1048 (Figs 1B, 9). Upper part of the Pitinga Formation (Azevedo-Soares and Grahn 2005). Assemblages 4 and 5, see Fig. 13. Similar specimens have been reported from lower part of the Manacapuru Formation (Late Ludlow?–Early Pridoli) in the Urubu area of the Amazonas Basin (Grahn and Melo 2003).

Cingulochitina aff. *C. serrata* (Taugourdeau and Jekhowsky 1960)
Plate III, fig. 5

1971 *Desmochitina cingulata* – Costa, p. 88–89, Plate 18, fig. 3
1971 *Desmochitina cingulata serrata* – Costa, p. 89–90, Plate 18, figs 4–8
1992 *Cingulochitina* sp. aff. *serrata* – Grahn and Paris, Plate 1, fig. 10
2003 *Cingulochitina* aff. *C. serrata* – Grahn and Melo, p. 377, Plate 4, fig. 10

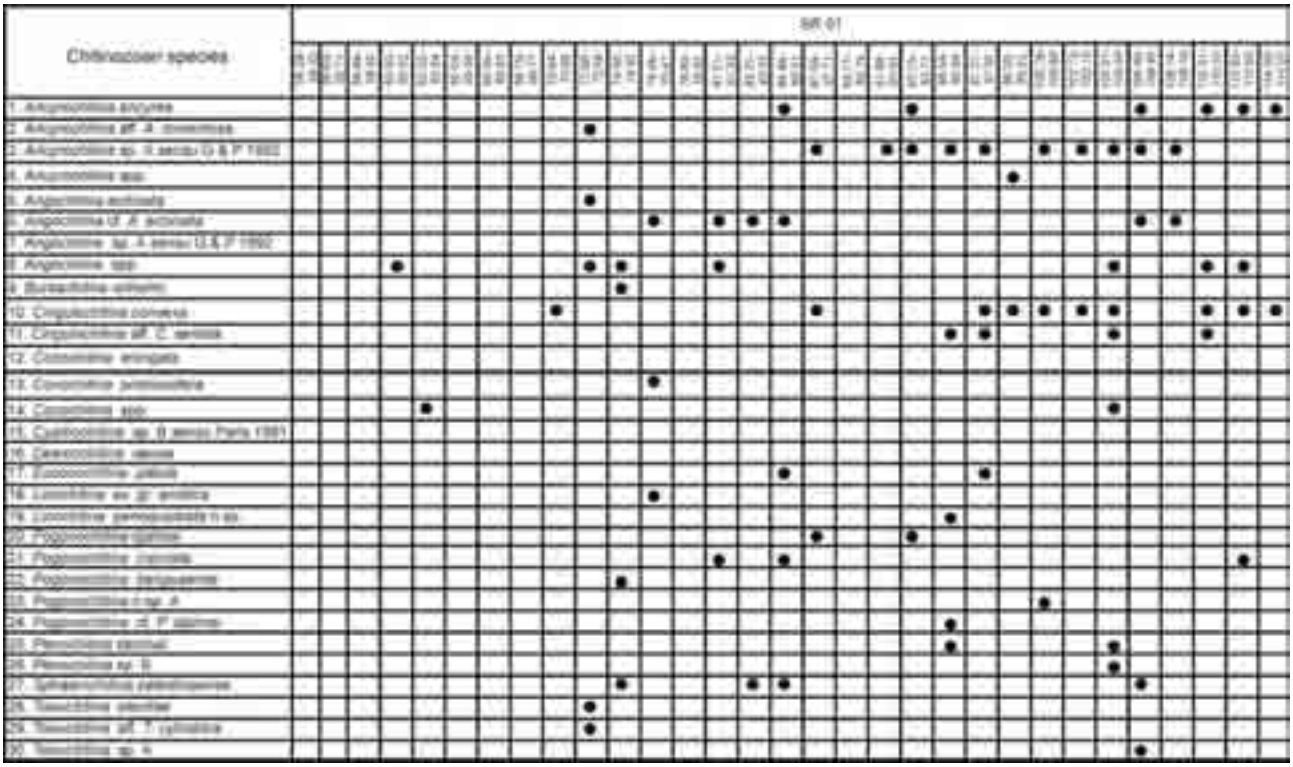

Figure 6. Chitinozoan distribution chart for the SR 01 well on the southern margin of the Amazonas Basin. For the location see Fig. 3B.

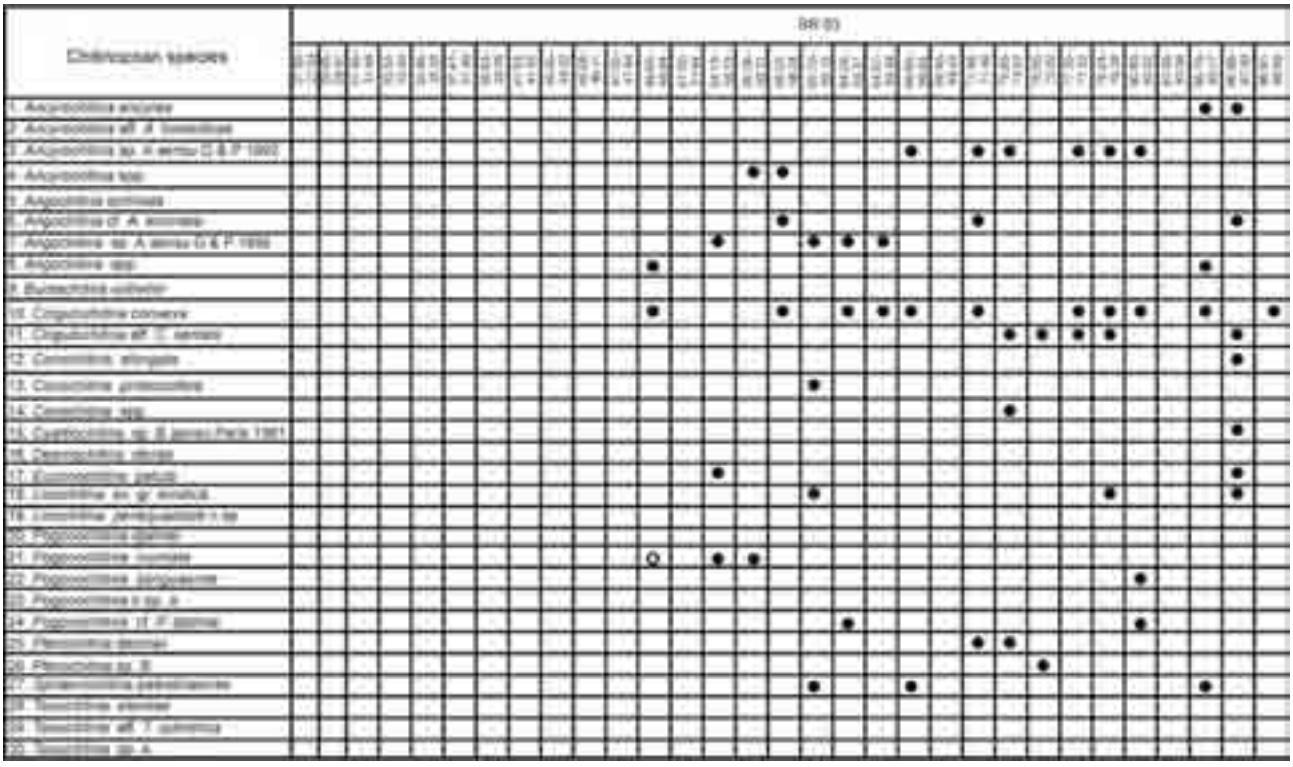

Figure 7. Chitinozoan distribution chart for the SR 03 well on the southern margin of the Amazonas Basin. For the location see Fig. 3B.

Discussion: This species was discussed by Grahn and Melo (2003). *Cingulochitina serrata* (Taugourdeau and Jekhowsky 1960) has straighter flanks and a longer neck than *C.* aff. *C.* serrata.

Dimensions (37 specimens measured): Total length 60–150 µm, maximum width 54 (43)–120 (96) µm, width of aperture 41 (33)–90 (72) µm, length of neck 1/3–1/2 of the total length.

Occurrence: Amazonas Basin, PETROBRAS 1-AM-1-AM, 1-UI-2-AM, 1-CM-2-PA, 1-MU-3-AM, and 2-MU-1-AM wells (Figs 1A, 2A, 4, 5, 11), shallow boreholes SM 1017, SM 1047, SM 1048, SR 01, SR 03, SR 07,

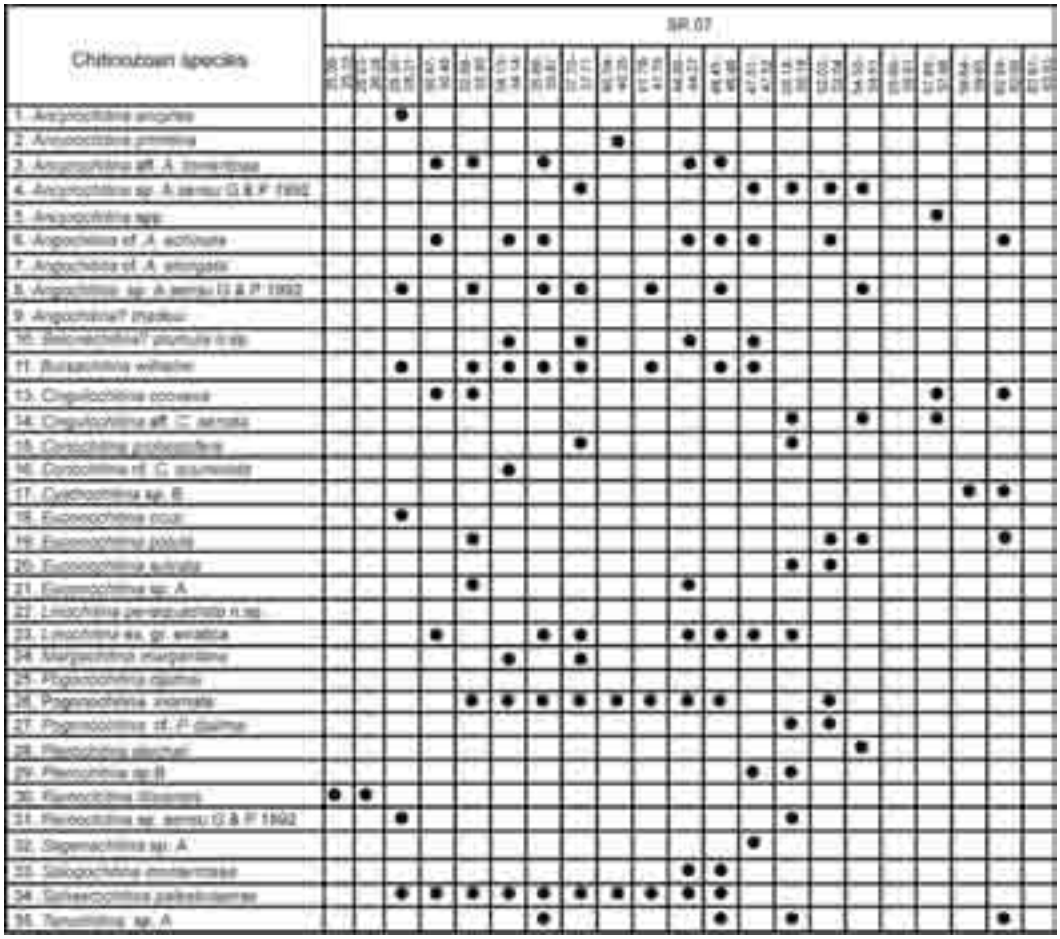

Figure 8. Chitinozoan distribution chart for the SR 07 well on the southern margin of the Amazonas Basin. For the location see Fig. 3A.

and SR 10 (Figs 1B, 2B, 3A–B, 6–8, 10), outcrop localities AM 83, AM 84, Igarapé da Rainha and Igarapé Ipiranga (Figs 1B, 3C, 5, 11). Lower part of the Pitinga Formation in the Trombetas – Xingu area. Assemblages 2 and 3, see Fig. 12, and lower part of the Manacapuru Formation (Late Ludlow–Early Pridoli) in the Urubu area (Grahn and Melo 2003).

Subfamily Margachitininae Paris 1981

Genus *Margachitina* Eisenack 1968

Margachitina aff. *M. saretensis* Boumendjel 2002
Plate IV, fig. 2

2002 *Margachitina* aff. *M. saretensis* – Jaglin and Paris, p. 346–348, Plate 1, fig. 4 (see for additional references)
2003 *Margachitina aff. M. saretensis* – Grahn and Melo, p. 377, Plate 5, figs 7–8
2005 *Margachitina* aff. *M. saretensis* – Azevedo-Soares and Grahn, Fig. 6:2

Discussion: For a discussion of this species, see Jaglin and Paris (2002).

Dimensions (five specimens measured): Total length (excl. peduncle) 100–115 µm, maximum width 98 (77)–118 (94) µm, width of aperture 75 (60)–96 (77) µm, length of peduncle 60–73 µm.

Occurrence: Amazonas Basin, PETROBRAS 1-AM-1-AM and 1-UI-2-AM wells (Figs 1A, 2A, 4, 11), shallow boreholes SM 1015, SM 1018, SM 1047, and SM 1048 (Figs 1B, 9), outcrop locality AM 75 (Figs 1B, 6). Upper part of the Pitinga (Grahn and Melo 2003, Azevedo-Soares and Grahn 2005) and possibly lowermost part of the Manacapuru formations. Assemblages 4 and 5, see Fig. 13. Jaglin and Paris (2002) described this species from the middle Pridoli (*Margachitina elegans* Zone) in the upper part of the Altemances Gréso-argileuses Formation, well A1-61, Tripolitania, northwest Libya.

Margachitina? sp.
Plate VII, fig. 3

Discussion: Only one specimen of this taxon was found, and the lack of essential morphological information concerning the vesicle precludes description.

Dimensions (one specimen measured): Total length (excluding peduncle) unknown, maximum width 91(73) µm, width of aperture 57(46) µm, length of peduncle unknown.

Occurrence: Amazonas Basin, outcrop locality Igarapé da Rainha 4-65-73 (Figs 3C, 11). Lower part of the Pitinga Formation. Assemblage 4, see Fig. 12.

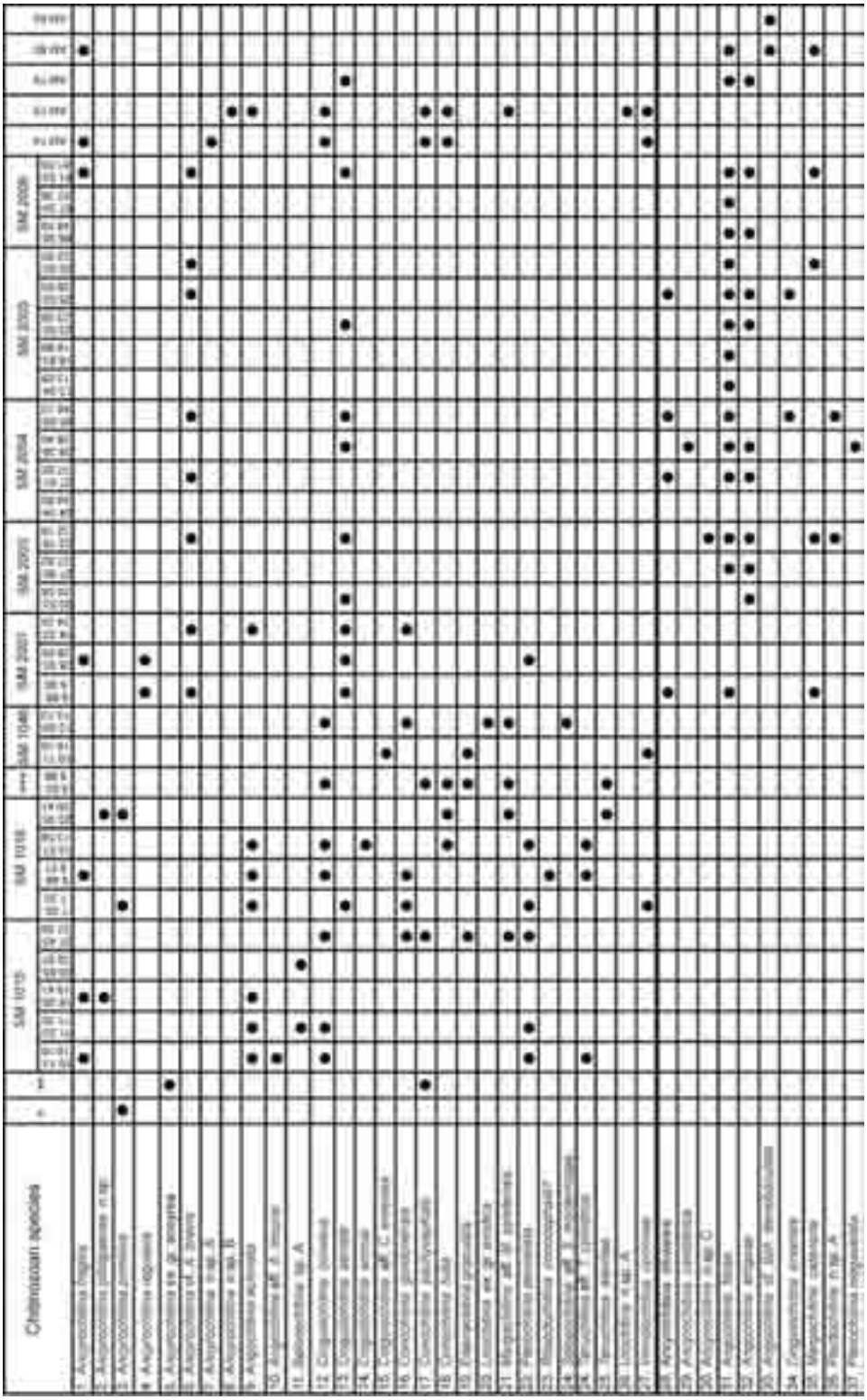

Figure 9. Chitinozoan distribution chart for various wells and outcrops containing assemblages 4–7 on the northern margin of the Amazonas Basin. * – 1-CM-2-PA core 43, ** – 2-MN-1-AM core 42, *** – SM 1047, C – core. For localities see Fig. 1.

Genus *Linochitina* Eisenack 1968 restr. Paris 1981

Linochitina penequadrata n. sp.
Plate VI, fig. 18, Plate VII, fig. 1

Derivation of name: Latin, *pene*, almost, and *quadratum*, four-cornered, referring to the rectangular shape of the species.

Diagnosis: A small *Linochitina* species with a rectangular vesicle outline and bearing a short copula.

Holotype: Plate VI, fig. 18 (lower specimen). UERJ/DEPA SEM collection 04608

Type locality: Well SR 01 (95.54–95.56 m).

Description: Species is easily recognized by its small vesicle size, rectangular vesicle and short copula. The vesicle wall is smooth. A thick rim is present on the basal margin.

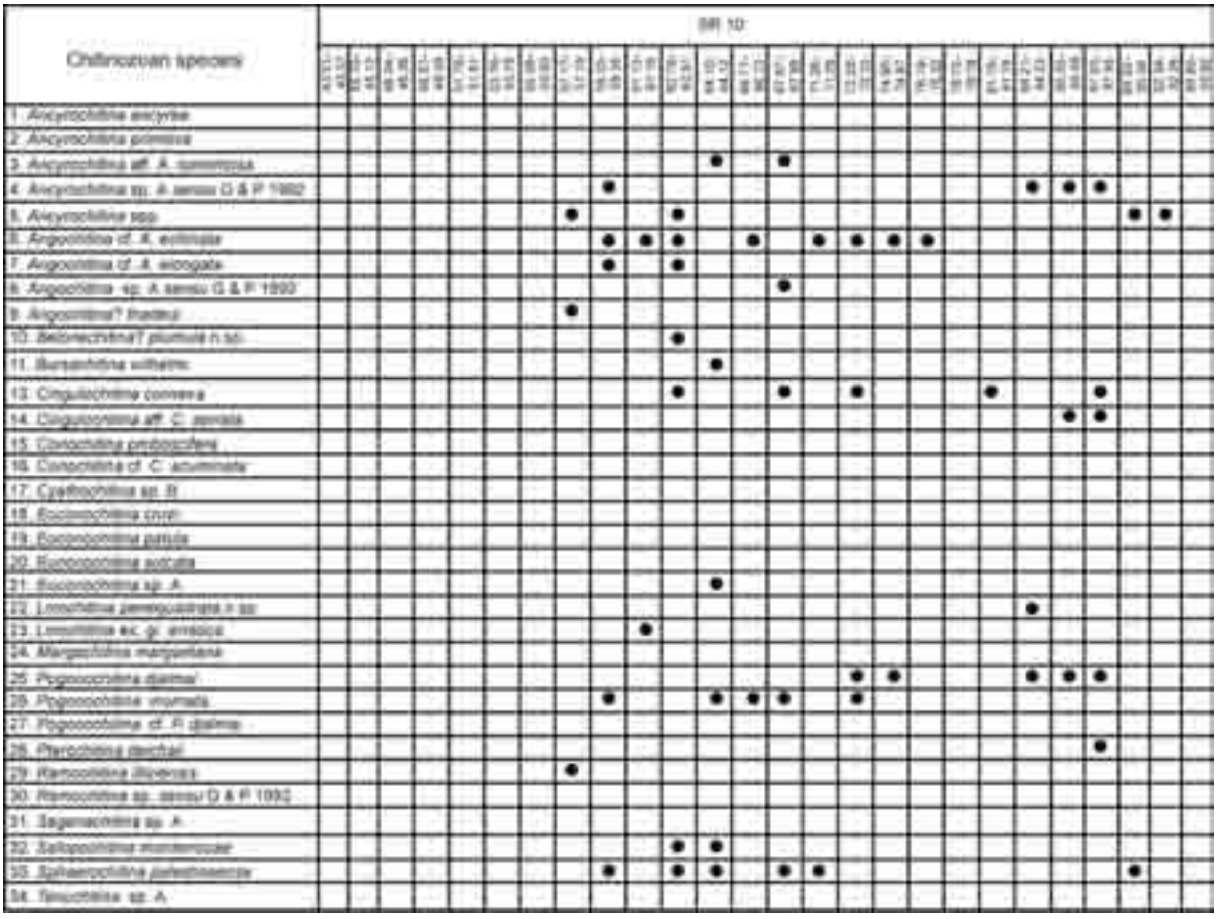

Figure 10. Chitinozoan distribution chart for the SR 10 well on the southern margin of the Amazonas Basin. For the location see Fig. 3A.

Dimensions (six specimens measured): Total length 100–146 µm. Holotype 118 µm, maximum width 71 (57)–121 (97) µm. Holotype 71(57) µm, width of aperture 59 (47)–106 (85) µm. Holotype 59(47) µm.

Occurrence: Amazonas Basin, shallow boreholes SR 01 and SR 10 (Figs 3A–B, 6, 10). Lower part of the Pitinga Formation. Assemblage 3, see Fig. 12.

Linochitina ex. gr. *erratica* (Eisenack 1931)
Plate III, fig. 27, Plate V, fig. 17

1971 *Desmochitina erratica* – Costa, p. 87–88, Plate 18, figs 1–2

Discussion: For a description of *Linochitina erratica*, see Laufeld (1974). *Linochitina* ex. gr. *erratica* differs from the Baltic specimens in having an ovoid base and indistinct flexure.

Dimensions (29 specimens measured): Total length 94–164 µm, maximum width 31 (25)–64 (51) µm, width of aperture 25 (20)–50 (40) µm, length of neck 1/2 of the total length.

Occurrence: Amazonas Basin, PETROBRAS 1-AM-1-AM and 1-UI-2-AM wells (Figs 1A, 2A, 4, 11), shallow boreholes SM 1048, SR 01, SR 03, SR 07, and SR 10 (Figs 1B, 2B, 3A–B, 6–10), outcrop locality Igarapé da Rainha (Figs 3C, 11). Lower part of the Pitinga Formation. Assemblages 3 and 4, see Fig. 12. Costa (1971) described this species from the Igarapé da Rainha 4-65-68 outcrop.

Subfamily Eisenackitininae Paris 1981

Genus *Eisenackitina* Jansonius 1964

Eisenackitina cf. *E. bohemica* (Eisenack 1934)
Plate III, fig. 19

1967 Tipos 76–77 – Lange, Plate 6, figs 76–77
1992 *Eisenackitina* cf. *bohemica* – Grahn and Paris, Plate 3, fig. 10
2003 *Eisenackitina* cf. *E. bohemica* – Grahn and Melo, p. 377–378, Plate 5, figs 1–2
2005 *Eisenackitina* cf. *E. bohemica* – Azevedo-Soares and Grahn, Fig. 4:18

Discussion: This species was discussed by Grahn and Melo (2003). *Eisenackitina* cf. *E. bohemica* is shorter and has a wider aperture than typical *E. bohemic*a.

Dimensions (two specimens measured): Total length 140–206 µm, maximum width 123 (98)–162 (130) µm, width of aperture 69 (55)–73 (58) µm.

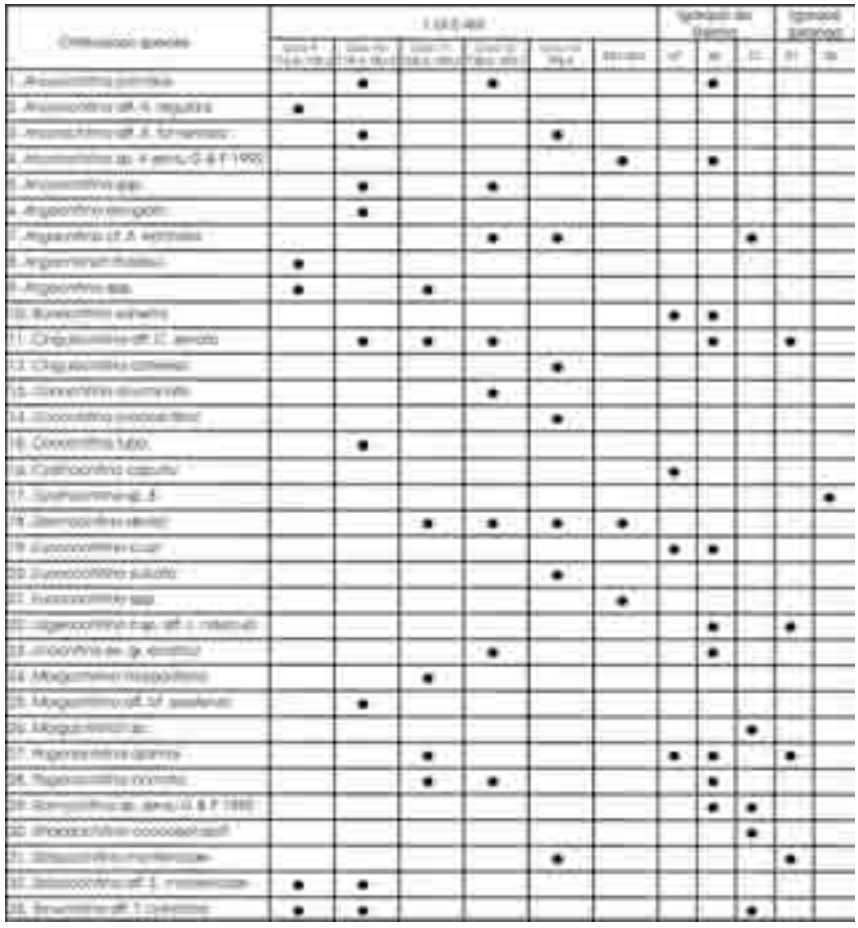

Figure 11. Chitinozoan distribution chart in the 1-UI-2-AM well and the outcrops along Igarapé da Rainha and Igarape Ipiranga rivers, southern margin of the Amazonas Basin. For the location see Figs 2A and 3C.

Occurrence: Amazonas Basin, PETROBRAS 1-AM-1-AM well (Figs 1A, 4). Upper part of the Manacapuru Formation. Assemblage 7, see Fig. 13. Grahn and Paris (1992) and Azevedo-Soares and Grahn (2005) reported *E.* cf. *E. bohemica* from the same interval, which includes the lower part of the Jatapu Member of the Maecuru Formation (Fig. 4).

Subfamily Orbichitininae Achab, Asselin and Soufiane 1993

Genus *Salopochitina* Swire 1990

Salopochitina aff. *S. monterrosae* (Cramer 1969)
Plate IV, fig. 15

1967 Tipos 89 a–b, 90 – Lange, Plate 7, figs 89 a–b, 90
1968 *Conochitina filifera* – Jardiné and Yapaudjian, Plate 6, figs 1, 2
2003 *Salopochitina* aff. *S. monterrosae* – Grahn and Melo, p. 379, Plate 6, figs 12, 14, 15

Discussion: This species was described by Grahn and Melo (2003). *Salopochitina* aff. *S. monterrosae* has a granulated vesicle in contrast to *S. monterrosae* which has a smooth vesicle.

Dimensions (three specimens measured): Total length 175–231 µm, maximum width 111 (89)–155 (124) µm, width of aperture 68 (54)–86 (69) µm, length of neck 1/5–1/3 of the total length, length of appendices ≤ 76 µm.

Occurrence: Amazonas Basin, PETROBRAS 1-AM-1-AM and 1-UI-2-AM wells (Figs 1A, 2A, 4, 11), shallow borehole SM 1048 (Figs 1B, 9). Uppermost part of the Pitinga and possibly lowermost part of the Manacapuru (Lange 1967, Grahn and Melo 2003) formations. Assemblage 4, see Fig. 12. Jardiné and Yapaudjian (1968) reported the species as *Conochitina filifera* from the Early Ludlow Médarba Formation, Polignac Basin, Algerian Sahara.

Order Prosomatifera Eisenack 1972
Family Conochitinidae Eisenack 1931 emend. Paris 1981
Subfamily Conochitininae Paris 1981

Genus *Euconochitina* Taugourdeau 1966 emend. Paris et al. 1999

Euconochitina sp. A
Plate VI, figs 14, 15

Discussion: A cylindrical species with a slightly flaring aperture, which is provided with small spines. A thick rim is present on the basal margin. The base is rounded.

Dimensions (three specimens measured): Total length 193–282 µm, maximum width 50 (40)–73 (58) µm, width of aperture 50 (40)–68 (54) µm.

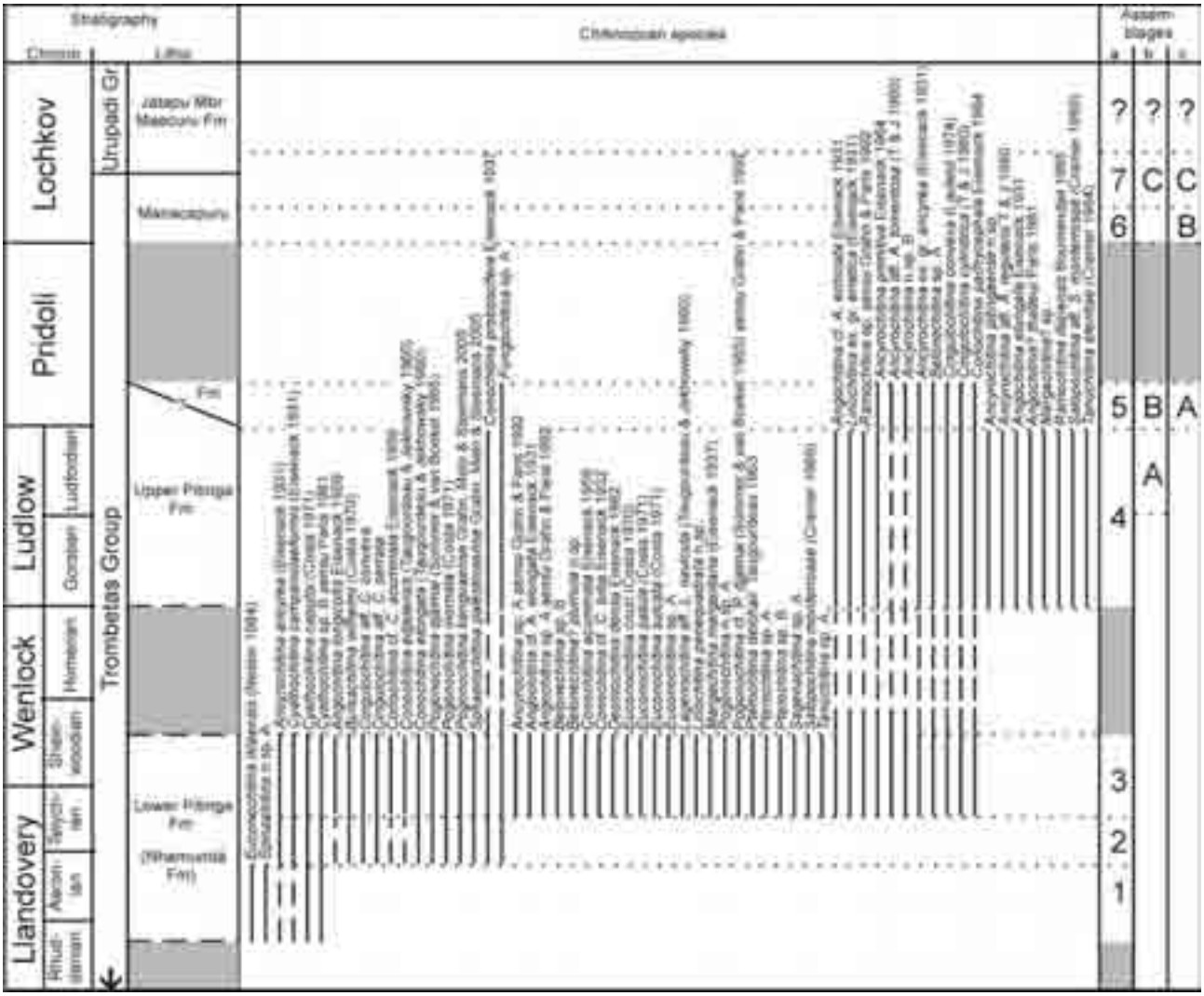

Figure 12. Composite chitinozoan range chart for the Pitinga Formation. a – this paper, b – Grahn and Melo (2003), c – Azevedo-Soares and Grahn (2005), dotted lines – inferred range.

Occurrence: Amazonas Basin, shallow boreholes Sr 07 and SR 10 (Figs 2B, 3A, 8, 10). Lower part of the Pitinga Formation. Assemblage 3, see Fig. 12.

Genus *Conochitina* Eisenack 1931 emend. Paris et al. 1999

Conochitina cf. *C. acuminata* Eisenack 1959
Plate VI, fig. 12

Discussion: For a discussion of *Conochitina acuminata* see Laufeld (1974). *Conochitina* cf. *C. acuminata* differs from the type in having an ovoidal base and a smaller mucron.

Dimensions (two specimens measured): Total length 292–296 µm, maximum width 158 (126)–167 (134) µm, width of aperture 113 (90)–130 (104) µm.

Occurrence: Amazonas Basin, PETROBRAS 1-NO-3-AM well (Figs 1A, 5), shallow boreholes SM 1017, SM 1018, SM 1047, and SR 07 (Figs 1B, 5, 8). Lower part of the Pitinga Formation. Assemblages 2 and 3 see Fig. 12.

Conochitina cf. *C. tuba* Eisenack 1932
Plate V, fig. 15

Discussion: *Conochitina* cf. *C. tuba* differs from *C. tuba* Eisenack 1932 by its convex flanks and ovoid base.

Dimensions (five specimens measured): Total length 226–360 µm, maximum width 115 (92)–153 (122) µm, width of aperture 67 (54)–92 (74) µm, length of neck 1/3 of the total length.

Occurrence: Amazonas Basin, PETROBRAS 1-AM-1-AM well (Figs 1A, 4). Lower part of the Pitinga Formation. Assemblage 3, see Fig. 12.

Genus *Rhabdochitina* Eisenack 1931

Rhabdochitina conocephala? Eisenack 1931 *sensu* Boumendjel 1987
Plate IV, fig. 12

1967 Tipos 51, 99–100 – Lange, Plate 4, fig. 51, Plate 8, figs 99–100

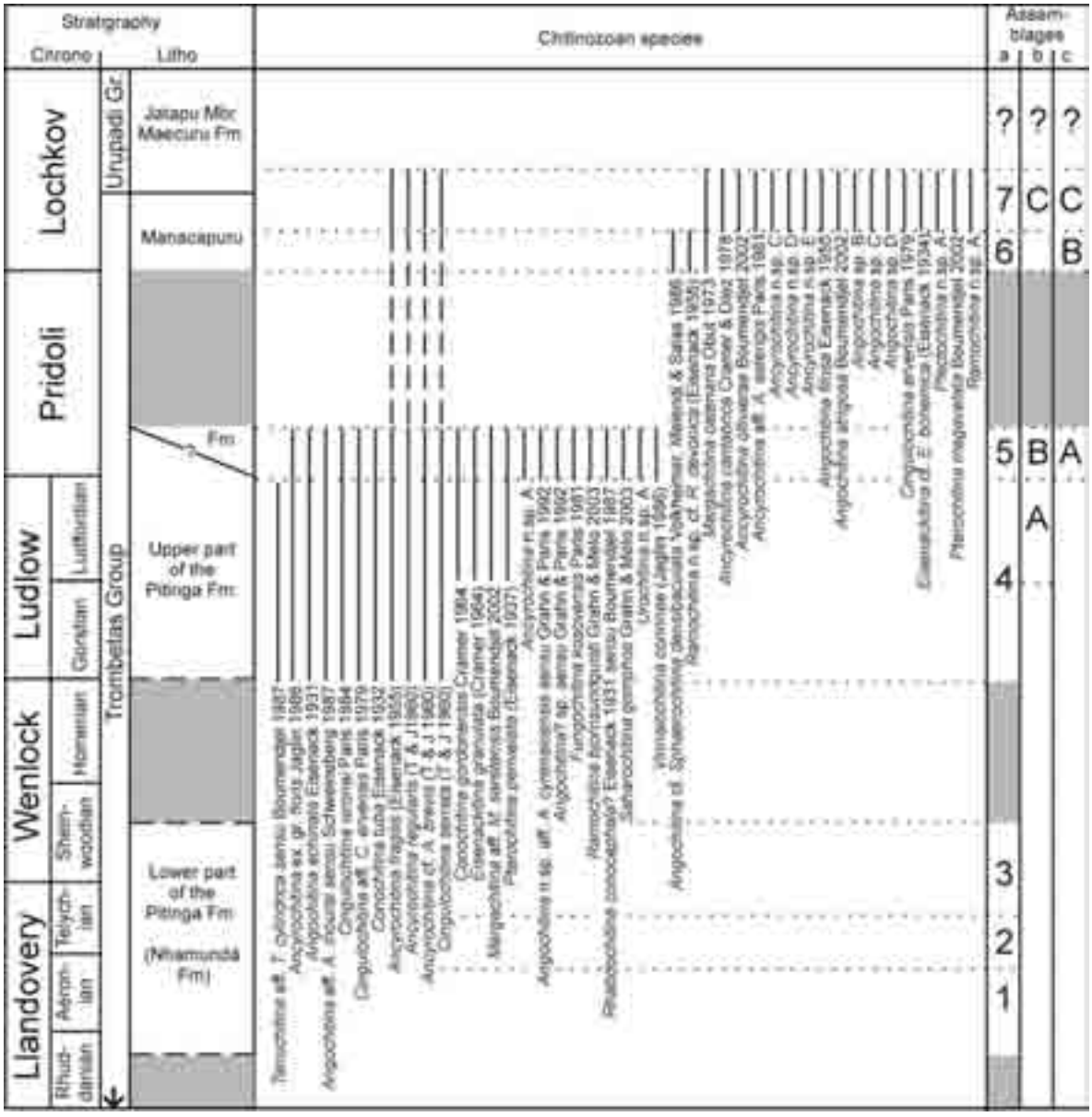

Figure 13. Composite chitinozoan range chart in the upper part of the Pitinga and Manacapuru formations. a – this paper, b – Grahn and Melo (2003), c – Azevedo-Soares and Grahn (2005), dotted lines – inferred range.

1987 *Rhabdochitina conocephala*? – Boumendjel, p. 73–74, Plate 2, figs 4–8
1992 *Rhabdochitina conocephala*? – Grahn and Paris, Plate 2, fig. 7
2003 *Rhabdochitina conocephala*? – Grahn and Melo, p. 379, Plate 6, fig. 13
2005 *Rhabdochitina conocephala*? – Azevedo-Soares and Grahn, Plate 2, fig. 6

Discussion: For a description of this species, see Boumendjel (1987).

Dimensions (three specimens measured): Total length 500–1433 μm, maximum width 85 (68)–158 (126) μm, width of aperture 70 (56)–167 (134) μm.

Occurrence: Amazonas Basin, PETROBRAS 1-AM-1-AM well (Figs 1A, 4), shallow borehole SM 1018 (Figs 1B, 9), outcrop locality Igarapé da Rainha (Figs 3C, 11). Uppermost part of the Pitinga (Lange 1967, Grahn and Paris 1992, Grahn and Melo 2003, and Azevedo-Soares and Grahn 2005) and lowermost part of the Manacapuru formations. Assemblage 5, see Fig. 13. Boumendjel (1987) described *R. conocephala*? from Lower Ludlow beds in the lower part of the Mehaiguène Formation, Oued Mya Basin, Algerian Sahara.

Subfamily Tanuchitininae Paris 1981

Genus *Tanuchitina* Jansonius 1964

Tanuchitina aff. *T. cylindrica* (Taugourdeau and Jekhowsky 1960) *sensu* Boumendjel 1987
Plate IV, fig. 20

?1967 Tipo 97 – Lange, Plate 4, fig. 97

1987 *Tanuchitina* sp. aff. *cylindrica* – Boumendjel, p. 74, Plate 1, figs 4, 8, 9
1992 *Tanuchitina* sp. aff. *cylindrica* – Grahn and Paris, Plate 2, fig. 12
2003 *Tanuchitina* aff. *T. cylindrica* – Grahn and Melo, p. 380, Plate 6, fig. 5

Discussion: For a description of this species, see Boumendjel (1987).

Dimensions (six specimens measured): Total length 360–930 µm, maximum width 80 (64)–120 (96) µm, width of aperture 60 (48)–120 (96) µm, width of carina ca 5 µm.

Occurrence: Amazonas Basin, PETROBRAS 1-AM-1-AM and 1-UI-2-AM wells (Figs 1A, 2A, 4, 11), shallow boreholes SM 1015, SM 1018, and SR 01 (Figs 1B, 2B, 3B, 4, 6, 9), outcrop locality Igarapé da Rainha (Figs 3C, 11). Uppermost part of the Pitinga (Lange 1967, Grahn and Paris 1992, Grahn and Melo 2003) and possibly lowermost part of the Manacapuru formations. Assemblage 4, see Fig. 13. Boumendjel (1987) described *T.* aff. *T. cylindrica* from Lower Ludlow beds in the Mederba Formation, Illizi Basin, Algerian Sahara.

Tanuchitina sp. A
Plate VII, fig. 10

Discussion: A *Tanuchitina* species with an elongated ovoid body, which is slightly convex at the base, and a cylindrical neck. A short carina is present below the basal margin. The aperture is straight.

Dimensions (four specimens measured): Total length 233–300 µm, maximum width 89 (71)–96 (77) µm, width of aperture 68 (54)–77 (62) µm, width of carina 4 µm.

Occurrence: Amazonas Basin, shallow boreholes SR 01 and SR 07 (Figs 2B, 3A–B, 6, 8). Lower part of the Pitinga Formation. Assemblage 3, see Fig. 12.

Subfamily Pogonochitininae Paris et al. 1999

Genus *Pogonochitina* Taugourdeau 1961

Pogonochitina cf. *P. djalmai* (Sommer and van Boekel 1965) *sensu* Grahn and Paris 1992
Plate IV, fig. 6

1971 *Conochitina intermedia* – Costa, p. 34–35, Plate 2, fig. 1
1992 *Pogonochitina* cf. *djalmai* – Grahn and Paris, Plate 2, figs 3, 9a–b

Discussion: *Pogonochitina* cf. *P. djalmai* differs from *P. djalmai* by its wider neck and barrel-shaped body.

Dimensions (six specimens measured): Total length 118–146 µm, maximum width 63 (50)–71 (57) µm, width of aperture 43 (34)–53 (42) µm, length of neck 1/4–1/3 of the total length.

Occurrence: Amazonas Basin, PETROBRAS 1-MU-3-AM well (Figs 1A, 5), shallow boreholes SM 1048, SR 01, SR 03, and SR 07 (Figs 1B, 2B, 3A–B, 5, 6–8). Lower part of the Pitinga Formation. Assemblage 3, see Fig. 12.

Pogonochitina n. sp. A
Plate VII, fig. 4

Discussion: This species has an elongated conical body and a cylindrical neck slightly widening at the straight aperture. The vesicle wall is smooth. A crown with minute simple spines is present at the basal margin.

Dimensions (one specimen measured): Total length 256 µm, maximum width 56 (45) µm, width of aperture 50 (40) µm, length of neck 2/5 of the total length.

Occurrence: Amazonas Basin, shallow borehole SR 01 (Figs 2B, 3B, 6). Lower part of the Pitinga Formation. Assemblage 3, see Fig. 12.

Subfamily Belonechitininae Paris 1981

Genus *Belonechitina* Jansonius 1964

Belonechitina sp. A
Plate V, figs 3–4

Discussion: A conical to subcylindrical species with a wide straight aperture. Base slightly convex. The vesicle wall is covered by small simple spines.

Dimensions (one specimen measured): Total length 191 µm, maximum width 110 (88) µm, width of aperture 71 (57) µm, length of neck 1/3 of the total length.

Occurrence: Amazonas Basin, PETROBRAS 1-AM-1-AM and 1-CM-2-PA wells (Figs 1A, 4, 5), shallow borehole SM 1015 (Figs 1B, 9). Pitinga Formation. Assemblages 3–5, see Fig. 12.

Belonechitina sp. B
Plate V, fig. 13

Discussion: An elongate slender species with a subcylindrical body and a cylindrical neck. The vesicle wall is ornamented by simple spines, which are concentrated on the anteapertural part.

Dimensions (one specimen measured): Total length 400 µm, maximum width 121 (97) µm, width of aperture 92 (74) µm, length of neck 1/3 of the total length.

Occurrence: Amazonas Basin, PETROBRAS 1-CM-2-PA well (Figs 1A, 5). Lower part of the Pitinga Formation. Assemblage 3, see Fig. 12.

Belonechitina? *plumula* n. sp.
Plate VI, figs 8–11

1971 *Illichitina multiplex* Scallreuter – Costa, p. 69–70, Plate 12, fig. 5

Derivation of name: Latin, *plumula*, diminutive of *pluma*, plume, referring to the ornamentation at the aperture.

Diagnosis: A species with a conical body and ovoid base, with a thick ridge at the basal margin. A plume of long simple spines occurs at the aperture.

Holotype: Plate VI, fig. 8. UERJ/DEPA SEM collection 12710

Type locality: Well SR 10 (64.10–64.12 m).

Description: This species is easily distinguished from other chitinozoan species by the plume of long simple spines at the aperture, and a thick ridge along the basal margin. A mucron is present on the base. The vesicle wall is smooth below the aperture. The flexure is indistinct.

Dimensions (five specimens measured): Total length 163–197 µm. Holotype 191 µm; maximum width 59 (47)–75 (60) µm. Holotype 89 (71) µm, width of aperture 59 (47)–72 (58) µm. Holotype 70 (56) µm, length of spines ≤ 74 µm. Holotype 48 µm.

Occurrence: Amazonas Basin, shallow boreholes SR 07 and SR 10 (Figs 2B, 3A, 8, 10). Lower part of the Pitinga Formation. Assemblage 3, see Fig. 12.

Subfamily Spinachitininae Paris 1981

Genus *Spinachitina* Schallreuter 1963

Spinachitina n. sp. A
Plate IV, fig. 16; Plate V, fig. 12

Discussion: A slender conical *Spinachitina* species with a constriction aperturewards of the sharp basal margin, which has a crown of simple appendages. Base flat. Neck cylindrical and slightly widened towards the spiny aperture. *Spinachitina* n. sp. A differs from other Early Silurian *Spinachitina* species (i.e. *S. fragilis*, *S. harringtoni*, *S. maennili*, *S. wolfarti*) by the constriction aperture ward of the basal margin.

Dimensions (two specimens measured): Total length 300–425 µm, maximum width 100 (80)–120 (96) µm, width of aperture 50 (40)–65 (74) µm, length of appendices 7–10 µm, length of neck 1/3 of the total length.

Occurrence: Amazonas Basin, shallow borehole SM 1017 (Figs 1B, 5). Lower part of the Pitinga Formation. Assemblage 1, see Fig. 12.

Family Lagenochitinidae Eisenack 1931 emend. Paris 1981
Subfamily Lagenochitininae Paris 1981

Genus *Lagenochitina* Eisenack 1931 emended Paris et al. 1999

Lagenochitina n. sp. aff. *L. navicula* Taugourdeau and Jekhowsky 1960
Plate VI, figs 16, 17

1971 *Angochitina amazonica* – Costa, p. 60–61, Plate 11, fig. 6
1971 *Angochitina crumena* – Costa, p. 61–62, Plate 11, figs 7–8
1971 *Lagenochitina sommeri* – Costa, p. 73–75, Plate 14, figs 5–8
1971 *Lagenochitina ovoidea* – Costa, p. 75, Plate 14, figs 9–10
1992 *Lagenochitina* n. sp. aff. *navicula* – Grahn and Paris, Plate 1, fig. 11

Discussion: *Lagenochitina* n. sp. aff. *L. navicula* differs from *L. navicula* by having a much shorter neck and almost spherical body. *L. navicula* has elongated ovoid body.

Dimensions (eight specimens measured): Total length 126–177 µm, maximum width 88 (70)–91 (73) µm, width of aperture 44 (35)–47 (38) µm, length of neck 1/4 of the total length.

Occurrence: Amazonas Basin, outcrop localities Igarapé da Rainha 4-65-68 and Igarapé Ipiranga 4-65-81 (Figs 3C, 11). Lower part of the Pitinga Formation (Grahn and Paris 1992). Assemblage 3, see Fig. 12.

Subfamily Cyathochitininae Paris 1981

Genus *Sagenachitina* Jenkins 1970

Sagenachitina sp. A
Plate VII, fig. 9

Discussion: This is a species of *Sagenachitina* with a conical body and a cylindrical neck. The basal margin contains a reticulate carina. The aperture is straight and vesicle wall is smooth.

Dimensions (1 specimen measured): Total length 439 µm, maximum width 156 (125) µm, width of aperture 89 (71) µm, length of neck 1/2 of the total length.

Occurrence: Amazonas Basin, shallow borehole SR 07 (Figs 2B, 3A, 8). Lower part of the Pitinga Formation. Assemblage 3, see Fig. 12.

Genus *Cyathochitina* Eisenack 1955b emend. Paris et al. 1999

C*yathochitina* sp. B *sensu* Paris 1981
Plate III, fig. 15, Plate VI, fig. 13

1971 *Cyathochitina caputoi* – Costa, p. 79–80, Plate 15, fig. 6
1981 *Cyathochitina* sp. B – Paris, p. 299, Plate 19, figs 2–3
1992 *Cyathochitina* sp. – Grahn and Paris, Plate 2, fig. 2
2000 *Cyathochitina* sp. B – Grahn in Grahn et al., Plate 3, fig. 7

Discussion: For a description, see Paris (1981). This small and characteristic species differs from *Cyathochitina caputoi* Costa 1971 in having a much shorter carina and in not having longitudinal ribs on the body.

Dimensions (six specimens measured): Total length 200–250 µm, maximum width 146 (117)–250 (200) µm, width of aperture 58 (46)–88 (70) µm, width of carina ≤ 16 µm, length of neck 1/3 of the total length.

Occurrence: Amazonas Basin (Grahn and Paris 1992), PETROBRAS 1-AM-1-AM well (Figs 1A, 4), shallow boreholes SR 03 and SR 07 (Figs 2B, 3A–B, 7, 8), outcrop locality Igarapé Ipiranga (Figs 3C, 11). Lower part of the Pitinga Formation. Assemblages 1–3, see Fig. 12. Grahn et al. (2000) reported *Cyathochitina* sp. B from Aeronian and Telychian strata, east Paraguay, and Paris (1981) described the species from the Late Llandovery (*turriculatus* Zone) Lande Murée Formation in France, and from coeval beds from Syria.

Subfamily Urochitininae Paris 1981

Genus *Urochitina* Taugourdeau and Jekhowsky 1960

Urochitina n. sp. A
Plate IV, figs 22, 23

2005 *Urochitina* n. sp. A – Azevedo-Soares and Grahn, Plate 2, figs 9, 11.

Discussion: This is a species of *Urochitina* with a hemispherical body and a cylindrical neck. The flexure is distinct and the aperture straight. The vesicle wall is glabrous and the base has a peduncle that tapers distally.

Dimensions (two specimens measured): Total length 230–260 μm, maximum width 97 (78)–116 (93) μm, width of aperture 49 (39)– 63 (50) μm, length of peduncle ≤ 95 μm, length of neck 1/2–2/3 of the total length.

Occurrence: Amazonas Basin, outcrop sample AM 75 (Figs 1B, 9). Upper part of the Pitinga Formation (Azevedo-Soares and Grahn 2005). Assemblage 5, see Fig. 13.

Subfamily Angochitininae Paris 1981

Genus *Fungochitina* Taugourdeau 1966

Fungochitina sp. A
Plate III, fig. 26

2003 *Fungochitina* sp. A – Grahn and Melo, p. 380, Plate 5, figs 3, 4

Discussion: This species was described by Grahn and Melo (2003). It is a *Fungochitina* species with simple spines and few other characteristic features.

Dimensions (four specimens measured): Total length 152–186 μm, maximum width 96 (77)–112 (90) μm, width of aperture 32 (26)–45 (36) μm, length of neck 2/5–1/2 of the total length.

Occurrence: Amazonas Basin, shallow boreholes SM 1017 and SM 1047 (Figs 1B, 5). Pitinga and possibly lowermost part of the Manacapuru formations (Grahn and Melo 2003). Assemblages 2–5, see Fig. 12.

Genus *Angochitina* Eisenack 1931

Angochitina n. sp. aff. *A. cyrenaicensis* Paris 1988
Plate II, fig. 7

1992 *Angochitina* n. sp. aff. *A. cyrenaicensis* – Grahn and Paris, Plate 3, figs 3a–b
2005 *Angochitina* n. sp. aff. *A. cyrenaicensis* – Azevedo-Soares and Grahn, Fig. 24:8

Discussion: For a description of *Angochitina cyrenaicensis*, a Late Givetian species, see Paris (1988). The specimens from the Silurian in the Amazonas Basin are striking in their similarity in the overall shape, but differ in having long hair-like spines and in lacking a collar. *Angochitina cyrenaicensis* has shorter spines arranged in lamellae, simple or multirooted.

Dimensions (one specimen measured): Total length 233 μm, maximum width 56 (45) μm, width of aperture 40 (32) μm, length of neck 1/2 of the total length.

Occurrence: Amazonas Basin, PETROBRAS 1-AM-1-AM well (Figs 1A, 4). Upper part of the Pitinga Formation (Grahn and Paris 1992, Azevedo-Soares and Grahn 2005). Assemblage 5, see Fig. 13.

Angochitina sp. aff. A. *mourai* non Lange 1952 *sensu* Schweineberg 1987
Plate V, fig. 2

1987 *Angochitina* sp. aff. *A. mourai* – Schweineberg, p. 62–63, Plate 4, figs 5–11
2003 *Angochitina* sp. aff. *A. mourai* – Grahn and Melo, p. 380, Plate 2, figs 9, 10

Discussion: This species was discussed by Grahn and Melo (2003). It differs from *A. mourai* Lange 1952 in having simple spines.

Dimensions (two specimens measured): Total length 128–153 μm, maximum width 58 (46)–95 (76) μm, width of aperture 40 (32)–43 (34) μm, length of neck 1/3 of the total length.

Occurrence: Amazonas Basin, shallow borehole SM 1015 (Figs 1B, 6). Upper part of the Pitinga Formation. Assemblages 4, 5, see Fig. 13. Schweineberg (1987) described this species from Upper Ludlow beds in the upper part of the Las Arroyacas Formation, Cantabric Mountains, Palencia, northern Spain.

Angochitina cf. *A. echinata* Eisenack 1931 *sensu* Grahn and Paris 1992
Plate VI, figs 6, 7

Discussion: For a description of *A. echinata* see Laufeld 1974. Specimens of *Angochitina* cf. *A. echinata* differ from the former by having long, simple hair-like spines.

Dimensions (14 specimens measured): Total length 140–229 μm; maximum width 67 (54)–98 (78)

µm, width of aperture 37 (30)–56 (45) µm, length of neck 2/5–1/2 of the total length, length of spines ≤ 10 µm.

Occurrence: Amazonas Basin, PETROBRAS 1-UI-2-AM well (Figs 2A, 11), shallow boreholes SR 01, SR 03, SR 07, and SR 10, outcrop localities Igarapé da Rainha (Figs 2B, 3, 11) and AM 76 (Figs 1B, 5). Lower part of the Pitinga Formation. Assemblages 3, 4, see Fig. 12.

Angochitina cf. *A. elongata* Eisenack 1931
Plate VI, fig. 5

Discussion: For a description of *A. elongata*, see Laufeld (1974). *Angochitina* cf. *A. elongata* differs from *A. elongata* in having a denser ornamentation. In the Brazilian populations, specimens of *A. elongata* s.s. have a more dense ornamentation than those of the Baltic type area.

Dimensions (two specimens measured): Total length 187–239 µm, maximum width 67 (54)–71 (57) µm, width of aperture 33 (26)–36 (29) µm, length of neck 2/5–1/3 of the total length, length of spines 7 µm.

Occurrence: Amazonas Basin, shallow borehole SR 10 (Figs 2B, 3A, 10). Upper part of the Pitinga Formation. Assemblage 3, see Fig. 12.

Angochitina sp. A *sensu* Grahn and Paris 1992
Plate II, figs 9, 13

1971 *Ancyrochitina spinosa* – Costa, p. 57–58, Plate 11, figs 1–2
1992 *Angochitina* sp. A – Grahn and Paris, Plate 2, figs 11a–b

Discussion: A short *Angochitina* species with a spherical body and cylindrical neck that widens slightly towards the aperture. The vesicle is covered by randomly distributed long and simple spines.

Dimensions (seven specimens measured): Total length 105–188 µm, maximum width 81 (65)–100 (80) µm, width of aperture 46 (37)–75 (60) µm, length of neck 2/5–1/2 of the total length, length of spines ≤ 12 µm.

Occurrence: Amazonas Basin, PETROBRAS 1-MU-3-AM, 2-NO-1-AM, and 2-SL-1-AM wells (Figs 1A, 5), shallow boreholes SM 1018, SR 03, SR 07, and SR 10 (Figs 1B, 5, 7, 8, 10). Lower part of the Pitinga Formation. Assemblage 3, see Fig. 12.

Angochitina sp. B
Plate II, fig. 15

2005 *Angochitina* n. sp. B – Azevedo-Soares and Grahn, Fig. 6:7

Discussion: This characteristic species has an ovoid body, and a broad cylindrical neck that widens slightly at the aperture. The vesicle is covered by randomly distributed, minute, simple spines.

Dimensions (three specimens measured): Total length 200–243 µm, maximum width 100 (80)–187 (150) µm, width of aperture 86 (69)–125 (100) µm, length of neck 1/3–2/5 of the total length.

Occurrence: Amazonas Basin, PETROBRAS 1-AM-1-AM well (Figs 1A, 4). Lower part of the Jatapu Member of the Maecuru Formation. Assemblage 7, see Fig. 13.

Angochitina sp. C
Plate II, fig. 16

2005 *Angochitina* n. sp. C – Azevedo-Soares and Grahn, Fig. 6:9

Discussion: This species has a spherical body and a cylindrical neck widening towards the aperture. The vesicle is covered by randomly distributed simple spines.

Dimensions (one specimen measured): Total length 250 µm, maximum width 96 (77) µm, width of aperture 67 (54) µm, length of neck 1/2 of the total length.

Occurrence: Amazonas Basin, PETROBRAS 1-AM-1-AM well (Figs 1A, 4). Uppermost part of the Manacapuru Formation. Assemblage 7, see Fig. 13.

Angochitina sp. D
Plate II, fig. 17

Discussion: An *Angochitina* species with an ovoid body and a short cylindrical neck widening towards the aperture. The vesicle is covered by randomly distributed simple spines.

Dimensions (one specimen measured): Total length 218 µm, maximum width 107 (86) µm, width of aperture 61 (49) µm, length of neck 1/3 of the total length.

Occurrence: Amazonas Basin, PETROBRAS 1-AM-1-AM well (Figs 1A, 4). Uppermost part of the Manacapuru Formation. Assemblage 7, see Fig. 13.

Angochitina? sp.
Plate II, figs 18, 19

1992 *Angochitina*? sp. – Grahn and Paris, Plate 3, fig. 11
2005 *Angochitina*? sp. – Azevedo-Soares and Grahn, Fig. 4:10

Discussion: A slender species questionably referred to *Angochitina* because its general shape. The body is ovoid to spherical, with a long cylindrical neck that widens at the aperture. Small simple spines cover the vesicle. *Angochitina hemeri* Paris and Al-Hajri 1995 is similar but has no ornamentation on the neck.

Dimensions (three specimens measured): Total length 264–333 µm, maximum width 53 (42)–77 (62) µm, width of aperture 27 (22)–36 (29) µm, length of neck 2/3 of the total length.

Occurrence: Amazonas Basin, PETROBRAS 1-AM-1-AM well (Figs 1A, 4). Upper part of the Pitinga Formation (Grahn and Paris 1992, Azevedo-Soares and Grahn 2005). Assemblage 5, see Fig. 13.

Angochitina cf. *Sphaerochitina densibaculata* Volkheimer et al. 1986
Plate II, fig. 14

2005 *Sphaerochitina* aff. *S. densibaculata* – Azevedo-Soares and Grahn, Fig. 6:6, 8

Discussion: For a description of *Sphaerochitina densibaculata*, see Volkheimer et al. (1986). The ornamentation of the *Angochitina* specimens from the Amazonas Basin shows a striking similarity to those of *Sphaerochitina densibaculata*.

Dimensions (nine specimens measured): Total length 147–233 µm, maximum width 100 (80)–116 (93) µm, width of aperture 54 (43)–67 (54) µm, length of neck 1/3–2/3 of the total length, length of spines 5–10 µm.

Occurrence: Amazonas Basin, PETROBRAS 1-AM-1-AM well (Figs 1A, 4), outcrop localities AM 80 and AM 82 (Figs 1B, 9). Lower-middle part of the Manacapuru Formation (Azevedo-Soares and Grahn 2005). Assemblage 6, see Fig. 13.

Genus *Ramochitina* Sommer and van Boekel 1964, emended Paris et al. 1999

Ramochitina n. sp. cf. *R. devonica* Eisenack 1955b
Plate IV, fig. 11

2005 *Ramochitina* n. sp. cf. *R. devonica* – Azevedo-Soares and Grahn

Discussion: This species has an ovoid body and a cylindrical neck. The vesicle displays eight crests of spines that branch at their tips. Each branch is further divided into two branches. *Ramochitina devonica* has its ornamentation concentrated in the lower anteapertural part of the body, and on the upper neck towards the aperture. The neck is also longer than that of *Ramochitina* n. sp. cf. *R. devonica*, which has its ornamentation all along the vesicle. Furthermore, *R. devonica* is a Middle Devonian species.

Dimensions (one specimen measured): Total length 200 µm, maximum width 90 (72) µm, width of aperture 61 (49) µm, length of neck 2/5 of the total length, length of spines *Angochitina hemeri* 30 µm.

Occurrence: Amazonas Basin, PETROBRAS 1-AM-1-AM well (Figs 1A, 4). Lower-middle part of the Manacapuru Formation (Azevedo-Soares and Grahn 2005). Assemblage 6, see Fig. 13.

Ramochitina n. sp. A
Plate I, fig. 14

2005 *Ramochitina* n. sp. B – Azevedo-Soares and Grahn, Fig. 6:18

Discussion: This species has an elongated ovoid body and a short flared neck. The flexure is indistinct. The vesicle has eight crests with long simple spines.

Dimensions (one specimen measured): Total length 197 µm; maximum width 128 (102) µm, width of aperture 43 (34) µm, length of neck 1/3 of the total length, length of spines 41 µm.

Occurrence: Amazonas Basin, PETROBRAS 1-AM-1-AM well (Figs 1A, 4). Upper part of the Manacapuru Formation (Azevedo-Soares and Grahn 2005). Assemblage 7, see Fig. 13.

Ramochitina sp. sensu Grahn and Paris 1992
Plate VII, figs 7, 8

1992 *Gotlandochitina* sp. – Grahn and Paris, Plate 2, fig. 10

Discussion: A *Ramochitina* species with an elongated body and a cylindrical neck. The vesicle has 10 or more crests comprised of long simple spines. The neck widens slightly at the aperture. The vesicle wall between the spines is tuberculate.

Dimensions (three specimens measured): Total length 129–222 µm, maximum width 67 (54)–98 (78) µm, width of aperture 35 (28)–54 (43) µm, length of neck 1/2 of the total length, length of spines *Angochitina hemeri* 24 µm.

Occurrence: Amazonas Basin, shallow borehole SR 07 (Figs 2B, 3A, 8), outcrop locality Igarapé da Rainha. Pitinga Formation (Grahn and Paris 1992). Assemblages 3 and 4, see Fig. 12.

Subfamily Ancyrochitininae Paris 1981

Genus *Ancyrochitina* Eisenack 1955a

Ancyrochitina pitingaense n. sp.
Plate I, figs 15, 16, Plate II, fig. 1

2003 ?*Ancyrochitina* n. sp. A – Grahn, Plate 1, fig. 4

Derivation of name: Latin, *pitingaense*, referring to the Pitinga Formation, from where the holotype is described.

Diagnosis: An *Ancyrochitina* species with 7–8 simple, wide, and tapering appendages at the basal margin, and similar shaped spines on the neck near the aperture. The vesicle wall is covered with minute simple spines.

Holotype: Plate I, fig. 15. UERJ/DEPA SEM collection 25050

Type locality: Well SM 1015 (19.38–19,41 m).

Description: This species has an ovoid body and a cylindrical neck widening at the aperture. The vesicle wall is covered by randomly distributed minute and simple spines. At the basal margin there are seven to eight appendages with wide bases, and which taper towards their tips. The same number of similarly shaped spines occurs on the neck near the aperture. These are thinner and curve aborally, in contrast to the appendages that tend to project aperturally.

Dimensions (seven specimens measured): Total length 200–326 µm. Holotype 326 µm; maximum width 92 (74)–168 (134) µm. Holotype 148 (118) µm, width of aperture

53 (42)–80 (64) µm. Holotype 78 (62) µm, length of neck 1/2 of total length; length of appendages 82–120 µm. Holotype 109 µm, length of spines 51–87 µm. Holotype 87 µm.

Occurrence: Amazonas Basin, shallow boreholes SM 1015 and SM 1018 (Figs 1B, 9). Upper part of the Pitinga Formation. Assemblage 4, see Fig. 12. Doubtful specimens designated as *Ancyrochitina* n. sp. A were reported from the Copo Formation, Chaco-Paraná Basin, northeast Argentina (Grahn 2003).

Ancyrochitina cf. *A. brevis* Taugourdeau and Jekhowsky 1960
Plate I, figs 4, 5

1989 *Ancyrochitina fragilis brevis* – Quadros, p. 28–30, Plate 1
2005 *Ancyrochitina* cf. A. *brevis* – Azevedo-Soares and Grahn, Fig. 5:15, 17

Discussion: For a description of *Ancyrochitina* brevis see Jaglin and Paris (2002). *Ancyrochitina* cf. *A. brevis* differs in having much longer appendages than typical *A. brevis*, which has a maximum length of 40 µm.

Dimensions (12 specimens measured): Total length 176–229 µm, maximum width 68 (54)–121 (97) µm, width of aperture 34 (27)–88 (70) µm, length of neck 1/3–2/3 of the total length, length of appendages 56–122 µm.

Occurrence: Amazonas Basin, PETROBRAS 1-AM-1-AM well (Figs 1A, 4), shallow boreholes SM 2001, SM 2003, SM 2004, SM 2005, and SM 2006 (Figs 1B, 9). Upper part of the Pitinga and lower part of the Manacapuru formations (Quadros 1989, Azevedo-Soares and Grahn 2005). Assemblages 4, 5 and 7, see Fig. 13.

Ancyrochitina aff. *A. asterigis* Paris 1981
Plate I, fig. 3

2005 *Ancyrochitina* aff. *A. asterigis* – Azevedo-Soares and Grahn, Fig. 6:2

Discussion: For a description of *Ancyrochitina asterigis*, see Paris (1981). *Ancyrochitina* aff. *A. asterigis* differs in having thinner appendages, and less pronounced spiny ornamentation on the neck.

Dimensions (one specimen measured): Total length 212 µm, maximum width 112 (90) µm, width of aperture 82 (66) µm, length of neck 2/5 of the total length, length of appendices ≤ 91 µm.

Occurrence: Amazonas Basin, 1-AM-1-AM well (Figs 1A, 4). Uppermost part of Manacapuru Formation (Azevedo-Soares and Grahn 2005). Assemblage 7, see Fig. 13.

Ancyrochitina aff. *A. regularis* Taugourdeau and Jekhowsky 1960
Plate VI, fig. 2

Discussion: For a description of *Ancyrochitina regularis* see Jaglin and Paris (2002). *Ancyrochitina* cf. *A. regularis* differs in having a neck that widens at the aperture.

Dimensions (one specimen measured): Total length 134 µm, maximum width 69 (55) µm, width of aperture 47 (38) µm, length of neck 1/2 of the total length, length of appendices ≤ 34 µm.

Occurrence: Amazonas Basin, PETROBRAS 1-UI-2-AM well (Figs 2A, 11). Upper part of the Pitinga Formation. Assemblage 4, see Fig. 12.

Ancyrochitina aff. *A. tomentosa* Taugourdeau and Jekhowsky 1960
Plate I, fig. 13

1987 *Ancyrochitina tomentosa* – Boumendjel, p. 90, Plate 16, fig. 9
2005 *Ancyrochitina* aff. *A. tomentosa* – Azevedo-Soares and Grahn, Fig. 4:3

Discussion: *Ancyrochitina* aff. *A. tomentosa* has a conical body and a cylindrical neck. The vesicle wall is covered with randomly distributed minute and simple spines, which are bigger just above the flexure towards the aperture. The basal margin has eight to ten appendages that branch at their tips. Each of these branches is generally subdivided twice. *Ancyrochitina tomentosa* is a badly characterized species that has become a waste basket. *Ancyrochitina* aff. *A. tomentosa* is much bigger, and has a comparatively longer neck, than the specimens of *A. tomentosa* illustrated by Paris (1981).

Dimensions (11 specimens measured): Total length 133–222 µm, maximum width 65 (52)–124 (99) µm, width of aperture 45 (36)–113 (90) µm, length of neck 2/5–3/5 of the total length, length of appendages ≤ 75 µm; length of spines ≤ 33 µm.

Occurrence: Amazonas Basin, PETROBRAS 1-AM-1-AM, 1-NO-3-AM, and 1-UI-2-AM wells (Figs 1A, 2A, 4–5, 11), shallow boreholes SR 01, SR 07, and SR 10 (Figs 2B, 3A–B, 6, 8, 10). Pitinga Formation (Azevedo-Soares and Grahn 2005). Assemblages 3 and 5, see Fig. 12. Boumendjel (1987) described similar specimens from the Late Lochkovian part of the Mehaiguène Formation, Oued Mya Basin, Algerian Sahara.

Ancyrochitina ex. gr. *ancyrea* (Eisenack 1931)
Plate I, fig. 2

1967 Tipo 13 – Lange, Plate 2, fig. 13.
2003 *Ancyrochitina* ex. gr. *ancyrea* – Grahn and Melo, p. 382, Plate 2, figs 11, 12

Discussion: This chitinozoan species was discussed by Grahn and Melo (2003). They are more slender than *A. ancyrea* s.s.

Dimensions (two specimens measured): Total length 163–263 µm, maximum width 100 (80)–127 (102) µm, width of aperture 48 (38)–55 (44) µm, length of neck 1/2–2/5 of the total length, length of appendages ≤ 61 µm.

Occurrence: Amazonas Basin, PETROBRAS 1-AM-1-AM and 2-MN-1-AM wells (Figs 1A, 4, 9), shallow borehole SM 1018 (Figs 1B, 5). Pitinga (Lange 1967, Grahn and Melo 2003) and lowermost part of the Manacapuru formations. Assemblages 3–5, see Fig. 12.

Ancyrochitina ex. gr. *floris* Jaglin 1986
Plate I, fig. 7

2003 *Ancyrochitina* ex. gr. *floris* – Grahn and Melo, p. 382, Plate 2, figs 13–14
2005 *Ancyrochitina* ex. gr. *floris* – Azevedo-Soares and Grahn, Fig. 4:4

Discussion: These chitinozoans were discussed by Grahn and Melo (2003). In contrast to *A. floris* they have a glabrous body.

Dimensions (one specimen measured): Total length 155 µm, maximum width 129 (103) µm; width of aperture 51 (41) µm, length of neck 2/5 of the total length, length of appendages ≤ 56 µm.

Occurrence: Amazonas Basin, PETROBRAS 1-AM-1-AM well (Figs 1A, 4). Uppermost part of the Pitinga (Grahn and Melo 2003, Azevedo-Soares and Grahn 2005) and possibly lowermost part of the Manacapuru formations. Assemblages 4 and 5, see Fig. 13.

Ancyrochitina sp. A *sensu* Grahn and Paris 1992
Plate VI, fig. 3

1971 *Plectochitina saharica* – Costa, p. 59, Plate 11, figs 3–5
1971 *Sphaerochitina collinsoni* – Costa, p. 66-67, Plate 12, fig. 2
1971 *Cyathochitina campanulaeformis* – Costa, p. 77–79, Plate 15, figs 4–5
1992 *Ancyrochitina* sp. A – Grahn and Paris, Plate 1, fig. 5

Discussion: *Ancyrochitina* species with conical body and cylindrical neck. The basal margin is well-rounded and has ten long appendages. The vesicle wall is covered with randomly distributed simple spines. Flexure is pronounced.

Dimensions (13 specimens measured): Total length 109–184 µm, maximum width 74 (59)–113 (90) µm, width of aperture 26 (21)–52 (42) µm, length of neck 2/5–3/5 of the total length, length of appendices ≤ 80 µm.

Occurrence: Amazonas Basin, PETROBRAS 1-UI-2-AM well (Figs 2A, 11), shallow boreholes SR 01, SR 03, SR 07, and SR 10 (Figs 2B, 3A–C, 6–8, 10). Lower part of the Pitinga Formation. Assemblage 3 , see Fig. 12.

Ancyrochitina n. sp. A
Plate II, fig. 2

1974 *Ancyrochitina ancyrea* – Cramer, Díez and Cuerda, Fig. 3, Figs 5a–g

Discussion: This species has an ovoid body and a cylindrical neck. Six thick appendages with basket-like structures at the tips, and a corresponding number of similarly-shaped spines on the neck. The vesicle wall is covered with randomly distributed minute and simple spines. *Ancyrochitina* n. sp. A differs from *Ancyrochitina pitingaense* n. sp. in having thinner appendages and spines provided with basket-like structures.

Dimensions (two specimens measured): Total length 159–203 µm, maximum width 85 (68)–103 (82) µm, width of aperture 44 (35)–50 (40) µm, length of neck 1/2 of the total length, length of appendices ≤ 97 µm, length of spines ≤ 78 µm.

Occurrence: Amazonas Basin, outcrop locality AM 74 (Figs 1B, 9). Upper part of the Pitinga Formation. Assemblage 5, see Fig. 13. Cramer et al. (1974) documented this species as a Bolivian variant of *A. ancyrea* from Ludlow? beds of the Kirusillas Formation at Cochabamba, Bolivia.

Ancyrochitina n. sp. B
Plate II, fig. 3

Discussion: An *Ancyrochitina* species with an ovoid body and a cylindrical neck. The basal margin has eight simple, tapering appendages that project anteaperturally. Minute simple spines randomly cover the vesicle wall.

Dimensions (five specimens measured): Total length 180–230 µm, maximum width 90 (72)–111 (89) µm, width of aperture 52 (42)–55 (44) µm, length of neck 1/2 of the total length, length of appendages ≤ 70 µm, length of spines ≤ 63 µm.

Occurrence: Amazonas Basin, PETROBRAS 1-AM-1-AM well (Figs 1A, 4), outcrop locality AM 75 (Figs 1B, 9). Pitinga Formation. Assemblages 3 and 5, see Fig. 12.

Ancyrochitina n. sp. C
Plate II, fig. 4

Discussion: This species has an ovoid body and a cylindrical neck. The vesicle wall is covered with minute and simple spines. At the basal margin occur six simple, tapering appendages that branch at their tips. On the neck there are four similarly-shaped spines.

Dimensions (one specimen measured): Total length 243 µm, maximum width 100 (80) µm, width of aperture 55 (44) µm, length of neck 2/5 of the total length, length of appendages ≤ 50 µm.

Occurrence: Amazonas Basin, shallow borehole SM 2003 (Figs 1B, 9). Uppermost part of the Manacapuru Formation. Assemblage 7, see Fig. 13.

Ancyrochitina n. sp. D
Plate II, fig. 5

Discussion: *Ancyrochitina* n. sp. D has an ovoid body and a cylindrical neck. The vesicle wall is covered by randomly distributed minute and simple spines that increase in size on the neck. The basal margin has six simple appendages that taper towards the tips and are curved aperturally.

Dimensions (one specimen measured): Total length 211 µm, maximum width 104 (83) µm, width of aperture 85 (68) µm, length of neck 2/3 of the total length, length of appendages ≤ 74 µm.

Occurrence: Amazonas Basin, PETROBRAS 1-AM-1-AM well (Figs 1A, 4). Uppermost part of the Manacapuru Formation. Assemblage 7, see Fig. 13.

Ancyrochitina n. sp. E
Plate II, fig. 6

Discussion: An *Ancyrochitina* species with an ovoid body and flared neck. The vesicle wall is covered with randomly distributed minute and simple spines. The basal margin has 10–12 simple, long, tapering appendages that are curved antiaperturally.

Dimensions (one specimen measured): Total length 211 µm, maximum width 104 (83) µm, width of aperture 85 (68) µm, length of neck 2/3 of the total length, length of appendages ≤ 74 µm.

Occurrence: Amazonas Basin, PETROBRAS 1-AM-1-AM well (Figs 1A, 4). Uppermost part of the Manacapuru Formation. Assemblage 7, see Fig. 13.

Genus *Plectochitina* Cramer 1964

Plectochitina n. sp. A
Plate IV, fig. 3

2005 *Plectochitina* n. sp. A – Azevedo-Soares and Grahn, Fig. 6:15

Discussion: This very characteristic *Plectochitina* species has a short conical body and a flared neck. The vesicle wall is glabrous. The basal age has eight massive appendages that branch at their tips. Each of these branches may be further subdivided into thinner branches. The total number of these thinner branches has not been recorded in the study material.

Dimensions (three specimens measured): Total length 213–233 µm, maximum width 117 (94)–133 (106) µm, width of aperture 73 (58)–92 (74) µm, length of neck 2/3–1/2 of the total length, length of appendages ≤ 125 µm.

Occurrence: Amazonas Basin, shallow boreholes SM 2003 and SM 2004 (Figs 1B, 9). Uppermost part of the Manacapuru Formation (Azevedo-Soares and Grahn 2005). Assemblage 7, see Fig. 13.

Chitinozoan biostratigraphy

Chitinozoans from the upper part of the Autas-Mirim Formation were described by Grahn (1992b), who recognized a characteristic late Ashgill (Rawtheyan) assemblage in the PETROBRAS 1-AM-1-AM well at level 2091 m that includes *Armoricochitina nigerica*? (Bouché 1965), *Lagenochitina prussica* Eisenack 1931, and *Tanuchitina anticostiensis* (Achab 1977) among others. The Nhamundá Formation is indirectly dated by the interfingering and overlying shales of the lower part of the Pitinga Formation. The chitinozoan biostratigraphy of the Pitinga and Manacapuru formations have been discussed by Grahn (1992a), Grahn and Paris (1992), and Grahn and Melo (2003). In the present data set of seven chitinozoan assemblages are distinguished (Figs 12, 13), i.e. 1–3 (lower Pitinga Formation), 4 (upper Pitinga Formation), 5 (at the transition between the Pitinga and Manacapuru formations), 6 (lower-middle Manacapuru Formation), and 7 (upper Manacapuru Formation). Reworking is very common in the Lower Silurian beds due to three glacial events during that time (Grahn and Caputo 1992). The assemblages are described in ascending stratrigraphic order below.

Assemblage 1

Assemblage 1 (Fig. 12) is of Late Rhuddanian–Early Aeronian age. The appearance of *Spinachitin*a species (i.e. *Spinachitina* n. sp. A) is characteristic of the early Aeronian, and in the Lower Silurian strata of the intracratonic basins of Brazil and Paraguay this genus does not range into the Telychian (Grahn et al. 2000, Grahn et al. 2005). Another diagnostic chitinozoan species in the Amazonas Basin is *Euconochitina iklaensis*, a species ranging from the Upper Rhuddanian to Aeronian (Verniers et al. 1995). *Ancyrochitina ancyrea* and the *Cyathochitina* species present have long ranges, and are known from the Early Llandovery elsewhere.

Assemblage 2

Assemblage 2 (Fig. 12) is of the latest Aeronian–Early Telychian age. In the Paraná Basin many species that appear in the uppermost Aeronian range into the Upper Telychian (Grahn et al. 2000), and this distribution pattern is also true for the Amazonas Basin. Assemblage 2 is well developed in the Parnaíba Basin (Grahn et al. 2005). The majority of the species in this assemblage probably represents an Early Telychian age. The absence of typical and common species for the Late Telychian–Early Sheinwoodian, and the absence of *Spinachitina* species, are characteristic of the assemblage.

Assemblage 3

Assemblage 3 (Fig. 12) is of Late Telychian–Early Sheinwoodian age. The assemblage is well developed in the Amazonas and Paraná basins. Diagnostic species in the Amazonas Basin include *Angochitina* sp. A *sensu* Grahn and Paris 1992, *Belonechitina*? *plumula* n. sp., *Conochitina acuminata, Desmochitina densa, Euconochitina cruzi, Euconochitina patula, Euconochitina sulcata, Linochitina penequadrata* n. sp., *Margachitina margaritana, Pterochitina deichaii*, and *Salopochitina monterrosae*. This chitinozoan assemblage characterizes the upper lower part of the Pitinga Formation in the Amazonas Basin, and the up-

per part of the Vargas Peña Formation in the Paraná Basin (Grahn et al. 2000).

Assemblage 4

Assemblage 4 (Figs 12 and13) is of Ludlow age, the only other definite report of which is from the upper part of the Pitinga Formation in the Amazonas Basin (Azevedo-Soares and Grahn 2005). Grahn and Melo (2003) reported Upper Ludlow beds from possibly lowermost Manacapuru Formation along the Urubu River. Species like *Ancyrochitina pitingaense* n. sp., *Ramochitina illiziensis, Salopochitina* aff. *S. monterrosae, Tanuchitina elenitae*, and *Tanuchitina* aff. *T. cylindrica* characterize this assemblage. Most of the species present in this assemblage range into lower Pridoli beds which contain Assemblage 5. Assemblage A of Grahn and Melo (2003) corresponds to the upper part of Assemblage 4 in this study (see Figs 12 and 13).

Assemblage 5

Assemblage 5 (Figs 12 and 13) is of early Pridoli age. Beds of this age are known from the Amazonas Basin (Azevedo-Soares and Grahn 2005) and probably from the Solimões Basin (Grahn et al. 2003) as well. Many chitinozoan species in this zone range from Late Ludlow. The species restricted to this assemblage in the Amazonas Basin include *Angochitina* n. sp. aff. *A. cyrenaicensis, Angochitina*? sp. *sensu* Grahn and Paris 1992, *Fungochitina kosovensis, Ramochitina bjornsundquisti, Rhabdochitina conocephala*?, *Saharochitina gomphos, Urochitina* n. sp. A, and *Vinnalochitina corinnae*. These species are representative of the uppermost Pitinga and lowermost Manacapuru formations in the Amazonas Basin (Azevedo-Soares and Grahn 2005). Assemblage 5 corresponds to Assemblage A of Azevedo-Soares and Grahn (2005) and Assemblage B of Grahn and Melo (2003, see Fig. 13).

Assemblage 6

Assemblage 6 (Fig. 13) is an earliest Lochkovian assemblage, which so far has only been reported from the Amazonas Basin. The presence of *Margachitina catenaria* confirms the Lochkovian age, and its stratigraphic position above Lower Pridoli beds, and below typical Lower Lochkovian beds, does not contradict, a lowermost Lochkovian correlation. Characteristic species are *Angochitina* cf. *Sphaerochitina densibaculata* and *Ramochitina* n. sp. cf. *R. devonica* (cf. Azevedo-Soares and Grahn 2005). The Silurian-Devonian boundary was discussed in detail by Azevedo-Soares and Grahn (2005), who identified a gap between Lower Pridoli and Lower Lochkovian strata, and the assemblage corresponds to their Assemblage B (see Fig. 13).

Assemblage 7

Assemblage 7 (Fig. 13) is of the Early Lochkovian age, and is present in the Solimões and Amazonas basins (Grahn and Melo 2003; Grahn et al. 2003). Characteristic species include *Ancyrochitina* aff. *A. asterigis, Ancyrochitina cantabrica, Ancyrochitina ollivierae, Angochitina filosa, Angochitina strigosa, Cingulochitina ervensis, Eisenackitina* cf. *E. bohemica, Plectochitina* n. sp. A, and *Pterochitina megavelata*. Assemblage 7 corresponds to Assemblage C by Azevedo-Soares and Grahn (2005) and Grahn and Melo (2003, see Fig. 13).

Concluding remarks

Chitinozoans from the Trombetas Group documented herein have been compared with coeval faunas from other parts of Gondwana, to which they have a pronounced affinity. The PETROBRAS 1-AM-1-AM well has been selected as a reference section for the Trombetas Group chitinozoan succession. Seven Siluro-Devonian chitinozoan assemblages can be defined from the Late Rhuddanian–Early Aeronian (1), latest Aeronian–Early Telychian (2), Late Telychian–Early Sheinwoodian (3), Ludlow (4), Early Pridoli (5), earliest Lochkovian (6), and Early Lochkovian (7). Assemblages 4, 5, and 7 were also defined in the Urubu area in the western part of the Amazonas Basin although designated by different schemas (see Figs 12 and 13; Grahn and Melo 2003). These assemblages have also been distinguished in coeval rocks from other intracratonic basins in Brazil and Paraguay.

The basal Autas-Mirim Formation is Late Ordovician (Caradoc? – Ashgill; Grahn 1992a, b), and the overlying Nhamundá Formation is indirectly dated by the interfingering and overlying shales of the lower part of the Pitinga Formation, which is Llandovery–early Wenlock in its type area. It consists of three transgressive cycles (Late Rhuddanian–Early Aeronian, latest Aeronian–Early Telychian, and Late Telychian–Early Sheinwoodian). The upper part of the Pitinga Formation is dated as Ludlow–Early Pridoli, and is well developed in shallow borings in the Trombetas area. The lower part of the Manacapuru Formation is of Early Pridoli age in the Trombetas area, but may be as old as Late Ludlow in the Urubu area (Grahn and Melo 2003). A badly characterized earliest Lochkovian interval occurs transgressively over Lower Pridoli strata in the Trombetas area. A characteristic Early Lochkovian chitinozoan assemblage is present in the uppermost part of the Manacapuru Formation, and in the lower part of the Jatapu Member of the Maecuru Formation (Urupadi Group). Of the 104 species present, 51 are left in open nomenclature and only three species, *Ancyrochitina pitingaense*, *Belonechitina*? *plumula* and *Linochitina penequadrata*, are described as new.

Acknowledgements. The author thanks the Faculty of Geology at Universidade do Estado do Rio de Janeiro (UERJ), and Dr. Egberto Pereira, head of the post-graduate program at the Faculty of Geology at UERJ for access to the facilities. PETROBRAS is thanked for permission to publish this material, as is the Conselho Nacional de Desenvolvimento Científico e Tecnológico (CNPq, PQ 303777/02-8), which made my work possible through grants. Danièle Bernard (Rennes, France) is gratefully acknowledged for processing some of the SEM films. Through the cour-

tesy of Dr. Sylvia Maria Couto dos Anjos, head of BPA at CENPES (PETROBRAS, Rio de Janeiro), and Prof. Florentin Paris (Rennes, France), we had access to Scanning Electron Microscopes. Dr. Merrell A. Miller (Dhahran, Saudi Arabia) is acknowledged for checking the English, and Dr. Florentin Paris (Rennes, France) made the French translations. I am very grateful to Drs. Theresa Winchester-Seeto (Sydney, Australia) and Radek Morávek (Prague, Czech Republic) for their careful revisions of the final version of the manuscript, which led to a much improved work. All technical help from Jorge Louiz dos Santos and Maria Rosalva Campos Coelho at UERJ and Rogério da Silva Martins da Costa at CENPES is greatly appreciated. My sincere thanks to all.

References

For completeness and to avoid confusion all references pertaining to the authorship of chitinozoan genera and species are included here.

Achab A. (1977): Les chitinozoaires de la zone à *Dicellograptus complanatus* Formation de Vauréal, Ordovicien supérieur, Ile d'Anticosti, Québec. Can. J. Earth Sci. 14, 413–425.

Achab A., Asselin E., Soufiane A. (1993): New morphological characters observed in the Order Operculatifera and their implications for the suprageneric Chitinozoan classification. Palynology 17, 1–9.

Azevedo-Soares H. L., Grahn Y. (2005): The Silurian–Devonian boundary in the Amazonas Basin, northern Brazil. Neues Jahrb. Mineral.-Abh. 236, 79–94.

Babin C., Deunff J., Melou M., Paris F., Pelhate H., Plusquellec Y., Racheboeuf P. (1979): La coupe de Porz Ar Vouden (Pridoli de la Presqu'ile de Crozon) Massif Armoricain, France. Lithologie et Biostratigraphie. Palaeontogr. Abt. B-Palaophytol. 164, 52–84.

Bouché P. M. (1965): Chitinozoaires du Silurien s.l. du Djado (Sahara nigérien). Rev. Micropaleontol. 8, 151–164.

Boumendjel K. (1985): Nouvelles espèces de chitinozoaires dans le Silurien et le Dévonien du bassin d'Illizi (S.E. du Sahara algérien). Rev. Micropaleontol. 28, 155–166.

Boumendjel K. (1987): Les Chitinozoaires du Silurien supérieur et Devonien du Sahara algérien. PhD Thesis, Université de Rennes.

Boumendjel K. (2002): Nouvelles espèces de chitinozoaires du Silurien Supérieur et du Dévonien Inférieur du bassin de Timimoun (Sahara central, Algeria). Rev. Palaeobot. Palynology 118, 29–46.

Costa N. M. (1970): *Pallachitina* e *Spathachitina*, dois novos gêneros de quitinozoáiros do Siluriano brasileiro. An. Acad. Bras. Cienc. 42, 207–218.

Costa N. M. (1971): Quitinozoários silurianos do Igarapé da Rainha, Estado do Pará. Departamento Nacional da Produção Mineral. Div. Geol. Mineral. Bol. 255.

Cramer F. H. (1964): Microplankton from three Palaeozoic formations in the province of León (NW Spain). Leidse Geol. Meded. 30, 255–361.

Cramer F. H. (1969): Possible implications for Silurian paleogeography from phytoplankton assemblages of the Rose Hill and Tuscacora formations of Pennsylvania. J. Paleontol. 43, 485–491.

Cramer F. H., Díez M. C. R. (1978): Iberian chitinozoans. 1. Introduction and summary of pre-Devonian data. Palinología, num. Extraord. 1, 149–201.

Cramer F. H., Díez M. C. R., Cuerda A. J. (1974): Late Silurian chitinozoans and acritarchs from Cochabamba, Bolivia. Neues Jahrb. Geol. Palaontol.-Monatsh. 1, 1–12.

Derby O. A. (1878): Contribuições para a geologia da região do Baixo Amazonas. Arch. Mus. Nac. 2, 77–104.

Eisenack A. (1931): Neue Mikrofossilien des baltischen Silurs. I. Paläontol. Z. 13, 74–118.

Eisenack A. (1932): Neue Mikrofossilien des baltischen Silurs. II. Paläontol. Z. 14, 267–277.

Eisenack A. (1934): Neue Mikrofossilien des baltischen Silurs III und neue Mikrofossilien des böhmischen Silurs I. Paläontol. Z. 16, 52–76.

Eisenack A. (1937): Neue Mikrofossilien des baltischen Silurs IV. Paläontol. Z. 19, 217–243.

Eisenack A. (1955a): Chitinozoen, Hystrichosphaeren und andere Mikrofossilien aus den Beyrichiakalk. Senckenb. lethaea 36, 157–188.

Eisenack A. (1955b): Neue Chitinozoen aus dem Silur des Baltikums und dem Devon der Eifel. Senckenb. lethaea 36, 311–319.

Eisenack A. (1959): Neotypen baltischer Silur Chitinozoen und neue Arten. Neues Jahrb. Geol. Palaontol. 108, 1–20.

Eisenack A. (1962): Neotypen baltischer Silur Chitinozoen und neue Arten. Neues Jahrb. Geol. Palaontol. 114, 291–316.

Eisenack A. (1964): Mikrofossilien aus dem Silur Gotlands. Chitinozoen. Neues Jahrb. Geol. Palaontol.-Abh. 120, 308–342.

Eisenack A. (1968): Über Chitinozoen des baltischen Gebietes. Palaeontogr. Abt. A 131, 137–198.

Eisenack A. (1972): Beitrage zur Chitinozoen-Forschung. Palaeontogr. Abt. A 140, 117–130.

Grahn Y. (1988a): Chitinozoan biostratigraphy of the pre-Carboniferous sequence of well 1-AM-1-AM, Amazonas Basin. Age and correlation of the Pitinga Shale. Internal report, PETROBRAS/Cenpes/Divex/ /Sebipe no. 915.

Grahn Y. (1988b): Chitinozoan biostratigraphy of the pre-Carboniferous sequence of the Amazonas Basin, with comments on the Upper Tapajós Basin. Internal report, PETROBRAS/Cenpes/Divex/Sebipe no. 943.

Grahn Y. (1990): The Late Silurian and Early Devonian of Brazil. New evidences from the chitinozoan biostratigraphy. Internal report. PETROBRAS/CENPES/DIVEX/SEBIPE no. 1115.

Grahn Y. (1992a): Revision of Silurian and Devonian strata of Brazil. Palynology 16, 35–61.

Grahn Y. (1992b): Ordovician Chitinozoa and stratigraphy of Brazil. Geobios 25, 703–723.

Grahn Y. (2003): Silurian and Devonian chitinozoan assemblages from the Chaco Paraná Basin, northeastern Argentina and central Uruguay. Rev. Esp. Micropaleontol. 35, 1–8.

Grahn Y., Caputo M. V. (1992): Early Silurian glaciations in Brazil. Paleogeogr. Paleoclimatol. Paleoecol. 99, 9–15.

Grahn Y., Loboziak S., Melo J. H. G. (2003): Integrated correlation of Late Silurian (Pridoli s.l.) – Devonian chitinozoans and miospores in the Solimões Basin, northern Brazil. Acta Geol. Pol. 53, 283–300.

Grahn Y., Melo J. H. G. (1990): Bioestratigrafia dos quitinozoários do Grupo Trombetas nas faixas marginais da Bacia do Amazonas. Petrobrás/CENPES Report MCT 67313079.

Grahn Y., Melo J. H. G. (2003): Silurian-Devonian chitinozoan biostratigraphy along the Urubu, Uatumã and Abacate rivers in the western part of the Amazonas Basin, northern Brazil. Bull. Geosci. 78, 373–391.

Grahn Y., Melo J. H. G., Steemans P. (2005): Integrated chitinozoan and miospore zonation of the Serra Grande Group (Silurian – lower Devonian), Parnaíba Basin, northeast Brazil. Revista Española de Micropaleontologia 37, 183–204.

Grahn Y., Paris F. (1992): Age and correlation of the Trombetas Group, Amazonas Basin, Brazil. Rev. Micropaleontol. 35, 20–32.

Grahn Y., Pereira E., Bergamaschi S. (2000): Silurian and Lower Devonian chitinozoan biostratigraphy of the Paraná Basin in Brazil and Paraguay. Palynology 24, 143–172.

Jaeger H. (1976): Das Silur und Unterdevon vom thüringischen Typ in Sardinien und seine regionalgeologische Bedeutung. Nova Acta Leopold. 45, 263–299.

Jaglin J. C. (1986): Nouvelles espèces de Chitinozoaires du Pridolí de Libye. Rev. Micropaleontol. 29, 44–54.

Jaglin J. C., Paris F. (2002): Biostratigraphy, biodiversity and palaeogeography of late Silurian chitinozoans from A1-61 borehole (north-west Libya). Rev. Palaeobot. Palynol. 118, 325–358.

Jansonius J. (1964): Morphology and classification of some Chitinozoa. Bull. Can. Pet. Geol. 12, 901–918.

Jardiné S., Yapaudjian L. (1968): Lithostratigraphie et palynologie du Dévonien - Gothlandien gréseux du basin de Polignac (Sahara). Rev. Inst. Fran. Petrol. 23, 439–469.

Jenkins W. A. M. (1970): Chitinozoa from the Ordovician Sylvan Shale of the Arbuckle Mountains, Oklahoma. Paleontology 13, 261–288.

Lange F. W. (1952): Quitinozoários do Folhelho Barreirinha, Devoniano do Pará. Dusenia 3, 373–386.

Lange F. W. (1967): Subdivisão bioestratigráfica e revisão da coluna siluro devoniana da Bacia do Baixo Amazonas. Atas do Simpósio sobre a Biota Amazônica (Geociências) 1, 215–326.

Lange F. W. (1972): Silurian of Brazil. In: Berry W. B. N., Boucot A. J. (eds) Correlation of the South American Silurian Rocks. Geol. Soc. Am. Spec. Pap. 154, 33–39.

Laufeld S. (1974): Silurian Chitinozoa from Gotland. Fossils and Strata 5, 120 p.

Melo J. H. G. (1988): The Malvinokaffric realm in the Devonian of Brazil. In: McMillan N. J., Embry A. F., Glass D. J. (eds) Devonian of the World. Can. Soc. Petrol. Geol. Mem., Vol. 1, 14, 669–703.

Nestor V. (1984): Distribution of chitinozoans in the Late Llandoverian Rumba Formation (*Pentamerus oblongus* beds) of Estonia. Rev. Palaeobot. Palynol. 43, 145–153.

Obut A. M. (1973): On the geographical distribution, comparative morphology, ecology, phylogeny and systematical position of the Chitinozoa. In: Betekhina O. A., Zhuraleva I. T. (eds) Morfologia i ekologiia vodnykh (in Russian). Nauka, Sibirskoe otdelenie 169, 72–84.

Paris F. (1981): Les Chitinozoaires dans le Paléozoïque du sudouest de l'Europe. Mem. Soc. Geol. Mineral. Bretagne 26.

Paris F. (1984): Nouvelles especes de Chitinozoaires a la limite Ludlow/Pridoli en Tchécoslovaquie. Rev. Palaeobot. Palynol. 43, 155–177.

Paris F. (1988): New chitinozoans from the Late Ordovician – Late Devonian of northeast Libya. In: El Arnauti A., Owens B., Thusu B. (eds) Subsurface Palynostratigraphy of Northeast Libya. Garyounis University, Benghazi, 77–87.

Paris F., Al-Hajri S. (1995): New chitinozoan species from the Llandovery of Saudi Arabia. Rev. Micropaleontol. 38, 311–328.

Paris F., Grahn Y., Nestor V., Lakova I. (1999): Proposal for a revised chitinozoan classification. J. Paleontol. 73, 549–570.

Quadros L. P. (1985): Natureza do contato entre as formações Trombetas e Maecuru (Bacia do Amazonas). Coletânea de trabalhos paleontológicos. Seção Paleontologia e Estratigrafia. VIII Congresso Brasileiro de Paleontologia 2, 435–441.

Quadros L. P. (1989): Ocorrência inédita de *Ancyrochitina fragilis brevis* (Chitinozoa) na área do rio Mapuera, Pará, Brasil. Boletim IG-USP. Publicação Especial 7, 27–33.

Ruedemann R. (1929): Descripção dos graptolitos do rio Trombetas. Monographias do Serviço Geologico e Mineralógico 7, 20–24.

Schallreuter R. (1963): Neue Chitinozoen aus ordovizischen Geschieben und Bemerkungen zur Gattung *Illichitina*. Paleontol. Abh. 1, 392–405.

Schweineberg J. (1987): Silurische Chitinozoen aus der Provinz Palencia (Kantabrisches Gebirge, N-Spanien). Gott. Arb. Geol. Palaontol. 33.

Sommer F. W., van Boekel N. M. (1964): Quitinozoarios do Devoniano de Goiás. An. Acad. Bras. Cienc. 36, 423–431.

Sommer F. W., van Boekel N. M. (1965): Novas espécies de quitinozoários do Furo 56, Bom Jardim, Itaituba, Pará. Ministerio das Minas e Energia. DNPM. Divisão de Geologia e Mineralogia. Notas preliminares e estudos 130, 1–20.

Swire F. (1990): New chitinozoan taxa from the Lower Wenlock (Silurian) of the Welsh Borderlands, England. J. Micropalaentol. 9, 107–113.

Taugourdeau P. (1961): Chitinozoaires du Silurien d'Aquitaine. Rev. Micropaleontol. 4, 135–154.

Taugourdeau P. (1963): Etudé de quelques espéces critiques de Chitinozoaires de la région d'Edjelé et compléments à la faune locale. Rev. Micropaleontol. 6, 130–144.

Taugourdeau P. (1966): Les Chitinozoaires. Techniques d'études, morphologie et classification. Mem. Soc. Geol. France, N. S. 45, 1–64.

Taugourdeau P., Jekhowsky B. (1960): Répartition et description des Chitinozoaires siluro-dévoniens de quelques sondages de la C.R.E.P.S., de la C.F.P.A. et de la S.N. Repal au Sahara. Rev. Inst. Fran. Petrol. 15, 1199–1260.

Verniers J., Nestor V., Paris F., Dufka P., Sutherland S. J. E., van Grootel G. (1995): A global Chitinozoa biozonation for the Silurian. Geol. Mag. 132, 651–666.

Volkheimer W., Melendi D. L., Salas A. (1986): Devonian Chitinozoans from Northwestern Argentina. Neues Jahrb. Geol. Palaontol.-Abh. 173, 229–251.

→

Plate I. Chitinozoans from the Trombetas Group. Scale bars represent 100 µm.
1 – *Ancyrochitina ancyrea* (Eisenack 1931), well 1-AM-1-AM, cuttings 1752–1755 m. 2 – *Ancyrochitina* ex. gr. *ancyrea* (Eisenack 1931), well 2-MN-1-AM, core 42 (1253.30–1252.40 m). 3 – *Ancyrochitina* aff. *A. asterigis* Paris 1981, well 1-AM-1-AM, core 37 (1522.00–1524.30 m). 4 – *Ancyrochitina* cf. *A. brevis* (Taugourdeau and Jekhowsky 1960), well SM 2001 (9.86–9.90 m). 5 – *Ancyrochitina* cf. *A. brevis* (Taugourdeau and Jekhowsky 1960), well SM 2004 (45.08–45.12 m). 6 – *Ancyrochitina cantabrica* Cramer and Díez 1978, well SM 2004 (38.36–38.40 m). 7 – *Ancyrochitina* ex. gr. *floris* Jaglin 1986, well 1-AM-1-AM, core 42 (1598.40–1599.30 m). 8 – *Ancyrochitina fragilis* Eisenack 1955, outcrop AM 85. 9 – *Ancyrochitina ollivierae* Boumendjel 2002, well 1-AM-1-AM, core 37 (1522.00–1524.30 m). 10 – *Ancyrochitina primitiva* Eisenack 1955, well 2-SL-1-AM, cuttings 591–606 m. 11 – *Ancyrochitina regularis* Taugourdeau and Jekhowsky 1960, well 1-AM-1-AM, cuttings 1630–1633 m. 12 – *Ancyrochitina regularis* Taugourdeau and Jekhowsky 1960, well 1-AM-1-AM, cuttings 1644–1647 m. 13 – *Ancyrochitina* aff. *A. tomentosa* (Taugourdeau and Jekhowsky 1960), well 1-AM-1-AM, core 37 (1522.00–1524.30 m). 14 – *Ramochitina* n. sp. A, well 1-AM-1-AM, core 37 (1522.00–1524.30 m). 15 – *Ancyrochitina pitingaense* n. sp., holotype, well SM 1048 (22.08–22,10 m). 16 – *Ancyrochitina pitingaense* n. sp., well SM 1048 (22.08–22.10 m).

→→

Plate II. Chitinozoans from the Trombetas Group. Scale bars represent 100 µm.
1 – *Ancyrochitina pitingaense* n. sp., well SM 1048 (22.08–22.10 m). 2 – *Ancyrochitina* sp. A, outcrop AM 74. 3 – *Ancyrochitina* sp. B, well 1-AM-1-AM, cuttings 1677–1680 m. 4 – *Ancyrochitina* sp. C, outcrop AM 75. 5 – *Ancyrochitina* sp. D, well SM 2003 (32.16–32.19 m). 6 – *Ancyrochitina* sp. E, well 1-AM-1-AM, core 37 (1522.00–1524.30 m). 7 – *Angochitina* n. sp. aff. *A. cyrenaicensis* Paris 1988, IGR, well 1-AM-1-AM, core 46 (1607.00–1613.00 m). 8 – *Angochitina echinata* Eisenack 1931, well 1-AM-1-AM, core 46 (1607.00–1613.00 m). 9 – *Angochitina* sp. A *sensu* Grahn and Paris 1992, well SR 03 (54.13–54.15 m). 10 – *Angochitina filosa* Eisenack 1955, well SM 2003 (32.16–32.19 m). 11 – *Angochitina longicollis* Eisenack 1959, well 1-AM-1-AM, cuttings 1674–1677 m. 12 – *Angochitina strigosa* Boumendjel 2002, well SM 2005 (23.02-23.06 m). 13 – *Angochitina* sp. A sensu Grahn and Paris 1992, IGR, well 1-MU-3-AM, core 17 (1386.00–1388.00 m). 14 – *Angochitina* cf. *Sphaerochitina densibaculata* Volkheimer et al. 1986, well 1-AM-1-AM, cuttings 1536 m. 15 – *Angochitina* sp. B, well 1-AM-1-AM, core 35 (1503.80–1508.80 m). 16 – *Angochitina* sp. C, well 1-AM-1-AM, core 37 (1522.00–1524.30 m). 17 – *Angochitina* sp. D, well 1-AM-1-AM, core 37 (1522.00–1524.30 m). 18 – *Angochitina*? sp. sensu Grahn and Paris 1992, IGR, well 1-AM-1-AM, core 42 (1598.40–1599.30 m). 19 – *Angochitina*? sp. sensu Grahn and Paris 1992, well 1-AM-1-AM, core 42 (1598.40–1599.30 m). 20 – *Cingulochitina convexa* (Laufeld 1974), outcrop AM 76. 21 – *Cingulochitina* aff. *C. convexa* (Laufeld 1974), well 1-AM-1-AM, cuttings 1749–1752 m.

→→→

Plate III. Chitinozoans from the Trombetas Group. Scale bars represent 100 µm.
1 – *Cingulochitina convexa* (Laufeld 1974), outcrop AM 75. 2 – *Cingulochitina ervensis* Paris (in Babin et al. 1979), well 1-AM-1-AM, core 35 (1503.80–1508.80 m). 3 – *Cingulochitina* aff. *C. ervensis* Paris (in Babin et al. 1979), well 1-AM-1-AM, core 45 (1602.30–1602.50 m). 4 – *Cingulochitina serrata* (Taugourdeau and Jekhowsky 1960), well 1-AM-1-AM, core 46 (1607.00–1613.00 m). 5 – *Cingulochitina* aff. *C. serrata* (Taugourdeau and Jekhowsky 1960), well 1-AM-1-AM, cuttings 1749–1752 m. 6 – *Cingulochitina wronai* Paris 1984, well SM 1018 (13.57–13.59 m). 7 – *Cingulochitina ervensis* Paris (in Babin et al. 1979), well SM 2004 (45.08–45.12 m). 8 – *Conochitina acuminata* Eisenack 1964, well 2-NO-1-AM, core 14 (1253.60–1256.30 m). 9 – *Conochitina gordonensis* Cramer 1964, well 1-AM-1-AM, core 42 (1598.40–1599.30 m). 10 – *Conochitina tuba* Eisenack 1964, outcrop AM 75. 11 – *Conochitina pachycephala* Eisenack 1964, well 1-AM-1-AM, core 46 (1607.00–1613.00 m). 12 – *Conochitina pachycephala* Eisenack 1964, well 1-AM-1-AM, cuttings 1644–1647 m. 13 – *Conochitina proboscifera* Eisenack 1955, well SM 1017 (21.92–21.97 m). 14 – *Cyathochitina caputoi* Costa 1971, well 1-NO-3-AM, core 29 (3346.20–3347.40 m). 15 – *Cyathochitina* sp. B Paris 1981, well 1-AM-1-AM, cuttings 1749–1752 m. 16 – *Desmochitina densa* Laufeld 1974, well SM 1018 (21.60–21.64 m). 17 – *Desmochitina densa* Laufeld 1974, well 2-NO-1-AM, core 14 (1253.60–1256.30 m). 18 – *Cingulochitina cylindrica* (Taugourdeau and Jekhowsky 1960), well 1-MU-3-AM, core 17 (1386.00–1388.00 m). 19 – *Eisenackitina* cf. *E. bohemica* Eisenack 1934, outcrop Pt.10 (Urubu River; see Grahn and Melo 2003). 20 – *Eisenackitina granulata* Cramer 1964, well 1-AM-1-AM, core 46 (1607.00–1613.00 m). 21 – *Euconochitina iklaensis* Nestor 1984, well SM 1017 (21.92–21.94 m). 22 – *Euconochitina iklaensis* Nestor 1984, well SM 1017 (21.92–21.94 m). 23 – *Euconochitina patula* (Costa 1971), well 1-AM-1-AM, cuttings 1674–1677 m. 24 – *Euconochitina sulcata* (Costa 1971), well 1-NO-3-AM, core 28 (3291.20–3293.00 m). 25 – *Fungochitina kosovensis* Paris 1981, IGR, well 1-AM-1-AM, core 46 (1607.00–1613.00 m). 26 – *Fungochitina* sp. A, well SM 1017 (21.91–21.94 m). 27 – *Linochitina* ex. gr. *erratica* (Eisenack 1931), well SM 1018 (13.09–13.13 m). 28 – *Margachitina catenaria* Obut 1973, well SM 2005 (32.02–32.05 m).

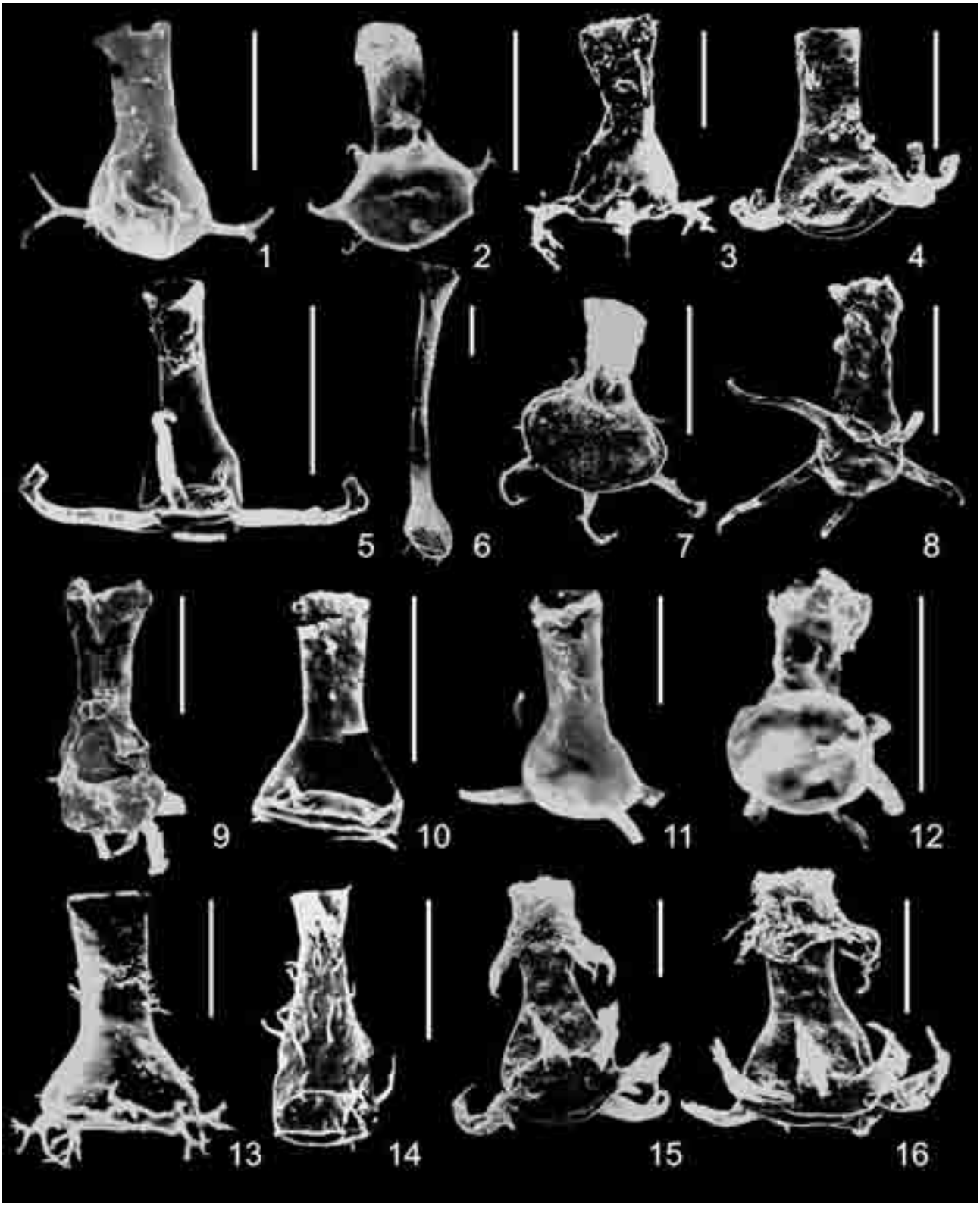
1
2
3
4
5
6
7
8
9
10
11
12
13
14
15
16


1
2
3
4
5
6
7
8
9
10
11
12
13
14
15
16
17
18
19
20
21

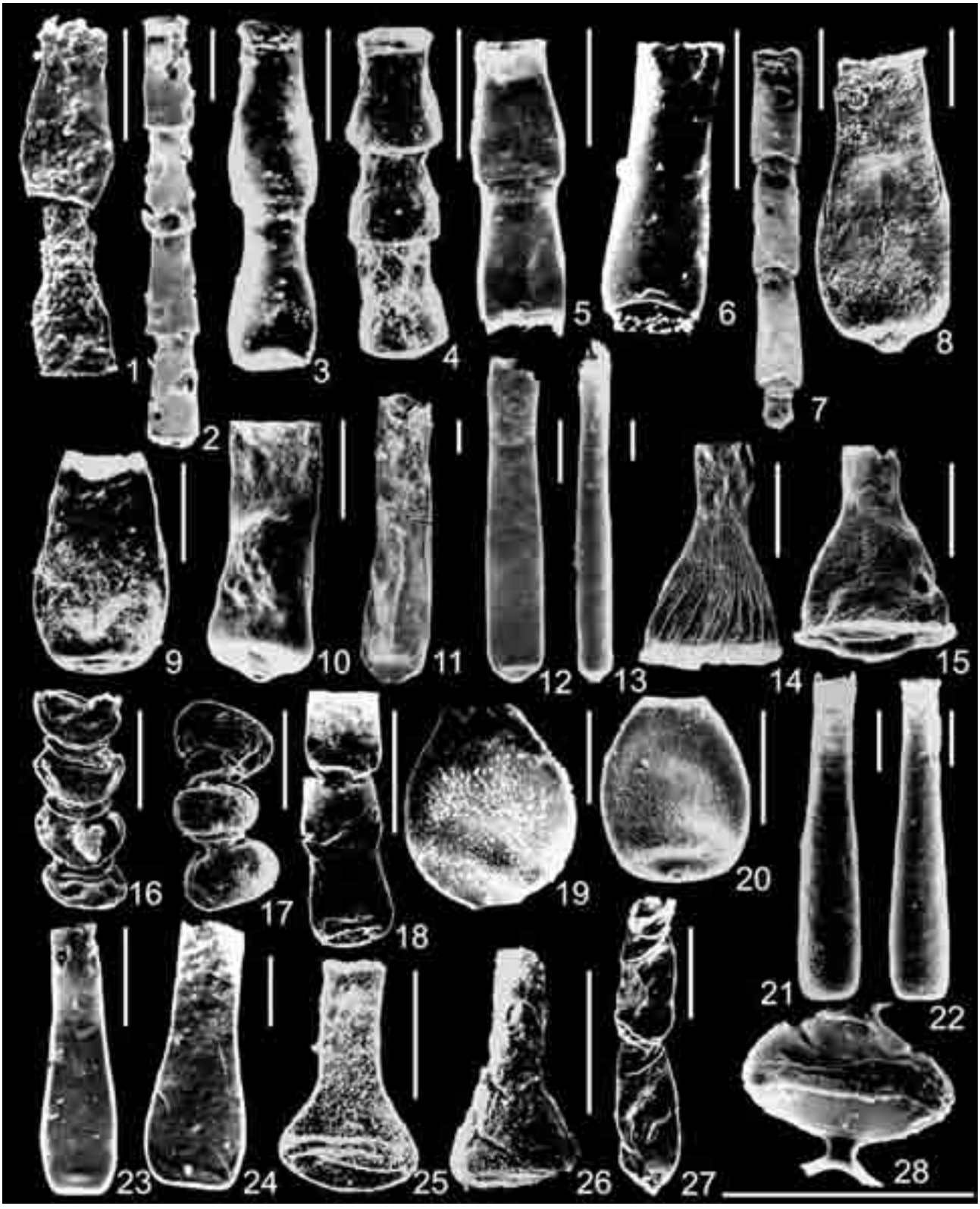
1
2
3
4
5
6
7
8
9
10
11
12
13
14
15
16
17
18
19
20
21
22
23
24
25
26
27
28

→

Plate IV. Chitinozoans from the Trombetas Group. Scale bars represent 100 μm.
1 – *Margachitina margaritana* Eisenack 1968, well 1-AM-1-AM, cuttings 1746–1749 m. 2 – *Margachitina* aff. *M. saretensis* Boumendjel 2002, well SM 1015 (37.45–37.50 m). 3 – *Plectochitina* n. sp. A, well SM 2003 (32.16–32.19 m). 4 – *Pogonochitina djalmai* (Sommer and van Boekel 1965), IGR, outcrop Igarapé da Rainha 4-65-68. 5 – *Pogonochitina djalmai* (Sommer and van Boekel 1965), outcrop AM 76. 6 – *Pogonochitina* cf. *P. djalmai* (Sommer and van Boekel 1965), well 1-MU-3-AM, core 18 (1388.00–1389.00 m). 7 – *Pogonochitina inornata* (Costa 1971), outcrop AM 76. 8 – *Pterochitina megavelata* Boumendjel 2002, well SM 2004 (38.36–38.40 m). 9 – *Pterochitina perivelata* (Eisenack 1937), IGR, well 1-AM-1-AM, core 46 (1607.00–1613.00 m). 10 – *Ramochitina bjornsundquisti* Grahn and Melo 2003, IGR, well 1-AM-1-AM, core 42 (1598.40–1599.30 m). 11 – *Ramochitina* n. sp. cf. *R. devonica* Eisenack 1955, well 1-AM-1-AM, cuttings 1533–1536 m. 12 – *Rhabdochitina*? *conocephala* Eisenack 1938, well SM 1018 (9.48–9.51 m). 13 – *Saharochitina gomphos* Grahn and Melo 2003, well 1-AM-1-AM, cuttings 1677–1680 m (contamination).14 – *Salopochitina monterrosae* (Cramer 1969), well 1-AM-1-AM, cuttings 1746–1749 m. 15 – *Salopochitina* aff. *S. monterrosae* (Cramer 1969), contamination, well SM 1018 (28.53–28.56 m). 16 – *Spinachitina* n. sp. A, well SM 1017 (21.92–21.97 m). 17 – *Sphaerochitina palestinaense* Grahn et al. 2005, well 1-NO-3-AM, core 29 (3346.20–3347.40 m). 18 – *Sphaerochitina palestinaense* Grahn et al. 2005, well SM 1015 (47.73–47.77 m). 19 – *Spinachitina tianguaense* Grahn and Melo 2003, well SM 1047 (1394.70–1347.20 m). 20 – *Tanuchitina* aff. *T. cylindrica* (Taugourdeau and Jekhowsky 1960) *sensu* Boumendjel 1987, well SM 1015 (10.13–10.16 m). 21 – *Tanuchitina elenitae* Cramer 1964, well SM 1048 (13.89–13.92 m). 22 – *Urochitina* n. sp. A, outcrop AM 75. 23 – *Urochitina* n. sp. A, outcrop AM 75. 24 – *Vinnalochitina corinnae* (Jaglin 1986), outcrop AM 74.

→→

Plate V. Chitinozoans from the Trombetas Group. Scale bars represent 100 μm.
1 – *Ancyrochitina primitiva* Eisenack 1964, well SM 1048 (22.08–22.10 m). 2 – Angochitina sp. aff. A. mourai *sensu* Schweineberg 1987, well SM 1015 (10.13–10.16 m). 3 – *Belonechitina* sp. A, well SM 1015 (11.32–11.35 m). 4 – *Belonechitina* sp. A, well 1-CM-2-PA, core 44 (952.00–955.10 m). 5 – *Bursachitina wilhelmi* (Costa 1970), well 2-MU-1-AM, core 28 (1394.70–1397.20 m). 6 – *Bursachitina wilhelmi* (Costa 1970), well SM 1015 (37.45–37.50 m). 7 – *Cyathochitina campanulaeformis* (Eisenack 1931), well 1047 (17.53–17.57 m). 8 – *Conochitina elongata* (Taugourdeau and Jekhowsky 1960), well 1-AM-1-AM, cuttings 1677–1680 m. 9 – *Conochitina edjelensis* (Taugourdeau and Jekhowsky 1960), well 1-AM-1-AM, cuttings 1647–1650 m. 10 – *Pterochitina* sp. A, well SM 1017 (21.92–21.94 m). 11 – *Pterochitina* sp. A, well SM 1047 (15.80–15.89 m). 12 – *Spinachitina* n. sp. A, well SM 1017 (21.92–21.97 m). 13 – *Belonechitina* sp. B, well 1-CM-2-PA, core 44 (952.00–955.10 m). 14 – *Conochitina edjelensis* (Taugourdeau and Jekhowsky 1960), well 1-NO-3-AM, core 29 (3346.20–3347.40 m). 15 – *Conochitina* cf. *C. tuba* Eisenack 1932, well 1-AM-1-AM, cuttings 1647–1650 m. 16 – *Euconochitina cruzi* (Costa 1970), IGR, outcrop Igarapé da Rainha 4-65-68. 17 – *Linochitina* ex. gr. *erratica* (Eisenack 1931), well 1-NO-3-AM, core 29 (3346.20–3347.40 m).

→→→

Plate VI. Chitinozoans from the Trombetas Group. Scale bars represent 100 μm.
1 – *Ancyrochitina* aff. *A. tomentosa* (Taugourdeau and Jekhowsky 1960), well SR 07 (46.45–46.46 m). 2 – *Ancyrochitina* aff. *A. regularis* (Taugourdeau and Jekhowsky 1960), well 1-UI-2-AM, core 9 (774.5 m). 3 – *Ancyrochitina* sp. A sensu Grahn and Paris 1992, well SR 03 (66.66–66.68 m). 4 – *Angochitina elongata* Eisenack 1931, well 1-UI-2-AM, core 10 (780.5 m). 5 – *Angochitina* cf. *A.* elongata Eisenack 1931, well SR 10 (62.79–62.81 m). 6 – *Angochitina* cf. *A. echinata* Eisenack 1931, IGR, outcrop Igarapé da Rainha 4-65-68. 7 – *Angochitina* cf. *A. echinata* Eisenack 1931, well SR 07 (44.26–44.27 m). 8 – *Belonechitina*? *plumula* n. sp., holotype, well SR 10 (64.10–64.12 m). 9 – *Belonechitina*? *plumula* n. sp., well SR 07 (47.51–47.52 m). 10 – *Belonechitina*? *plumula* n. sp., well SR 07 (34.13–34.14 m). 11 – *Belonechitina*? *plumula* n. sp., well SR 07 (37.70–37.71 m). 12 – *Conochitina* cf. *C. acuminata* Eisenack 1959, well SR 07 (34.13–34.14 m). 13 – *Cyathochitina* sp. B, IGR, two specimens in lateral view, outcrop Igarapé Ipiranga 4-65-82. 14 – *Euconochitina* sp. A, well SR 10 (62.79–62.81 m). 15 – *Euconochitina* sp. A, well SR 07 (44.26–44.27 m). 16 – *Lagenochitina* aff. *L. navicula* Taugourdeau and Jekhowsky 1960, IGR, three specimens in lateral view, outcrop Igarapé da Rainha 4-65-68. 17 – *Lagenochitina* aff. *L. navicula* Taugourdeau and Jekhowsky 1960, outcrop Igarapé da Rainha 4-65-68. 18 – *Linochitina penequadrata* n. sp., the lower specimen is the holotype, well SR 01 (95.54–95.56 m).

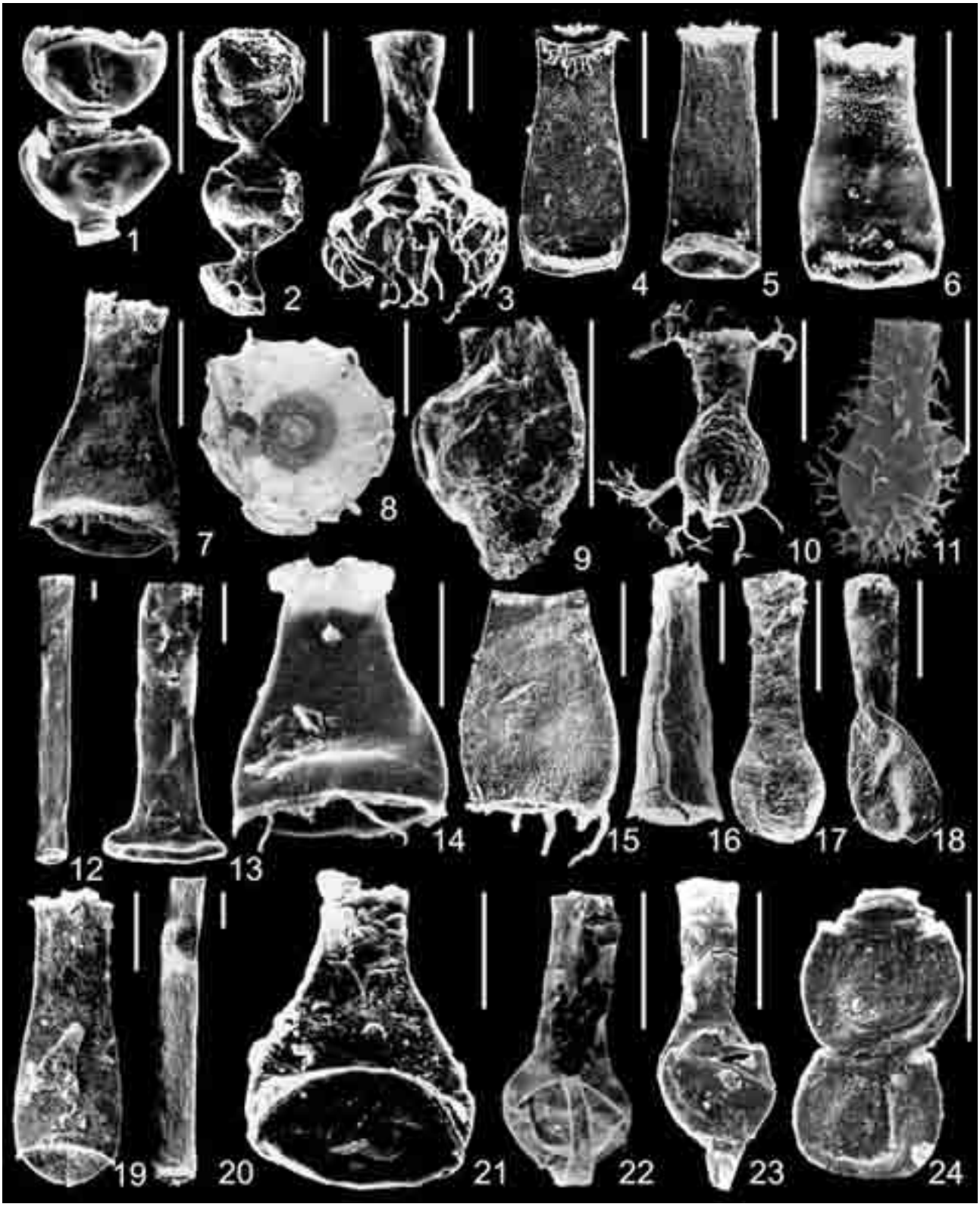
1
2
3
4
5
6
7
8
9
10
11
12
13
14
15
16
17
18
19
20
21
22
23
24

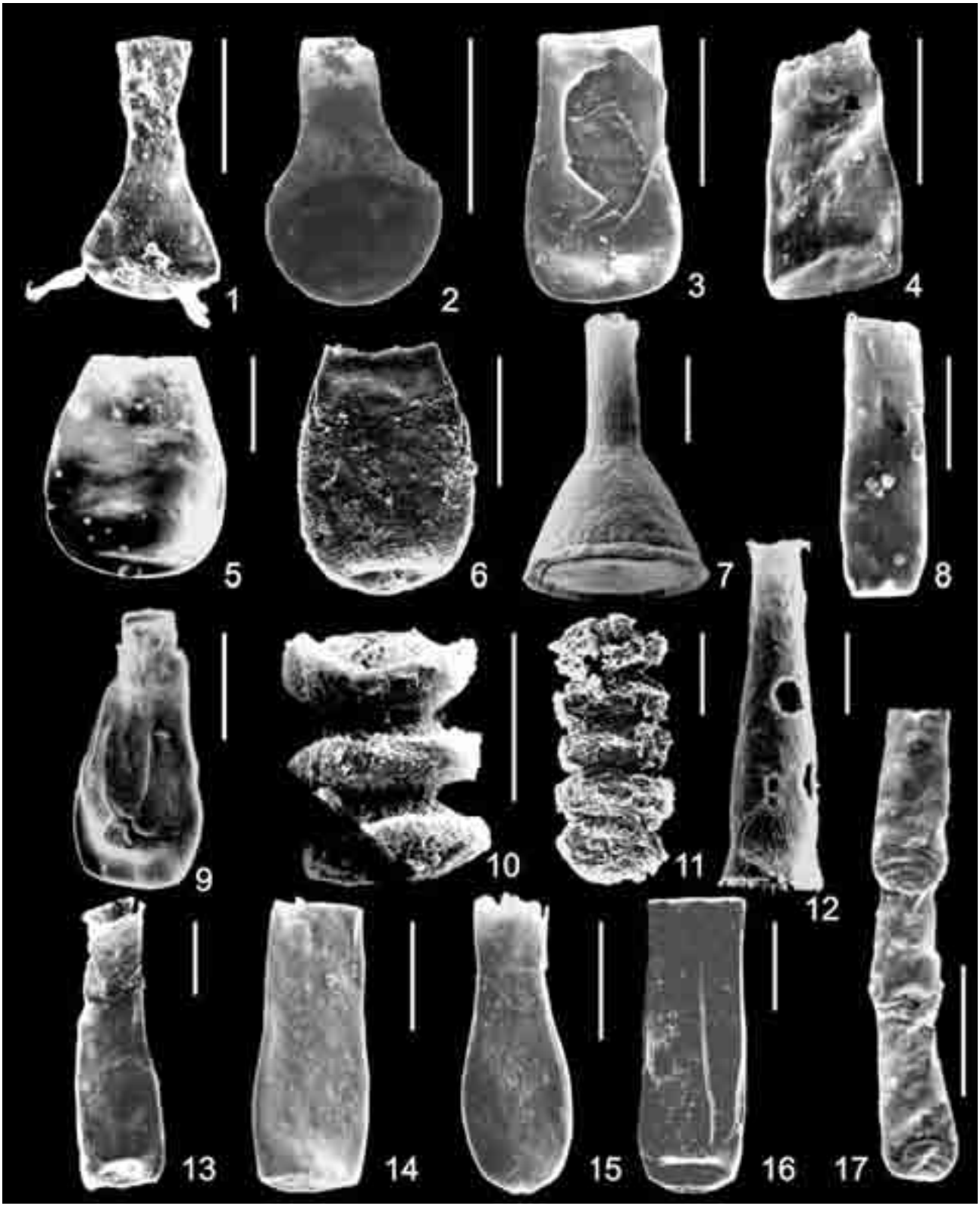
1
2
3
4
5
6
7
8
9
10
11
12
13
14
15
16
17

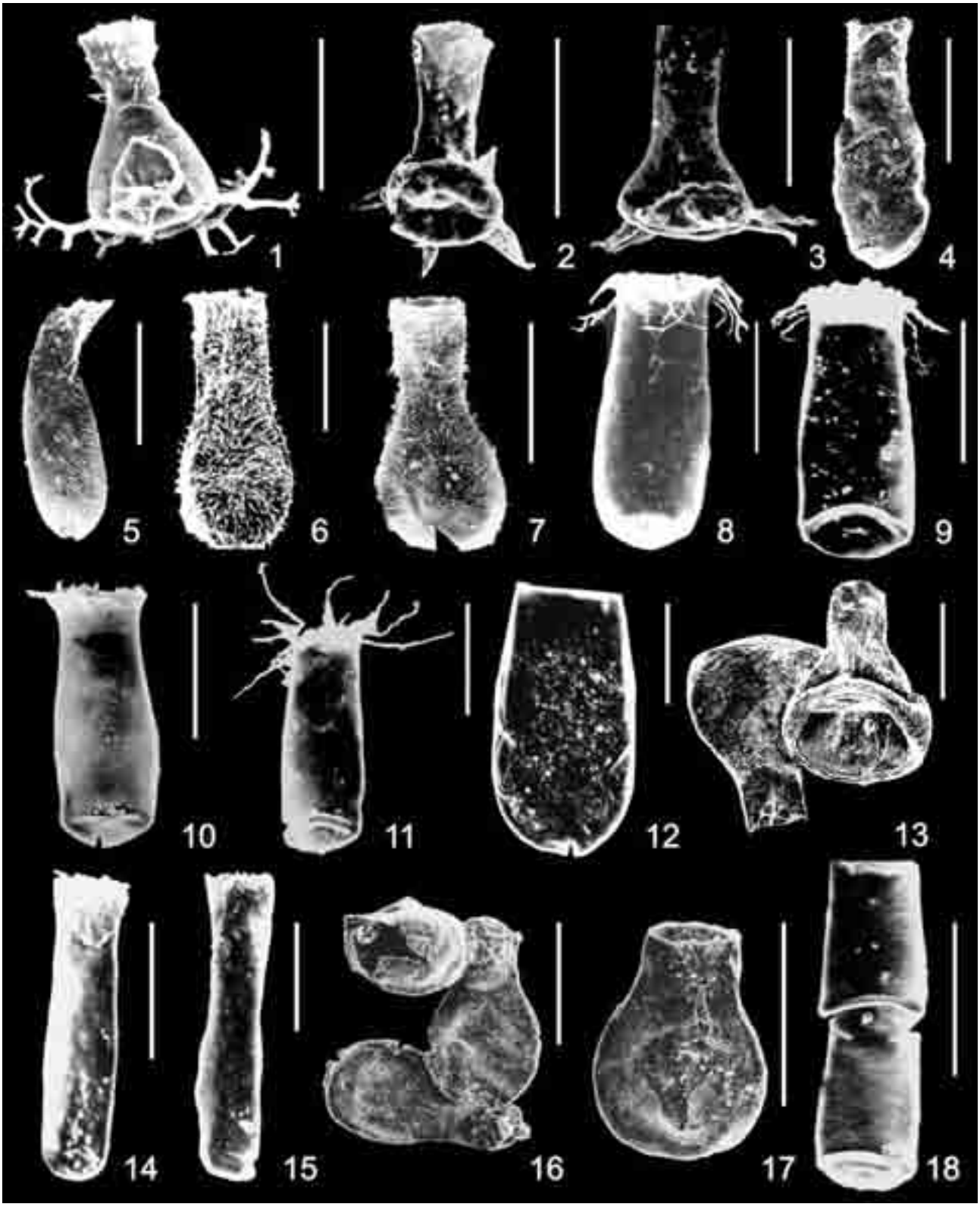
1
2
3
4
5
6
7
8
9
10
11
12
13
14
15
16
17
18

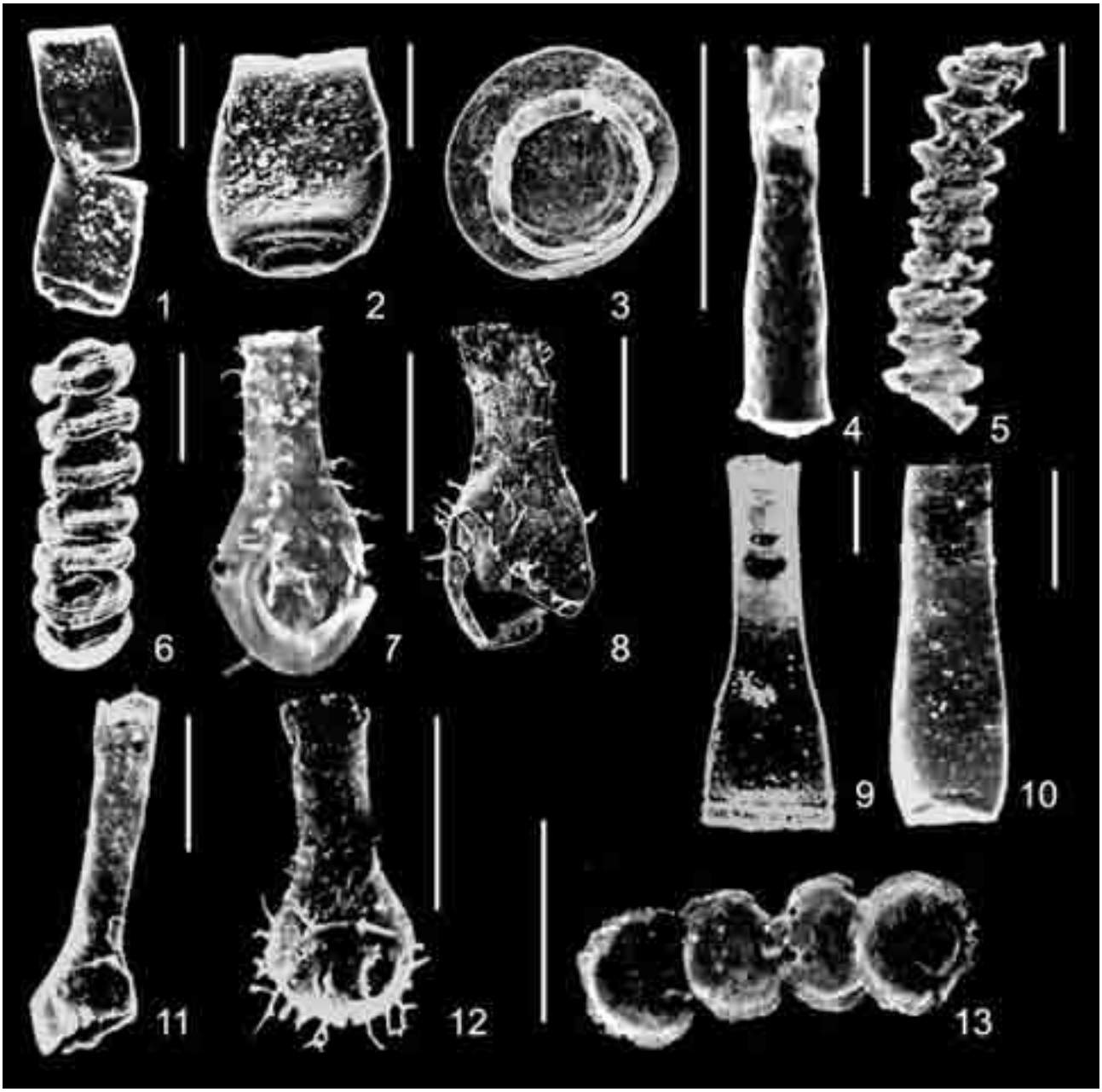

Plate VII. Chitinozoans from the Trombetas Group. Scale bars represent 100 μm.
1 – *Linochitina penequadrata* n. sp., two specimens in lateral view, well SR 07 (47.51–47.52 m). 2 – *Bursachitina wilhelmi* (Costa 1970), well SR 07 (47.51–47.52 m). 3 – *Margachitina*? sp., IGR, outcrop Igarapé da Rainha 4-65-73. 4 – *Pogonochitina* n. sp. A, well SR 01 (100.78–100.80 m). 5 – *Pterochitina* sp. B, well SR 01 (104.57–104.59 m). 6 – *Pterochitina* sp. B, well SR 07 (47.51–47.52 m). 7 – *Ramochitina* sp. sensu Grahn and Paris 1992, well SR 07 (28.30–28.31 m). 8 – *Ramochitina* sp. sensu Grahn and Paris 1992, IGR, outcrop Igarapé da Rainha 4-65-73. 9 – *Sagenachitina* sp. A, well SR 07 (47.51–47.52 m). 10 – *Tanuchitina* sp. A, well SR 07 (35.86–35.87 m). 11 – *Angochitina*? *thadeui* Paris 1981, well SR 10 (57.17–57.19 m). 12 – *Ramochitina illiziensis* Boumendjel 1985, well SR 07 (25.09–25.10 m). 13 – *Pterochitina deichaii* Taugourdeau 1963, chain with four specimens, well SR 03 (71.46–71.48 m).

Bulletin of Geosciences, Vol. 80, No. 4, 277–286, 2005
© Czech Geological Survey, ISSN 1214-1119

The Cinotepeque Range of central El Salvador: Geology, magma origin, and volcanism

Vladislav Rapprich [1, 2] – Petr Hradecký [1]

[1] Czech Geological Survey, Klárov 3, 118 21 Praha 1, Czech Republic. E-mail: rapprich@cgu.cz, hradecky@cgu.cz
[2] Charles University, Faculty of Science, Institute of Petrology and Structural Geology, Albertov 6, 128 43 Praha 2, Czech Republic

Abstract. The Cinotepeque Range is a geological block in NW El Salvador with a complicated volcanic history. Due to the absence of data concerning the geological basement, it remains unclear when volcanic activity started in this zone. The oldest rocks found in the Cinotepeque Range are rhyolitic basal ignimbrites produced from unknown sources. Volcanic activity then proceeded with the silicic pyroclastic products of calderas, the activity of which can be traced up to the Holocene. It is difficult to identify the exact sources of individual pumiceous deposits. Their potential candidates are the three calderas Ilopango Antiguo, Old Coatepeque, and Chilamatal. Later, extrusions of lava sheets of "inferior" and "superior" andesites, interrupted by the deposition of agglomeratic pyroclastic flows, called "Rana", covered the majority of the landscape. The Rana pyroclastic flows were most probably produced from Texistepeque Caldera located between the towns of Santa Ana and Metapán. The youngest volcanism is represented in this area by monogenic volcanic cones. Source vents of these youngest volcanic products are situated mostly on faults that cut and displace all older volcanic rocks. Two different processes of magma origin occurred during the volcanic history of this part of El Salvador: a) during the first stage magma originated by flux melting at a subduction zone; b) during the next stage the decompressional melting in a back-arc environment occurred.

Key words: El Salvador, Cinotepeque Range, volcanostratigraphy, back-arc volcanism, Rana ignimbrite

Introduction

Geological research in El Salvador by the Czech Geological Survey began in the year 2003 with studies of the Conchagua Peninsula (Hradecký et al. 2003) and continued in the areas of Guazapa Volcano and Cinotepeque Range (Hradecký et al. 2004, Fig. 1). There is lack of geological knowledge of the Cinotepeque Range. The geological and volcanological interest in El Salvador is mainly focused on the active volcanic chain associated with the Central American Trench. Some geological observations from El Salvador in general, and of this area in particular, were presented by Weber et al. (1974), Wiesemann (1975), and Wiesemann et al. (1978) as the results of geological mapping of the country on the scale of 1 : 100 000, carried out by a German geological expedition during the years 1967–71.

Geological setting

Cinotepeque Range differs in its volcanic evolution from the geological block of Guazapa. It is situated north of Central Valley and east of Chilamatal Caldera, near the towns of Guazapa, Aguilares, San Juan Opico, San Pablo Tacachico, and Quezaltepeque. The range has been named after the dominant cone, Cinotepeque (665 m a.s.l.), which is situated in its northern part. The Cinotepeque Range is delimited by the Rio Lempa Valley in the north, by the Rio Acelhuate Valley to the east, and the northern boundary fault of the Central Valley depression on the south. On the west it passes continuously into the eastern slopes of the ?Pliocene Chilamatal Caldera. Acelhuate Valley is bound to the major N-S trending subsidence fault (fault *a*, Fig. 2), and is filled with pyroclactic and epiclastic material from the Ilopango Caldera. The Cinotepeque Block is uplifted in relation to the Guazapa Block along this fault.

The chain of volcanic cones of the Cinotepeque Range continues to the south across the northern boundary fault of the Central Valley depression (fault *b*, Fig. 2), to the surroundings of the town of Quezaltepeque. The volcanic edifices of the Cerro El Playón–Grandes Bloques System are situated to the west of Quezaltepeque town. These volcanic

Figure 1. Area of the geological research localized on a map of El Salvador. 1 – main cities, 2 – study area limits, 3 – calderas: a – Coatepeque, b – Ilopango, 4 – volcanoes of the volcanic front: c – Chingo, d – Santa Ana, e – Izalco, f – San Salvador, g – San Vicente, h – Usulutan, i – San Miguel, 5 – extinct volcanoes: k – Guazapa, l – Conchagua.

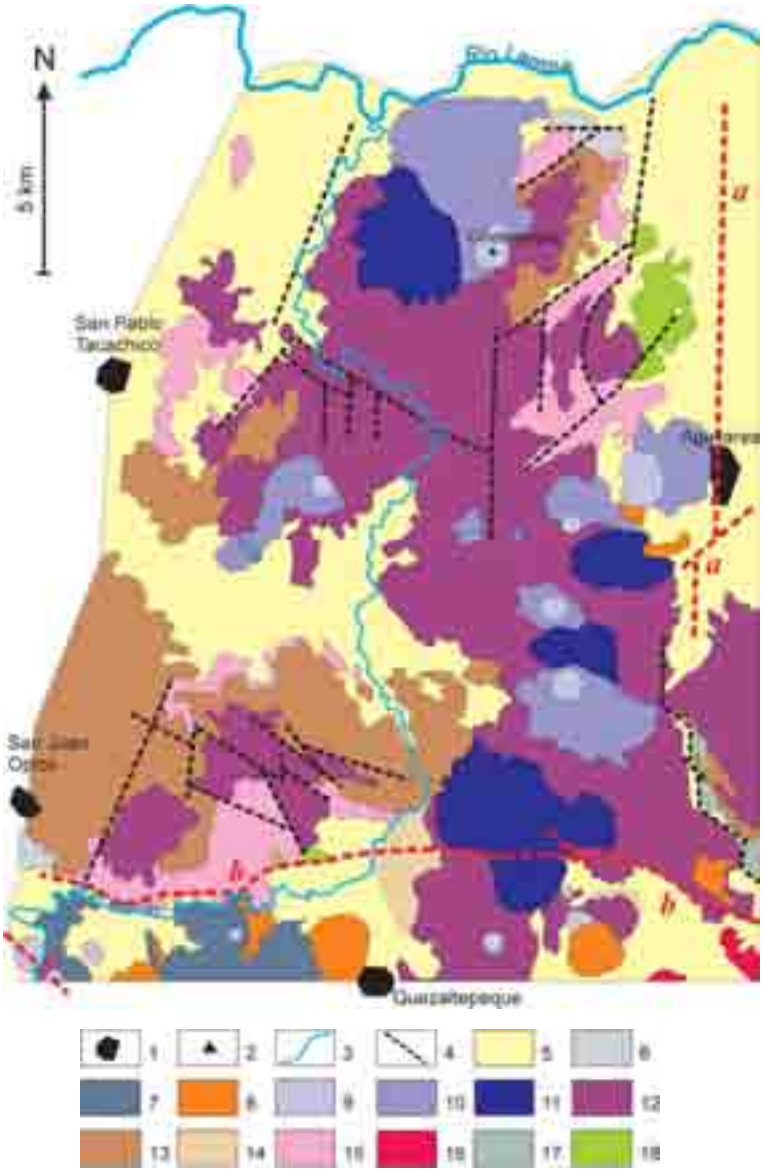

Figure 2. Simplified geological map of the Cinotepeque Range (after Hradecký et al. 2004, adapted): 1 – urban areas, 2 – dominant peak, 3 – river, 4 – major geological fault (those mentioned in text are in red: *a)* Rio Acelhuate valley Fault, *b)* Central Valley northern boundary fault and *c)* Cerro El Playón–Grandes Bloques Fault), 5 – sedimentary rocks (colluvial, fluvial, anthropogenic) almost alternating with Tierra Blanca and products of Coatepeque Caldera, 6 – deposits of debris avalanches, 7 – lavas of the El Playón – Grandes Bloques System, 8 – maar sequence, 9 – cinder cone, 10 – lava produced from cinder cone, 11 – lavas of smaller shield volcanoes and lava cones, 12 – Superior Andesites, 13 – Rana pyroclastic flows, 14 – San Antonio fall out tuffs, 15 – Inferior Andesites, 16 – lavas of Nejapa and Guaycume, 17 – Products of Ilopango antiguo, 18 – Basal Ignimbrites.

bodies are aligned along NW-SE trending fault (fault *c*, Fig. 2), which connects them with the magma chamber of the San Salvador Volcano. For additional information and geochemical data on the San Salvador Volcano and its adventive craters, see Sofield (1998, 2004).

There are neither written nor oral reports on the historical activity of the youngest cones of the Cinotepeque Range, but their juvenile shape and the freshness of their scoria fragments suggest that some are of Holocene age, and might even correspond to the period of historical settlement. Large areas of the southern part of Cinotepeque Range are covered with tuffs of the last Ilopango eruption – Tierra Blanca Jóven (TBJ). Some smaller amounts of Coatepeque tuffs also reach the western part of this range.

Methods

A new geological map on the scale 1 : 50,000 (see a simplified version in the Fig. 2) was compiled during eleven weeks of field work, supported by the study and interpretation of aerial photographs. Detailed mapping enabled the description of the spatial distribution of newly defined units. Documenting the observed sequence of individual members from numerous small-scale outcrops, and some larger ones, allowed us to work out the complex volcanostratigraphy of the Cinotepeque Range.

Laboratory investigations resulted in the petrologic characterization of the rock types. Silicate analyses were completed by roentgen-fluorescence analyses (XRF) for selected trace elements. All the analyses were carried out in the laboratories of the Czech Geological Survey in Prague. Analytical data were recalculated to a water-free base and plotted in diagrams using the GCDkit software (Janoušek et al. 2003). These diagrams were graphically corrected using CorelDraw software. The analytical data were grouped and interpreted according to affiliation with the individual volcanic sequences. The TAS diagram of Le Bas et al. (1986) and the Nb/Y–Zr/TiO_2 diagram of Winchester and Floyd (1977) were used for the classification of the rocks. For description of main geochemical characteristics, AFM (Irvine and Baragar 1971) and SiO_2–K_2O (Peccerillo and Taylor 1976) diagrams were used. Diagrams of MgO–Nb and MgO–Ba/La (after Walker et al. 2000) were constructed for distinguishing the volcanic rocks of the volcanic front ("VF") from those from behind the volcanic front ("BVF").

The volcanostratigraphy of Cinotepeque was evaluated and compared with that of the Conchagua Peninsula (Hradecký et al. 2003) towards understanding which stratigraphical units are of regional distribution, and which are only local.

Results

Geology and stratigraphy

The spatial distributions of the lithological units are shown on the geological map (Fig. 2). Sedimentary and volcanic sequences are arranged chronologically in the legend. For a better understanding of the stratigraphic relations, we draw attention to the proposed stratigraphical column in Fig. 3.

The oldest rock formation observed in the area of Cinotepeque Range is designated as the Basal Ignimbrite (Fig. 2, No. 18). This formation consists of strongly welded, rhyolitic ignimbrites that may be correlated with the Basal Ignimbrites on Zacatillo Island and Conchagua Volcano in eastern El Salvador (Hradecký et al. 2003). The Basal Ignimbrites occur in two separated areas of the Cinotepeque Range. Massive grey ignimbrites with black glassy fiamme (up to 3 cm) and tiny phenocrysts (quartz and feldspars up to 1mm across, clinopyroxene, orthopyroxene, and Fe-Ti oxides – all of X0 μm) occur in the vicinity of Atapasco village (SW margin of Cinotepeque Range – north of the town of Quezaltepeque). This block was named the Atapasco Ignimbrite after the village. Deformed glass shards show no signs of hydratation and/or devitrification (see Fig. 4). On the NE rim of the Cinotepeque Range (NW of Aguilares), a second block of Basal Ignimbrites occurs, called the Delicias Ignimbrite. Stripes or fine laminae of grey and pink or violet colours are typical for these rocks. They are even more compacted and completely devitrified.

Two types of devitrification and secondary modification processes were observed within these originally glass-rich ignimbrites: a) the crystallization of chalcedony spherulites; and b) the recrystalization of silica-rich glass into microcrystalline quartz. These two processes are closely associated (see microphotograph on Fig. 5).

Basal Ignimbrites occur in tectonic relics or in erosional windows. Their original extent and source vents are unknown. They may represent the initial phase of Cenozoic volcanism in El Salvador, which created a basement of younger volcanic products. Stratigraphic comparison with other Central American ignimbrite phases remains unclear, which is why radiometric data are needed.

At some locations slightly welded pumiceous pyroclastic flow deposits, or dacitic Plinian fall-out tuffs, were observed beneath the Inferior Andesites or beneath the Rana flows (Fig. 15). These are believed to be ancient products of the Quaternary Ilopango or Coatepeque Calderas or the ?Pliocene Chilamatal Caldera. Lack of data on these ancient pumiceous deposits and bad exposure prevents these rocks from being more clearly distinguished, and the matching of individual deposits to their respective sources.

Paleobotanical findings from some silicic and intermediate pyroclastic deposits north and east of Guazapa probably correspond to the Chalatenango Formation (dated as Upper Miocene, Kvaček in Hradecký et al. 2004).

Extensive effusions of andesitic lavas represent a significant proportion of the Cinotepeque basement. Sheet effusions were divided into two groups, which differ in stratigraphic position and chemical composition. A similar subdivision was used during the 2003 studies in eastern El Salvador, and is reliably anchored in the Neogene volcanic stratigraphy of Central Nicaragua (Hradecký et al. 2003, 2004). Both of these individual groups comprise thick and laterally wide spread sheet-like lava fields. The older andesites, designated as "inferior" are of more acidic, andesitic s.s. composition. The Inferior Andesites were covered by thick younger volcanics and currently occur in tectonically or erosionally exposed margins of the Cinotepeque Block.

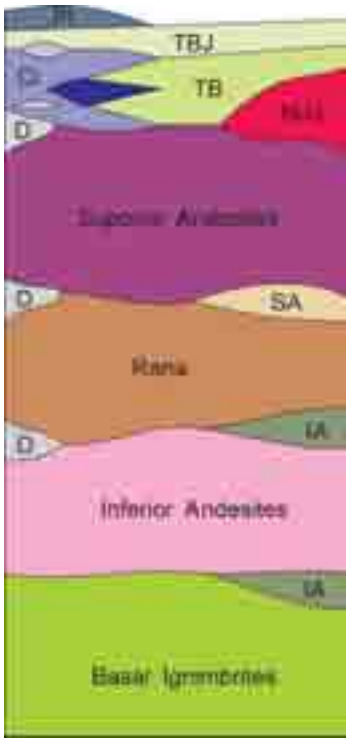

Figure 3. Stratigraphic column of the Cinotepeque Range based on field observations (no borehole data are available). The stratigraphic scheme is not in scale (maximum thickness of the Rana deposits in the Cinotepeque Range reaches 100 m, as does the thickness of the Superior Andesites, whereas thicknesses of young basaltic edifices vary from several meters to tens of metres). Thicknesses of Inferior Andesites, Ilopango antiguo or Basal Ignimbrites remain unknown. Colours correspond to the geological map on the Fig 2. Pl – lavas and scorias of El Playón – Grandes Bloques system, Ci – products of the Cinotepeque monogenic cones system, TBJ – tuffs and epiclastic material of Tierra Blanca Joven, TB – pyroclastic flow and fall-out deposits of Tierra Blanca

Andesitic agglomeratic "block and ash" pyroclastic flows, called the Rana deposits, were probably produced from the Texistepeque Caldera, which is located 6 km north of Santa Ana city. These deposits consist of moderately welded, poorly sorted andesitic agglomerates. Juvenile vesiculated andesitic fragments mostly of 8–12 cm across (sometimes up to 30 cm) are enclosed within a matrix of ash and small-scale lithics. The brown-violet colour corresponds well to the intermediate composition of this material. Weathering of these deposits produces surfaces that are reminiscent of the skin of toad (rana = toad in Spanish). Characteristic "warts" of more resistant andesitic fragments were exposed by small-scale selective removal of finer matrix. Rock fragments can be concentrated in the basal flow units (Fig. 14). On many outcrops, deposits of associated ground-surge and ash-cloud-surge were observed (see Fig. 6). The Rana deposits consist of multiple flow units from a series of eruptions. Short interruptions in activity of the Texistepeque Caldera were documented by thin intercalations of fluvial sediments or local thin lava flows between the individual flow units of the entire sequence. The complete thickness of the Rana sequence reaches about 100 m in the region of Cinotepeque Range. Agglomerates often built up vertical rock walls (Fig. 7). In some localities these steeply dipping cliffs were unstable and prone to collapse, and thus debris flows were triggered.

Figure 4. Microphotograph of the Atapasco Ignimbrite. Note the deformed glass-shards curving around rigid phenocrysts. Real size of the picture is 1.6 mm.

Figure 5. Microphotograph of the Delicias Ignimbrite. Two types of devitrification (spherulites and micro-quartz) alternate in very small distances. Real size of the picture is 3 mm.

Figure 6. Block of the Rana deposits – well developed ash-cloud surge structure and coarse units. Real scale of the block being showed is 0.8 x 1.2 m. (Photo by Petr Hradecký)

Similar phenomena can be seen also in the marginal parts of deeply eroded Texistepeque Caldera.

Younger lava sheets of basaltic to basaltic andesite composition covered the Rana pyroclastic flows. They are designated the Superior Andesites by the present authors because of their stratigraphic position. Their spatial extent and degree of weathering are quite similar to those of the inferior andesites, which sometimes complicates discriminating between them. However, they are easily distinguished at outcrops that show their relations to the Rana deposits (the Inferior Andesites underlying the Rana deposits, while the Superior Andesites overlie the Rana). Such local observations had to be applied also to the rest of the area.

Lavas of the Superior Andesites were produced from numerous sources. Later volcanic and tectonic activity destroyed the original sources or vents. Effusions of these more basic lavas began when extensional activity in the BVF environment occurred in this region. The decompressional melting of an uplifted mantle slab is demonstrated by the chemical composition of these lavas (discussed below). The Superior Andesites in central El Salvador are the oldest rocks showing the BVF character. Future radiometric dating will define the time span during which the extension and mantle slab emplacement started.

The youngest, freshest, and morphologically most distinctive volcanic forms in the Cinotepeque Range are the ?Upper Pleistocene to Holocene monogenic cones. They were subdivided into two groups according to their geotectonic position, composition, and magmatic affinity.

A NW-SE trending fault is located on the SW margin of the Cinotepeque Range, west of Quezaltepeque city and south of San Juan Opico (fault *b* in Fig. 2). This fault runs southeastward to the center of the San Salvador Volcano. Several scoria cones and maars located on this fault erupted with a more differentiated magma (basaltic andesite) than became current in the cases of such monogenic cones. Their chemical composition (sample No. 81 in this paper, see also Sofield 1998) corresponds to that of the lavas of the San Salvador Volcano. This magmatic system, known as the Cerro El Playón–Grandes Bloques System, is therefore related to the magma chamber of San Salvador. Magmatism associated with this fault is still active. The last strombolian eruptions associated with lava effusions (Cerro El Playón) occurred in the years 1575 and 1658. This system differs in more differentiated composition and melt origin (flux melting at subduction zone, discussed below) from the Cinotepeque System.

Monogenic cones of the Cinotepeque System are located on several N-S and NW-SE trending faults. This relatively young local volcanism of primitive magma is represented in several types of volcanic forms. Aside from common cinder cones and maars, some smaller shield volcanoes and lava cones were also observed. The direction of this system of faults is oblique to the Salvadorian part of the Central American Trench, and they are of extensional character (Baratoux in Hradecký et al. 2004). The chemistry of the lavas and scorias of the Cinotepeque System shows the origin of their magmas by decompressional melting in the BVF environment. There is no report on the historical activity of the cones of the Cinotepeque

Range, but their well-preserved shape and the freshness of their scoria should indicate a very young (probably Holocene) age. Unfortunately, no carbonized wood to be used for ^{14}C dating was found within deposits of these volcanoes. The southern parts of the Cinotepeque Range are often covered by distal fall-outs of the last Ilopango eruption.

Volcanism

As the origin and composition of the magmas erupted in the Cinotepeque were changing during the history of this region, the eruption style likewise varied. After voluminous, silicic, explosive activity from large calderas, the effusion of the inferior andesites took place. The sources of the Basal Ignimbrites and the Inferior Andesites are no longer preserved.

The newly described Rana volcanic sequence may have been produced by multiple eruptions of the Texistepeque Caldera. The character of these pyroclastic flows suggests that they resulted from lava dome explosions or the over boiling of gas-rich magma from andesitic-caldera faults.

The effusive activity of the Superior Andesites was probably similar to that of the inferior ones. Basic to intermediate lavas (basalt to basaltic andesite) accumulated to thicknesses of several tens to one hundred metres.

Small-scale local forms represent volcanism of the last eruptive episode of the Cinotepque Range. Common cinder cones are accompanied by several maars, some smaller shield volcanoes, and by lava cones. In some cases, selective erosion has exposed one dyke and two isometric compact vent fillings. Successions of phreatomagmatic and Strombolian/Hawaiian activity were observed at many of these occurrences. A list of the individual younger volcanic forms (some of them newly observed) is presented in Table 1.

Five well-preserved maar structures have been documented, another three represent erosional remnants. Phreatomagmatic activity is evinced in the base surge deposits, and some bigger fragments of fall origin are preserved with bomb-sags structures (Fig. 9). Most of maar structures are situated in the southern part of the studied area.

Several cinder cones have been located in the area, some of which are situated close to the maar craters and represent the continued dry activity of the magma chambers. Some cones are associated with small lava flows. Both scoria and lava show the primitive basaltic composition. Several forms of lava without pyroclastic deposits were documented in the area. In the geological map in Fig. 2, we have tried to differentiate between the lavas of the lava cones and those associated with scoria cones, according to the differences in activity style. The term "lava cone" is used for the smaller-scale effusive vents of slightly higher viscosity lavas that do not create flat shields, but elevated volcanic edifices of conical form. Their higher viscosity was probably due to lower temperature and higher degree of crystallinity, as the chemical composition is very similar to the lavas of the cinder cones and shield volcano. Usage of this term distinguishes these forms and their activity from the more explosive activity of cinder cones and

Figure 7. High cliffs of Rana pyroclastic flow deposits on the NE margin of the Cinotepeque Range. (Photo by Vladislav Rapprich)

Figure 8. Cinotepeque scoria cone. Prominent, fresh-looking volcanic body. (Photo by Petr Hradecký)

the lower viscosity of lavas erupted from shield volcanoes. Lava cones are current in the Guazapa Block, but scarce in the Cinotepeque area. Their lavas have a basaltic to basaltic andesite composition.

In the Cinotepeque area one shield volcano was identified, named Ojo del Agua (points 50, 52). It is probably of the same age as the young monogenic volcanic forms around it. Its lavas are less viscous compared with those of the cinder cones. Most of the lavas flowed northwards. The volcano is situated on the fault that delimits the regional Central Graben (fault *b* in Fig. 2). The fault was reactivated after the volcanic activity, and cut the volcanic edifice into two parts. The southern part subsided some 50 metres.

In some cases erosion has destroyed the original volcanic surfaces, and only vent-filling rock remained from the former volcano. Such a case was documented as a point 431 at the small hill of Cantón Segura (467 m a.s.l.), which is situated 6 km SW of Aguilares. Its vent consists of massive basalt. Another small vent-filling body lies in Caserio Los Anzora (482 m a.s.l.), 7 km west of Aguilares, with the associated small lava flow (point 432). Loma Chata, which is at a low elevation 5 km SE of San Pablo Tacachico, is a dyke surrounded by an old volcanic edifice. In the south, the youngest TBJ ashes cover most of these monogenic forms.

Table 1. List of young monogenic volcanic forms of the Cerro El Playón–Grandes Bloques ("P-GB" in table) and the Cinotepeque ("CINO" in table) systems. CC – cinder cone, LC – lava cone, SV – shield volcano, p. – documentation point.

Name	Type	System	Location	Description
Loma Caldera	maar	P-GB	S of small volcano Laguna Caldera	ring of maar deposits, partly covered by strombolian scoria of Laguna Caldera
Caldera Escondida (Sofield 1998)	maar	P-GB?	1 km SE of Cerro Las Viboras	greater part of maar structure is covered by Las Flores lava
Pueblo Viejo (Hradecký et al. 2004)	maar	P-GB?	W of Pueblo Viejo village (p. 87 in Hradecký et al. 2004), 5 km W of Quezaltepeque	base surge and fall-out deposits were documented in the relic of maar. Maar has been destroyed by the Sucio river and its tributaries and partly buried by lavas of El Playón (1658) and La Primavera.
Lava Caldera (Sofield 1998)	maar	??	2.5 km WNW of Quetzaltepeque (p. 71 in Hradecký et al. 2004)	most of the structure is filled by El Playón lavas. Small scoria cone rests in the bottom of the crater.
Quetzaltepeque	maar	??	W limits of town of Quetzaltepeque	tuff ring is composed of basaltic surge and falls with fragments up to 2–5–20 cm in diameter
La Tabla (Hradecký et al. 2004)	maar + CC	CINO	5 km E of Quetzaltepeque (p. 24, 67 and 68 in Hradecký et al. 2004)	surge and fall deposits are mostly covered by the TBJ Ilopango ashes. Continuing explosive activity formed small Cerro La Tabla scoria cone in N limits of maar crater.
Acelhuate (Hradecký et al. 2004 and Wiesemann et al. 1978)	maar	CINO	7.5 km ENE of Quetzaltepeque (p. 62 and 407 in Hradecký et al. 2004)	structure is cut by the Acelhuate River. This maar is situated upon the N-S trending fault. Faulting caused the lithologic differences in W and E crater walls.
La Esperanza (Hradecký et al. 2004)	maar	CINO	1.5 km SW of Aguilares (p. 502 in Hradecký et al. 2004)	two relics of former maar structure: one of them crops out beneath the Cerro Chino scorias, another forms the half ring elevation in the S. Badly sorted fall deposits reveal the bomb-sag structures. W part of the maar is covered by lavas of Cerro Las Tunas volcano and by colluvial deposits.
Laguna Caldera	CC	P-GB	3 km S of San Juan Opico (p. and analyses 23 and 74 in Sofield 1998)	cone built after the phreatic activity of the volcano which destroyed the Joya de Cerén Mayan settlement
Laguna Ciega (Sofield 1998)	CC	P-GB	0.5 km SE of Laguna Caldera (p. and analyses 67 in Sofield 1998)	small cinder cone
Las Viboras (Sofield 1998)	CC	P-GB?	1.5 km E of Laguna Caldera (p. 89 in Hradecký et al. 2004)	small cinder cone
El Pollo (Hradecký et al. 2004)	CC	??	3 km WNW of Quetzaltepeque (p. 86 in Hradecký et al. 2004)	low scoria cone inside the Lava Caldera maar
Buenos Aires (Hradecký et al. 2004)	CC	CINO	2.5 km NE of Quetzaltepeque (p. 21 in Hradecký et al. 2004)	scoria cone located upon the elevated tectonic block composed of superior andesite
Mulunga (Hradecký et al. 2004)	CC	CINO	5 km ENE of Quetzaltepeque (p. 25 in Hradecký et al. 2004)	small cinder cone situated on the NW-SE trending fault
Cerro Redondo (Hradecký et al. 2004)	CC	CINO	1 km S of Tutultepeque, 6 km SSW of Aguilares (p. 11 in Hradecký et al. 2004)	cinder cone with basaltic lava erupted to south
Cerro Segura (Hradecký et al. 2004)	CC	CINO	5 km SW of Aguilares (p. 499 in Hradecký et al. 2004)	deposits of Strombolian and Hawaiian activity were accompanied by lava effusion. The cone is cut by dextral fault NE-SW which was also a conduit of volcanic eruption.
Santa Rita (Hradecký et al. 2004)	CC	CINO	4 km WSW of Aguilares (p. 406 in Hradecký et al. 2004)	cinder cone and basaltic lava flow
Cerro Chino	CC	CINO	1.2 km W of Aguilares (p. 416, 417 and 419 in Hradecký et al. 2004)	one of the largest cinder cones in the area with 1.2 km^2 of area covered by edifice
San Augustín (Hradecký et al. 2004)	CC	CINO	6 km SE of San Pablo Tacachico (p. 386 in Hradecký et al. 2004)	cinder cone with associated basaltic lava flow (point 387)
Cerro Cinotepeque	CC	CINO	6 km NW of Aguilares (p. 404 in Hradecký et al. 2004)	cone with very fresh morphology almost without vegetation. Crater is well preserved, opened towards the W. Long lava flow (p. 436) reaches up to 4 km of distance from the cone and covers wide area. Another, small flow was produced towards the S.
Santa Rosa (Hradecký et al. 2004)	CC	CINO	1.5 km NE of San Matias, 5 km E of San Juan Opico (p. 411 in Hradecký et al. 2004)	relic of cinder cone, destroyed by erosion, situated in the Santa Rosa village. It is situated upon the NW-SE trending normal fault; part NE of cone down-tilted several tens of meters. This faulting started the cone destruction.

Table 1, continued

Name	Type	System	Location	Description
Las Tunas (Hradecký et al. 2004)	LC	CINO	3 km SW of Aguilares	cone formed of basaltic lavas
Picado (Hradecký et al. 2004)	LC	CINO	5 km SW of Aguilares	cone formed of basaltic lavas
Los Dos Cerros (Hradecký et al. 2004)	LC	CINO	6 km NE of San Pablo Tacachico	cone formed of basaltic lavas
Ojo del Agua (Hradecký et al. 2004)	SV	CINO	4 km NE of Quetzaltepeque (p. 50 and 52 in Hradecký et al. 2004)	shield volcano cut by N marginal fault of Central Graben

Chemical composition and magma origin

The results of major element and selected trace element analyses are presented in Table 2. Classification was based on comparison of the TAS diagram (Le Bas et al. 1986 – see Fig. 10) with the Nb/Y–Zr/TiO_2 diagram (Winchester and Floyd 1977 – see Fig. 11). The application of these two diagrams was necessary due to content of water in the samples of pyroclastic materials. A wide spectrum of compositions is shown in these diagrams. The oldest rock, represented by the Atapasco Basal Ignimbrite, is of rhyodacitic or rhyolitic composition, in agreement with macroscopic and microscopic observations.

Samples of the Rana pyroclastic flow deposits have been affected by weathering (total water content is over 17 %), and are strongly depleted in alkalis (see Fig. 10). This is why the Nb/Y–Zr/TiO_2 diagram was also used to classify this rock. This diagram showing the proportions of immobile elements confirmed the andesitic composition deduced from the TAS diagram and macroscopic observations.

The difference between the Inferior and Superior Andesites is very similar to that between equivalent rocks in eastern El Salvador. Similarly, in the Conchagua Peninsula and in central El Salvador the Inferior Andesites are more evolved and silicic than the Superior ones (see Fig. 10 for comparison with rocks from eastern El Salvador).

The most basic rocks are represented in lavas and scorias of young monogenic cones. We draw the attention to the relatively wide compositional range of the magmas of these monogenic cones, where no differentiation could be made. The lavas of Cerro El Playón have a more evolved composition (basaltic andesite) in comparison to the Cinotepeque System. This can be explained by a possible connection between the cones of the Cerro El Playón–Grandes Bloques System and the more evolved magmatic system of San Salvador Volcano. On the other hand, the products of the Cinotepeque System are of a more primitive character (see Fig. 10).

Walker et al. (2000) presented numerous diagrams to demonstrate differences between VF and BVF volcanites, of which their MgO-Nb and MgO-Ba/La diagrams are of the most value. In their other diagrams, the distinction between both defined groups is unclear, while their main discriminating factor, "distance from volcanic front", is doubtful. In the MgO–Nb and MgO–Ba/La diagrams (Figs 12 and 13) two clusters of data are distinctive. High MgO/high Nb values characterize rocks of BVF, whereas

Figure 9. Balistic deposits of phreato-magmatic eruption with bomb-sag structures beneath larger fragments. Maar Rio La Esperanza 1.5 km SW of Aguilares. (Photo by Vladislav Rapprich)

low MgO/low Nb values characterize rocks of VF in the MgO–Nb diagram. In the MgO–Ba/La diagram, high MgO values are accompanied with low Ba/La in the case of BVF volcanics, whereas high Ba/La values accompany the low MgO values in the VF volcanics. The clustering of values and their interpretation are the same in these two diagrams.

Analyses of the Inferior Andesites, Rana deposits, Basal Ignimbrites, and lava 1575 from Cerro El Playón cluster in the field of VF volcanics. Therefore, it can be supposed that the magmas of all these sequences were produced by flux melting at a subduction zone. Concerning Cerro El Playón lava 1575, our analyses evince a connection with the magmatic system of the San Salvador Volcano, and a distinction of the Cerro El Playón–Grandes Bloques System from the Cinotepeque System.

BVF rocks are characterized by higher MgO and Nb, and lower Ba/La values, which can be interpreted as a result of decompressional melting in the BVF environment (Walker et al. 2000). Two samples of BVF in the VF cluster (one of lavas of Cinotepeque System, and one sample of the Superior Andesites from eastern El Salvador) could be wrongly classified in the field.

Discussion

Field work together with laboratory investigation from the area of the Cinotepeque Range allow the volcanostratigraphic comparison of central El Salvador with that of eastern El Salvador. The main point deduced from this compa-

Table 2. Chemical analyses of the volcanic rocks of Cinotepeque range.

Sample Sequence	1	41	81	336	416	427	432	436	438	521	617
oxides (wt.%)	Inferior Andes.	Cinot. sys.	Playón 1575	Basal Ignim.	Cinot. sys.	Cinot. sys.	Cinot. sys.	Cinot. sys.	Cinot. sys.	Super. Andes.	Rana
SiO_2	58.03	52.81	55.48	67.76	49.68	53.7	52.85	51.04	51.33	52.38	49.51
TiO_2	0.78	1.02	1.31	0.55	0.92	0.99	0.97	1.13	1.08	0.92	1.1
Al_2O_3	17.41	17.32	15.1	14.56	17.38	19.19	17.03	17.82	17.66	17	19.82
Fe_2O_3	4.17	3.1	4.17	2.06	4.34	7.14	3.52	2.4	3.72	3.18	7.92
FeO	1.52	5.86	6.96	0.57	5.48	1.27	4.97	6.57	5.12	5.15	0.03
MgO	1.91	4.86	2.95	0.47	6.45	1.72	5.71	5.99	5.93	5.64	1.02
MnO	0.133	0.181	0.273	0.106	0.199	0.178	0.178	0.191	0.175	0.168	0.107
CaO	6.03	8.3	6.9	1.68	10.22	7.57	8.54	9.28	8.62	8.88	1.43
Na_2O	4.03	3.26	3.91	3.97	2.68	3.87	3.31	3.36	3.48	3.24	0.77
K_2O	1.6	1.45	1.75	4.01	0.68	1.52	1.3	1.07	1.21	1.26	0.72
P_2O_5	0.244	0.388	0.338	0.084	0.189	0.24	0.275	0.27	0.314	0.282	0.044
H_2O^+	2.38	0.9	0.31	3.32	0.84	1.3	0.67	0.44	0.42	0.95	8.96
H_2O^-	1.3	0.22	0.08	0.43	0.26	0.68	0.31	0.21	0.22	0.47	8.11
Total	99.54	99.67	99,53	99,57	99,32	99,37	99,63	99,77	99,28	99,52	99,54
Minor and trace elements (ppm)											
Cr	3	72	9	*	149	6	112	71	107	109	179
Ni	*	32	*	6	56	5	42	35	44	36	50
Cu	17	59	127	7	79	47	80	80	50	73	105
Zn	81	85	116	70	76	70	82	70	73	79	95
As	6	4	6	8	4	4	3	6	5	5	6
Rb	45	32	50	95	25	44	31	26	28	29	39
Sr	437	506	346	179	473	492	425	534	507	450	133
Zr	165	185	162	251	65	138	160	128	157	162	145
Nb	3	6	2	5	3	4	7	9	7	6	5
Pb	5	5	9	7		3	9	*	*	2	*
Y	22.3	38.7	37.6	50.8	20	46.8	37.1	19.4	21.5	21.5	29.6
La	12	20.5	11.5	24.5	7.1	20.9	16.9	10.5	13.3	14.4	17.4
Ba	689.7	600.1	707.6	1316.7	358.3	886.7	519.5	376.2	447.9	1289.8	824

Inferior Andes. – Inferior Andesites, Cinot. sys. – lavas and scorias of monogenic cones of the Cinotepeque system, Basal Ignim. – Basal Ignimbrites, Super. Andes. – Superior Andesites, * – not detected.

rison is that not all the earlier and/or newly defined volcanostratigraphic units can be applied regionally. On the other hand, some stratigraphic units are of regional validity. The ages could be estimated by stratigraphic relationships and the correlation of ages known from of the generally similar sequences in Nicaragua and/or Honduras. Radiometric data are needed for the better determination of the volcanostratigraphy of El Salvador.

In the development of the Cinotepeque Range, BVF volcanism played an important role. The composition of the BVF volcanics is similar to the basalts of volcanologically identical areas in Guatemala and Honduras described by Walker et al. (2000). The hypothesis of decompressional melting of a mantle slab emplaced in the space vacated after the breaking-off of a subducted slab is also accepted for the case of central El Salvador. The break-off of a subducted slab was well documented in lower crust/mantle tomography of Central America published by Rogers et al. (2002). As shown above, this petrogenic process can be applied for some older sequences as well. Magmas of the Superior Andesites were produced also by decompressional melting in the BVF environment. Moreover, the Superior Andesites are widely distributed in El Salvador behind the active volcanic chain, thus extensional stress and decompressional melting took place, and perhaps still occurs, along entire El Salvador. Because the exact age of the Superior Andesites remains unknown, it is impossible to say when the processes of decompressional melting in the Salvadorian part of BVF zone began.

Conclusion

Rock composition and stratigraphy of the Cinotepeque Range is comparable with those of eastern El Salvador

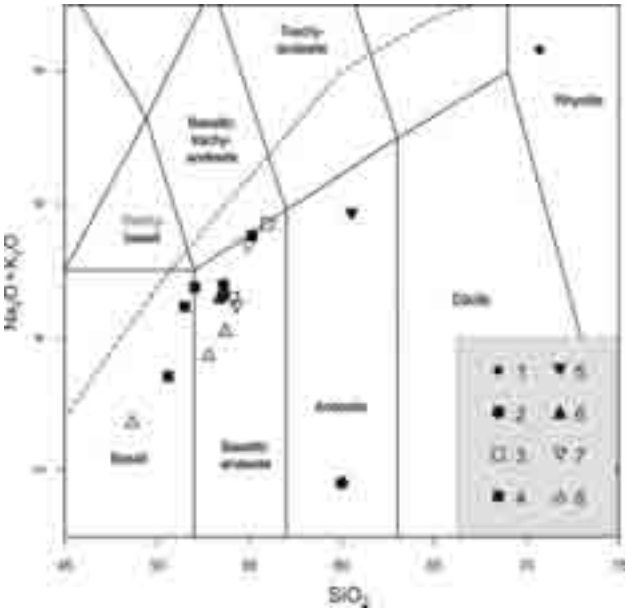

Figure 10. Detail of TAS diagram (Le Bas et al. 1986) with rocks of Cinotepeque Range. For comparison data of Inferior and Superior Andesites from Conchagua Peninsula (E part of El Salvador – from Hradecký et al. 2003) were also plotted in this diagram.
Key: 1 – Basal Ignimbrite, 2 – Rana, 3 – Cerro El Playón lava from 1575, 4 – products of monogenic cones of the Cinotepeque system, 5 – Inferior Andesites, 6 – Superior Andesites, 7 – Inferior Andesites from eastern El Salvador (data from Hradecký et al. 2003), 8 – Superior Andesite from eastern El Salvador (data from Hradecký et al. 2003). Loss of alkalies and thus abnormal position of Rana (solid circle) in the TAS diagram was caused by weathering of clastic and porous Rana material. For this reason Winchester and Floyd diagram (see Fig. 11) is more relevant.

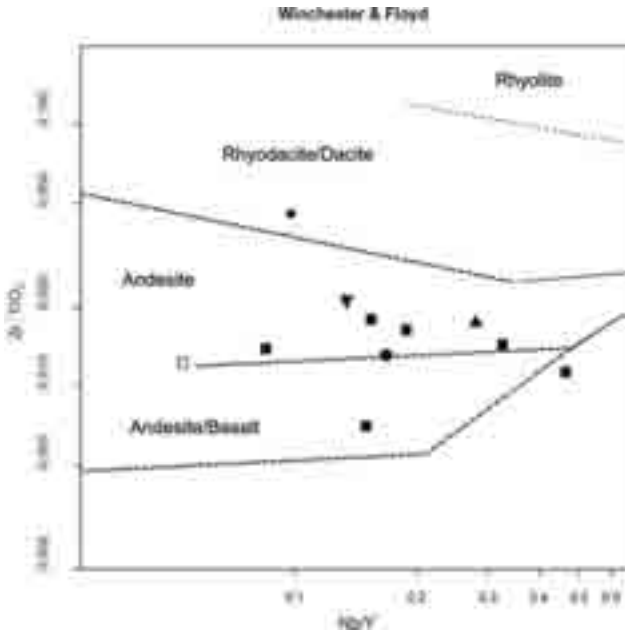

Figure 11. Detail of Nb/Y–Zr/TiO_2 diagram (Winchester and Floyd 1977) of the rocks of Cinotepeque Range. Andesites of eastern El Salvador are not plotted in this diagram. Used symbols correspond to the Fig. 10.

(Hradecký et al. 2003). The Basal Ignimbrites are of similar appearance and composition in the two areas. They possibly represent connected stratigraphic formations exposed in different parts of El Salvador. The presence

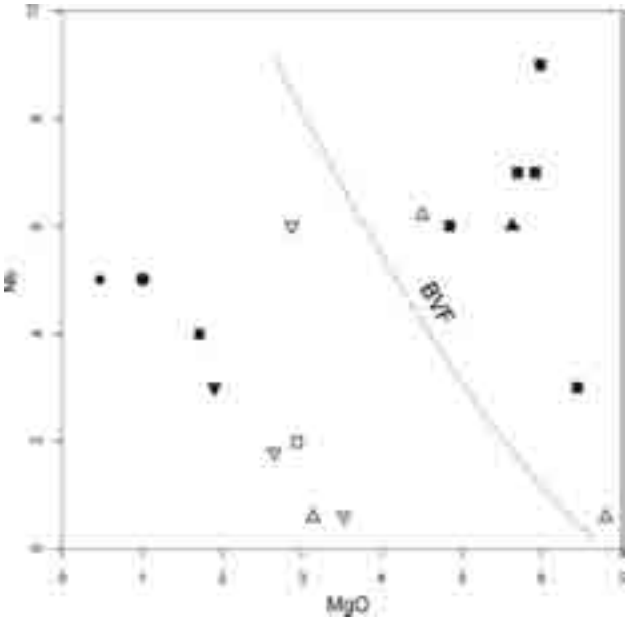

Figure 12. MgO–Nb diagram (after Walker et al. 2000) with plotted analyses of rocks from Cinotepeque Range. Used symbols correspond to the previous Figs. Grey curve deliminates volcanics of the BVF from volcanics of the VF.

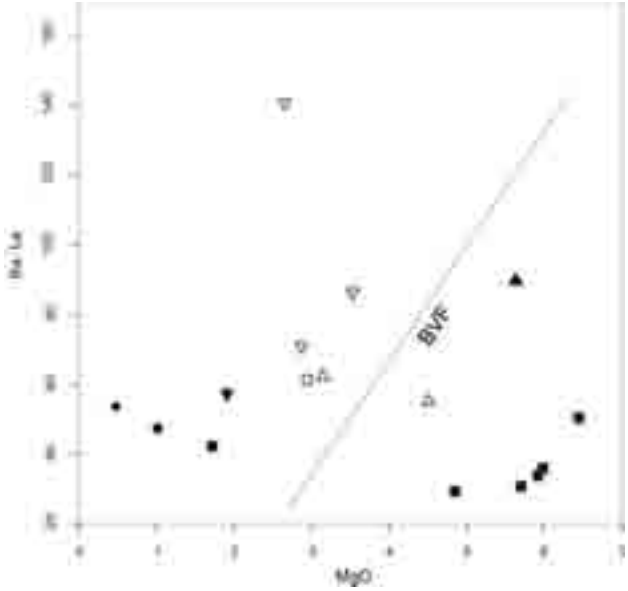

Figure 13. MgO–Ba/La diagram (after Walker et al. 2000) with plotted analyses of rocks from Cinotepeque Range. Used symbols correspond to the previous Figs. Grey curve deliminates volcanics of the BVF from volcanics of the VF.

of the Inferior and Superior Andesites shows another similarity between eastern and central El Salvador. In both areas, the older Inferior Andesites are of more differentiated character than the Superior ones. The main difference between the two areas is the presence of the San Alejo silicic complex of yet unknown source, which separates both andesitic suites in eastern El Salvador (Hradecký et al. 2003), whereas in central and NW El Salvador the two andesitic suites are separated by the Rana pyroclastic flow deposits. The origin of the magma of the

Figure 14. Fallen blocks of Rana agglomerate flow near Aguilares show flow units with concentration of big rock fragments at the base. (Photo by Petr Hradecký)

Figure 15. Coarse basal unit of Rana deposits rests upon Old Coatepeque silicic ignimbrite. (Photo by Petr Hradecký)

Superior Andesites differs from that of the Inferior ones in the two areas. The magma of Inferior Andesites was produced by flux melting, whereas the magma of the Superior ones originated by decompressional melting in the BVF environment.

Younger monogenic volcanic forms were subdivided into two systems, which differ in magma origin. The Cerro El Playón–Grandes Bloques System is situated on a NW-SE trending fault that continues to the San Salvador Volcano. The more evolved character of the magmas erupted in this system, and the VF petrochemical characteristics, lead us to interpret it as a system of adventive cones associated with the magma chamber of the San Salvador Volcano. On the other hand, magmas that belong to the Cinotepeque system are of primitive character and were produced by decompressional melting in the BVF environment.

Acknowledgment. This work has been financially supported by the Ministry of Foreign Affairs of the Czech Republic within the framework of the "Development Assistance Project", which is gratefully acknowledged. The authors would like to thank also all team members (in alphabetical order: L. Baratoux, P. Havlíček, D. Mašek, M. Opletal, J. Šebesta and T. Vorel from Czech Geological Survey), as well as all the analysts and technicians of the laboratories of the Czech Geological Survey who carried out chemical analyses of the sampled rocks and prepared a set of thin sections from the studied area. M. Zemková and V. Kopačková from the CGS-GIS digitized maps and produced a GIS database, and their comments were respected. Special thanks go to Carlos Pullinger, Walter Hernandéz, and Demetrio Escobar from Servicio Nacional de Estudiod Territoriales (SNET) for their assistance and help with the organization of work in El Salvador.

References

Hradecký P., Havlíček P., Mrázová Š., Rapprich V., Šebesta J., Ševčík J., Vorel T., Pullinger C., Hernandéz W. (2003): Geological study of natural hazards research in the region of La Unión and the Gulf of Fonseca, El Salvador. Unpublished report, Archives of CGS and SNET (in Czech and Spanish).

Hradecký P., Baratoux L., Guevara M., Havlíček P., Hernandéz W., Kvaček Z., Mašek D., Novák Z., Nováková D., Opletal M., Pullinger C., Rapprich V., Šebesta J., Vorel T. (2004): Geological research on natural hazards in central El Salvador in provinces of La Libertad, San Salvador and Cuscatlán. Unpublished report, Archives of CGS and SNET (in Czech and Spanish).

Irvine T. N., Baragar W. R. A. (1971): A guide to the chemical classification of the common volcanic rocks. Can. J. Earth. Sci. 8, 523–548.

Janoušek V., Farrow C., Erban V. (2003): GCDkit: new PC software for interpretation of whole-rock geochemical data from igneous rocks. Geochim. Cosmochim. Acta 67, A186.

Le Bas M. J., Le Maitre R. W., Streckeisen A., Zanettin B. (1986): A chemical classification of volcanic rocks based on the total alkali-silica diagram. J. Petrol. 27, 745–750.

Peccerillo R., Taylor S. R. (1976): Geochemistry of Eocene calc-alkaline volcanic rocks from the Kastamonu area, Northern Turkey. Contrib. Mineral. Petrol. 58, 63–81.

Rogers R. D., Kárason H., van der Hilst R. D. (2002): Epeirogenic uplift above a detached slab in northern Cenral America. Geology 30, 1031–1034.

Sofield D. J. (1998): History and Hazards of Volcán San Salvador, El Salvador. MSc thesis, Michigan Technological University.

Sofield D. J. (2004): Eruptive history and volcanic hazards of Volcan San Salvador. In: Rose W. I., Bommer J. J., Lopez D. L., Carr M. J., Major J. J. (eds) Natural hazards in El Salvador. Geol. Soc. Am., Spec. Pap. 375, Boulder, 147–158.

Walker J. A., Patino L. C., Cameron B. I., Carr M. J. (2000): Petrogenetic insights provided by compositional transects across the Central American arc. J. Geophys. Res. 105, 18949–18963.

Weber H. S., Wiesemann G., Wittekindt H. (1974): Mapa geológico General de la República de El Salvador 1 : 500 000 / Geologische Übersichtskarte der Republik El Salvador 1:500 000 (After geological maps 1 : 100 000 – 1967–71). Hannover.

Wiesemann G. (1975): Remarks on the geologic structure of the Republic of El Salvador, Central America. Mitt. Geol.-Paläont. Inst. Univ. Hamburg 44, 557–574.

Wiesemann G. et al. (1978): Mapa geológico de Republica de El Salvador, escala 1 : 100 000. Bundesanstalt für Geowissenschaften und Rohstoffe, Hannover.

Winchester J. A., Floyd P. A. (1977): Geochemical discrimination of different magma series and their differentiation products using immobile elements. Chem. Geol. 20, 325–343.

Bulletin of Geosciences, Vol. 80, No. 4, 287–290, 2005
© Czech Geological Survey, ISSN 1214-1119

A new *Parastriatopora* species (Anthozoa, Tabulata) from the Lower Devonian of Colle (Spain, Cantabrian Mountains)

Andreas May

Saint Louis University – Madrid campus, Avenida del Valle 34, E-28003 Madrid, Spain. E-mail: maya@madrid.slu.edu

Abstract. The paleontological collection of the Museo Geominero (Madrid) houses a new species of the tabulate coral *Parastriatopora*. It comes from the Lower Devonian of Colle (Prov. León) and probably originates from one of the biostromal levels in the upper part of the Valporquero Formation and the lower part of the Coladilla Formation (Upper Emsian). The new species, described under open nomenclature as *Parastriatopora* sp., is characterized primarily by its very large corallites and calices: the 5 to 7-cornered calices are 3.5–6.9 mm in diameter (mostly 5.5–6.0 mm). Furthermore, it shows very interesting paleobiogeographical relationships, because the morphologically closest related species is *Parastriatopora gigantea* (Knod 1908) from the Lower Devonian of Bolivia. *Parastriatopora* sp. could be an example of a close relationship between the Cantabrian Mountains and America during the Emsian.

Key words: Anthozoa, biogeography, Lower Devonian, systematics, tabulate corals

Introduction

Parastriatopora is a genus of ramose tabulate corals that is widespread in Silurian and Lower Devonian strata of Australia, Asia, Europe, North Africa, and America. However, only relatively few *Parastriatopora* specimens are known from Spain: *Parastriatopora* ex gr. *annulata* (Le Maître 1952) has been found in the Lower Devonian of the Cordoba Province (Crousilles et al. 1978, Lafuste et al. 1992). Tourneur and Fernández-Martínez (1991) found *Parastriatopora cantabrica* Tourneur and Fernández-Martínez 1991 in the Emsian (Lower Devonian) of the Cantabrian Mountains. May (1993, p. 87–88) describes *Parastriatopora fallacis* Yanet 1968 and *Parastriatopora obsoleta* Dubatolov 1969 from the Emsian of Asturias.

Consequently, the finding of a new *Parastriatopora* species in the collections of the Museo Geominero in Madrid is of particular interest. Even though only one specimen is known to exist, the exact lithostratigraphical level of which is not fully known, this species is of remarkable size and shows very interesting paleobiogeographical relationships that justify a description of this new species.

The Museo Geominero contains very important historical collections of fossils from Spain and the Western Sahara (Rabano and Arribas 1997). These collections are registered in an exemplary manner in the well-developed database (Rabano and Arribas 1997, p. 14), which makes them easily accessible for scientific research. However, the Paleozoic corals and stromatoporoids have not yet been revised.

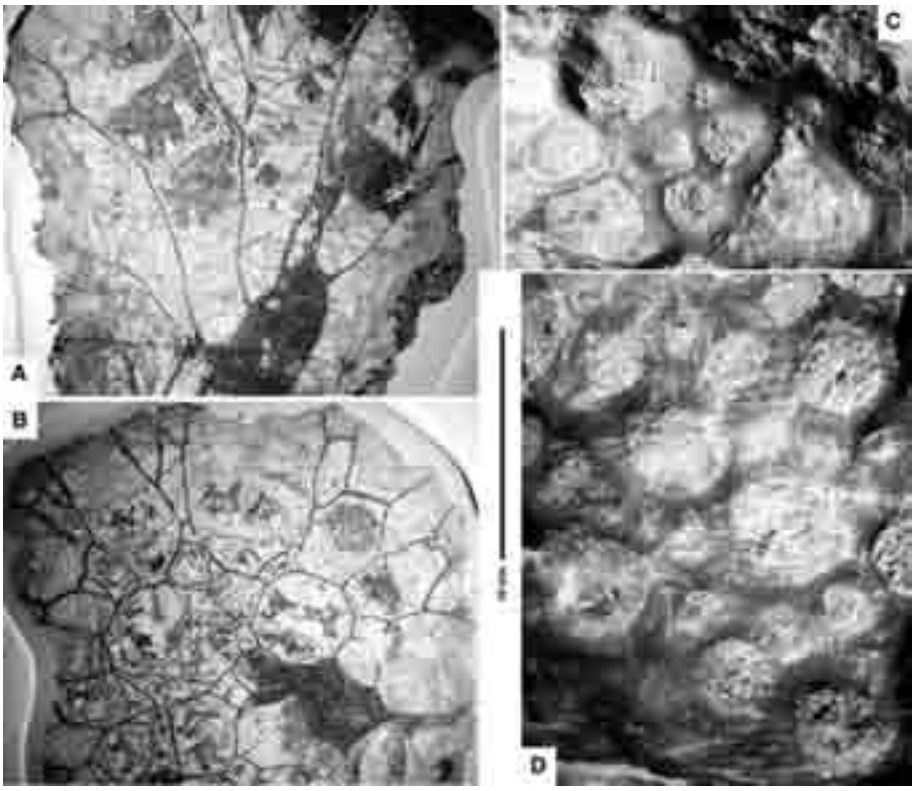

Figure 1. *Parastriatopora* sp., stock no. 791D, Upper Emsian of Colle (Province León). The scale is 10 mm long. A – longitudinal thin section. B – transversal thin section. C, D – surface of the branch, showing calices.

Systematic description

Class Anthozoa Ehrenberg 1834
Subclass Tabulata Milne-Edwards and Haime 1850
Order Favositida Wedekind 1937
Family Parastriatoporidae Chudinova 1959

Parastriatopora Sokolov 1949

Type species: *Parastriatopora rhizoides* Sokolov 1949.

Diagnosis and geographical and stratigraphical distribution see Hill (1981, p. 586–588) and May (1993, p. 86–87). A synonymy list of the genus *Parastriatopora* is given by May (1993, p. 86).

Remarks: Genus *Argentinella* Fernández-Martínez, Plusquellec and Tourneur 2002, with the type species *Favosites argentina* Thomas 1905, is closely related to *Parastriatopora. Argentinella* is distinguished by its marked development of the septal elements from typical *Parastriatopora* species (Fernández-Martínez et al. 2002).

Parastriatopora sp.

Diagnosis: A species of *Parastriatopora* in which 5 to 7-cornered calices are 3.5–6.9 mm in diameter (mostly 5.5–6.0 mm diameter). The branch has a diameter of about 30 mm. Within the outermost 1.5–2.5 mm of the branch, the corallite walls and tabulae are strongly thickened by skeletal substance showing secondary lamellation. No septal elements occur apart from weak septal ridges in the calice. Mural pores are rare and are about 0.2 mm in diameter. Horizontal skeletal elements dominate the central part of the branch tabulae, while the peripheral part of the branch is dominated by bubble-like tabellae.

Material: Only one incomplete corallum exists. This is the reason for describing this new species only under open nomenclature. The specimen is stored in the paleontological collection of the Museo Geominero (Madrid) under the stock no. 791D. Photographs are shown in Fig. 1.

Provenance of the material: Due to the fact that the corallum was collected before 1900, we know only that it came from the Devonian of Colle (Prov. León). Colle is a small village on regional road LE-3143, approximately 5 km east of Boñar.

On the slope of the hill where the church of Colle is situated, there is an outcrop that has been famous since the 19th century for the quality and wealth of its fossil deposits. Modern descriptions of this locality are given in Fernández et al. (1995, p. 43), García-Alcalde (1999), and Schröder and Soto (2003). In this locality the upper part of the Valporquero Formation and the lower part of the Coladilla Formation emerge, which is the upper part of the La Vid Group. The sequence belongs to the Upper Emsian (Fernández et al. 1995, García-Alcalde 1999, García-Alcalde et al. 2002), and contains several biostromal levels built by rugose and tabulate corals. Further information about these biostromal levels can be found in Fernández et al. (1995, p. 43), Méndez-Bedia et al. (1994, p. 162), Soto (1982 and 1986, p. 29) and Stel (1975).

Parastriatopora sp. originates very probably from one of these biostromal levels in the upper part of the Valporquero Formation and the lower part of the Coladilla Formation (Upper Emsian).

Description: Before the preparation of both thin sections, *Parastriatopora* sp. was a 67 mm long fragment of an isolated, well-preserved branch of 33 mm in maximum diameter. The surface of the branch is a little worn. However, some calices show faint, radially oriented septal ridges. The calices are polygonal and of very different diameters: 4-cornered calices are 3.2–4.5 mm in diameter, and the 5 to 7-cornered calices are 3.5–6.9 mm in diameter (mostly 5.5–6.0 mm).

The transversal thin section through the branch shows that in the middle of the branch the corallites have a polygonal to rounded polygonal outline. New corallites originate by peripheral intracalicular increase, and are about 0.9 mm in diameter. The large corallites, 4.4–5.5 mm in diameter in the middle of the branch, and 4.5–6.4 mm in the peripheral part of the branch, come slowly to the surface and intersect it at an acute angle. In the middle of the branch, the observed corallite diameters vary between 0.9 mm and 5.5 mm. In the peripheral part of the branch, smaller corallites of 1–4.5 mm diameter occur between the larger corallites.

Within the largest part of the branch, the common wall between the corallites is only 0.06–0.16 mm thick with a broad dark median suture.

The longitudinal thin section of the branch shows that in a relatively broad zone in the middle of the branch the corallites run more or less parallel to its longitudinal axis. Approximating to the surface of the branch the corallite bends slowly. Close to the surface the corallites have diameters of 4–6 mm. Mural pores are rare and are about 0.2 mm in diameter.

In the central part of the branch among the horizontal skeletal elements tabulae dominate, which are horizontal or slightly inclined and slightly curved in an irregular undulating manner. Bubble-like tabellae occur only occasionally. The distance between the tabulae in the central part of the branch varies between 0.4 mm and 3.5 mm. At a distance of 10 mm the number of tabulae amount to 6–11.

In the peripheral part of the branch, bubble-like tabellae dominate. The distance between the tabellae in the peripheral part of the branch varies between 0.3 mm and 1.6 mm. In most parts of the branch, the horizontal skeletal elements are microcrystalline and thin (only 0.015–0.040 mm thick).

In the outermost part of the branch a 1.3–3.8 mm (mostly 2–2.5 mm) thick stereozone has developed. The skeletal elements (walls, tabellae, and tabulae) are thickened within this stereozone by a skeletal substance showing secondary lamellation (Hill 1981, p. 454). The horizontal skeletal elements are especially thickened by a secondary lamellate skeletal substance lying on the upper side of the thin microcrystalline skeletal element. These layers are

mostly 0.03–1.2 mm thick. However, one coherent thickening can be up to 2.0 mm thick.

Neither in the transversal thin section nor in the longitudinal thin section do any septal elements occur.

Comparisons: The branch shows the typical characteristics of the genus *Parastriatopora* Sokolov, 1949. *Argentinella argentina* (Thomas 1905) from the Lochkovian of Argentina, the type species of the closely related genus *Argentinella* Fernández-Martínez, Plusquellec and Tourneur 2002, shows some similarity, but is clearly distinguished by its strongly developed septal elements and smaller calices (Fernández-Martínez et al. 2002).

The branch shows greater diameters of corallites and calices than on any other species of *Parastriatopora.* Consequently, it is considered as a new species. However, because of the lack of material, it is named under open nomenclature *Parastriatopora* sp. Most species of *Parastriatopora* need not be compared with *Parastriatopora* sp., because the diameter of their corallites and calices is less than half that of *Parastriatopora* sp. For example, the calices are 0.75–2.4 mm in diameter in *Parastriatopora fallacis* Yanet 1968 and *Parastriatopora obsoleta* Dubatolov 1969 from the Emsian of Asturias (May 1993, p. 87–88).

Parastriatopora sp. demonstrates the closest similarity to *Parastriatopora gigantea* (Knod 1908) from the Pragian or Emsian of Bolivia (Tourneur et al. 2000). *Parastriatopora gigantea* (Knod 1908) is distinguished by a combination of the following features. On the one hand, *P. gigantea* has smaller corallites and calices (Tourneur et al. 2000). The corallites are only up to 3.8 mm diameter in the middle of the branch (Tourneur et al. 2000, p. 712). Even though the 6 to 8-cornered calices in *P. gigantea* have a maximum diameter of 7.5 mm (Tourneur et al. 2000, p. 715), the average diameter of the 6 to 8-cornered calices in *P. gigantea* is only 4–5.1 mm (Tourneur et al. 2000, Fig. 6). On the other hand, the stereozone in the outermost part of the branch is much broader in *P. gigantea*.

Parastriatopora sanjuanina Fernández-Martínez, Plusquellec and Tourneur, 1999 from the Lochkovian of Argentina (Fernández-Martínez et al. 1999) is more closely related to *Parastriatopora gigantea* (Knod, 1908) than to *Parastriatopora* sp.: The calices of *P. sanjuanina* are only up to 6 mm in diameter, and the stereozone in the outer part of the branch is broad and well developed (García-López and Fernández-Martínez 1995, p. 178–180, Fig. 3 and Fernández-Martínez et al. 1999). Furthermore the branches of *P. sanjuanina* are only 7–20 mm thick.

Parastriatopora cantabrica Tourneur and Fernández-Martínez 1991 from the Emsian (Lower Devonian) of the Cantabrian Mountains is very similar to *Parastriatopora* sp., but has significantly smaller corallites and calices: the largest calices are 3.5–4.5 mm (maximum 5.0 mm) in diameter, and the biggest corallites are 2.0–4.5 mm in diameter (Tourneur and Fernández-Martínez 1991). Furthermore, the peripheral stereozone is slightly differently developed: the stereozone is broader, but the skeletal elements are less strongly thickened by a secondary lamellate skeletal substance than in *Parastriatopora* sp.

Dubatolov (1980, p. 110, Plate 11, fig. 3) describes from the Rudny Altai a similar coral as *Parastriatopora* sp. that has calices of 4.0–5.0 mm in diameter. Consequently, the calices are significantly smaller than in here described *Parastriatopora* sp.

Parastriatopora grandissima Dubatolov in Dubatolov and Spasskij 1964 is another species from the Lower Devonian of Siberia that is similar to *Parastriatopora* sp. However, in *Parastriatopora grandissima* the large corallites are only 2.2–3.0 mm in diameter (Dubatolov and Spasskij 1964, p. 121–123, Plates 4–6).

Parastriatopora annulata (Le Maître 1952) and *Parastriatopora floralis* (Le Maître 1952), two species from the Lochkovian and Pragian of Algeria, show some similarity to *Parastriatopora* sp., but the corallites in the peripheral part of the branch have diameters of only 2.1–4.0 mm, and the stereozone in the outer part of the branch is broader than in *Parastriatopora* sp. (for details see: Le Maître 1952, p. 67–68, Plates 5, 6, 9 and Plusquellec 1976, p. 206–208).

The *Parastriatopora* ex gr. *annulata* (Le Maître 1952) found in the Lower Devonian of the Cordoba Province (Crousilles et al. 1978; Lafuste et al. 1992) is very similar to the both Algerian species. It is clearly distinguished from *Parastriatopora* sp. by its smaller corallite diameter and the broader stereozone (Lafuste et al. 1992, p. 6, Fig. 1).

Conclusions

The finding of *Parastriatopora* sp. is very remarkable. It is not only the *Parastriatopora* species with the greatest diameter of the corallites and calices, but it also shows very interesting paleobiogeographical relationships: The morphologically closest related species is *Parastriatopora gigantea* (Knod 1908) from the Pragian or Emsian of Bolivia. It would be plausible to construct a phylogenetic sequence from *Parastriatopora sanjuanina* Fernández-Martínez, Plusquellec and Tourneur 1999 from the Lochkovian of Argentina via *P. gigantea* to *Parastriatopora* sp. In this case, *Parastriatopora* sp. would be an example of close relationships between the Cantabrian Mountains and America during the Emsian – a phenomenon which Soto (1979, 1982) and Fernández-Martínez and Tourneur (1995) were able to observe in different groups of rugose and tabulate corals.

However, the possibility cannot yet be excluded that *Parastriatopora* sp. is derived from *Parastriatopora cantabrica* Tourneur and Fernández-Martínez 1991 or other unknown Lower Devonian *Parastriatopora* species of the Cantabrian Mountains.

Acknowledgements. This investigation would not have been possible without the support of the following persons: Antonio Perejón Rincon (Universidad Complutense Madrid) proposed me to investigate the collections of the Museo Geominero. Isabel Rábano Gutiérrez del Arroyo, the director of the Museo Geominero, permitted me to carry out this research and supported it. Silvia Menéndez Carrasco, the custodian of the palaeontological collections of the Museo Geominero, supported my re-

search in various ways. Peter Brittain (Munich) proofread the English of the manuscript. Author is thankful for all this support.

This article is a contribution to the IGCP 499 "Devonian land-sea interaction: evolution of ecosystems and climate".

References

Crousilles M., Dixsaut C., Lafuste J. (1978): Données nouvelles sur les calcaires du Dévonien inférieur de la Province de Cordoue (Espagne). C.R. Hebd. Seances Acad. Sci., Ser. D, Sci. Nat. 286, 507–509.

Dubatolov V. N. (1980): Tip Coelenterata. Podklass Tabulata. In: Kul'kov N. P. (ed.) Biostratigrafija nižnego y srednego devona Rudnogo Altaja. Akademija Nauk SSSR, Sibirskoe otdelenie, Institut geologii i geofiziki, Trudy 425, 95–117.

Dubatolov V. N., Spasskij N. J. (1964): Stratigrafičeskij i geografičeskij obzor devonskich korallov SSSR. Nauka, Moskva.

Fernández L. P., Fernández-Martínez E., Méndez-Bedia I., Rodríguez S., Soto F. (1995): VII International Symposium on Fossil Cnidaria and Porifera, Field Trip A, September 5–11, 1995: Devonian and Carboniferous reefal facies from the Cantabrian Zone (NW Spain). Madrid.

Fernández-Martínez E., Plusquellec Y., Tourneur F. (2002): Revisión de *Favosites argentina* Thomas, 1905, especie tipo de *Argentinella* nov. gen., coral tabulado del Devónico inferior de Argentina. Rev. Esp. Paleontol. 17, 1, 101–116.

Fernández-Martínez E., Plusquellec Y., Tourneur F., Herrera Z. (1999): Nueva especie de tabulado del Devónico inferior de Argentina. Rev. Esp. Paleontol. 14, 1, 37–57.

Fernández-Martínez E., Tourneur F. (1995): Tabulate coral faunas from the Lower Devonian of Colle and "Plataforma de Arnao" (Cantabrian Mountains, NW Spain). Paleogeographical affinities. In: Comas-Rengifo M. J., Perejón A., Rodríguez S., Sando W. J. (eds) VII International Symposium on Fossil Cnidaria and Porifera, Madrid, Spain, September 12–15, 1995. Abstracts, Madrid, 23–24.

García-Alcalde J. L. (1999): Terebratúlidos (Braquiópodos) del Emsiense superior de Colle (Sabero, León, N. de España). Trab. Geol. 21, 159–176.

García-Alcalde J. L., Carls P., Pardo Alonso M. V., Sanz López J., Soto F., Truyols-Massoni M., Valenzuela-Ríos J. (2002): Devonian. In: Gibbons W., Moreno T. (eds) The Geology of Spain. Geological Society, London, 67–91.

García-López S., Fernández-Martínez E. (1995): The genus *Parastriatopora* Sokolov, 1949 (Tabulata) in the Lower Devonian of Argentina: palaeobiogeographic implications. Geobios 28, 2, 175–183.

Hill D. (1981): Rugosa and Tabulata. In: Teichert, C. (ed.) Treatise on Invertebrate Paleontology, Part F [Coelenterata] Suppl. 1. Boulder/Colorado & Lawrence/Kansas.

Lafuste J., Fernández-Martínez E., Tourneur F. (1992): *Parastriatopora* (Tabulata) de las calizas del Lorito (Devónico inferior, Provincia de Córdoba): Morfología y microestructura. Rev. Esp. Paleontol. 7, 1, 3–12.

Le Maître D. (1952): La faune du Dévonien inférieur et moyen de la Saoura et des abords de l'Erg el Djemel (Sud-Oranais). Materiaux pour la carte géologique de l'Algérie, 1er Série Paléontologie 12, 1–171.

May A. (1993): *Thamnopora* und verwandte ästige tabulate Korallen aus dem Emsium bis Unter-Eifelium von Asturien (Devon; Nord-Spanien). Geologica et Palaeontologica 27, 73–101.

Méndez-Bedia I., Soto F., Fernández-Martínez E. (1994): Devonian reef types in the Cantabrian Mountains (NW Spain) and their faunal composition. Cour. Forsch. Inst. Senckenberg 172, 161–183.

Plusquellec Y. (1976): Les Polypiers – Tabulata. In: Lardeux H. (ed.): Les schistes et calcaires eodevoniens de Saint-Céneré (Massif Armoricain, France). Mem. Soc. Geol. mineral. Bretagne 19, 183–215.

Rabano I., Arribas A. (1997): Los ejemplares tipo y figurados de las colecciones paleontológicas del Museo Geominero. I. Invertebrados e icnofosiles paleozoicos. Bol. Geol. Miner. 108, 3, 229–233.

Schröder S., Soto F. (2003): Lower Devonian (Emsian) rugose corals from the Cantabrian Mountains, northern Spain. Acta Palaeontol. Pol. 48, 4, 547–558.

Soto F. (1979): Considérations paléobiogéographiques sur les Streptelasmatina (Coelenterata, Rugosa) solitaires du Dévonien des Monts Cantabriques (NW de l'Espagne). Geobios, 12, 3, 399–409.

Soto F. (1982): *Synaptophyllum* (Rugosa) aus dem Unterdevon des Kantabrischen Gebirges (Colle, Prov. León). Neues Jahrb. Geol. Palaontol.-Abh. 163, 2, 236–238.

Soto F. (1986): Asociaciones coralinas del Devónico astur-leonés (Cordillera Cantábrica, NO de España). Trab. Geol. 16, 25–35.

Stel J. H. (1975): The influence of hurricanes upon the quiet depositional conditions in the Lower Emsian La Vid Shales of Colle (NW Spain). Leidse Geol. Meded. 49, 3, 475–486.

Tourneur F., Fernández-Martínez E. (1991): *Parastriatopora cantabrica*, nueva especie de tabulado del Devónico inferior (Emsiense) de la Cordillera Cantábrica (NO de España). Rev. Esp. Paleontol. 6, 1, 3–19.

Tourneur F., Plusquellec Y., Fernández-Martínez E. M., Díaz Martínez E. (2000): Revision of *Parastriatopora gigantea* (Knod, 1908) (Anthozoa, Tabulata) from the Devonian of Bolivia. Geobios 33, 6, 709–724.

Bulletin of Geosciences, Vol. 80, No. 4, 291–305, 2005
© Czech Geological Survey, ISSN 1214-1119

The Jurassic floor of the Bohemian Massif in Moravia – geology and paleogeography

Josef Adámek

Czech Geological Survey, Leitnerova 22, 658 69 Brno, Czech Republic. E-mail: adamek@cgu.cz

Abstract. The lithofacies, paleogeography, and tectonics of the Jurassic sediments were studied in the footwall of the Carpathian Foredeep and outer units of the Carpathian Flysch Belt in southern Moravia. The major lithofacies were correlated and shown in a set of well logs and regional geological cross-sections. The distribution of facies types is demonstrated in their thicknesses and geological structures. Both cross sections and regional maps (structural and thickness maps) include informations based on deep borehole data and seismic investigation. Some remarks refer to petroleum geology.

Key words: autochthonous and parautochthonous Jurassic, NE European Platform, Western Carpathians, geology, lithostratigraphy, tectonics, depositional topography, petroleum geology

Introduction

Jurassic sediments have been known for a long time in the autochthonous sedimentary cover of the SE margin of the European Platform and in the Flysch Belt of the Western Carpathians. In the vicinity of the city of Brno and the Moravian Karst they are known from some outcrops. In the 1940s they were explored in wells situated in the shallow part of the Carpathian Foredeep. But these wells and outcrops documented only partial sections of the carbonate platform facies. In 1959 the first step into deeper parts of the area was made in Lower Austria by the deep well Staatz-1, which documented mainly pelitic sediments as a basinal facies of Malmian age and primarily clastic sediments of the Dogger (Wessely 1988). In the 1970s, these investigations in former Czechoslovakia were connected (like in Austria) to oil and gas exploration. Otherwise, Jurassic rocks have been mentioned in the literature as tectonic klippen in the Pavlovské Vrchy Hills of southern Moravia and in the Waschberg Zone of Lower Austria for more than 170 years. The exploration and scientific activities on both sides of the border resulted in valuable data on the autochthonous Jurassic as well as the character of the Jurassic of the Outer Carpathians. This paper presents a summary of data concerning Jurassic sediments in the area of interest (Fig. 1), with particular focus on their geological setting and development. The author had been interested in the Jurassic sediments during his long professional activity with the company Moravské Naftové Doly a. s., and some previously non-published information were used in this paper.

Method

Lithological profiles controlled by cuttings, cores, paleontological assemblages, and microfacies, compared with standard microfacies by Wilson (1975) and logs from many deep wells and seismic profiles, have been used to study the autochthonous Jurassic. The multidisciplinary data set formed the basis for well log correlation in the area of interest, and was integrated into a 2D seismic interpretation to construct regional geological cross-sections and to generate structural and thickness maps. Drilling and seismic investigation have revealed many facts on the geological structure and development of Jurassic facies as well as the influence of some significant faults.

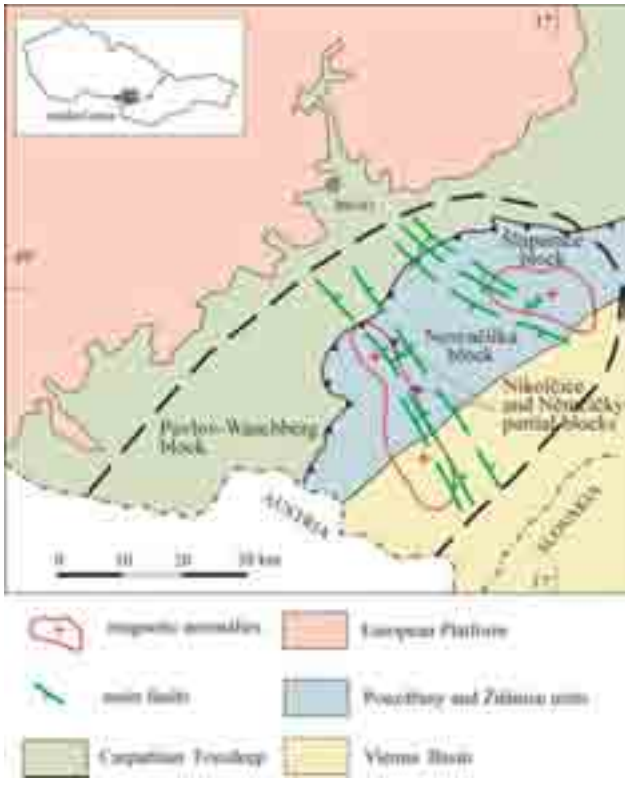

Figure 1. Geological map with individual tectonic blocks.

Geological setting

The geology of the autochthonous and allochthonous Jurassic units of this area has been described by Eliáš (1962, 1969, 1974, 1981, 1984, 1992), Stráník et al. (1968, 1979, 1993), Špička (1976), Vašíček (1980), Adámek (1986, 1990, 2001), Adámek et al. (1980), Eliáš and Wessely (1990), Jiříček (1990), Ciprys et al. (1995), and Wessely (in print).

In this region, the encountered rock complexes belong to three structural levels, the Cadomian, Variscan, and Neoid, all of which are buried below the overthrust flysch complexes of the Western Carpathians. The Cadomian level is composed of metamorphites, granitoids to quartz diorites, and rare ultrabasic rocks. They can be found in the Brunovistulicum unit (Dudek 1980). The Variscan level (?Cambrian, Lower Devonian to Upper Carboniferous) begins with prevailingly red-coloured, coarse-grained clastics. This lithofacies has been identified as the Old Red Sandstone throughout the entire region and, by recent assumption, partly of Lower Cambrian age. Based on micropaleontological data from the Němčičky-3 and -6, and Měnín-1 wells (Jachowitz and Přichystal 1997, Fatka and Vavrdová 1998), middle Devonian deposits overlie the Old Red Sandstones, followed by Lower Carboniferous carbonates. At the onset of Hercynian Orogeny, the carbonate was replaced by the synorogenic flysch sedimentation (Culm), which in the Late Carboniferous was overlain by post-orogenic molasse sediments of the Upper Carboniferous, which are comprised mostly of sandstones containing coal seams (Namurian – A). The Mesozoic Tethyan cycle (Neoid level) began with rifting and deposition of basal, mostly terrigenous, clastic sediments and marine marly shales in the Middle Jurassic (Dogger). This sedimentation was followed by a further transgression of the Tethyan Sea. The development of the Malm is predominantly carbonatic in the shallow depth area, and marly and carbonatic in the basinal facies in a deeper area, continuing to the end of the Jurassic (Malm, Tithonian). The general characteristics of the particular lithostratigraphic units of the Jurassic and their thicknesses are displayed in Fig. 2.

After the Jurassic, the terrain was uplifted and re-peneplaned (except the Pavlov-Waschberg block) up to the Tertiary. A marine transgression locally occurred at the Pavlov-Waschberg block during the end of the Lower Cretaceous. During most of the Lower Cretaceous, the Moravian part of the North European Platform was uplifted and locally eroded, and only rare occurrences of Aptian to Albian rocks are found (Krystek and Samuel 1978, Řehánek 1984). Afterwards, the Middle–Upper Cretaceous sedimentation started. During this major transgression, sedimentation from Turonian to Maastrichtian (Adámek 1986), Turonian to Campanian (Řehánek 1978), or Upper Cenomanian to Lower Campanian continued. During the Laramide Orogeny (Late Cretaceous to Early Paleogene), this area was uplifted and deeply eroded by rivers in the tectonically predisposed Nesvačilka and Vranovice depressions. In both of these depressions most of the Mesozoic sediments were removed. The heavily eroded pre-Tertiary basement in both depressions was gradually filled with sediments during Paleogene. During the orogenic phases in the Early Miocene most of the Paleogene fill in the northwestern shallow parts of both depressions was not tectonically deformed. The distribution of Autochthonous Paleogene deposits is presently much smaller than originally, due to intense denudation and tectonic abrasion during thrusting of the flysch nappes. The Miocene fill of the Carpathian Foredeep was covered by

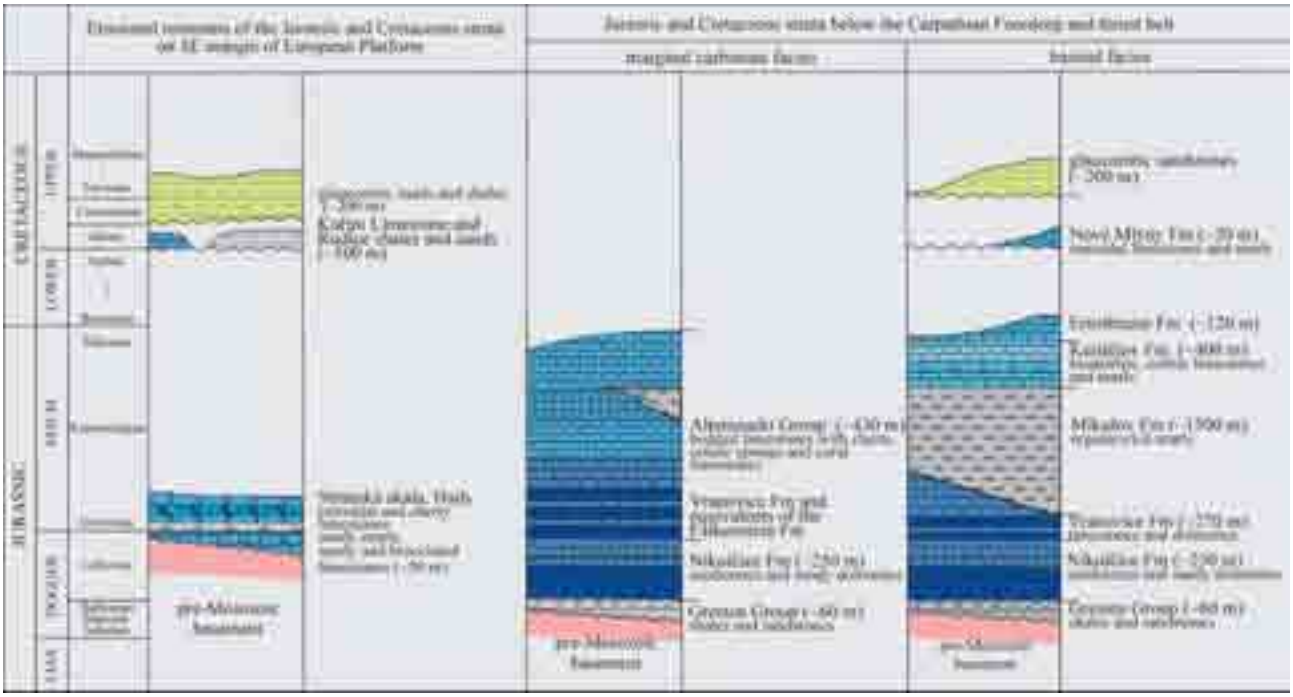

Figure 2. Lithostratigraphic units of the Autochthonous Mesozoic.

overthrust nappes in some parts of the area in front of the flysch. These deposits were preserved to a larger extent, but reduced in thickness under the flysch nappes, primarily on the Nikolčice-Kurdějov horst. The thicknesses of Paleogene, Miocene, and Mesozoic sediments on the Pavlov-Waschberg block were markedly influenced by nappes and were locally incorporated into the basal part of the flysch nappes. The Western Carpathian Flysch Belt comprises the Outer (Menilite-Krosno) group of nappes represented by the Pouzdřany and Ždánice units.

Structural setting

The southeastern margin of the North European Platform (in Czech geological articles often denominated as the southeastern slopes of the Bohemian Massif) in the area of interest was early divided in a transversal direction into two main tectonic blocks: The South Moravian block (subsequently named the Pavlov-Waschberg block) in the SW, and the Central Moravian block in the NE (Chmelík 1969, Špička 1976). The boundary between them was originally considered to be the Nesvačilka depression axis. In the next stage, the individual blocks were established on the basis of the actual knowledge of structural development of the area (Dvořák 1978, Adámek et al. 1980, Adámek 1990, Krejčí et al. 1996). The present article discusses both of the above-mentioned main blocks, as well as the subsequently-formed partial blocks (Fig. 1). These partial blocks, from SW to NE, are: the Nikolčice-Němčičky, the Nesvačilka, and partly the Šlapanice block. Drilling data and geophysical investigations have revealed new facts concerning the fault system separating the main and partial blocks, and have enabled definition of the boundary between the Pavlov-Waschberg and Central Moravian blocks to the SW margin of the Nikolčice-Kurdějov Ridge (Adámek 1990). This ridge made it possible to distinguish partial blocks, such as the shallow Nikolčice and the deep Němčičky block. Interrelations among the blocks were described by Adámek et al. (1980). According to Pícha (1979) the autochthonous Jurassic strata of southern Moravia and northeastern Austria have been confined to a relatively narrow zone of the Carpathian Foreland between Brno and the Danube valley. The area relates to the NW-SE trending rift and modifies the regional depression. Pícha et al. (2005) subsequently defined the depression as the Dyje/Thaya depression.

Jurassic geological development

According to the development of the blocks, the Jurassic sediments lay unconformably on the pre-Mesozoic basement at the Cadomian (Crystalline) or Variscan level (?Cambrian, ?Lower Devonian to Upper Carboniferous). Deposition of Jurassic strata started in the Middle Doggerian (Upper Bajocian–Bathonian) in southern Moravia. These deposits are known in Lower Austria as the Gresten Beds, Gresten Group, or Gresten Formation, formerly in southern Moravia as the Diváky Beds (Eliáš 1974, 1981, Brix et al. 1977, Eliáš and Wessely 1990). Subsequently, the term Gresten Beds was accepted for similar sediments in the southern Moravian area (Adámek 1986, 2001, Řehánek et al. 1996).

In Austria the Gresten Group (except the underlying Porrau Diabase Complex) was subdivided into four members: Lower Quarzarenite Series, Lower Shale Horizon, Upper Quarzarenite Series, and Upper Shale Horizon (Wessely in Brix et al. 1977). The sedimentation was described as a product of combined delta and marine sedimentation of synrift type. The full facies variety is clearly visible in the Austrian territory, but in southern Moravia has not yet been identified. Only an incomplete development with different members of the Gresten Group was found on both of the main tectonic blocks. A more complete succession was found in the Nesvačilka block. The thickness of the sediments varies within tens of metres (at about 60 m on the above-mentioned block). According to information about the Austrian territory (Grün 1984, Sauer et al. 1992, Zimmer and Wessely 1996), there is a distinct SW-NE general drift of tectonic lines in Austria showing a dipping of the fault system towards SE. The thickness of deposits reaches more than 1700 m (in the area of Stockerau). The thickness depends on the position within the deltaic complex and the position within the synsedimentary tilted fault block system. In southern Moravia these sediments have been found locally and incompletely as relatively thin bodies in an uplifted position. A slightly different direction of faulting is found on the Nesvačilka block (Figs 7, 8).

In the Callovian time a new cycle started that was marked by an unconformable superposition on older sediments and tectonics. As a result of the global eustatic cycle by the Callovian regional transgression, mainly sandstones of the Nikolčice Formation and the corresponding Höflein Formation in Lower Austria were deposited on a regional plain surface. The cycle is characterized by carbonatic influence in the beginning, particularly on the Pavlov--Waschberg block, and by sandstones on the southern part of the Central Moravian block. Thicknesses of the both facies (sandstones and sandy dolomites) in southern Moravia range between 70–250 m. The prevailing terrestrial sedimentation was followed by a further transgression of the Tethyan sea and created a Malmian carbonate platform (Altenmarkt beds, Ladwein 1976), later renamed as the Altenmarkt Group (Eliáš and Wessely 1990) in the shallow northwestern peripheral part. This part developed along a passive continental margin in the west. Another one, the so-called Pavlov carbonate platform (Eliáš 1984) was probably developed on a horst block in the inner part of the Jurassic basin in the Late Jurassic (see the model of the depositional topography on Fig. 3). The upper part of the sediments of this platform was incorporated during the late Alpine deformation and thrusting into the frontal part of the Carpathian thrust belt (Jurassic and Cretaceous sediments of the Pavlovské Vrchy Hills). The surface of the

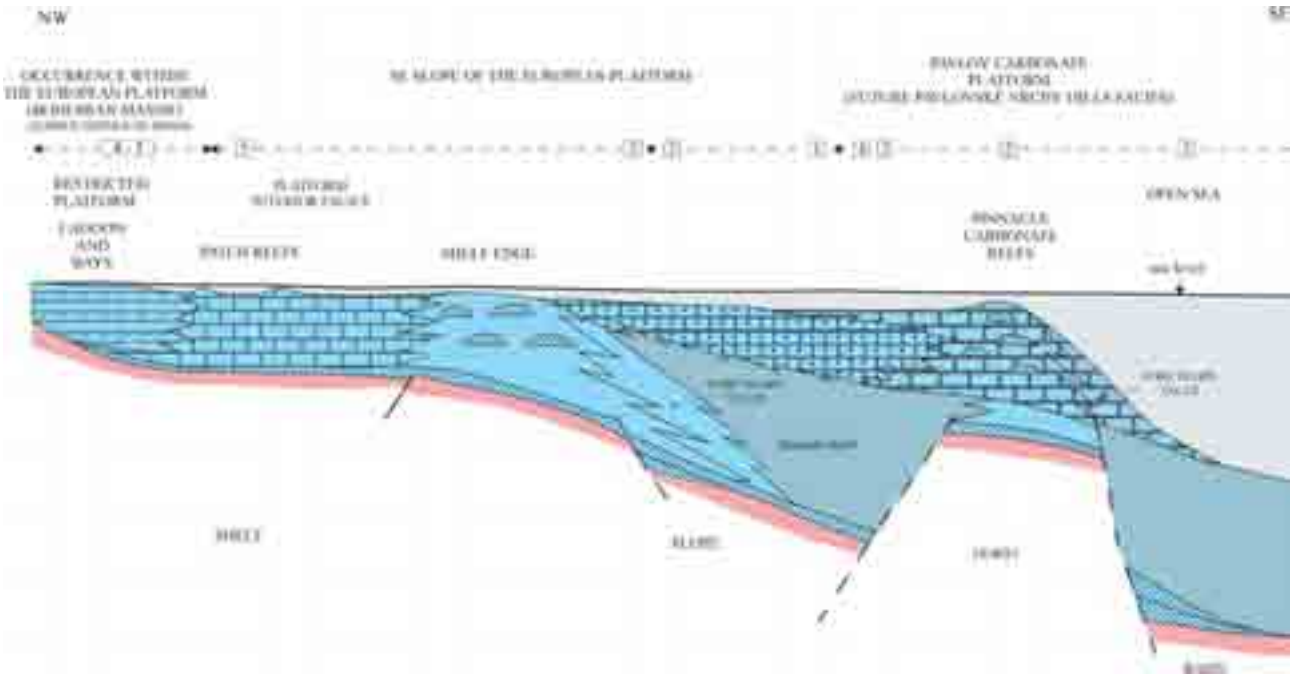

Figure 3. Jurassic on the SE margin of the European Platform – model of the depositional topography (horizontal and vertical dimensions not to scale). 1–8 – standard microfacies by Wilson (1975).

autochthonous Jurassic rocks is exposed only in the vicinity of Brno, and was described by Eliáš (1984). The 430 m thick sequence of the marginal carbonate facies, the Altenmarkt Group, begins with bedded limestones with some chert, grading upwards into bioclastic limestones containing algal-sponge associations and some rare coral patch-reefs. The moderate dip of the slope of the carbonate platform is characteristic of the study area, and, contrary to Lower Austria, does not contain any large reef complexes.

Predominantly marly sediments form a basinal pelitic-carbonatic development that was deposited in a deeper, more restricted marine environment (Kapounek et al. 1967, Stráník et al. 1968, Brix et al. 1977, Eliáš 1981, Adámek 1986, Eliáš and Wessely 1990). Upwards from the bottom the following lithostratigraphical units can be distinguished: Vranovice (limestone and dolomite), Mikulov (marl), Kurdějov (arenite) formations, and finally the Ernstbrunn Formation (limestone). The transitional series of the sediments between the marginal carbonate and the basinal, pelitic-carbonatic development is represented by the equivalent of the Vranovice Formation in Moravia and the Falkenstein Formation in Lower Austria. The Vranovice Formation fringes basinward, and its thickness decreases from 270 m at the front of the marginal carbonate platform (marginal carbonate facies) to only a few tens of metres in the pelitic-carbonatic development (basinal facies) further east. The Mikulov Formation (dark marl) is the most extensive member of the deeper pelitic-carbonatic development. The known thickness is about 2000 m, but often it is tectonically enlarged (Adámek 1986) by duplication (Fig. 6). The Mikulov Formation (marl) gradually passes upwards into the Kurdějov Formation (arenite) as the basin grew shallower. The up to 400 m thick dark to light Kurdějov Formation (arenite) developed from the Mikulov Formation (marl) by an upward transition. The Kurdějov Formation (arenite) consists of various types of detrital limestones alternating with layers of dark marls. The regression resulted in the development of carbonates of the Ernstbrunn Formation (limestone), which is very similar to the external klippen of the Carpathian nappes (Řehánek 1987). The Ernstbrunn Formation, containing the remains of mollusks, algae, and corals, terminated the Malmian sedimentation. Their thickness (known from deep wells) reached about 120 m.

All the individual facies complexes of Jurassic in the Czech territory have been described by Eliáš (1962, 1969, 1974, 1977, 1981) and Řehánek (1977, 1985). A comparison of the Ernstbrunn Formation between wells and outcrops in southern Moravia was published by Řehánek (1987). The description, compilation, and comparison of all of the lithofacies on both sides of the Czech/Austrian border have been presented by Adámek (1985, 1986) and Eliáš and Wessely (1990). Stratigaphy of the autochthonous Jurassic and Cretaceous deposits, their lithostratigraphic units, and their relationships are shown in Fig. 2.

Interpretation

The Jurassic stratigraphy and structure of southern Moravia described in the preceding sections is illustrated in five figures, each of which has two parts: a regional correlation of well logs, and a geological cross section. The regional profiles are based on seismic and well log data. The locations of the regional geology and regional correlations of well log profiles described in text are indicated on the map

(Fig. 10). Well log correlation and subsequent interpretation of the geologic cross sections document the geological development on the profiles with emphasis on the Jurassic strata. Well logs were used to identify the individual Jurassic facies (using spontaneous potential SP and resistivity gradient curve Rag). For the geological interpretation of each of the regional cross sections, the seismic lines were used. For a better understanding of the geological development of the area, the profiles had been situated perpendicular to the main geological features.

Cross sections

Transversal profiles (Figs 4–6) connect the shallow part of the Carpathian Foredeep with the Vienna Basin through the Carpathian Flysch Belt, or they terminate in the Carpathian Flysch. Each of them is about 30 km long, and the wells and seismic lines verify all the profiles. The profiles document both Doggerian and Malmian strata, marginal carbonate and basinal facies, as well as geology in general, including tectonic patterns with dominant normal faults and overthrusts. A well log cross section in the upper part and a regional geological cross section in the lower part of each of the individual figures show the thinning and developing of the Jurassic strata from southeast to northwest, and document the development and facies characteristics of the Jurassic.

In the southern part of the area (Fig. 4) the Gresten and Nikolčice formations of the Dogger are poorly developed in wells and hardly distinguished on seismic profiles. The cross section passes the western margin of the Jurassic with the marginal carbonate facies (Novosedly-1 and Březí-1 wells) through the Březí-2, Nový Přerov-2 and Mikulov-1 wells with basinal facies. The Sedlec-1 well represents the deeper part. The geological cross section illustrates the regional tilting of the eastern slope of the Bohemian Massif. In the shallow part of the profile, younger post-Jurassic, antithetic and basinward-directed normal faults are expected. Earlier faults, such as in the Dolní Dunajovice gas field, are also documented. In the deeper parts normal significant synthetic faults are expected.

The NNW part of the profile on Fig. 5 crosses the Vranovice depression, filled by Paleogene sediments, and continues through the Carpathian Flysch Belt to Vienna Basin (easternmost part of the profile). Except for the eastern slope of regional tilting, one can see the dominant younger faulting of the Jurassic (similar to that in Fig. 4). The profile passes the Pasohlávky-1 and Mušov-3G wells (both of which contain thermal water, Adámek and Michalíček 1990). It crosses the northern part of the Dolní Dunajovice gas field, which has been converted into an underground gas storage facility (Dunajovice-17 well), and continues to the deeper part of the region (Strachotín-2 and Bulhary-1 wells).

The profile situated on the Nikolčice-Kurdějov horst (Fig. 6) connects the shallow part of the Carpathian Foredeep with the so-called Měnín Hill, which consists of Paleozoic sediments. It then passes the marginal carbonate platform of the Jurassic (shallow Měnín Counterflush Cf wells and Nikolčice-4 well), and reaches the basinal deeper part of the Jurassic development below the flysch nappes (Nikolčice-6, 1A, 2A, Němčičky-5, 2, 1 and Kobylí-1 wells). From the view of the geological development of the separate blocks the profile is situated in the southern part of the Central Moravian block. The structural extension related to Dogger rifting is recognized in the shallow part of the area – on the Nikolčice partial blocks. The Cadomian level, composed of granitoid rocks, was encountered only in the Nikolčice block. Because of the great thickness of the overlying sediments it has not been reached by drilling in the deeper parts of the area, as in the Němčičky block. The tectonic style of the area is a bit different than on both previous transversal profiles (Figs 5, 6).

All transversal profiles document the different kind of sedimentary cover of the Dogger and Malm. But except for the Doggerian tectonics, all the Jurassic complexes of sediments are disturbed by normal-synthetic fault steps down to the subthrust floor. There are also a few significant normal-antithetic faults (faults systems) in the shallow part of the Carpathian Foredeep, some of which are of importance from the hydrogeological, hydrodynamic, and petroleum perspective (Adámek 1977, 1978, 1985, 1986, Polesňák and Adámek 1983, 1986). The faults were formed as a result of thrust loading over the foreland in the Neogene. Their mechanism and pattern, and their significance for hydrocarbon accumulation, have been described by Harding and Tuminas (1989).

Longitudinal regional correlation profiles of well logs, and geologic cross sections (Figs 7, 8), pass through the Pavlov-Waschberg block region in the SW part. The central parts of profiles pass through the Nikolčice–Kurdějov horst and the Nesvačilka depression, and continue to the Ždánice high (Šlapanice or Uhřice individual fault blocks). This means that the profile connects both main regional blocks in the area of interest: the Pavlov-Waschberg and Central Moravian blocks. Studies permit the determination the southwestern margin of the Variscan area of sedimentation preserved on the Nikolčice-Kurdějov horst, and the identification of the structure of this region near the limits of the Variscan tectogene. NW-SE striking tectonic elements in this region subdivide the whole area between the Pavlov-Waschberg block and the Ždánice high into numerous step-like blocks with faults that evidently disturb the Variscan level and the lower part of Jurassic sediments. The profile in Fig. 7 was situated in the deeper part of the Carpathian Flysch Belt, while the profile in Fig. 8 was situated in the shallow part of the area (Carpathian Foredeep and the frontal part of Carpathian Flysch Belt). The cross sections illustrate the geological and tectonic pattern on the profiles, and the tectonic style of both main blocks (Pavlov-Waschberg and Central Moravian blocks) and the individual-partial blocks.

The profile situated in the deeper southeastern part of the area (Fig. 7) passes the marginal part of the Vienna Basin (Nové Mlýny-2 well), the Pálava Hills (Nové Mlýny-3 well) with the Nikolčice-Kurdějov horst and the Uhřice

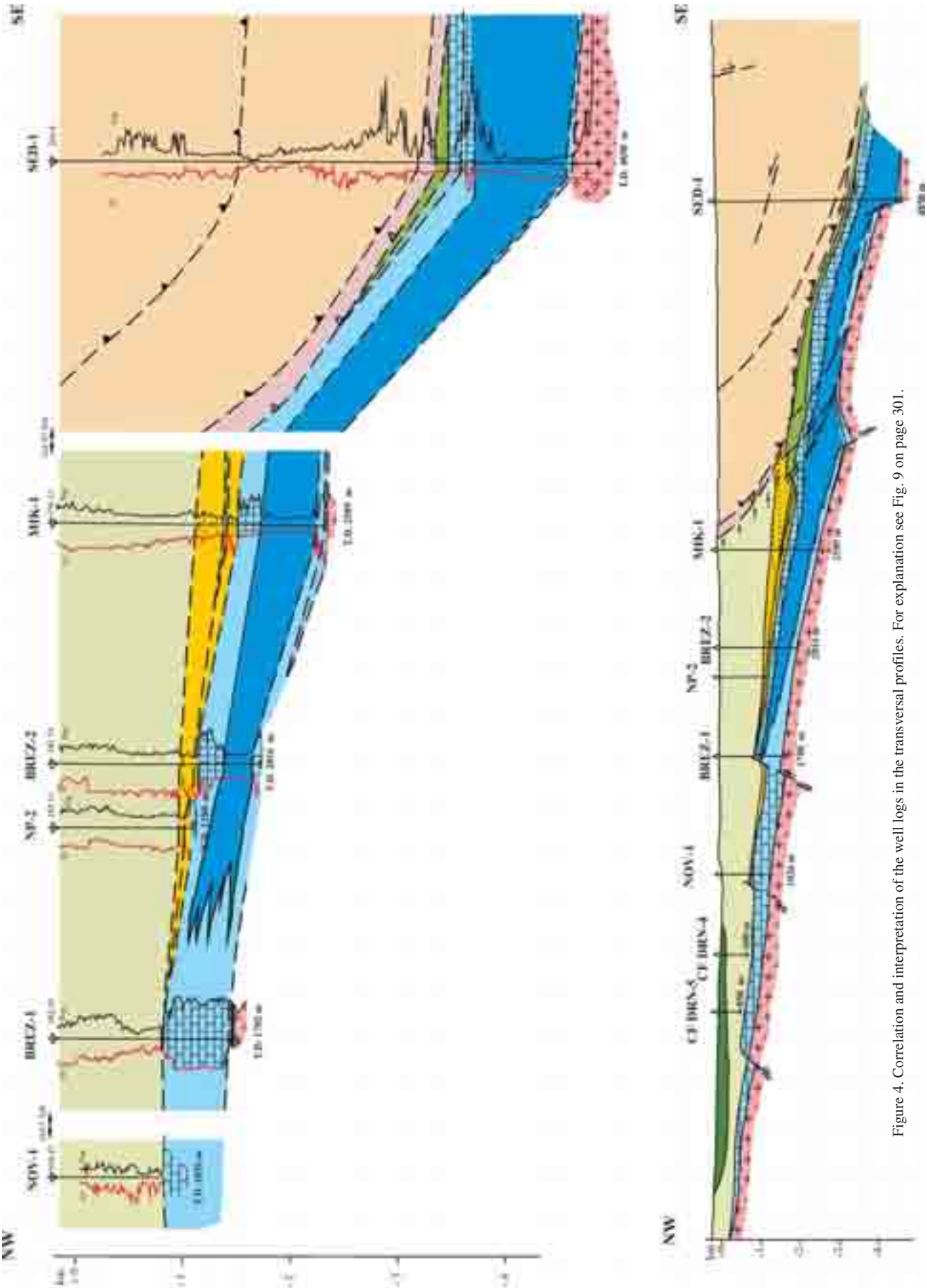

Figure 4. Correlation and interpretation of the well logs in the transversal profiles. For explanation see Fig. 9 on page 301.

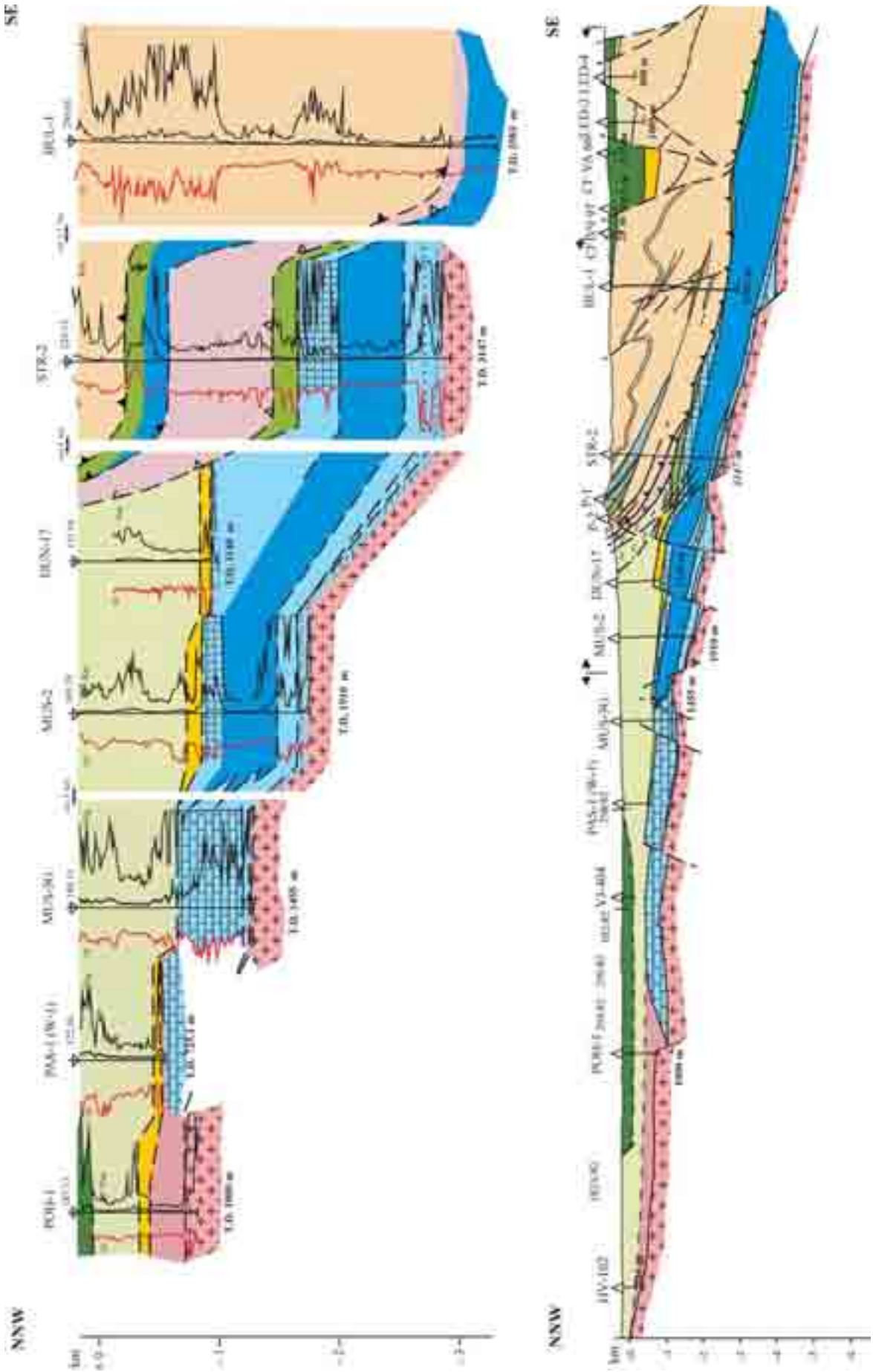

Figure 5. Correlation and interpretation of the well logs in the transversal profiles. For explanation see Fig. 9 on page 301.

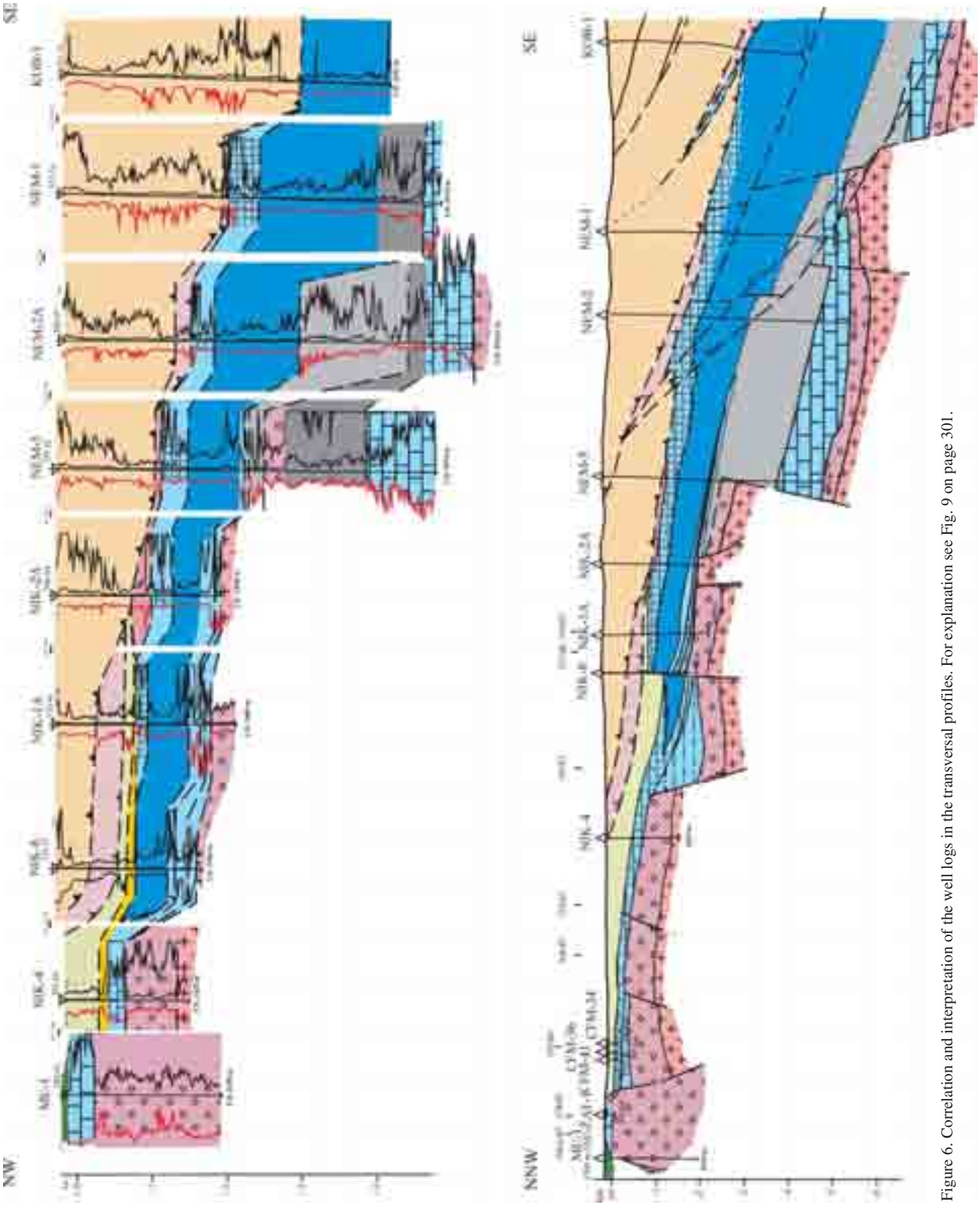

Figure 6. Correlation and interpretation of the well logs in the transversal profiles. For explanation see Fig. 9 on page 301.

blocks on the SW slope of the Ždánice high. The profile was verified by wells and seismic lines, and crosses the Vranovice and Nesvačilka depressions filled with autochthonous Paleogene deposits. All the area is overthrusted by flysch nappes (Pouzdřany and Ždánice units). The Jurassic sediments are mostly preserved on the Waschberg-Pavlov block, the Nikolčice-Kurdějov horst, and partly on the Šlapanice block. The geologic cross section illustrates the trends on the flanks of the Nikolčice-Kurdějov horst as well as on SW slope of the Ždánice high (Uhřice blocks). In the central, axial parts of the Vranovice and the Nesvačilka depressions we do not expect (based on well logs and seis-

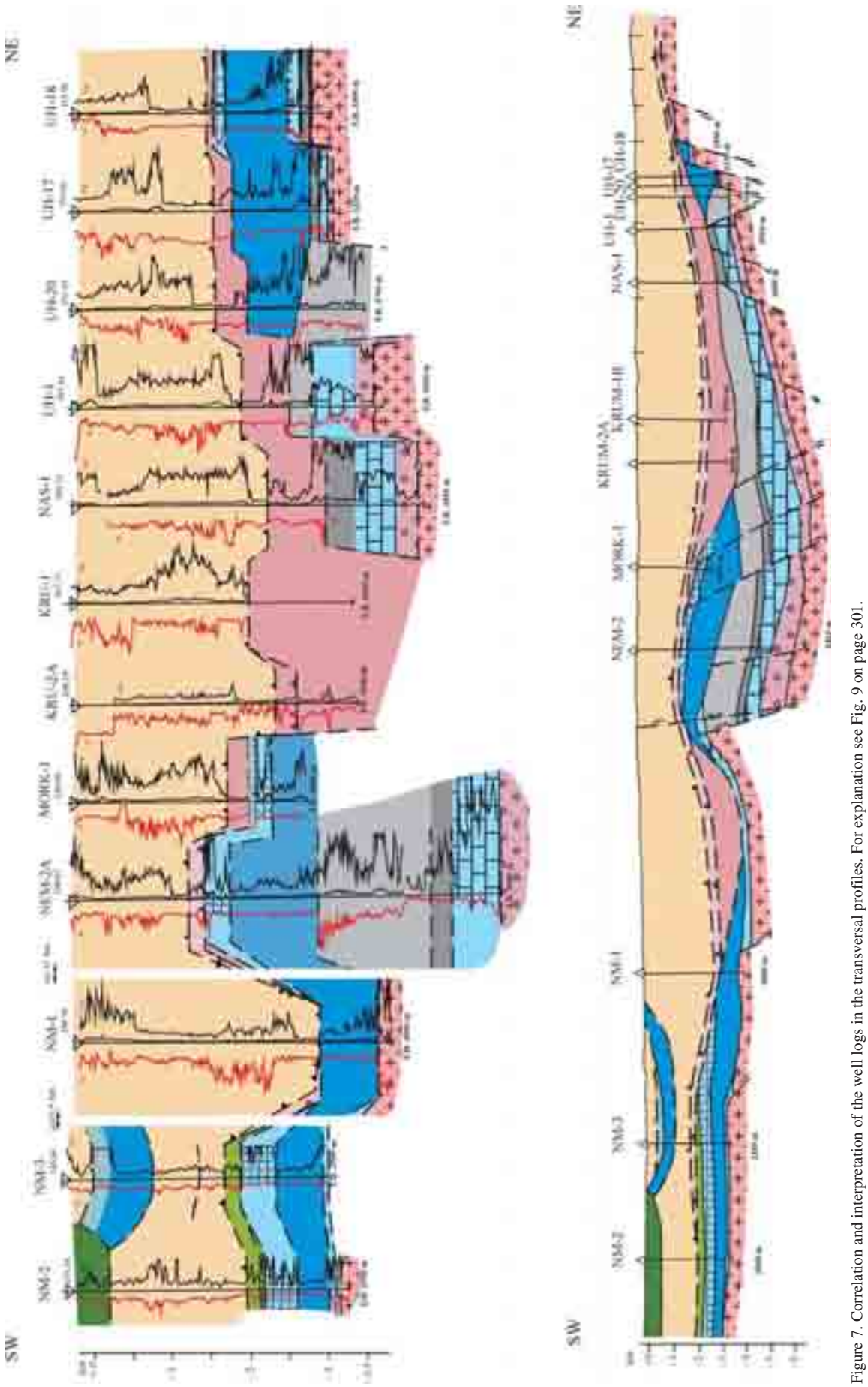

Figure 7. Correlation and interpretation of the well logs in the transversal profiles. For explanation see Fig. 9 on page 301.

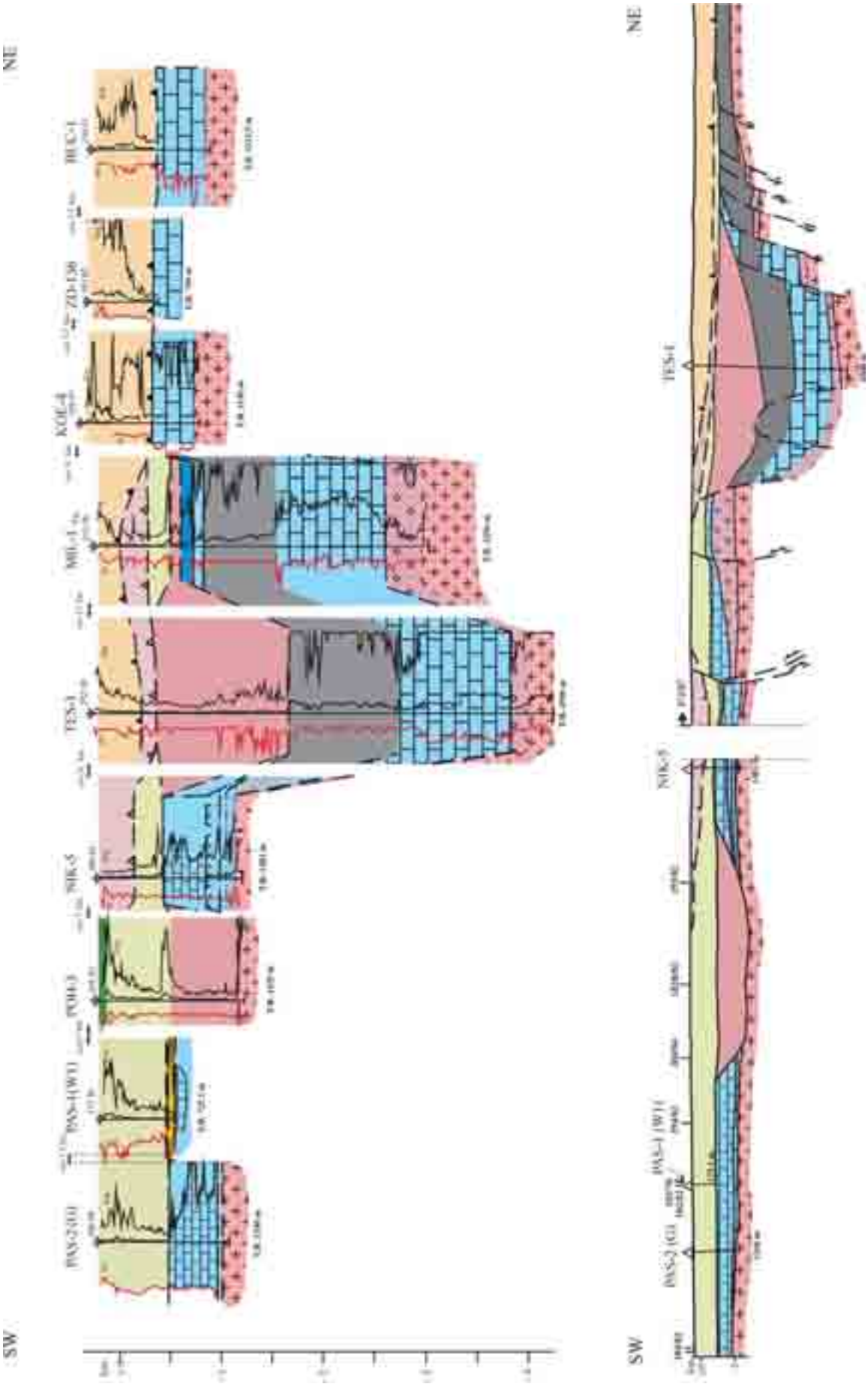

Figure 8. Correlation and interpretation of the well logs in the transversal profiles. For explanation see Fig. 9 on page 301.

mic investigations) almost any thickening of Jurassic sediments, which have been largely removed by long-term erosion in both depressions. On the SW slope of the Ždánice high they were left as remnants in tectonically limited blocks on the downthrown blocks (NE part of the profile), or due to the inversion on individual, partial, upthrown blocks.

The profile (Fig. 8) in the shallow northwestern part of the area passes the part of Carpathian Foredeep (Pasohlávky-1, 2G wells) with the Nikolčice-Kurdějov horst (Nikolčice-5 well), crosses the Vranovice and the Nesvačilka depressions, and ends on the SW flank of the Ždánice high. This profile was verified in the above-mentioned wells, and generally documents the marginal carbonate platform. The thickness of the Jurassic sediments reaches about 500 m. According to the profile in Fig. 7, the development of both Paleogene depressions was similar. In contrast to the profile situated in the deeper part of the area (Fig. 7), erosion has clearly been the dominant controlling mechanism for the Vranovice depression.

Structurae and isochore maps

The structural contour map of the top of the pre-Tertiary relief (Fig. 10) shows essential features and structural elements. The contour interval is 100 m in the shallow part and 200 m in the deepest part of the area. Elevation is indicated in metres above sea level. The NW-SE trend of the regional tilting of the individual blocks (Vranovice, Nesvačilka and Nikolčice-Kurdějov high) is evident, as well as a relatively gradual slope in the deeper part of the area to the southeast. The roughly NW-SE trending depressed zones are the most prominent elements within the pre-Tertiary relief, and the map displays their deepening towards the SE. In the largest part of the area of the Vranovice depression, and partly in the area of the Nesvačilka depression, the Jurassic sediments were largely removed by deep but selective erosion. Thus, the crystalline basement and the Lower Carboniferous Culm or sediments of Dogger age form the pre-Tertiary relief. Only remnants exist on tectonically limited blocks, namely on the SW slope of the Nesvačilka depression (Figs 7, 8).

Isochore map

The Jurassic isochore map (Fig. 11) clearly shows the thicknesses of both Jurassic developments in the area of interest, except the non-depositional area in the Vranovice and the Nesvačilka depressions. While the deposition on the Pavlov-Waschberg block is symmetric, that on the Nikolčice-Kurdějov high and the Nesvačilka depression is distinctly asymmetric due to the different tectonic development of these blocks. Thicknesses reach up to 1100 m on the Pavlov-Waschberg block, 2000 m on the Nikolčice-Kurdějov high, and at about 500 m on the Uhřice block. The Jurassic sediments of the marginal carbonate platform have been identified as remains, while the thickness of the basinal facies (Mikulov marls) increases eastward under the flysch nappes. The continuation of the Ju-

Figure 9. Explanations for Figs 4–8.

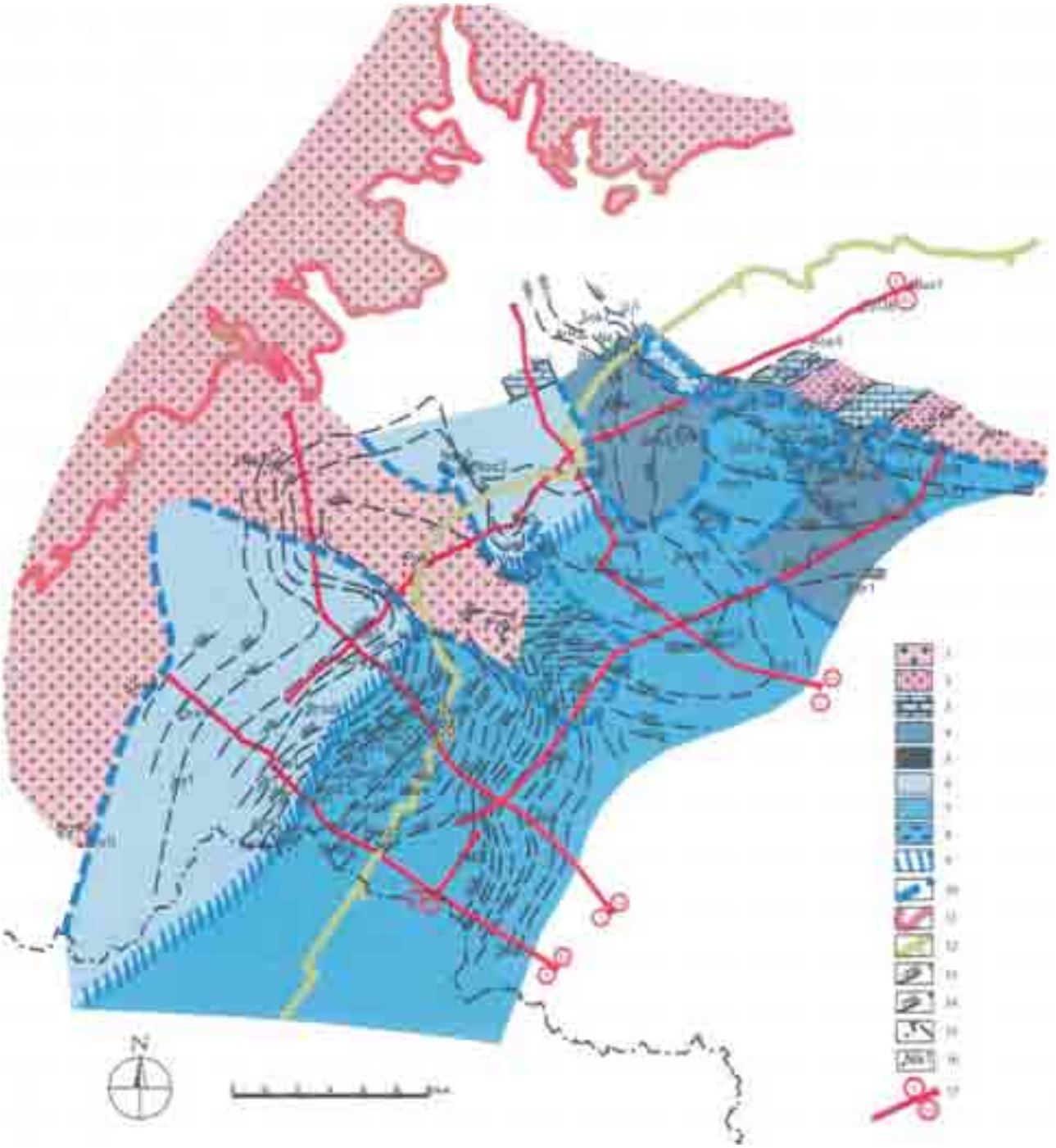

Figure 10. Structure contour map on the pre-Tertiary basement and situation of wells.
1 – Crystalline and Paleozoic basement, 2 – Paleozoic (?Cambrian–?Old-Red), 3 – Devonian, 4 – Lower Carboniferous, 5 – Upper Carboniferous with coal, 6 – Jurassic, carbonate platform, 7 – Jurassic, basinal development, 8 – Gresten Group and Nikolčice Formation, 9 – Mušov, transition zone of Jurassic facies, 10 – extension of Jurassic sediments, 11 – outcrop of Crystalline and Paleozoic basement, 12 – Carpathian thrust front, 13 – contours, 14 – isochors, 15 – state border, 16 – selected wells, 17 – direction of profiles.

rassic sediments to the Bohemian Massif (to the NW) and to the Western Carpathians (to the SE) is not depicted. Marginal carbonates, basinal facies, and the transition zone between both Jurassic developments are depicted on this map, and the transition zone is indicated by a dashed line. The transition zone named as the Mušov Zone (Adámek 1974, 1977) represents the changing of the facies in the seismic image between both main facies developments, which, together with normal faulting, plays a very important role from the petroleum perspective. The marginal carbonate platform seems to be an open hydrogeological structure, while the basinal facies (pelitic-carbonatic development), is closed and of interest for petroleum exploration (Polesňák and Adámek 1983, 1986).

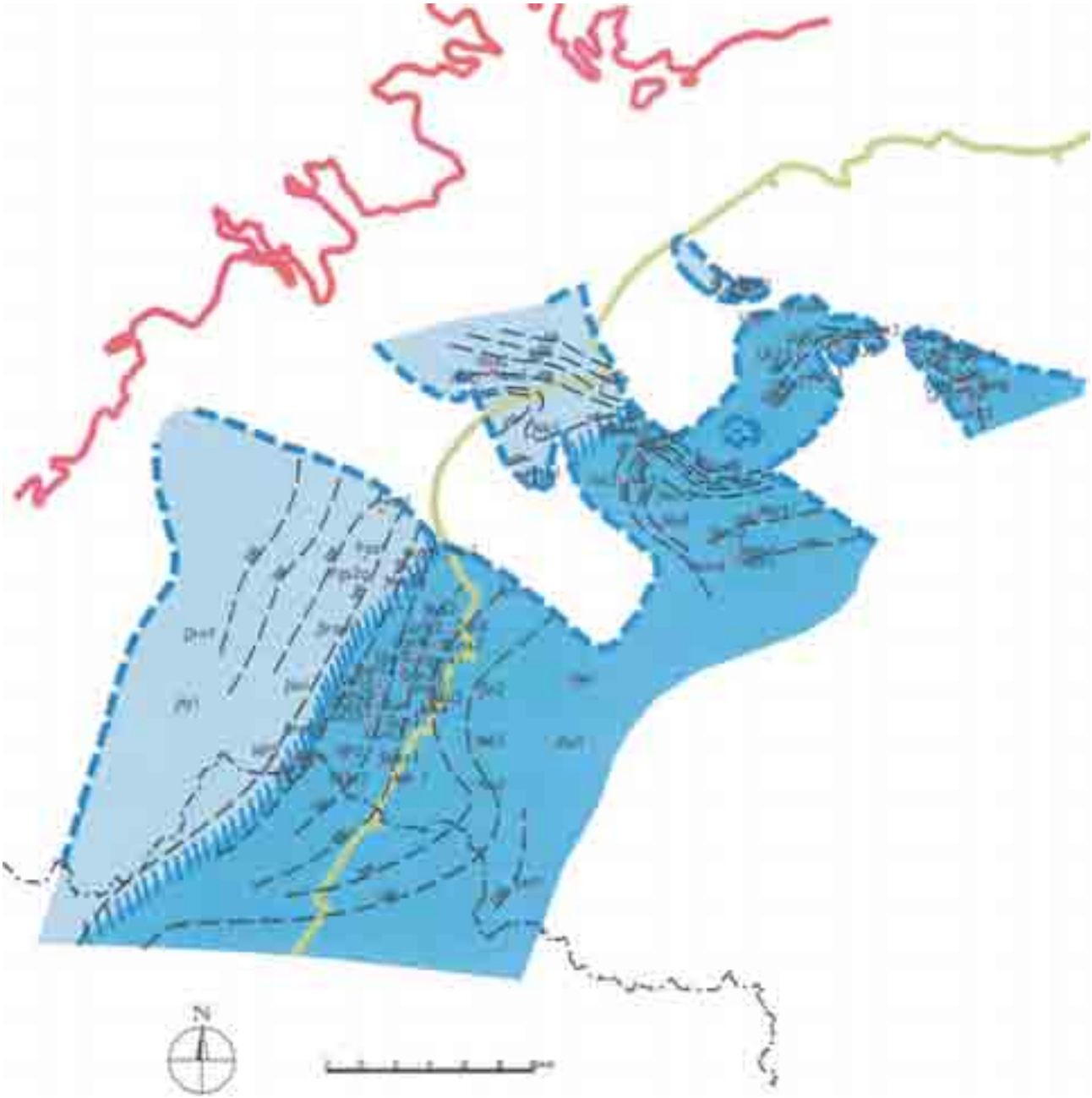

Figure 11. Isochore map of Malmian sediments and facies distribution.

Petroleum geology

Reservoir rocks

In the study area, the most important reservoir rocks are the Gresten Group (Dogger sandstone facies), the Nikolčice Formation (Callovian sandstones and sandy dolomites), and the Vranovice Formation (Oxfordian limestones and dolomites). In these lithostratigraphic units the most important hydrocarbon reservoirs are situated not only in southern Moravia (Dambořice, Žarošice and Uhřice – south oil fields), but also in Lower Austria (Höflein). Within the Gresten sandstone facies, the values of porosity in the Dambořice oil field range between 15–25 %, while their permeability ranges from 100 to 1000 (8000) md (Kostelníček and Thonová 1994). In the Höflein field, the Höflein and Gresten lithostratigraphic units are stated as the gass-bearing strata. For the Höflein Formation (analogous to the dolomitic development of the Nikolčice Formation in southern Moravia), porosity values reach 25.4 % and permeability values vary between 131–1119 md. In the Gresten Sandstone underlying the Höflein fields, the Höflein Formation porosity and permeability values are 21.2 % and 516–3236 md, respectively (Grün 1984, Sauer et al. 1992, Zimmer and Wessely 1996).

Source rocks

The Mikulov Formation (marl facies) buried under the flysch units is indicated as the prominent hydrocarbon

source rocks based on a series of geochemical studies (Ladwein 1988, Franců et al. 1996, Pícha and Peters 1998). The total TOC values recognized within the Mikulov Formation vary between 0.2–10 % with an average value of 1.9 %. Marl of the Mikulov Formation is considered to be the principal hydrocarbon source not only for the hydrocarbon deposits in the Vienna Miocene sedimentary fill, but also for its foreland in southern Moravia and adjacent regions (Pícha 1966, Krejčí et al. 1994, Ciprys et al. 1995, Franců et al. 1996, Zimmer and Wessely 1996). The source rock potential of the Mikulov Formation evidently increases eastward under the flysch nappes. There were found indications of noncommercial hydrocarbon accumulations in the area of interest and adjacent areas in all the potential sedimentary sequences. We suppose that the hydrocarbon indications confirm the idea of young Miocene migration processes, and hence of possible subsequent hydrocarbon filling of the potential traps. Practically all of the hydrocarbons could have been generated after the overthrusting of the flysch nappes. Migration processes took place both laterally and vertically. Migration pathways within fractured rocks along the young or older Miocene reactivated fault systems had great importance.

Sealing

The pelitic facies of Jurassic (Mikulov Formation) are generally considered as the sealing horizon for the older Dogger and Malm (Gresten-Group sandstone facies, Nikolčice and Vranovice formations). Besides lateral facies changes, normal faults played an important sealing role, depending on their displacement and the thickness of the facies.

Conclusions

In this article, an interpretation of the Jurassic strata under the Miocene sediments of the Carpathian Foredeep and the flysch nappes in the southwestern part of the Carpathians is presented. The cross sections document in detail the Doggerian and Malmian sediments, carbonatic and basinal facies, as well as geology in general, including tectonic patterns with dominant normal faults and overthrusts. The development of both the Doggerian and the Malmian sediments was different. From the petroleum perspective, the Doggerian clastics are important reservoir rocks for the whole Jurassic strata. A model for the distribution of the Malmian facies was demonstrated. The moderately dipping slope of the carbonate platform is characteristic of the study area. The longitudinal profiles exhibit the southwestern margin of the Variscan area with different structural features of the Jurassic on the Pavlov-Waschberg and the SW part of Central Moravian blocks. Isopachs and facies maps show the extent of Malmian sediments by means of seismic and well data. The structural contour map displays the essential features and structural elements of the pre-Tertiary relief. The isochore map shows the thicknesses of both of the Jurassic developments and the non-depositional areas in the Vranovice and the Nesvačilka grabens.

Acknowledgements. The author wishes to thank the Moravské Naftové Doly a. s., Hodonín for geological data.

Constructive comments from RNDr. Z. Stráník, DrSc. and RNDr. V. Dvořáková contributed to final form of the manuscript. Z. Jurová and H. Repková drew the figures. The author appreciates especially the assistance of Dr. G. Wessely who carefully reviewed the paper.

References

Adámek J. (1974): Projekt geologických prací. Pionýrský průzkum oblasti Mušov-Dolní Dunajovice, II. etapa. MS MND Hodonín (in Czech).

Adámek J. (1977): Několik poznámek o nových výsledcích v oblasti jižní části karpatské předhlubně. Zem. Plyn Nafta 22, 1, 7–12 (in Czech).

Adámek J. (1978): Plynové ložisko Dolní Dunajovice a geologická stavba jižní části karpatské předhlubně. Zem. Plyn Nafta 24, 1, 11–21 (in Czech).

Adámek J. (1985): Výsledky a perspektivy průzkumu na ropu a zemní plyn v úseku Jih jv. svahů Českého masívu. Geol. Průzk. 27, 2, 35–38 (in Czech).

Adámek J. (1986): Geologické poznatky o stavbě mezozoika v úseku Jih jv. svahů Českého Masivu. Zem. Plyn Nafta 31, 4, 453–484 (in Czech).

Adámek J. (1990): New findings of the deep structure of the southeastern slopes of the Bohemian Massif (southern section – Němčičky Block). In: Minaříková H., Lobitzer H. (eds) Thirty years of geological cooperation between Austria and Czechoslovakia. Federal geological Survey Vienna – Geological Survey Prague, Praha, 11–16.

Adámek J. (2001): Regionálně-geologické zhodnocení sedimentů jury v oblasti jihovýchodních svahů Českého masívu. (Regional-geological evaluation of the Jurassic sediments on the southeast margin of the Bohemian Massif). Zpr. geol. Výzk. v Roce 2001, 9–11 (in Czech).

Adámek J., Dvořák J., Kalvoda J. (1980): Příspěvek ke geologické stavbě a naftově geologickému hodnocení nikolčicko-kurdějovského hřbetu. Zem. Plyn Nafta 25, 4, 379–441 (in Czech).

Adámek J., Michalíček. (1990): Mušov-3 (G) První vyhledávací vrt na termální vodu na jižní Moravě. Zem. Plyn Nafta 35, 2, 113–122 (in Czech).

Brix F., Kröll A., Wessely G. (1977): Die Molassezone und deren Untergrund in Niederösterreich. Erdöl Erdgas Z. 93, Sonderausgabe, 12–35.

Ciprys V., Adámek J., Benada S. (1995): Petroleum geology of the Carpathian Foredeep and overthrust zones in the Czech Republic. Petrol. Geosci. 1, 89–96.

Dudek A. (1980): The crystalline basement block of the Outer Carpathians in Moravia: Bruno-Vistulicum. Rozpr. ČSAV řad. mat.-přírod. 90, 8, 1–85.

Dvořák J. (1978): Geologie paleozoika v podloží Karpat jv. od Drahanské vrchoviny. Zem. Plyn Nafta 23, 2, 185–203 (in Czech).

Eliáš M. (1962): Zpráva o sedimentárně petrografickém výzkumu klentnických vrstev a ernstbrunnských vápenců. Zpr. geol. Výzk. ÚÚG v roce 1961, 196–198 (in Czech).

Eliáš M. (1969): Zpráva o sedimentologickém výzkumu brněnské jury. Zpr. geol. Výzk. ÚÚG v roce 1968, 216–219 (in Czech).

Eliáš M. (1974): Mikrofaciální výzkum karbonátů naftonadějných oblastí na příkladě autochtonní jury jv. svahů Českého masivu. Zem. Plyn Nafta 19, 3, 359–374 (in Czech).

Eliáš M. (1977): Paläogeographische Entwicklung des Mesozoikums und des Tertiärs am Rande der Karpaten und des Böhmischen Massifs. Erdöl Erdgas Z. 93. Sonderausgabe, 5–11.

Eliáš M. (1981): Facies and paleogeography of the Jurassic of the Bohemian Massif. Sbor. geol. Věd, Geol. 35, 75–144.

Eliáš M. (1984): Facies and paleogeography of the Jurassic in the western part of the Outer Flysch Carpathians in Czechoslovakia. Sbor. geol. Věd, Geol. 39, 105–170.

Eliáš M. (1992): Sedimentology of the Klentnice Formation and the

Ernstbrunn Limestone (Ždánice–Subsilesian unit of the Outer West Carpathians). Bull. Czech Geol. Surv. 67, 3, 179–192.

Eliáš M., Wessely G. (1990): The autochthonous Mesozoic on the eastern flank of the Bohemian Massif – an object of mutual geological efforts between Austria and Czechoslovakia. In: Minaříková H., Lobitzer H. (eds) Thirty years of geological cooperation between Austria and Czechoslovakia. Federal Geological Survey Vienna – Geological Survey Prague, Praha, 78–83.

Fatka O., Vavrdová M. (1998): Early Cambrian Acritarcha from sediments underlying the Devonian in Moravia (Měnín-1 borehole, Czech Republic). Bull. Czech Geol. Surv. 73, 1, 55–60.

Franců J., Radke M., Schaefer R. G., Poelchau H. S., Čáslavský J., Boháček Z. (1996): Oil-oil and oil-source rock correlations in the northern Vienna basin and adjacent Carpathian Flysch Zone (Czech and Slovak area). In: Wessely G., Liebl W. (eds) Oil and gas in Alpidic thrustbelts and basins of Central and Eastern Europe. EAGE Special Publication 5, Geological Society, London, 343–353.

Grün W. (1984): Die Erschliesung von Lagerstätten im Untergrund der alpin-karpatischen stirnzone Niederösterreichs (The exploration of reservoirs in the basement of the Alpine-Carpatian frontal zone of Lower Austria). Erdöl Erdgas Z. 100, 9, 292–295.

Harding T. P., Tuminas A. C. (1989): Structural interpretation of hydrocarbon traps sealed by basement normal block faults at stable flank of foredeep basins and at rift basins. AAPG Bull. 78, 812–840.

Chmelík F. (1969): Základní rysy geologického vývoje a stavby karpatského pásma střední Moravy. Zpr. geol. Výzk. v Roce 1967, 196–198 (in Czech).

Jachowicz M., Přichystal A. (1997): Nález spodnokambrických sedimentů v hlubokých vrtech na jižní Moravě. Zpr. geol. Výzk. Mor. Slez. v Roce 1996, 64 (in Czech).

Jiříček R. (1990): Paleogeografie mezozoika na styku alpsko-karpatské oblasti. Biostratigrafické a sedimentologické studie v mezozoiku Českého masivu a Západních Karpat. Knih. Zem. Plyn Nafta 9b, 147–184 (in Czech).

Kapounek J., Kröll A., Papp A., Turnovsky K. (1967): Der Mezozoische Sedimentmantel des Festlandsockels der Böhmischen Masse. Jb. Geol. Bundesanst. 110, Wien.

Kostelníček P., Thonová H. (1994): Nové výsledky průzkumné činnosti na ložisku Dambořice (Uhřice II). 2nd International Conference, Oil and gas business activities. Luhačovice, 19–25 (in Czech).

Krejčí O., Franců J., Müller P., Pereszlenyi M., Stráník Z. (1994): Geologic structure and hydrocarbon generation in the Carpathian flysch belt of southern Moravia. Bull. Czech Geol. Surv. 69, 13–26.

Krejčí O., Franců J., Poelchau H. S., Müller P., Stráník Z. (1996): Tectonic evolution and oil and gas generation at the border of the North European Platform with the West Carpathians (Czech Republic). In: Liebl W., Wessely G. (eds) Oil and Gas in Alpidic Thrustbelts and Basins of Central and Eastern Europe. EAGE Special Publication 5, Geological Society, London, 177–185.

Krystek I., Samuel O. (1978): Výskyt kriedy karpatského typu severne od Brna (Kuřim). Geol. práce. Spr. 71 (in Slovak).

Ladwein, H. W. (1976): Sedimentologische Untersuchungen an Karbonatgesteinen des autochthonen Malm in NÖ (Raum Altenmarkt – Staatz). Diss. Phil. Fak. Univ. Innsbruck.

Ladwein H. W. (1988): Organic Geochemistry of Vienna Basin: Model for Hydrocarbon Generationin Overthrust Belts. AAPG Bull. 72, 586–599.

Polesňák P., Adámek J. (1983): Hydrogeochemické hodnocení širší oblasti Dolních Dunajovic v moravské části karpatské předhlubně. Zem. Plyn Nafta 28, 4, 529–549 (in Czech).

Polesňák P., Adámek J. (1986): Hydrogeologické hodnocení širší oblasti ložiska Dolní Dunajovice. Geol. Průzk. 28, 4, 97–100 (in Czech).

Pícha J. F. (1966): Exploring for hydrocarbons under thrust belts – a challenging new frontier in the Carpathians and elsewhere. AAPG Bull. 80, 4, 1547–1564.

Pícha J. F. (1979): Nesvačilka Formation – a new name for the strata of the autochthonous Paleogene in South Moravia. Čas. Mineral. Geol. 24, 3, 305–311 (with English summary).

Pícha J. F., Peters E. (1998): Biomarker oil-to-source rock correlation in the Western Carpathians and their foreland, Czech Republic. Petrol. Geosci. 4, 289–302.

Pícha J. F., Stráník Z., Krejčí O. (in print): Geology and hydrocarbon resources of the outer West Carpathians and their foreland, Czech Republic. In: Golonka J., Pícha J. F. (eds) The Carpathians and their foreland: geology and hydrocarbon resources. AAPG Memoir 84.

Řehánek J. (1977): Problematika mikrofaciálního studia mezozoických karbonátů jv. svahů ČM. Zem. Plyn Nafta 22, 1, 71–78 (in Czech).

Řehánek J. (1978): Mikrofacie a mikrofauna (Incertae sedis) písčito-glaukonitové série svrch. křídy v podloží karpatské předhlubně a vnějšího flyšového pásma na jižní Moravě. Zem. Plyn Nafta 23, 4, 327–345 (in Czech).

Řehánek J. (1984): Nález mořského svrchního albu Českého masivu na jižní Moravě. Geol. práce 81, 87–101 (in Czech).

Řehánek J. (1985): Cadosinidae Wanner and Stomiosphaeridae Wanner (incertae sedis) from the Mesozoic limestones of southern Moravia. Čas. Mineral. Geol. 30, 4, 367–380.

Řehánek J. (1987): Faciální vývoj a biostratigrafie ernstbrunnských vápenců (stř.–svrch. tithon, jižní Morava). Geol. Práce, Zpr. 87, 27–60 (in Czech).

Řehánek J., Leereveld H., Verreussel R. M. C. H., Salaj J. (1996): Biostratigraphy and lithofacies pattern of the Gresten Formation (Dogger) in South Moravia (Czech Republic), with emphasis on reworked Triassic material. Jb. Geol. B.-A. 139, 4, 505–521.

Sauer R., Seifert P., Wessely G. (1992): Guidebook to Excursions in the Vienna Basin and the adjacent Alpine-Carpathian Thrustbelt in Austria. Mitt. Österr. Geol. Ges. 85, Wien.

Stráník Z., Adámek J., Ciprys Z. (1979): Geologický profil karpatskou předhlubní, flyšovým pásmem a vídeňskou pánví v oblasti Pavlovských vrchů. Tektonické profily Západných Karpat. Geol. úst. D. Štúra, 7–12 (in Czech).

Stráník Z., Benešová E., Pícha F. (1968): Geologie hlubinného vrtu Bulhary–1. Sborník geol. věd. Geol. 13, 75–131 (in Czech).

Stráník Z., Dvořák J., Krejčí O., Müller P., Přichystal A., Suk M., Tomek Č. (1993): The contact of the North European Platform with the West Carpathians. J. Czech. Geol. Soc. 38, 1–2, 21–29.

Špička V. (1976): Hlubinná geologická stavba autochtonu na jižní Moravě a jeho perspektivnost pro ropu a plyn. Sbor. geol. Věd, Geol. 28, 7–128 (in Czech).

Vašíček Z. (1980): Příspěvek k biostratigrafii autochtonního malmu na jv. svazích Českého masívu. Sbor. věd. Prací Vys. Šk. báň. v Ostravě, Ř. horn.-geol. 24 (1978), 1, 29–46 (in Czech).

Wessely G. (1988): Der Tiefenaufschluß im Wiener Becken und der Molassezone als Ausgangspunkt für die Alpenexploration in Österreich. Erdöl Erdgas Kohle Z. 11, 435–440.

Wessely G. (in print): Geologie von Niederösterreich. Geologische Bundesanstalt Wien.

Wilson J. L. (1975): Carbonate facies in geologic history. Springer, Berlin.

Zimmer W., Wessely G. (1996): Exploration results in thrust and subthrust complexes in the Alps and below the Vienna Basin in Austria. In: Wessely G., Liebl W. (eds) Oil and gas in Alpidic Thrustbelts and Basins of Central and Eastern Europe. EAGE Special Publication 5, Geological Society, London, 81–107.

Bulletin of Geosciences, Vol. 80, No. 4, 307–319, 2005
© Czech Geological Survey, ISSN 1214-1119

Pb-Zn-Ag vein mineralization of the central part of the Českomoravská vrchovina Upland (Czech Republic): S, C, and O stable isotope study

Karel Malý [1] *– Zdeněk Dolníček* [2]

[1] Muzeum Vysočiny Jihlava, Masarykovo náměstí 55, 586 01 Jihlava, Czech Republic. E-mail: maly@muzeum.ji.cz
[2] Palacký University, Department of Geology, tř. Svobody 26, 771 46 Olomouc, Czech Republic. E-mail: dolnicek@prfnw.upol.cz

Abstract. The central part of the Českomoravská vrchovina Upland (Czech Republic) is characterized by the presence of base-metal vein mineralizations of various origins. Three groups of mineralizations were distinguished based on sulfur isotope analyses of sulfides and barite (329 analyses in total), and the carbon and oxygen isotope analyses of carbonates (124 analyses in total). 1) High-temperature mineralizations (ca 400–500 °C) show source sulfur values between +3 and +5 ‰ CDT, and are derived from metamorphic or granitic rocks of the Moldanubicum. $\delta^{18}O$ values of carbonates are high; $\delta^{13}C$ values are low, indicating the involvement of originally organic carbon in the hydrothermal process. 2) Mesothermal mineralizations (ca 200–350 °C) show source sulfur values that are either markedly positive (up to +10 ‰ CDT) or within the range of ca –3 to +3 ‰ CDT. The $\delta^{18}O$ values of water in the hydrothermal fluid were usually higher than 5 ‰ SMOW, with water of low $\delta^{18}O$ values being sometimes involved in the final stages of the mineralization processes (meteoric or marine waters). The values of $\delta^{13}C$ correspond to homogenized carbon of the Earth's crust, locally affected by carbon from marbles/limestones. 3) Low-temperature mineralization (< 130 °C) shows markedly negative sulfane fluid values, whereas the sulfate values range from +11 to +14 ‰ CDT. In its $\delta^{13}C$ values, the carbon of the fluids corresponds to homogenized crustal values (with local influence of carbon from limestones and oxidized organic matter). The water of the hydrothermal fluid shows values around 0 ‰ SMOW, thus indicating a prevalence of (i) marine water, (ii) meteoric water, or (iii) a mixture of waters of various origins in the hydrothermal system. The first and the third mineralization types can be considered as distinct genetic categories (minerogenetic type): high-temperature mineralizations are genetically associated with Variscan magmatic and metamorphic processes, while the low-temperature mineralizations are genetically associated with hypersaline brines of a still controversial but possibly marine origin. The mesothermal type most probably includes mineralizations genetically linked with a variety of geological processes.

Key words: polymetallic mineralization, stable isotopes, Českomoravská vrchovina Upland

Introduction

The Českomoravská vrchovina Upland is constrained by the western exocontact of the Moldanubian pluton in the west, the rim of the Boskovice Graben in the east, and by sediments of the Bohemian Cretaceous Basin in the north. The metallic ores deposits of the central part of this unit are typical of numerous occurrences of Pb-Zn-Ag vein mineralization. Most of the sites have been mined or at least explored using mining techniques as early as the Middle Ages, and the last prospecting and mining took place there in the mid-20th century. Some deposits constitute historically significant ore districts with numerous sites (e.g., Jihlava Ore District, Havlíčkův Brod Ore District), while others are completely isolated. The deposits are hosted by various regional-geological units.

The metallogenic characteristics of these sites are not unified and have been the subject of controversy (e.g., Bernard 1991, Češková 1978). Most of the sites have not been subjected to modern methods of study, or else the relevant data are unpublished or scattered in a number of incomplete scientific reports. Only one deposit has so far been investigated using modern analytical methods: the Rožná uranium deposit (with vein-sulfide, stratiform barite-hyalophane etc. type mineralizations, e.g., Hladíková et al. 1995, Kříbek et al. 1996). This deposit is therefore not discussed here.

The present article is intended to summarize all available data on the S, C, and O stable isotope geochemistry of these deposits, and to supplement it with new analytical data. The material thus gathered was used for establishing some genetic conditions of the origin of the Pb-Zn-Ag vein mineralization in this part of the Bohemian Massif. The present study is also a contribution to the discussion on metallogenic subdivision of the Bohemian Massif and on the metallogenic typology of this mineralization type.

Characteristics of the studied sites

The site locations are shown in Fig. 1. Their general economic-geological characteristics are given below (Table 1). Combined characteristics are given for historically or geographically delimited ore districts consisting of two or more deposits. Mineralogical and economic-geological studies are referred only if published in the recent past.

Methods

Sulfur, carbon, and oxygen isotope analyses were carried out on a Finnigan MAT 251 mass spectrometer in the laboratories of the Czech Geological Survey (analysts K. Žák, J. Hladíková). The samples were prepared for measurement using standard methods: sulfides were oxidized by CuO to SO_2 at 800 °C (Grinënko 1962); SO_2 from barite was liberated by heating with a mixture of V_2O_5 and SiO_2 at

Figure 1. Position of the studied sites in a schematic geological map.

1050 °C; carbonates were decomposed by 100% H_3PO_4 (McCrea 1950). The measured values were related to conventional standards: CDT ($\delta^{34}S$), PDB ($\delta^{18}O$, $\delta^{13}C$ of carbonates), and SMOW ($\delta^{18}O$ of water). Measurement precision was ±0.2 ‰ for $\delta^{34}S$ in sulfides; ± 0.3 ‰ for $\delta^{34}S$ in barite; ±0.1 ‰ for $\delta^{18}O$ in carbonates; ±0.1 ‰ for $\delta^{13}C$ in carbonates.The $\delta^{34}S$ values of the source sulfur and isotope thermometry was determined using the equation of Ohmoto and Rye (1979). $\delta^{18}O$ values of hydrothermal fluids were estimated from those of carbonates, in accordance with O'Neil et al. (1969).

Most of the data presented here are original, with some being adopted from earlier published studies. In contrast, most isotope data for minerals from the Jihlava Ore District (site 5) come from an unpublished study by Vosáhlo (1988). Some data on the Havlíčkův Brod Ore District (site 2) come from a published source (Bernard and Žák 1992) and an unpublished database by Žák (Czech Geological Survey, Praha). The data sources are not specified in the text below.

Results

The results of isotope analyses of sulfur in sulfides and barite are summarized in Fig. 2 (329 analyses in total). The results of the isotope analyses of C and O in the carbonates are summarized in Fig. 3 (124 analyses in total).

Discussion

Sulfur isotopes in sulfides and barite

Isotopic relations among minerals

The data and their distribution permit the characterization of some properties of the hydrothermal fluids (or, more exactly, the degree of variability of these properties), which control the establishment of $\delta^{34}S$ values of the minerals formed (sulfides and possibly barite). These properties include the $\delta^{34}S$ value of source sulfur in the hydrothermal fluid, temperature, pH, Eh and sulfur activity in the fluid.

It can be stated that:

– Data dispersal is relatively small for most sites. This evinces minor variability of the above parameters.
– Site 14 in the Tišnov area and site 16 in Maršov are exceptional. Here, the variability in the $\delta^{34}S$ values in sulfides is probably due to major local Eh differences in the hydrothermal fluid. A prominent dispersal in $\delta^{34}S$ values was also observed at site 3 in the Dačice-Slavonice area. This can also be explained by the low Eh stability in the fluid. Another less likely possibility is that the sulfides analyzed may belong to different mineralization stages, characterized by different temperatures of mineral crystallization, and different $\delta^{34}S$ values of sulfane in the fluid. This possibility cannot be excluded due to the poorly known succession of relations at the site.
– Prominent outliers in the $\delta^{34}S$ values of pyrite were observed in some cases (e.g., site 6 Měřín, site 3 Dačice-Slavonice area). This can be explained by the fact that, in most cases, pyrite is formed throughout the existence of the hydrothermal fluid, and its isotope composition reflects changes in fluid properties. For example, pyrite with value $\delta^{34}S = -15.7$ ‰ from the site 6 Měřín was formed only in the final stage of mineralization, during which an increase in oxygen fugacity can be presumed. Another possible explanation is a different mechanism of pyrite (and chalcopyrite) formation: their precipitation from sulfane-containing fluids requires an oxidation mechanism, contrary to that of simple sulfides (Ohmoto 1986).
– $\delta^{34}S$ values of individual minerals at most of the studied sites indicate the establishment of isotopic equilibrium (with a few exceptions – mostly in pyrite). $\delta^{34}S$ values can be therefore used for thermometric calculations (see below). The absence of isotope equilibrium among sulfur-containing minerals is evident only at site 3 Dačice-Slavonice, site 14 Tišnov, and site 16 Maršov: the application of isotope thermometry on the deposits at those sites is therefore problematic or impossible.

Sulfur isotope thermometers

Sphalerite-galena pairs were preferably used for the purpose of isotope thermometry. These minerals are common at sulfidic deposits and show sufficiently contrasting fractionation with respect to sulfane. Thermometry pairs with pyrite do not generally yield geologically realistic temperatures (see explanation above).

Sulfide-barite isotope pairs from the studied sites did not yield geologically realistic temperatures. This may be explained as follows:

– Barite was formed at a different stage of fluid development than were the sulfides (sphalerite, galena), thus precluding the establishment of isotopic equilibrium. This explanation can be suggested (based on succession relations) for site 5 Jihlava, mineralizations 5.2,

Table 1. Characteristics of the studied sites

Locality – Ore district	Site examples	Sites studied	Regional-geological unit	Host rock of the deposit	Ore minerals			Gangue minerals		Relative size of the deposit (occurrence)	Principal mineralogical and economic-geological studies
					major	minor	accessory	major	minor		
1. Pelhřimov Ore District	Pavlov, Branišov, Vyskytná, Proseč, Rohozná, Těšenov, Zadní Pole	Nemojov	Moldanubicum	granite (Moldanubian pluton), paragneiss	pyrite, Fe-sphalerite	arsenopyrite, galena, pyrrhotite	chalcopyrite, tetrahedrite, freibergite, acanthite	quartz	siderite, ankerite, dolomite	minor deposits mined in the past	Litochleb (2001)
2. Havlíčkův Brod Ore District	Česká Bělá, Stříbrné Hory, Utín, Mírovka, Dlouhá Ves, Bartoušov, Pohled, Svatý Kříž	Česká Bělá, Stříbrné Hory, Utín, Dlouhá Ves, Bartoušov, Pohled	Moldanubicum	paragneiss, granite (Moldanubian pluton), granite porphyry	pyrite, pyrrhotite, Fe-sphalerite	galena, arsenopyrite	tetrahedrite, pyrargyrite, marcasite, chalcopyrite, cassiterite, argentite, stannite	quartz	Fe-Mg-Mn carbonate	large deposits mined from the Middle Ages to 20th century	Pokorný (1964), Holub and Tenčík (1973), Dobeš and Malý (2001)
3. Dačice-Slavonice area	Vlastkovec, Radlice, Horní Radíkov, Valtínov, Český Rudolec-Markvarec	Vlastkovec, Radlice, Horní Radíkov	Moldanubicum	Granite (Moldanubian pluton), paragneiss	pyrite, sphalerite, galena	chalcopyrite	argentite, chalcocite, covellite, silver, naumannite	quartz		minor deposits mined in the past	no studies
4. Dobrá Voda			Moldanubicum	paragneiss, granite (Moldanubian pluton)	pyrite, Fe-sphalerite, galena	arsenopyrite, chalcopyrite, pyrrhotite	tetrahedrite	quartz	siderite	minor deposits mined in the past	Stýblo (1972)
5. Jihlava Ore District Pluskal and Vosáhlo (1998) distinguish six types of mineralization in the Jihlava Ore District:											
5.1. black sphalerite + Fe-sulphide ± carbonates	Kamenná, Jihlava-Rudný, Jihlava-Pfaffenhof, Jezdovice	Kamenná, Hybrálec, Ježená, Hosov, Popice, Jezdovice	Moldanubicum	paragneiss, granite (Moldanubian pluton), durbachite (Jihlava Massif)	pyrite, sphalerite, galena	chalcopyrite, arsenopyrite, pyrrhotite	tetrahedrite, argentite, pyrargyrite	quartz	carbonates Fe-Mg-Mn type, dolomite – ankerite	large deposits mined from the Middle Ages	Pluskal and Vosáhlo (1998), Vosáhlo (1988)
5.2. dark brown sphalerite ± barite ± carbonates	Malý Beranov, Kosov, Sasov	Malý Beranov, Kosov, Sasov	Moldanubicum	paragneiss, granite (Moldanubian pluton), durbachite (Jihlava Massif)	sphalerite, galena	chalcopyrite	tetrahedrite, silver, argentite, pyrargyrite	quartz, barite	dolomite – ankerite, calcite	large deposits mined from the Middle Ages	Pluskal and Vosáhlo (1998), Vosáhlo (1988)

Table 1, continued

Locality – Ore district	Site examples	Sites studied	Regional-geological unit	Host rock of the deposit	Ore minerals			Gangue minerals		Relative size of the deposit (occurrence)	Principal mineralogical and economic-geological studies
					major	minor	accessory	major	minor		
5.5. quartz ± pyrite	Ježená, Hlávkov, Jezdovice, Vílanec	it was not studied in this article	Moldanubicum	paragneiss, granite (Moldanubian pluton), durbachite (Jihlava Massif)	pyrite			quartz			Pluskal and Vosáhlo (1998), Vosáhlo (1988)
5.6. psilomelane ± chalcedony	Malý Beranov, Kosov	it was not studied in this article	Moldanubicum	paragneiss, granite (Moldanubian pluton), durbachite (Jihlava Massif)	psilomelane			quartz, chlacedony			Pluskal and Vosáhlo (1998), Vosáhlo (1988)
6. Měřín	Měřín	Měřín	Moldanubicum	paragneiss, durbachite (Třebíč Massif)	sphalerite, galena	pyrite, chalcopyrite	pyrargyrite, tetrahedrite	quartz	barite	minor deposits mined in the past	Malý (2003)
7. Velké Meziříčí	Velké Meziříčí	Velké Meziříčí	Moldanubicum	durbachite (Třebíč Massif)	galena	sphalerite, pyrite, chalcopyrite	tetrahedrite, ullmanite	calcite, ankerite	siderite	mineralogical occurrence	no studies
8. Ptáčov	Ptáčov	Ptáčov	Moldanubicum	durbachite (Třebíč Massif)	chalcopyrite, galena			calcite, dolomite – ankerite		mineralogical occurrence	no studies
9. Jemnice	Jemnice	Jemnice	Moldanubicum	paragneiss, granulite	sphalerite, galena	chalcopyrite, pyrite	tetrahedrite – freibergite, polybasite	quartz	calcite, dolomite – ankerite	minor deposits mined in the past	Houzar and Pošmourný (1991), Zimák and Šendová (1999)
10. Štěpánov nad Svratkou Ore District Malý and Dobeš (2001) distinguish two types of mineralization in the Štěpánov Ore District											
10.1. Pb-Zn(-Sb) type	Horní Čepí, Švařec, Koroužné	Švařec, Koroužné	Moravicum – Svratka Dome, Olešnická Group	paragneiss, micaschist, marble, quartzite	galena, sphalerite	chalcopyrite	pyrite, antimonite, bournonite, tetrahedrite, freibergite, boulangerite, pyrargyrite	quartz	calcite, dolomite – ankerite	intermediate deposits mined in the past	Mátl (1965), Malý and Dobeš (2001), Houzar and Malý (2002)
10.2. Cu-Pb(-Zn) type	Borovec	Borovec	Moravicum – Svratka Dome, Olešnická Group	paragneiss, micaschist, marble, quartzite	galena, chalcopyrite	sphalerite	pyrite, tetrahedrite	quartz, barite	calcite	intermediate deposits mined in the past	Mátl (1965), Malý and Dobeš (2001), Houzar and Malý (2002)

Table 1, continued

Locality – Ore district	Site examples	Sites studied	Regional-geological unit	Host rock of the deposit	Ore minerals			Gangue minerals		Relative size of the deposit (occurrence)	Principal mineralogical and economic-geological studies
					major	minor	accessory	major	minor		
11. Rozseč nad Kunštátem	Rozseč nad Kunštátem	Rozseč nad Kunštátem	Moravicum – Svratka Dome, Olešnická Group	micaschist, marble, paragneiss	sphalerite, galena	tetrahedrite, bournonite	chalcopyrite, pyrite, marcasite, arsenopyrite, boulangerite	quartz, dolomite – ankerite	calcite	minor deposits mined in the past	Šouba and Mátl (1961), Malý (1999)
12. Štěchov-Lačnov	Štěchov- Lačnov	Štěchov-Lačnov	Moravicum – Svratka Dome, Olešnická Group	marble, micaschist	sphalerite, galena	pyrite		ankerite – dolomite		minor deposits mined in the past	Malý (1999)
13. Horní Loučky	Horní Loučky	Horní Loučky	Moravicum – Svratka Dome, Olešnická Group	paragneiss, marble, micaschist	sphalerite, galena	pyrite	arsenopyrite, marcasite	quartz	dolomite – ankerite, calcite	mineralogical occurrence	Hrazdil et al. (2003)
14. Tišnov area	Dřínová, Květnice, Dolní Loučky, Štěpánovice	Dřínová, Květnice, Dolní Loučky, Štěpánovice	Moravicum – Svratka Dome, (para-)autochthon unit	limestone, metagranitoid, quartzite	chalcopyrite, galena	pyrite	sphalerite, tetrahedrite, bravoite, gersdorffite	barite, calcite	quartz, fluorite	minor deposits mined in the past (barite)	Mátl (1960), Dolníček (1999), Dolníček (2001), Dolníček and Malý (2003), Dolníček (2004)
15. Heroltice	Heroltice	Heroltice	Moravicum – Svratka Dome, (para-)autochthon unit	limestone	galena, sphalerite	chalcopyrite	tetrahedrite, hessite	quartz	dolomite – ankerite, calcite	minor deposits mined in the past	Češková and Orel (1971), Malý (2004)
16. Maršov-Javůrek area	Maršov	Maršov	Moravicum – Svratka Dome, Bílý potok Group	micaschist, quartzite, limestone	chalcopyrite, galena	sphalerite, tetrahedrite, pyrite		quartz, barite	fluorite	minor deposits mined in the past	Mátl (1963), Malý and Dobeš (2002)
17. Jasenice	Jasenice	Jasenice	Moravicum – Svratka Dome, Olešnická Group	marble, paragneiss, micaschist	sphalerite, galena	tetrahedrite, chalcopyrite, pyrite, marcasite		quartz	barite, calcite, dolomite – ankerite	minor deposits mined in the past	Malý (2000)
18. Letovice	Letovice	Letovice	Letovice Crystalline Unit	serpentinite, amphibolite	galena, magnetite	chalcocite, chalcopyrite, covellite, sphalerite, bornite, pyrite, marcasite		dolomite	calcite	mineralogical occurrence	no studies

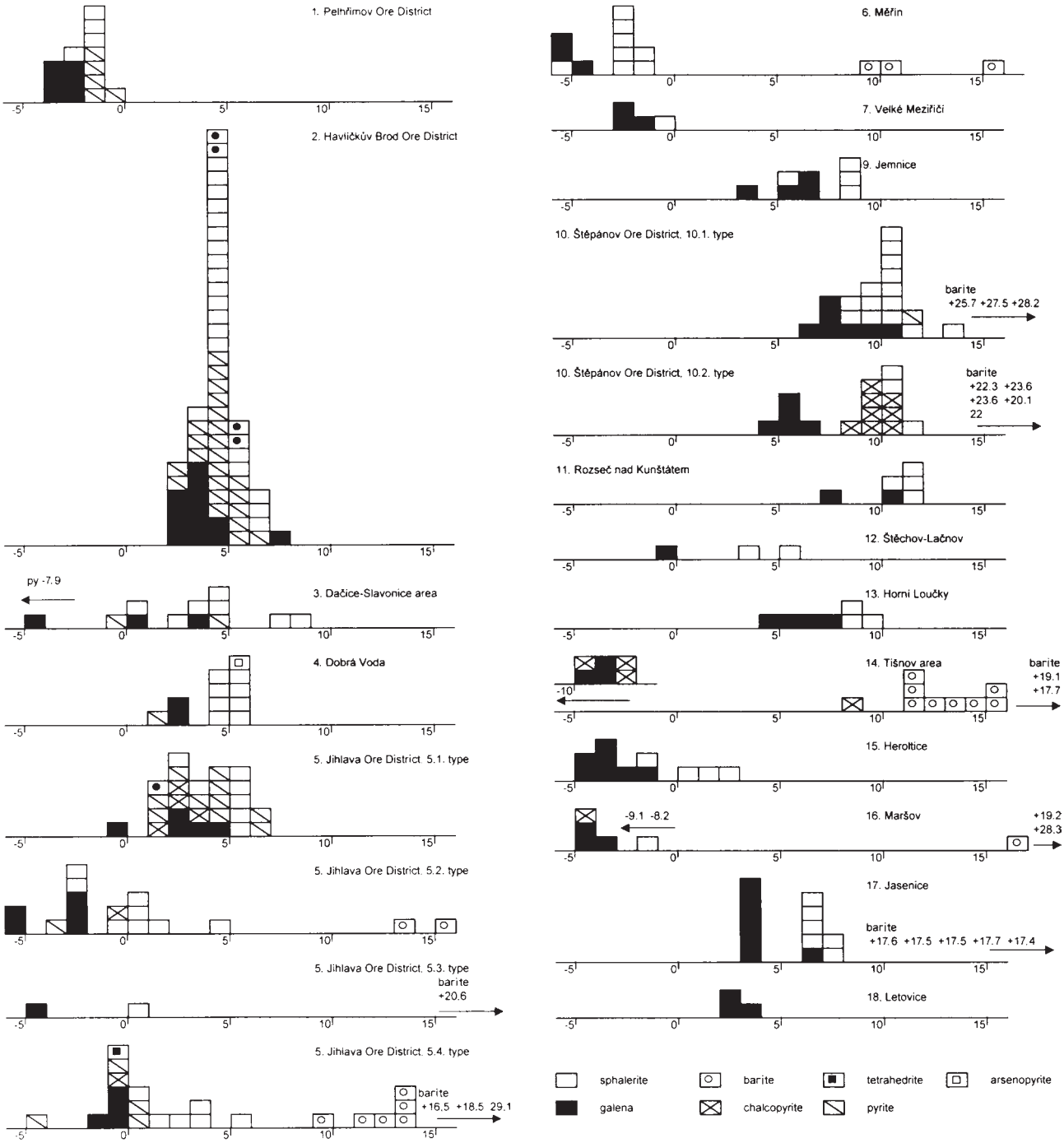

Figure 2. Isotope analyses of sulfur in sulfides and barite ($\delta^{34}S$ ‰, CDT).

5.3, 5.4, site 6 Měřín, site 10.1 Štěpánov Ore District, mineralization Pb-Zn(-Sb), and for site 17 Jasenice.

– The slow rate of isotope exchange reactions between sulfane and sulfate in the fluid at low temperatures (Ohmoto and Lasaga 1982), in which no isotopic equilibrium was established. This was probably the cause for sulfide-barite pair failure at all studied sites where barite is present.

Table 2 summarizes the geologically realistic temperatures of isotopic equilibria. These temperatures were calculated from average $\delta^{34}S$ values of sulfides at the given sites (outliers in $\delta^{34}S$ values were not included in the mean value calculation). Where a thermometric pair was available from a single hand specimen, the results are listed (including the minerals used) – temperatures thus obtained can be considered more realistic.

Based on the results of sulfur isotope thermometry, the studied sites can be subdivided into three groups:

1. High-temperature ore occurrences and deposits (ca 350 to 450 °C). This group includes site 1, the Pelhřimov Ore District; site 2, the Havlíčkův Brod Ore District; site 4, Dobrá Voda; and site 5, Jihlava, mineralization 5.1. Temperatures markedly exceeding 500 °C were sometimes obtained by isotope thermometry: such values

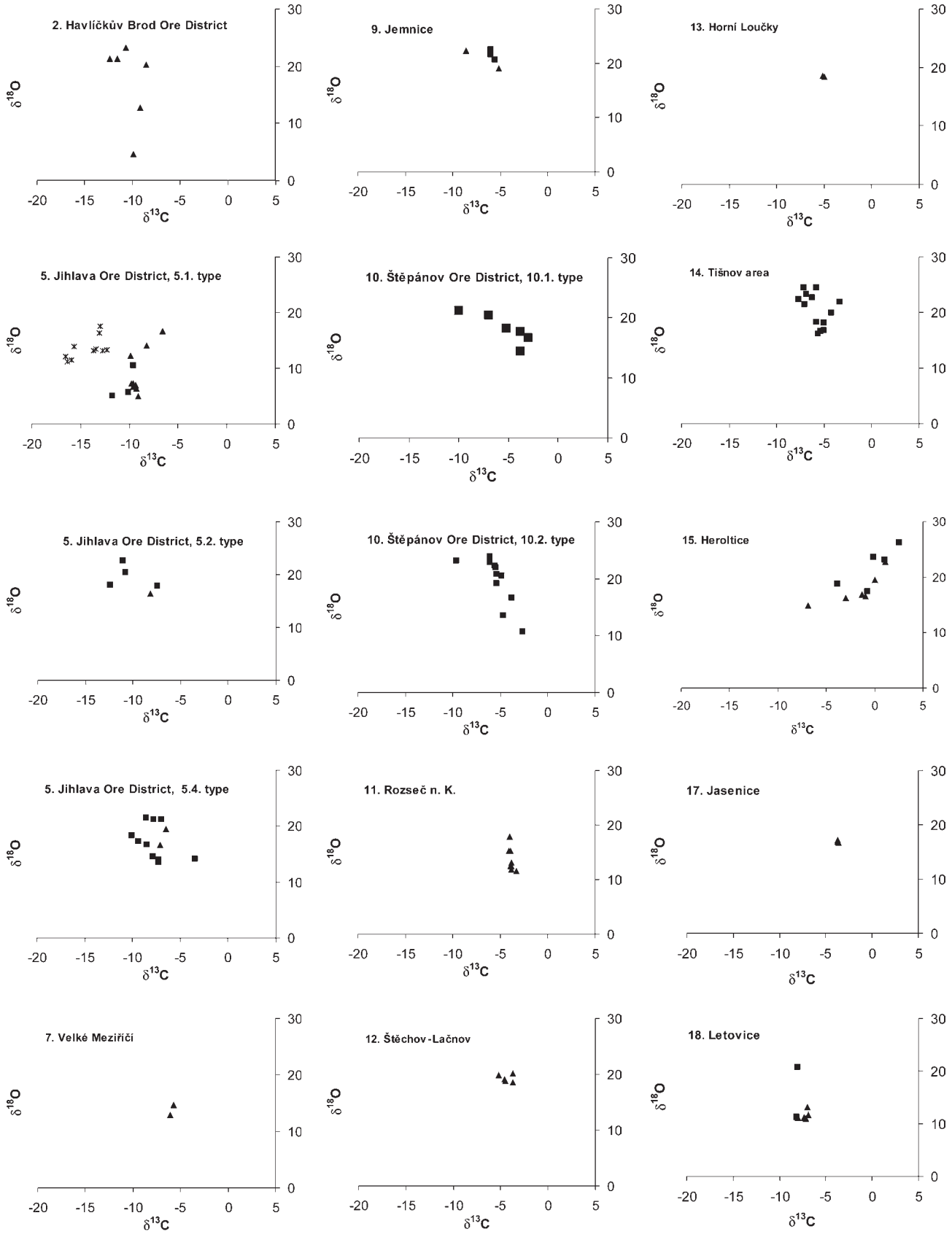

Figure 3. Isotope analyses of carbon and oxygen in carbonates ($\delta^{13}C$ ‰, PDB, $\delta^{18}O$ ‰ SMOW). ▲ – dolomite-ankerite-kutnohorite, ■ – calcite, ∗ – siderite.

Table 2. Sulfur isotope thermometers

Locality		Temperature from one hand-specimen		Temperature from average $\delta^{34}S$ data	
		t (°C)	minerals	t (°C)	minerals
1. Pelhřimov Ore District	Nemojov	449	sf–ga	279	sf–ga
		463	py–ga	483	py–ga
		653	py–ga		
		411	py–ga		
2. Havlíčkův Brod Ore District	Česká Bělá	382	py–sf		
	Stříbrné Hory	542	sf–ga	382	sf–ga
	Utín	581	sf–ga	507	sf–ga
		529	py–ga	593	sf–py
				529	py–ga
	Pohled	593	py–sf		
	Dlouhá Ves			593	sf–py
	Bartoušov	441	sf–ga	581	sf–ga
		653	py–ga		
3. Dačice-Slavonice area		non-realistic temperature			
4. Dobrá Voda		402	sf –ga	317	sf–ga
5. Jihlava Ore District	5.1. black sphalerite ± sulphide ± carbonates	370–410	according Pluskal and Vosáhlo (1998)	507	sf–ga
	5.2. dark brown sphalerite ± barite ± carbonates	280–340	according Pluskal and Vosáhlo (1998)	184	sf–ga
	5.3. dark brown sphalerite + barite + fluorite	250	according Pluskal and Vosáhlo (1998)	171	sf–ga
	5.4. light brown sphalerite ± barite ± carbonates	230–260	according Pluskal and Vosáhlo (1998)	109	sf–ga
6. Měřín		257	sf–ga	303	sf–ga
7. Velké Meziříčí				364	sf–ga
8. Ptáčov	no data				
9. Jemnice				267	sf–ga
10. Štěpánov Ore District	10.1. Pb-Zn(-Sb)	247	sf–ga	303	sf–ga
				174	sf–py
				255	py–ga
	10.2. Cu-Pb(-Zn)			95	sf–ga
				96	sf–chp
				94	ch–ga
11. Rozseč nad Kunštátem		220	sf–ga	303	sf–ga
12. Štěchov-Lačnov				121	sf–ga
13. Horní Loučky				257	sf–ga
14. Tišnov area		non-realistic temperature			
15. Heroltice		205	sf–ga	165	sf–ga
16. Maršov-Javůrek area				113	sf–ga
17. Jasenice				197	sf–ga
18. Letovice	no data				

were considered irrelevant (this was especially the case of thermometric pairs with pyrite – see explanation above).

2. Mesothermal ore occurrences and deposits (ca 200–250 °C). This group includes site 5, Jihlava Ore District, mineralizations 5.3 and 5.4; site 6, Měřín; site 9, Jemnice; site 10, Štěpánov Ore District, mineralization 10.1. site 11, Rozseč nad Kunštátem; site 12, Štěchov-Lačnov; site 13, Horní Loučky; site 15, Heroltice; and site 17, Jasenice.

Where homogenization temperatures of fluid inclusions are available, they are consistent with the results obtained from isotope thermometry (Malý and Dobeš 2001, Malý 2003, Hrazdil et al. 2003).

3. Low-temperature ore occurrences and deposits (below ca 130 °C). This group includes site 10, Štěpánov Ore District, mineralization 10.2; site 14, Tišnov area; and site 16, Maršov. The results of isotope thermometry clearly show that the mineralization 10.2 of the Štěpánov Ore District occurred at low temperatures. No exact data could be obtained for site 14 Tišnov and site 16 Maršov. These conclusions are supported by the results of fluid inclusion studies (Malý and Dobeš 2002, Dolníček 1999).

Formation temperatures of ca 350 °C were indicated for site 5 Jihlava Ore District, mineralization 5.2, and site 7 Velké Meziříčí by isotope thermometry. With respect to the small amount of analytical data, however, these values should be considered preliminary.

Isotopic composition of source sulfur and its origin

Determination of the $\delta^{34}S$ value for sulfur of the hydrothermal fluid (the so-called source sulfur) is generally problematic, as it is generally impossible to determine the oxidized vs. reduced sulfur ratio in the fluid. The presence of pyrrhotite (stable), temperatures below 500 °C, and fluid pH values less than 6 seem to suggest the dominance of H_2S as a sulfur carrier in the fluid (isotopic composition of sulfides then corresponds to source sulfur). The simultaneous formation of pyrite and hematite is thought to indicate the prevalence of sulfate in the fluid, in which case the $\delta^{34}S$ values of sulfides may widely differ from those of the source sulfur.

The assumed formation conditions for the deposits studied, and the inferred $\delta^{34}S$ values of source sulfur, are summarized in Table 3.

In principle, the sulfur sources of hydrothermal fluids at the studied sites include the following:

1. Deep-seated sulfur with $\delta^{34}S$ values around 0 ‰.

This source of sulfur can be assumed only for site 7 (Velké Meziříčí) and site 15 (Heroltice). At the latter site, however, this interpretation is contrary to the following considerations: lead at this site is derived from upper crustal rocks (Vaněček et al. 1985); the source of carbon for hydrothermal fluids was strongly affected by the host limestone; and the salinity of the hydrothermal fluid is merely ca 6 wt.% NaCl equiv. (Malý 2004). The effect of fluids derived from a deep-seated source was therefore probably weak at this site, and the source of sulfur in the ambient rocks should be considered.

2. Sulfur derived from rocks in which the ore mineralization occurred.

Bernard and Žák (1992) reported 28 isotope analyses of accessory (stratiform) sulfides (pyrite, pyrrhotite) from rocks in the surroundings of the Moldanubian pluton. The values of $\delta^{34}S$ encompass a wide range from ca –15 ‰ CDT to +6 ‰ CDT; a prominent peak is, however, observed in the interval of ca 0 to +5 ‰ CDT. Sulfur of this isotopic composition could have posed a direct source for hydrothermal fluids at site 2 Havlíčkův Brod Ore District, site 4 Dobrá Voda, and site 5 Jihlava Ore District, mineralizations 5.1 and 5.3.

Six analyses of rock sulfur have been performed from different rocks and different regional-geological units of the Svratka Dome of the Moravicum (Dolníček 2004, Malý – unpublished data). The $\delta^{34}S$ values range from +1.1 to +14.7 ‰ CDT, with most data concentrated in the interval of ca +5 to +10 ‰ CDT. Sulfur of this isotope composition could have posed a direct source for hydrothermal fluids at site 10 Štěpánov Ore District, site 11 Rozseč nad Kunštátem, site 12 Štěchov-Lačnov, site 13 Horní Loučky, and site 17 Jasenice.

Without the knowledge of $\delta^{34}S$ values of the rock types in the ambience of a specific ore occurrence, reference to the ambient rocks as a source of the sulfur is somewhat speculative. This category includes ore occurrences in the Moldanubicum with negative $\delta^{34}S$ values of source sulfur (i.e. site 1 Pelhřimov Ore District; site 5 Jihlava Ore District, mineralizations 5.2 and 5.4; site 6 Měřín) and sites with markedly positive $\delta^{34}S$ values of source sulfur (site 9 Jemnice, site 18 Letovice).

3. Permian-Triassic marine sulfate.

This source is believed to be responsible for the formation of barite-dominating Upper Permian–Lower Triassic (Dolníček et al. 2003) mineralizations in the Svratka Dome (Maršov and Tišnov sites). Barite $\delta^{34}S$ values are higher than those of the host rocks, precluding sulfur sources in the mobilized sulfur (i.e. oxidized to sulfate) derived from the host rocks because no significant isotopic fractionation occurs during pyrite oxidation (Bottrell et al. 2001). Nevertheless, we cannot exclude host rocks as a direct source of sulfur. Theoretically, the superimposed bacterial reduction of mobilized host rock sulfur may explain the observed $\delta^{34}S$ values, although temperatures above ~80 °C terminate the bacterial activity. Alternatively, most barite sulfur isotope data fall within the range reported for Permian-Triassic marine sulfate (Claypool et al. 1980). A marine evaporitic origin of the parent fluids may also be supported by other methods (high Br/Cl ratios in fluid inclusion leachates, oxygen isotope composition of the parent fluid; Dolníček 2004).

The values of $\delta^{34}S$ can be expected to vary depending on the host lithology at the sites where sulfur is believed to come from the ambient rocks. This trend is readily apparent: mineralizations hosted in metamorphic rocks (of the Olešnice Group of the Svratka Dome Moravicum) show positive $\delta^{34}S$ values (usually highly positive values) in all cases; mineralization 15 Heroltice (autochthonous part of the Svratka Dome of the Moravicum) is located in different rocks (limestones) and shows $\delta^{34}S$ values of around 0 ‰. Mineralizations hosted by Moldanubian metamorphic rocks show $\delta^{34}S$ values in the range of ca –3 to +3 ‰.

The idea of local material sources is also supported by lead isotope geochemistry (Table 4): mineralizations hosted by the same regional-geological (or lithological) unit have practically identical lead isotope compositions. No correlation is visible between the lead isotope composition and other properties of the mineralizations (formation temperature, $\delta^{34}S$ values, presumed mineralization ages). This is well documented by mineralizations in the Moravicum: lead at all of the studied sites (meso- and epithermal) is markedly enriched in radiogenic isotopes compared to other sites.

Table 3. $\delta^{34}S$ value of source sulfur (‰, CDT)

Locality		t (°C)	H_2S/SO_4^{2-} ratio	$\delta^{34}S_{\Sigma S}$
1. Pelhřimov Ore District	Nemojov	400–500	$H_2S > SO_4^{2-}$	–1 to –2
2. Havlíčkův Brod Ore District	Česká Bělá	400–450	$H_2S > SO_4^{2-}$	+3 to +5
	Stříbrné Hory	450–500	$H_2S > SO_4^{2-}$	+3 to +5
	Utín	450–550	$H_2S > SO_4^{2-}$	+4 to +5
	Pohled	about 500	$H_2S > SO_4^{2-}$	+4 to +5
	Dlouhá Ves	450–550	$H_2S > SO_4^{2-}$	+3 to +4
	Bartoušov	450–550	$H_2S > SO_4^{2-}$	+4 to +5
3. Dačice-Slavonice area		160–200*	probably extremely variable Eh	?
4. Dobrá Voda		400–450	$H_2S > SO_4^{2-}$	+4 to +5
5. Jihlava Ore District	5.1. black sphalerite ± sulphide ± carbonates	350–450	$H_2S > SO_4^{2-}$	+3 to +5
	5.2. dark brown sphalerite ± barite ± carbonates	250–350	variable $H_2S > SO_4^{2-}$	0 to –3
	5.3. dark brown sphalerite + barite + fluorite	about 250	variable $H_2S > SO_4^{2-}$	+1 to +3
	5.4. light brown sphalerite ± barite ± carbonates	about 250	variable $H_2S > SO_4^{2-}$	0 to –3
6. Měřín		about 250	variable $H_2S > SO_4^{2-}$	–3 to –4
7. Velké Meziříčí		350 ?	$H_2S > SO_4^{2-}$	about 0
8. Ptáčov	no data			
9. Jemnice		about 250	$H_2S > SO_4^{2-}$	+7 to +8
10. Štěpánov Ore District	10.1. Pb-Zn(-Sb)	about 250	variable $H_2S > SO_4^{2-}$	+8 to +10
	10.2. Cu-Pb(-Zn)	100–150	variable $H_2S > SO_4^{2-}$	+9 to +10 (main mineralization stage)
11. Rozseč nad Kunštátem		200–250	$H_2S > SO_4^{2-}$	+10 to +12
12. Štěchov-Lačnov		200–250 ?	$H_2S > SO_4^{2-}$	+2 to +4
13. Horní Loučky		about 250	$H_2S > SO_4^{2-}$	+8 to +9
14. Tišnov area		80–120**	variable $H_2S > SO_4^{2-}$ $SO_4^{2-} > H_2S$	–8 sulfane, +11 to +14 sulphate
15. Heroltice		200–250	$H_2S > SO_4^{2-}$	+1 to –1
16. Maršov-Javůrek area		up to 130	variable $H_2S > SO_4^{2-}$ $SO_4^{2-} > H_2S$	–1 to –6 sulfane
17. Jasenice		200–250	variable $H_2S > SO_4^{2-}$	+6 to +7
18. Letovice		200–250*	$H_2S > SO_4^{2-}$	+5 to +6

* according Th of fluid inclusion (Dobeš, Malý – unpublished data)
** according Th of fluid inclusion (Dolníček 1999)

Carbon isotopes in carbonates

In common hydrothermal fluids, H_2CO_3 and HCO_3^- are the main carriers of oxidized carbon to be considered in isotope studies of carbonates. At temperatures above 100 °C, the main carrier of carbon is H_2CO_3 (Ohmoto 1986).

If temperatures used in the study of isotope geochemistry of sulfur are considered for the origin of carbonates (see above), the sites studied here can be divided into three groups based on the calculated $\delta^{13}C$ values of fluids:

1. At a majority of the sites, the values of source $\delta^{13}C$ fall within the range typical of the homogenized carbon of Earth crust, or deep-seated carbon (ca –5 to –8 ‰ CDT).
2. Some sites falling within this range show a trend towards more negative $\delta^{13}C$ values of source carbon. Such a trend can be interpreted as showing the more prominent involvement of organic carbon in the hydrothermal process. This applies to site 2 Havlíčkův Brod Ore District and site 5 Jihlava Ore District, mineralization 5.1 and 5.2.
3. In contrast, some sites show a shift towards more positive $\delta^{13}C$ values of source carbon: site 12 (Štěchov-Lačnov), site 15 (Heroltice), site 17 (Jasenice), and to a lesser degree also site 14 (Tišnov area). This trend can be interpreted as the involvement of carbon from the marbles and limestones that hosted the hydrothermal mineralization process. Alternatively, the decrease of crystallization temperature also increases the $\delta^{13}C$ values of younger carbonates (site 14, Tišnov area).

Table 4. Isotope composition of sulfur and lead (data for lead after Vaněček et al. 1985)

Locality		Pb isotope ratios			
		$\delta^{34}S_{\Sigma S}$ ‰, CDT	206/204	207/204	208/204
1. Pelhřim Ore District		–1 to –2	18.16	15.59	38.36
2. Havlíčkův Brod Ore District	Stříbrné Hory	+3 to +5	18.12	15.59	38.12
	Bartoušov	+4 to +5	18.14	15.61	38.25
3. Dačice-Slavonice area		?	18.11	15.65	38.29
5. Jihlava Ore District	5.1. black sphalerite ± sulphide ± carbonates	+3 to +5	18.17	15.59	38.18
	5.2. dark brown sphalerite ± barite ±carbonates	0 to –3	18.22	15.65	38.34
	5.3. dark brown sphalerite + barite + fluorite	+1 to +3	18.11	15.52	38.25
	5.4. light brown sphalerite ± barite ± carbonates	0 to –3	18.15	15.59	38.21
10. Štěpánov Ore District	10.1. Pb-Zn(-Sb)	+8 to +10	18.81	15.64	38.57
			18.76	15.68	38.70
			18.74	15.59	38.42
	10.2. Cu-Pb(-Zn)	+9 to +10	18.99	15.76	38.66
11. Rozseč nad Kunštátem		+10 to +12	18.82	15.77	38.61
12. Štěchov-Lačnov		+2 to +4	18.35	15.58	38.34
			19.02	15.82	38.80
14. Tišnov area*	Květnice	–8 (H_2S)	18.55	15.64	38.29
15. Heroltice		+1 to –1	18.78	15.60	38.37
16. Maršov-Javůrek area		–1 to –6 (H_2S)	18.78	15.76	38.66
			18.90	15.82	38.91
			18.69	15.64	38.60

* Dolníček and Slobodník – unpublished data

Oxygen isotopes in carbonates

Provided that the temperatures used in the study of isotope geochemistry of sulfur, and the temperatures obtained from the study of Th from fluid inclusions in carbonates (see above), are considered for the origin of carbonates, approximate $\delta^{18}O$ values for the water of the hydrothermal fluids can be determined. These values allow the division of the studied sites into two groups:

1. Most sites show high $\delta^{18}O$ values for the water of the hydrothermal fluid, from ca +4 to +10 (even higher values can be presumed in some cases). These values are typical for fluids subjected to isotopic equilibration with the host rock at high temperatures.
2. At some sites, the number of analyzed samples, and the knowledge of their paragenetic position, permitted a more detailed isotope study. It revealed that water with lower $\delta^{18}O$ values was involved in the hydrothermal process during final stages of mineralization. This was the case at site 5 (Jihlava, mineralization 5.1), site 10 (Štěpánov Ore District, mineralization 10.2), and site 11 (Rozseč nad Kunštátem). Such a trend can be explained by the involvement of water of a different type in the system (probably water of meteoritic or marine origin).

At site 14 (Tišnov area), $\delta^{18}O$ values of water in hydrothermal fluids focus around 0 ‰ (±3 ‰) SMOW. This indicates a prevalence of (i) marine water, (ii) meteoric water (with possible O-exchange with the rock environment at relatively low temperatures), or (iii) a mixture of waters of different origins in the hydrothermal system. The proportion of meteoritic water was increasing during the final stages of mineralization: –5 to –1 ‰ SMOW (Dolníček 2004).

Conclusion

Based on our interpretation of the obtained isotope data, the studied sites can be divided into three types:

1. High-temperature mineralization (ca 400–500 °C, depending on isotope thermometer) with source sulfur having $\delta^{34}S$ values mostly between +3 and +5 ‰ (with the exception of site 1 Pelhřimov Ore District). As suggested by mineralogical, isotopic, and geochemical data, the hydrothermal fluids were characterized by a marked dominance of sulfane over sulfate (more reducing environment). Analytical data indicate (at some sites) an increase in oxygen fugacity in the final stages of the mineralization process. The source of sulfur is believed to have been the metamorphic rocks, or possibly the granitic rocks, of the Moldanubicum. The values of $\delta^{18}O$ in carbonates of the main mineralization stage are high (due to high-temperature isotope exchange reactions with oxygenated host-rock miner-

als); the low $\delta^{13}C$ values indicate the involvement of carbon of organic origin in the hydrothermal process.

This group includes the following sites:

1. Pelhřimov Ore District
2. Havlíčkův Brod Ore District
4. Dobrá Voda
5. Jihlava Ore District, mineralization 5.1

This type of mineralization fits the characteristics of the Kutná Hora type Lower Permian Fe-Zn-Pb-Ag vein mineralization in the sense of Bernard and Žák (1992), as well as the mineralization of the "kb+eb Erzformation" type (Baumann 1958) or "k-pol" type (Bernard 1991). Bernard and Žák (1992) suggest that this mineralization has temporal and genetic relationships to middle Variscan metamorphism and magmatism.

2. Mesothermal mineralization (200–350 °C, based on isotope thermometry). The values of $\delta^{34}S_{\Sigma S}$ are either markedly positive (max. +8 to +10 % CDT) or lie within the range of ca –3 to +3 ‰ CDT. The sulfur source can be expected in rocks surrounding the ore occurrences (this fact has been confirmed at some sites and is presumed at others). Hydrothermal fluids were more oxidative than those of the preceding mineralization type; their oxidative character usually became even more distinct during the final stages of mineral formation. Waters of hydrothermal fluids generally show $\delta^{18}O$ values higher than 5 ‰ SMOW (due to isotope exchange reactions with oxygenated host-rock minerals). The involvement of water with low $\delta^{18}O$ values in the final stages of the mineralization process was documented in some cases (probably meteoritic or marine water). The values of $\delta^{13}C$ correspond either to homogenized carbon of the Earth's crust or its mixture with carbon from marbles/limestones (at sites where ores are hosted by these lithologies).

This group includes the following sites:

3. Dačice-Slavonice area
5. Jihlava Ore District, mineralizations 5.2, 5.3 and 5.4
6. Měřín
7. Velké Meziříčí
8. Ptáčov
9. Jemnice
10. Štěpánov Ore District, mineralization 10.1
11. Rozseč nad Kunštátem
12. Štěchov-Lačnov
13. Horní Loučky
17. Jasenice
18. Letovice

In some parameters, the mineralizations correspond to, for example, the "Lower Permian Pb-Zn-Cu-Ag veins: Ratibořské Hory type" in the sense of Bernard and Žák (1992) or to the "pol" mineralizations *sensu* Bernard (1991). It is, however, very probable that mineralizations of this group were in fact formed due to different processes and are of different ages. The establishment of this group cannot therefore be considered as genetic.

While the genesis of some sites is fairly constrained, that of others remains uncertain. Mineralization in the Svratka Dome of the Moravicum (site 10 Štěpánov Ore District, site 11 Rozseč nad Kunštátem, site 12 Štěchov-Lačnov, site 13 Horní Loučky, and site 17 Jasenice) are traditionally genetically linked to the final stages of Variscan metamorphism (Malý and Dobeš 2001). Mineralization in the Třebíč Massif and its envelope (site 6 Měřín, site 7 Velké Meziříčí, and site 8 Ptáčov) is probably genetically linked with local tectonic structures such as the Třebíč and Sázava Faults (cf. Chmelař 1986).

3. Low-temperature mineralization (below 130 °C). The $\delta^{34}S$ values of sulfane in the hydrothermal fluid were markedly negative, while those of sulfate range from ca +11 to +14 ‰ CDT. Sulfane was introduced from an external source by migrating fluids or was formed in lower-temperature areas of the hydrothermal system by the process of bacterial sulfate reduction. The sulfate sulfur may have been sourced from the host rocks or from the sulfate of the marine water (the stable isotope signature of which may be locally modified by other processes and sources). Carbon in the fluids has $\delta^{13}C$ values most commonly in the range of –6 to –11 ‰ PDB, which indicates the prevalence of "deep-seated" or homogenized crustal carbon (with limited effects of carbon from the host limestone, and local effects of carbon from oxidized organic matter from the ambient metasediments or possibly hydrocarbons of the hydrothermal fluid). Water of the hydrothermal fluid most commonly shows values around 0 ‰ SMOW. This may indicate a prevalence of marine water in the hydrothermal system. Although this interpretation is not the only possible one, it may be further supported by independent results (Br/Cl in fluid inclusion leachates; Dolníček 2004). Significant changes in redox conditions occurred in the course of the mineralization process.

This group includes the following sites:

14. Tišnov area
16. Maršov

In its parameters, the mineralization perfectly corresponds to the "fba" association *sensu* Bernard (1991). Its genesis can be linked with hypersaline fluids of primarily marine origin. The age of the mineralization has been established as the Late Permian to Early Triassic at site 14 (Tišnov area; Dolníček et al. 2003).

A distinct position is occupied by the mineralization at site 10 Štěpánov Ore District, mineralization 10.2. It is clearly a low-temperature occurrence, but fully corresponds to the mineralizations of group 2 in other aspects.

The definitions of group 1 (high-temperature) and group 3 (low-temperature) are quite certain: their features are characteristic enough to make them distinct genetic types.

Acknowledgements. The authors thank the Grant Agency of Czech Republic (grant No. 205/02/P104) for financial support.

References

Baumann L. (1958): Tectonics and origin of the ore deposits Freiberg – central part. Freiberger Forschungs Hefte, C46, 1–208 (in German).

Bernard J. H. (1991): Empirical types of ore mineralizations in the Bohemian Massif. Czech Geological Survey, Prague.

Bernard J. H., Žák K. (1992): Stable isotope study of Variscan vein Pb-Zn-Ag mineralization of the Bohemian Massif. Explor. Mining Geol. 1, 81–84.

Bottrell S. H., Crowley S., Self C. (2001): Invasion of a karst aquifer by hydrothermal fluids; evidence from stable isotopic composition of cave mineralization. Geofluids 1, 103–121.

Claypool G. E., Holser W. T., Kaplan I. R., Sakai H., Zak I. (1980): The age curves of sulphur and oxygen isotopes in marine sulphate and their mutual interpretation. Chem. Geol. 28, 199–260.

Češková L. (1978): Metalogenetic characterization of some geological units near the east margin of the Czech Massif. Folia Univ. J. E. Purkyně 19, 3, 7–99 (in Czech).

Češková L., Orel P. (1971): Vein and metasomatic type of the polymetallic mineralization near Heroltice. Sbor. geol. Věd, řada LG 14, 41–63 (in Czech).

Dobeš P., Malý K. (2001): Mineralogy of polymetallic ore occurrences in central part of ore district Havlíčkův Brod. Vlastivěd Sbor. Vysočiny, Odd. Věd přír. 15, 51–85 (in Czech).

Dolníček Z. (1999): Mineral paragenesis of the barite veins from surrounding of Tišnov. MSc Thesis, Masaryk University, Brno (in Czech).

Dolníček Z. (2001): Mineralogy of the barite veins from Květnice Hill near Tišnov. Acta Mus. Moraviae, Sci. geol. 86, 59–73 (in Czech).

Dolníček Z. (2004): Mineralogy and formation conditions of the fluorite and barite mineralizations in the Brunovistulicum. PhD Thesis, Masaryk University, Brno (in Czech).

Dolníček Z., Chadima M., Pruner P. (2003): Age determination of the barite veins from Tišnov using palaeomagnetic method. In: Zimák J. et al. (eds) Mineralogie Českého masivu a Západních Karpat 2003, Olomouc, 4–9 (in Czech).

Dolníček Z., Malý K. (2003): Mineralogy and genesis of the epithermal veins from the quarry in Dolní Loučky near Tišnov. Acta Mus. Moraviae, Sci. geol. 88, 149–166 (in Czech).

Griněnko V.A. (1962): Prigotovljenie dvuokisi sery dlja izotopnovo analiza. Žurnal Neorgan. Chimiji 7, 2478–2483 (in Russian).

Hladíková J., Kříbek B., Fojt B., Aichler J. (1995): The strontium and sulphur isotopic composition of sulphates and sulphides from the Fe-Cu-Pb-Zn-(Ba) stratabound mineralisations of the Bohemian Massif (Czech Republic). In: Pašava J., Kříbek B., Žák K. (eds) Mineral deposits: from their origin to their environmental impacts. A. A. Balkema, Rotterdam, 271–274.

Holub M., Tenčík I. (1973): The contribution to the metallogeny of the southeast part of the Bohemian Massif. Hornická Příbram ve vědě a technice, řada G, 25–48 (in Czech).

Houzar S., Malý K. (2002): Mineralogy, ore deposits situation and history of the Štěpánov Ore District in the Western Moravia. Acta Mus. Moraviae, Sci. geol. 87, 5–59 (in Czech).

Houzar S., Pošmourný K. (1991): Ag-Pb-Zn mineralization near Jemnice, Western Moravia. Acta Mus. Moraviae 76, 95–103 (in Czech).

Hrazdil V., Malý K., Dobeš P., Houzar S. (2003): Pb-Zn mineralization near Horní Loučky in vicinity of Tišnov. Acta Mus. Moraviae, Sci. geol. 88, 139–148 (in Czech).

Chmelař J. (1986): Manifestations of hydrothermal mineralization of the Sázava deep-seated fault at the boundary of the Stráže Moldanubicum and the Třebíč Massif. Bull. Geol. Surv. 61, 6, 333–337 (in Czech).

Kříbek B., Hladíková J., Žák K., Bendl J., Pudilová M., Uhlík Z. (1996): Barite-hyalophane sulfidic ores at Rožná, Bohemian Massif, Czech Republic: metamorphosed black shale-hosted submarine exhalative mineralization. Econ. Geol. 91, 14–35.

Litochleb J. (2001): The Pelhřimov silver-bearing district (Bohemian-Moravian Highlands, SE Bohemia). Bull. Mineral.-Petrolog. Odd. Nár. Muz. (Praha) 9, 102–121 (in Czech).

Malý K. (1999): Mineralogy of ore occurrences near Rozseč nad Kunštátem and Štěchov-Lačnov villages (Svratka Dome). Acta Mus. Moraviae 84, 61–70 (in Czech).

Malý K. (2000): Mineralogy of ore occurrence near Jasenice (Moravicum, Svratka Dome). Acta Mus. Moraviae 85, 81–89 (in Czech).

Malý K. (2003): Mineralogy of polymetallic ore occurrence near Měřín (Moldanubicum, Czech Republic). Vlastivěd Sbor. Vysočiny, Odd. Věd přír. 16, 43–51 (in Czech).

Malý K. (2004): Mineralogy of polymetallic ore occurrence near Heroltice (Svratka Dome, Moravicum). Acta Mus. Moraviae, Sci. geol. 89, 81–89 (in Czech).

Malý K., Dobeš P. (2001): Stable isotope and fluid inclusion study of epithermal polymetallic mineralization near Štěpánov nad Svratkou (Svratka Dome, Moravicum). Bull. Czech Geol. Surv. 76, 15–21.

Malý K, Dobeš P. (2002): Mineralogy of polymetallic ore occurrences near Maršov and Javůrek villages (Svratka Dome, Moravicum). Acta Mus. Moraviae, Sci. geol. 87, 75–85 (in Czech).

Mátl V. (1960): Final account of the mineral exploration – Květnice. Unpub. Czech Geological Survey – Geofond Praha (in Czech).

Mátl V. (1963): The mineral exploration of Pb-Zn-Cu ores, Domašov – Javůrek. Unpub. Czech Geological Survey – Geofond Praha (in Czech).

Mátl V. (1965): The mineral exploration of Pb-Zn-(Cu) ores, Borovec near Štěpánov. 1959–1963. Unpub. Czech Geological Survey – Geofond Praha (in Czech).

McCrea J. M. (1950): On the isotopic chemistry of carbonates and a paleotemperature scale. J. Chem. Phys. 18, 849–857.

Ohmoto H. (1986): Stable isotope geochemistry of ore deposits. In: Valley J. W., Taylor H. P. Jr., O'Neil J. R. (eds) Stable isotopes in high temperature geological processes. Rev. Mineral. 16, Mineral. Soc. Amer., Washington, 491–560.

Ohmoto H., Lasaga A. C. (1982): Kinetics of reactions between aqueous sulfates and sulfides in hydrothermal systems. Geochim. Cosmochim. Acta 46, 1727–1745.

Ohmoto H., Rye R. O. (1979): Isotopes of sulfur and carbon. In: Barnes H. L. (ed.) Geochemistry of hydrothermal ore deposits. Wiley, New York, 509–567.

O'Neil J. R., Clayton R. N., Mayeda T. K. (1969): Oxygen isotope fractination in divalent metal carbonates. J. Chem. Phys. 51, 5547–5558.

Pluskal O., Vosáhlo J. (1998): Jihlava Ore District. Vlastivěd Sbor. Vysočiny, Odd. Věd přír. 13, 157–191 (in Czech).

Pokorný J. (1964): Final account of the mineral exploration of Pb-Zn deposits in Havlíčkův Brod Ore District. Unpub. Czech Geological Survey – Geofond Praha (in Czech).

Stýblo W. (1972): Polymetallic Pb-Zn-Ag mineralization near Dobrá Voda in metallogeny of the west margin of the Moldanubian Pluton. MSc Thesis, Charles Univ. Praha (in Czech).

Šouba M., Mátl V. (1961): Final account of the mineral exploration in 1959–60. Horničí. Unpub. Czech Geological Survey – Geofond Praha (in Czech).

Vaněček M., Patočka F., Pošmourný K., Rajlich P. (1985): The use of isotopic composition of ore leads in metallogenic analysis of the Bohemian Massif. Rozpr. Čs. Akad. Věd, Ř. mat. přír. Věd 95, 5, 1–114.

Vosáhlo J. (1988): The contribution to the minerogenesis of the hydrothermal polymetallic mineralization in Kamenná, Jihlava and Jezdovice Ore District. MSc Thesis, Charles Univ. Praha (in Czech).

Zimák J., Šendová P. (1999): New data on the historical ore deposit "U havířských jam" near Jemnice. Geol. výzk. Mor. Slez. v Roce 1998, 132–133 (in Czech).

Bulletin of Geosciences, Vol. 80, No. 4, 321–354, 2005
© Czech Geological Survey, ISSN 1214-1119

Cenomanian and Cenomanian-Turonian boundary in the southern part of the Bohemian Cretaceous Basin, Czech Republic

Stanislav Čech [1] – Lenka Hradecká [1] – Marcela Svobodová [2] – Lilian Švábenická [1]

[1] Czech Geological Survey, Klárov 131/3, CZ-118 21 Praha 1, Czech Republic. E-mail: cech@cgu.cz, hradecka@cgu.cz, svab@cgu.cz
[2] Academy of Sciences of the Czech Republic, Institute of Geology, Rozvojová 135, CZ-165 02 Praha 6, Czech Republic.
E-mail: msvobodova@gli.cas.cz

Abstract. Initial transgressive Cretaceous deposits are described from boreholes in the southern part of the Bohemian Cretaceous Basin, i.e. siliciclastic sediments of Cenomanian age (Peruc-Korycany Formation), and hemipelagic marlstones and limestones of the Turonian age (Bílá Hora Formation). Transgressive successions include fluvial, supratidal marsh, estuarine tidal flat and channel, estuarine and mouth sand, inner shelf and open marine facies assemblages interpreted on the basis of sedimentological and paleontological features. Fluvial-estuarine facies filled an incised valley that formed a tributary of the main paleovalley in the central part of the basin. Fluvial facies are characterized by either the prevalence of spores and the presence of freshwater green algae (swampy conditions), or the prevalence of angiosperm pollen grains (alluvial plain assemblage). Marsh and estuarine facies are characterized by the presence of marine microplankton tolerant to changing salinity conditions, acritarchs, prasinophycean algae, agglutinated foraminifers, thick-walled spores, and halophyte and taxodiaceous pollen. Inner shelf facies exhibit rare sporomorphs (often thick-walled), increase of gonyaulacean dinocyst, marine macrofauna, foraminifers with non-keeled planktonic foraminifera, and sparse calcareous nannofossils. Open shelf facies are characterized by hemipelagic sediments containing keeled planktonic foraminifers and diverse calcareous nannofossils. Concerning calcareous nannofossils, the base of the Turonian is marked by the first occurrence of *Eprolithus octopetalus* (within foraminiferal *Whiteinella archaeocretacea* Interval and Partial range Zone) just above prominent erosion surface at the base of the Bílá Hora Formation. The first appearance of nannofossil species *Eprolithus moratus* coincides with first occurrence of foraminiferal planktonic species *Helvetoglobotruncana helvetica* in hemipelagic sediments of the Bílá Hora Formation.

Key words: Bohemian Cretaceous Basin, Cenomanian, Cenomanin-Turonian boundary, lithostratigraphy, depositional environment, biostratigraphy, macrofauna, foraminifers, calcareous nannofossils, palynomorphs

Introduction

In the second half of the year 2000 and in the beginning of the following year, the Aquaprotec Company Ltd. drilled hydrogeological boreholes in the south-central part of the Bohemian Cretaceous Basin (BCB) (Fig.1). The boreholes were drilled with the aim of intensifying the sources of mineral water from Cenomanian deposits in the area between Nymburk and Poděbrady-Spa.

The lithology and micropaleontology of the Cretaceous sediments in these drill cores were studied in detail by the Czech Geological Survey (CGS) and the Institute of Geology, Academy of Sciences of the Czech Republic (IGAS).

Previous studies

Although the Cenomanian sediments have been known from boreholes ever since mineral water was discovered in 1909 in Poděbrady, there is little known about the sedimentology and biostratigraphy of the Cenomanian in this area (south-central part of the BCB).

Lithological and paleontological characteristics of the Cenomanian and Turonian sediments were introduced by Klein (1966) from the west-central part of the BCB, and by Klein et al. (1982) from the east-central part of the BCB. Some problems concerning the sedimentology, sequence stratigraphy, biostratigraphy, and geochemical anomalies at the Cenomanian-Turonian (Ce-Tu) boundary have been investigated in the west-central part of the Bohemian Cretaceous Basin by Uličný et al. (1993, 1997a, b). In the Poděbrady area, the lithology, paleogeography, and tectonics of the Cenomanian and Turonian sediments were studied from boreholes by Hruška et al. (1968), and more recently by Čech (2004).

Biostratigraphically, Upper Cenomanian macrofauna was characterized by Pražák in his unpublished report (1989) from the central part of the BCB, and by Svoboda (1998) from the SW margin of the BCB. Macrofaunal assemblages and the characteristics of the microfauna and microflora of rocky shore sediments from the southern margin of the BCB have been described by Eliášová (1997), Svobodová (1990), Štemproková-Jírová (1991), and Žítt et al. (1997a, b).

In the study area, Hercogová (1968) was the first to record early Turonian foraminifers in the cores of some boreholes (OP-4 Vrbice, OP-5 Velké Zboží, OP-6 Choťánky). Macrofauna, foraminiferal assemblages, and calcareous nannofossils from the Cenomanian-Turonian boundary interval have been described in this region from the borehole Kouty BJ-16 (Hradecká et al. 1997).

Calcareous nannofossils from the Cenomanian-Turonian boundary interval have already been studied in some localities and boreholes in the BCB, unfortunately without any success (Hradecká and Švábenická 1995). Cenomanian deposits were usually barren of this fossil group, whereas the lowermost Turonian sediments contained rich assemblages. Poor coccolith assemblages in Cenomanian

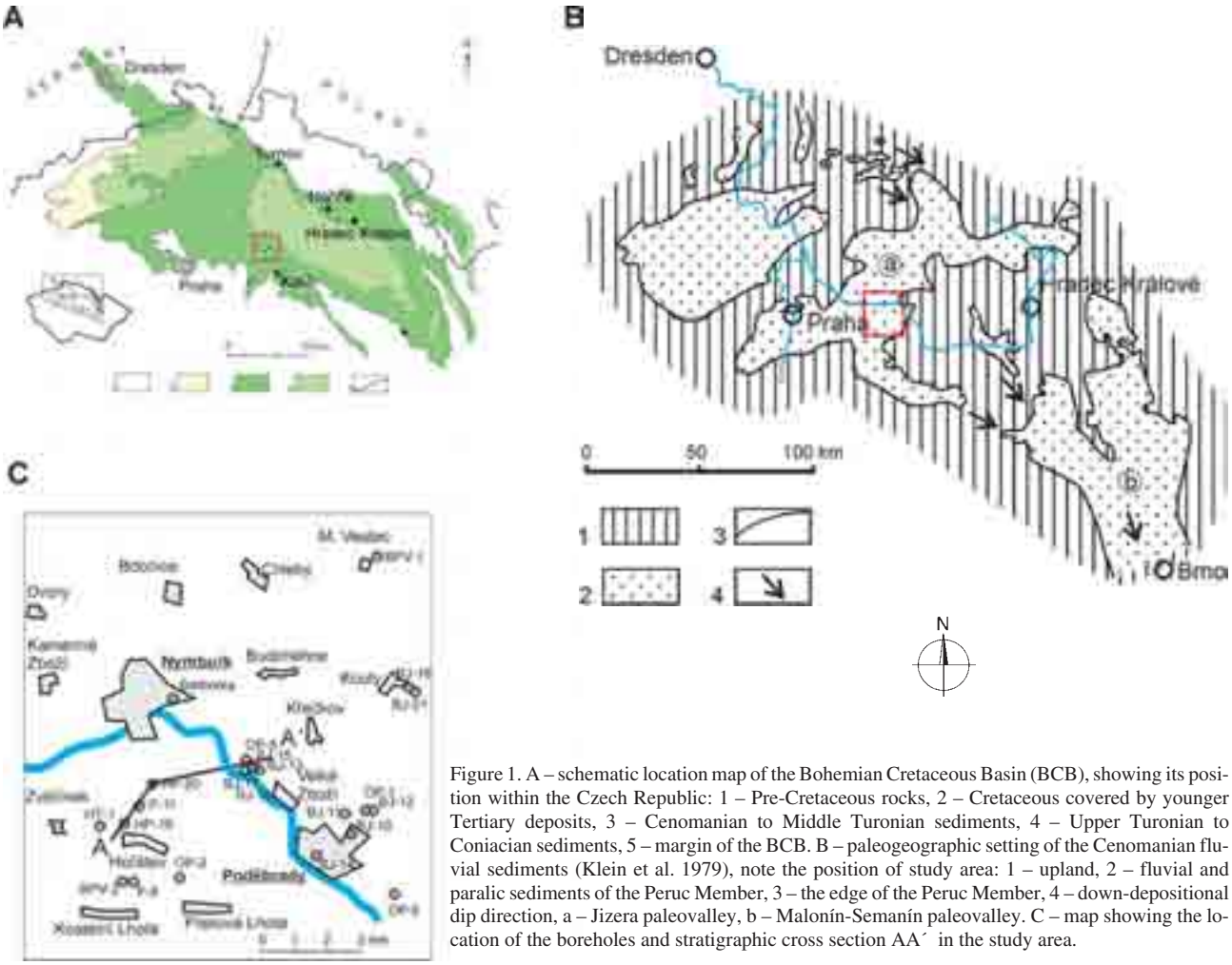

Figure 1. A – schematic location map of the Bohemian Cretaceous Basin (BCB), showing its position within the Czech Republic: 1 – Pre-Cretaceous rocks, 2 – Cretaceous covered by younger Tertiary deposits, 3 – Cenomanian to Middle Turonian sediments, 4 – Upper Turonian to Coniacian sediments, 5 – margin of the BCB. B – paleogeographic setting of the Cenomanian fluvial sediments (Klein et al. 1979), note the position of study area: 1 – upland, 2 – fluvial and paralic sediments of the Peruc Member, 3 – the edge of the Peruc Member, 4 – down-depositional dip direction, a – Jizera paleovalley, b – Malonín-Semanín paleovalley. C – map showing the location of the boreholes and stratigraphic cross section AA´ in the study area.

strata were recorded only in some boreholes situated in the central part of basin (Švábenická 2004). This study is the first to present data on calcareous nannofossils from the Cenomanian-Turonian interval of this area.

Middle–Late Cenomanian palynofacies (freshwater, transitional, and marine) and palynological assemblages from the west-central part of the BCB were studied by Pacltová and Svobodová (1993), Uličný et al. (1997 a, b), Svobodová et al. (1998), Méon et al. (2004).

Geological setting

The Bohemian Cretaceous Basin (Cenomanian-Santonian) is an intra-continental basin formed during the mid-Cretaceous as a seaway between the North Sea Basin and the Tethys Ocean. The BCB was formed by the reactivation of a fault system in the Variscan basement of the Bohemian Massif during the mid-Cretaceous (Uličný 1997, 2001).

Individual sub-basins and adjacent source areas (West and East Sudetic Islands, Central European Island) were separated by WNW to NW-trending, principal displacement fault zones (Uličný 1997). These fault zones, together with subordinate NW and NNE-directed fault zones, significantly influenced the basin topography and the basin filling in the initial stage of a marine transgression during the Cenomanian. The marine transgression created a fluvial-estuarine depositional setting with a system of paleovalleys separated by topographical highs. Two principal paleovalleys were recognized based on subsurface data: the SE trending Semanín-Malonín paleovalley in the SE part of the BCB directed to the Tethys ocean (Frejková and Vajdík 1974), and the NNE-oriented paleovalley in the central part of the basin (Klein et al. 1979, Uličný et al. 2003) (Fig. 1B).

In the study area, the Cenomanian fluvial-estuarine deposits represent the southern (landward) part of the paleodrainage system of the central paleovalley (Uličný et al. 2003, Čech 2004). New hydrogeological and balneological boreholes have penetrated the Upper Cretaceous sediments of the Bílá Hora (Lower-Middle Turonian) and Peruc-Korycany (Cenomanian) formations sensu Čech et al. (1980).

Material and methods

For correlation purposes, and for sedimentological and paleogeographical interpretations, older and recent balneological and hydrogeological boreholes, as well as some from the uranium industry, were studied (Fig. 1C). The division of Cenomanian strata into several facies associations was made on the basis of a detailed description of lithology, and the re-

cognition of major bounding surfaces in the cores together with characteristic faunal, floral, and biogenic contents, as was done in the Pecínov Quarry in the SW part of the BCB (Uličný et al. 1997a). Several stratigraphic cross sections were constructed across the area to provide a correlation framework. Lithostratigraphic subdivision of the Cretaceous deposits in the cores was used according to Čech et al. (1980). Regional genetic-stratigraphic units (CEN 1–6) based on the correlation of well-logs (Uličný et al. 2003) is still in progress and cannot be used in this paper.

Cores for litho- and biostratigraphic studies were obtained from boreholes Velké Zboží BJ-17 (83.0–110.4 m), BJ-18 (83.0–121.85 m), Hořátev HP-19 (76.0–148.6 m), Nymburk HP-20 (81.0–155.5 m), and Velké Zboží OP-5 (80.0–123.6 m) (Fig. 1C).

Samples for the study of foraminifers, calcareous nannofossils, and palynomorphs were disintegrated in the CGS Laboratory in Prague using standard methods. Macrofauna, foraminifers, and smear slides with nannofossils are housed in the CGS.

Foraminifers were separated under binocular microscope, and photographs of species were taken using scanning electron microscope. Planktonic zonation by Robaszynski and Caron (1995) was used for the correlation of the studied samples. Foraminiferal assemblages were compared with others of the same age from older material archived at CGS from the 1960s and 1970s.

Nannofossils and foraminifers were studied from the same samples. Suspension slides were prepared using a decantation method, separated fraction 3–30 μm. Slides were inspected with a Nikon light-microscope at 1000x magnification. Quantitative data are based on cca 300–500 specimens. Biostratigraphic data were correlated with the standard nannoplankton zones (CC) of Sissingh (1977), and with the Upper Cretaceous (UC) nannofossil zones of Burnett (1998).

Palynomorphs were studied only from the Cenomanian part of the boreholes. Palynological processing followed standard procedures involving HCl-HF-KOH, acetolysis, and HNO_3. Slides were examined on Zeiss-Amplival and OPTON light-microscopes. Quantitative analysis is based on 200 specimens. The slides and residues used in this study have been deposited in the Laboratory of Paleobiology and Paleoecology of the IGAS.

Results

Lithostratigraphy

Peruc-Korycany Formation

Based on the core samples, the Peruc-Korycany Formation can be subdivided into three members: the Peruc, Korycany (Čech et al. 1980), and Pecínov (Uličný 1992) members (Figs 2 and 3).

The lower part of the Peruc Member consists of fining-upward cycles of grey sandstones and conglomerates with interbeded light and dark grey mudstones. The upper part of the member also contains grey sandstones and conglomerates, but the mudstones dominate this section and have associated root zones. Carbonaceous plant debris is common. Fossil leaves are less common. In borehole HP-19, the sand-dominated, upward-coarsening cycles occur in the upper part of the Peruc Member. Driftwood fragments penetrated with borings of marine bivalves are sparsely distributed in this sandstone. In the uppermost part of the member, finely laminated black mudstones with lenses and interbeds of glauconitic siltstones and fine-grained sandstones are developed. Sand-filled burrows are conspicuous in this facies: *Thalassinoides, Planolites*, and *Teichichnus* are dominant. Thin layers of coarse-grained sandstones appear in the heterolithic beds.

The Korycany Member consists of well-sorted fine and medium grained quartzose sandstones and clayey sandstones. Sandstones locally contain a high amount of glauconite. Well-sorted sandstones contain thin layers of plant material and mud drapes, usually within cross-bed sets. Discrete sand-filled burrows of *Thalassinoides*, *Ophiomorpha*, *Diplocraterion*, and the absence of primary sedimentary lamination, indicate extensive bioturbation. In the middle and upper part of the Korycany Member, a thin heterolithic facies was observed in the core. The facies include interbedded sandstone and mudstone as sand streaks in mud, that pass into lenticular, wavy, and flaser bedded sandstone. The sediments are densely bioturbated. In some cores (HP-19, BJ-17), a thin pebbly bed (up to 0.1 m in thickness) with an erosive base was observed in the middle part of the Korycany Member.

The Pecínov Member (Uličný 1992) is characterized by dark grey, clayey, variably calcareous, very fine glauconitic siltstones that contain brown phosphatic nodules, pyrite, sponge spicules, numerous *Chondrites* burrows, and marine macrofauna in which bivalves dominate. A thin bed of glauconitic pebbly sandstone is developed at the base of the Pecínov Member. This bed is associated with a prominent erosional surface at its base.

Bílá Hora Formation

The Bílá Hora Formation is comprised of dark grey to grey marlstones and micritic limestones (Figs 2 and 3). At the base of the formation, a thin, very glauconitic, green, sandy marlstone bed is developed, associated with an erosive surface at the base of the bed (Fig. 15). This glauconitic marlstone bed contains dark brown phosphatic nodules, quartz pebbles, and dense *Chondrites* burrows. *Thallassinoides* burrows pipe glauconitic sediment down into the underlying siltstones of the Pecínov Member.

Macrofauna

A sparse marine macrofauna was recognized in the clayey siltstones of the lower part of the Pecínov Member (Figs 2 and 3). Broken shells of the bivalve *Perna cretacea* are common in the cores of HP-19 (113.1–113.95 m), HP-20 (116.55–117.0 m), and BJ-18 (107.1 m). Occasionally, the

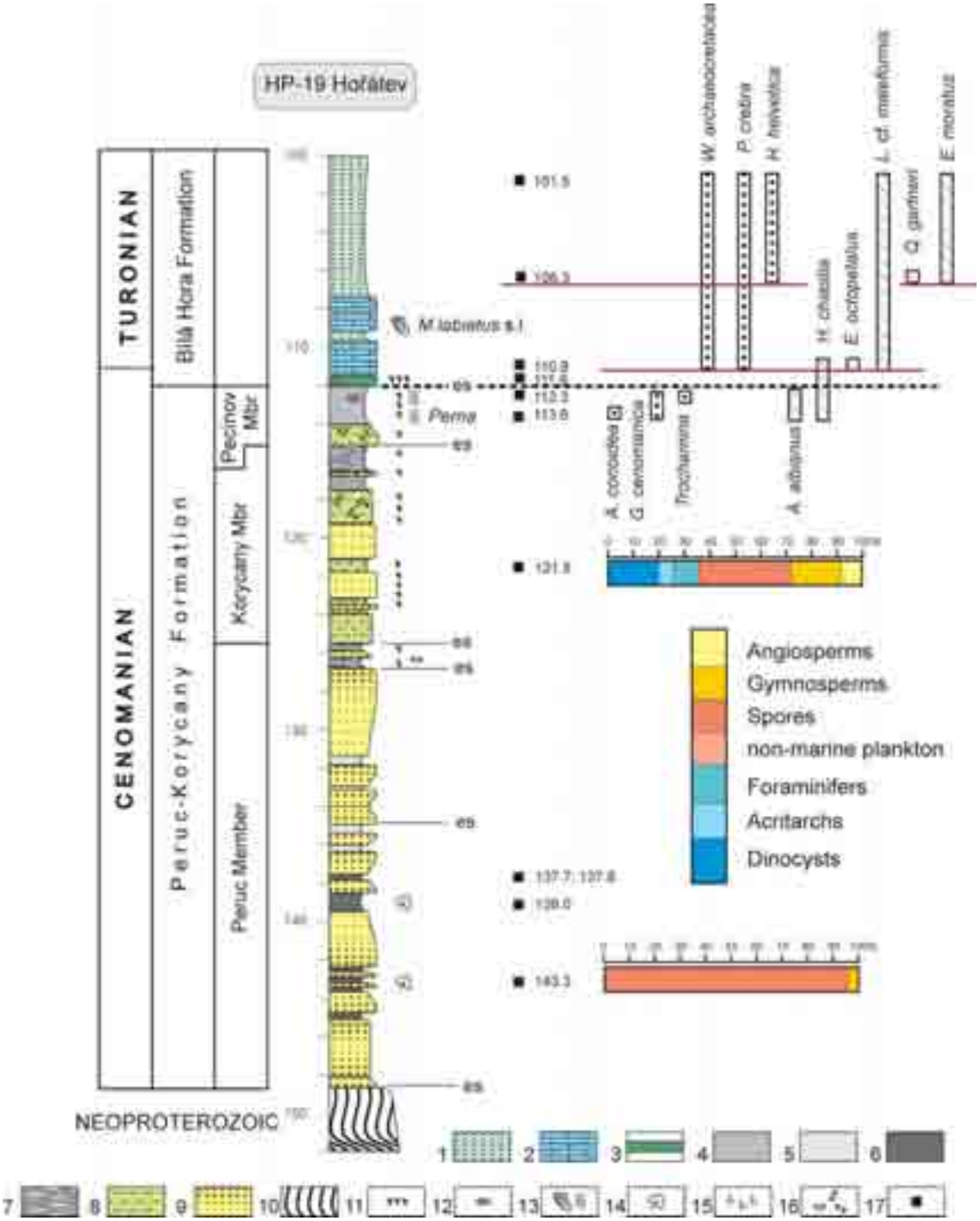

Figure 2. Lithology and distribution of macrofauna, foraminifers, calcareous nannofossils, and palynomorphs in the borehole Hořátev HP-19.
1 – marlstones, 2 – micritic limestones, 3 – glauconitic bed, 4 – calcareous clayey siltstones, 5 – claystones, 6 – carbonaceous claystones, 7 – alternation of sandstones and claystones, 8 – clayey sandstones, 9 – quartzose sandstones, 10 - metamorphosed rocks, 11 – glauconite, 12 – phosphatic nodules, 13 – macrofossils, 14 – plant macrofossils, 15 – plant roots, 16 – bioturbations, 17 – sample for micropaleontology analysis, es – erosion surface.

bivalve *Nuculana* sp. was recognized in the lower part of the Pecínov Member in borehole HP-20 (117.0 m), while the pectinid bivalve *Syncyclonema* sp. was found in borehole OP-5 (104.5 m), and *Chlamys robinaldina* in borehole BJ-18 (107.15 m).

The glauconitic bed at the base of the Bílá Hora Formation contains only small oysters. In the lower part of the Bílá Hora Formation, only fragments of the inoceramid bivalve *Mytiloides* sp. were observed in marlstones 3 m above the base of the Bílá Hora Formation in borehole HP-19 (108.9 and 105.7 m). Higher in the section, *Mytiloides* cf. *subhercynicus* appears approximately 17–19 m above the base of the Bílá Hora Formation in boreholes BJ-17 (86.5 m) and BJ-18 (87.8 m).

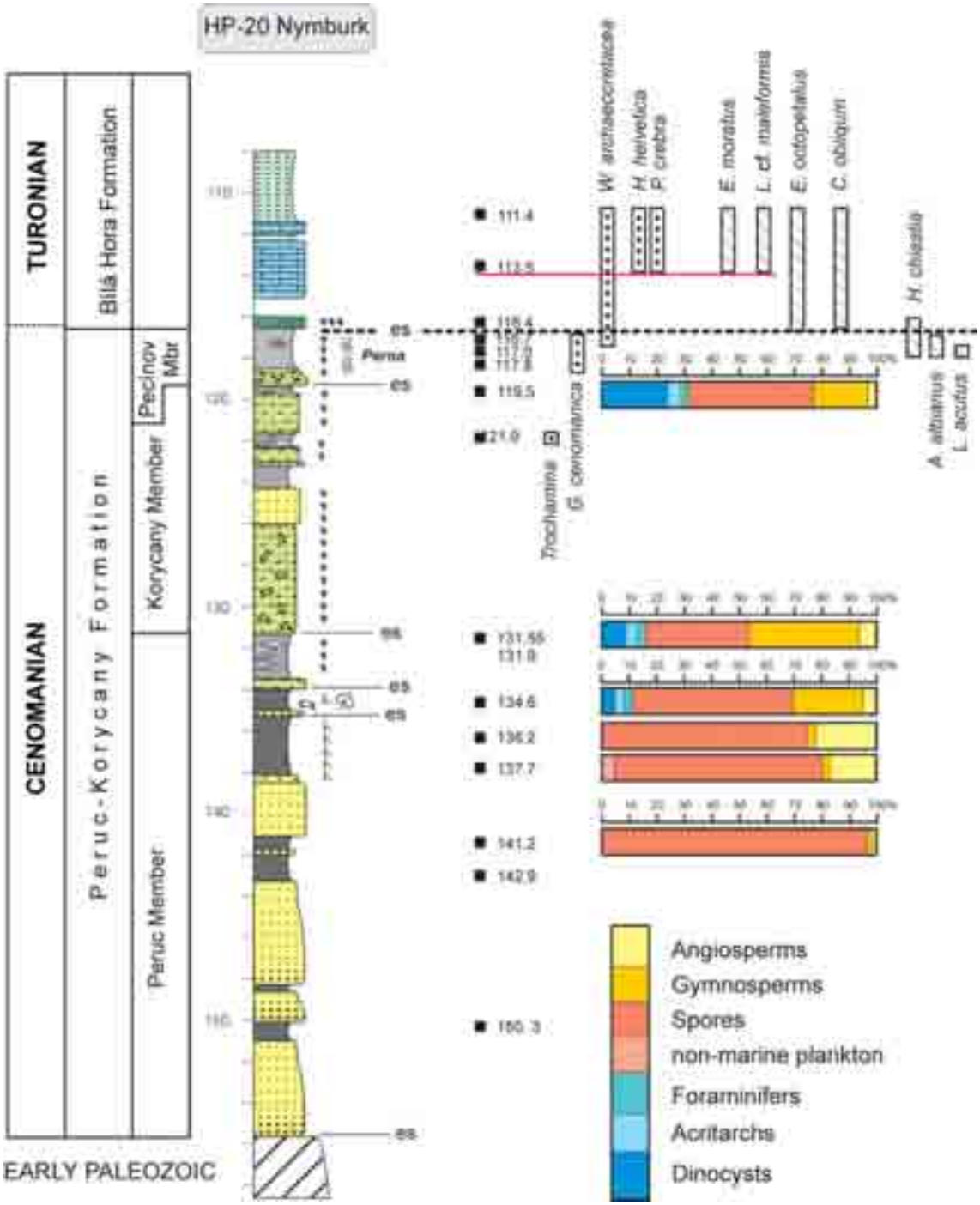

Figure 3. Lithology and distribution of macrofauna, foraminifers, calcareous nannofossils and palynomorphs in the borehole Nymburk HP-20.

Foraminifers

In borehole HP-19, *Gavelinella cenomanica* appears together with *Valvulineria lenticula* and *Ataxophragmium depressum* in siltstones of the Pecínov Member, 0.3–1.4 m below the base of glauconitic bed of the Bílá Hora Formation (Figs 2 and 4). In this stratigraphic level agglutinated species of *Arenobulimina, Haplophragmoides, Ammobaculites, Trochammina, Bigenerina*, and *Pseudotextulariella* are common. Minor components of these assemblages are calcareous forms represented mainly by *Gavelinella schloenbachi* and *Planularia complanata*. Moreover, planktonic species are again very rare. Only *Hedbergella delrioensis* and *Whiteinella brittonensis* were sporadically found.

The washed material from the lowermost Upper Cenomanian sample from borehole HP-20 (121.9 m) contained rare agglutinated species such as *Dorothia filiformis*, *Ammobaculoides lepidus*, and more frequently *Trochammina obliqua*. Only three specimens of *Gavelinella cenomanica* were found with decalcified and damaged tests. In general, agglutinated species of the genera *Arenobulimina, Haplophragmoides, Ammobaculites, Trochammina, Bigenerina*, and *Pseudotextulariella* were

abundant in the studied samples of this stratigraphic level (HP-19 113.6–112.3 m, HP-20 117.0–116.7 m, BJ-16 178.1–177.9 m, BJ-18 107.3 m). *Gavelinella schloenbachi* and *Planularia complanata* were rare here. From plankton only *Hedbergella delrioensis* and *Whiteinella brittonensis* were sporadically found (Fig. 5).

In the lower part of the glauconitic bed, at the base of the Bílá Hora Formation, inorganic material (glauconite and pyrite) prevailed in boreholes HP-19 (111.9 m) and HP-20 (116.4 m) (Figs 4–7). The foraminiferal assemblage is generally poor: only agglutinated *Arenobulimina preslii* and a few specimens of the calcareous *Lingulogavelinella* and *Gavelinella* were found.

Diversity of the foraminiferal assemblages increases gradually in the overlying sediments, i.e. in the upper part of the glauconitic bed (in boreholes BJ-17 from 103.2 m, BJ-18 from 106.5 m, and BJ-16 from 177.3 m) and the micritic limestones (in boreholes HP-19 from 110.9 m, and HP-20 from 113.5 m). The foraminiferal assemblage is characterized by the frequent occurrence of *Praebulimina crebra*, *Gavelinella polessica*, *G. belorussica, G. berthelini, Cassidella tegulata*, and *Valvulineria lenticula.* Planktonic foraminifera are represented by *Hedbergella, Whiteinella*, and *Heterohelix.* Some specimens of *Helvetoglobotruncana helvetica* were found in the micritic limestones and marlstones, approximately 3–8 m above the base of the Bílá Hora Formation. Foraminifera with agglutinated tests are represented by the genera *Gaudryina, Gyroidina*, and *Dorothia* (Figs 4 and 5).

Calcareous nannofossils

Calcareous nannofossils were found exclusively in the grey calcareous siltstone of the Pecínov Member (in boreholes Hořátev HP-19 (113.6–111.9 m), and Nymburk HP-20 (117.8–116.7 m) (Figs 8 and 9). These deposits contain low- to mid-abundance assemblages (10–20 specimens per 1 field of view of microscope) with medium-well or poorly preserved nannofossils. Coccoliths are etched, mostly in fragments, and the central areas of placoliths are usually dissolved. The assemblages contain the marker species *Axopodorhabdus albianus* (Plate III, figs 16–18) and *Helenea chiastia*, and relatively high numbers of *Watznaueria barnesae* (35–40 %, Plate IV, fig. 17), *Prediscosphaera columnata* (6–7 %), and *Broinsonia signata* (10–12 %). A characteristic phenomenon is the presence of large, broadly elliptical specimens of *Manivitella pemmatoidea* (see Plate IV, figs 31, 32).

Calcareous nannofossils from the Pecínov Member occur in the Nymburk HP-20 borehole at a depth of 117.8 m, representing only a small number of specimens of long-ranging taxa. The quantity and species diversity quickly increases in the overlying strata (see Fig. 11). The scarce presence of the stratigraphically significant *Lithraphidites acutus* (Plate IV, figs 33, 34) and *Corollithion kennedyi* (see Plate IV, figs 1, 2) was recorded from the Nymburk HP-20 borehole exclusively, at a depth of 117.0 m (see Plate 3, figs 1, 2 and 33, 34). The relatively common occurrence of *A. albianus*, and its sudden disappearance, were observed in both boreholes.

The character of the nannofossil associations is markedly different in the green glauconitic sandy marlstones (Bílá Hora Formation) of boreholes Velké Zboží BJ-17, BJ-18, Hořátev HP-19, and Nymburk HP-20 (Figs 8–11). High-abundance assemblages (40–50 specimens per field of view under the microscope) are typical for these strata. Nannofossils are well or medium-well preserved and remarkably small in size, especially in the lowermost part of the sequence. The deposits contained *Eprolithus octopetalus* (Plate III, figs 29, 30), *Ahmuellerella octoradiata,* and *Quadrum intermedium* (5 and 7 ray-like elements) among others. *Helenea chiastia* was recorded only in the lowermost part of these strata. Specimens of the genus *Broinsonia* becomes rare (*B. signata* 1 %, *B. enormis* 4 % in maximum). High content of *Watznaueria barnesae* varies between 43–47 %, and this percentage slightly decreases up to 35 % in the overlying beds. The size of nannofossils quickly returns to the standard norm. The character of nannofossil assemblages also remains very similar in the lower part of the overlying micritic limestones with an admixture of glauconite.

Up-section, the first occurrences of *Eprolithus moratus* (Plate III, figs 31, 32) and *Lucianorhabdus* cf. *maleformis* (Plate IV, figs 28–30) are observed, whereas *Eprolithus octopetalus* disappears (Figs 2 and 3). The assemblages contain higher numbers of the "subtle" specimens of the family Stephanolithiaceae, such as *Corollithion signum, C. exiguum, Cylindralithus biarcus*, and *Rotelapillus crenulatus*. Calcareous nannofossils were not studied from the deposits of borehole Velké Zboží OP-5.

Palynomorphs

The lower part of borehole Hořátev HP-19 (depth 143.3 m) is characterized by a well-preserved palynomorph assemblage consisting predominantly of fern spores (94 %) of Schizaeaceae and Gleicheniaceae. Gymnosperm pollen grains rarely occur (Figs 12, 13). Samples from the depth interval 137.7–139.0 m were barren. Marine microplankton (40 %) appear in the upper part of the HP-19 borehole (121.5 m). The terrestrial content includes bryophyte and pteridophyte spores (35 %), gymnosperm pollen (20 %), and angiosperm pollen grains (5 %). Pteridophyte spores consist of the Gleicheniaceae, Lycopodiaceae, and Cyatheaceae. *Classopollis classoides* and *Taxodiaceaepollenites hiatus* prevail among the gymnosperm pollen. *Classopollis/Corollina* pollen is often found in tetrads, suggesting a negligible distance of transport. The dinocyst assemblage includes littoral forms such as *Circulodinium distinctum* and *Epelidosphaeridia spinosa*, or neritic types such as *Spiniferites ramosus.*

In the mudstones of the lower part of borehole HP-20 Nymburk, a poor palynomorph assemblage of predominantly freshwater origin was found at 150.3 m, associated with a small percentage of acritarchs and halophyte pollen. A sample from 141.2 m contains an assemblage with a high percentage of angiosperms (42 %). A similar assemblage was recorded in the mudstone of Unit 1 of the Pecínov quarry (Uličný et al. 1997a, Svobodová et al. 1998). Two

HOŘÁTEV HP-19	Upper Cenomanian		Lower Turonian			
	Whiteinella archaeocretacea Zone				*Helvetoglobotruncana helvetica* Zone	
depth (m)	113.6	112.3	111.9	110.9	106.3	101.5
Gyroidina nitida					○	●
Hagenowina advena	x					
Arenobulimina preslii	x		x			
Ataxophragmium depressum	x	○				
Bigenerina selseyensis	x					
Haplophragmoides nonioninoides		x				
Trochammina obliqua		x				
Ammobaculites reophacoides		x				
Pseudotextulariella cretosa		x				
Dorothia gradata		x				
Haplophragmoides stelcki		x				
Trochammina globosa		x				
Gaudryina praepyramidata					○	
Dorothia filiformis					x	x
Gaudryina variabilis					x	
Praebulimina crebra				●	●	●
Lenticulina sp.	x		x		x	○
Gavelinella cenomanica	○	○				
Gavelinella schloenbachi	x			x		
Nodosaria obscura		x				
Valvulineria lenticula		○		○	●	●
Marginulina robusta		x				
Nodosaria bistegia		x				
Lingulogavelinella globosa			○	x		x
Gavelinella belorussica			○	x		
Gavelinella polessica				○	○	●
Cassidella tegulata				x	x	
Gavelinella berthelini			○	x		x
Frondicularia verneuiliana					x	
Ramulina globulifera						x
Vaginulina robusta						x
Lenticulina comptoni						x
Frondicularia inversa						x
Gavelinella baltica			x			x
Lingulogavelinella pazdroae						x
Whiteinella archaeocretacea				○	x	x
Hedbergella delrioensis	x			○	○	○
Whiteinella brittonensis			x	x	○	x
Whiteinella aprica			x	x		
Heterohelix pulchra				○	○	●
Helvetoglobotruncana helvetica					x	x
Praeglobotruncana delrioensis					x	x
Hedbergella simplex			x			
Hedbergella planispira					x	
Whiteinella baltica					○	
Dicarinella imbricata					x	

Figure 4. Distribution of foraminiferal species in Hořátev HP-19 borehole.
● abundant, ○ common, x rare, ? questionable

NYMBURK HP-20	Upper Cenomanian			Lower Turonian			
	Whiteinella archaeocretacea Zone					*H. helvetica* Zone	
depth (m)	121.9	117.8	117.0	116.7	116.4	113.5	111.4
Gaudryina praepyramidata						x	x
Gaudryina angustata							x
Dorothia filiformis	x					x	x
Gyroidina nitida							○
Gaudryina folium							x
Dorothia gradata				x			x
Gaudryina trochus						x	x
Textularia foeda							x
Trochammina obliqua	○						x
Marssonella oxycona						x	
Dorothia turris						x ?	
Haplophragmoides sp.			x	x			
Haplophragmoides ovalis				○			
Ammobaculites reophacoides				x			
Ataxophragmium depressum			○	x			
Ammodiscus gaultinus				x			
Spiroplectammina scotti		x					
Lituotuba incerta		x					
Ammobaculoides lepidus	○						●
Cassidella tegulata						x	
Praebulimina crebra						●	○
Dentalina sp.				x		x	x
Valvulineria lenticula					x	●	●
Lenticulina sp.				x		x	x
Ramulina globulifera						x	x
Vaginulina robusta							x
Gavelinella polessica						○	○
Frondicularia verneuiliana							x
Lenticulina comptoni				x		○	○
Frondicularia sp.						x	x
Planularia complanata			x	x			x
Nodosaria obscura							x
Gavelinella belorussica					x	x	
Gavelinella berthelini						○	
Lingulogavelinella globosa					○	x	
Gavelinella cenomanica	x ?	○	○	●			
Marginulina aequivoca				x			
Gavelinella schloenbachi		x					
Whiteinella brittonensis		x			○	○	●
Hedbergella delrioensis						○	●
Heterohelix globulosa							○
Whiteinella paradubia						x	○
Whiteinella archaeocretacea				x	x		x
Hedbergella planispira						x	x
Helvetoglobotrun. praehelvetica					x	x	○
Helvetoglobotruncana helvetica						x	x
Whiteinella aprica					x		x
Heterohelix pulchra						x	
Dicarinella imbricata							x
Whiteinella baltica						x	

Figure 5. Distribution of foraminiferal species in Nymburk HP-20 borehole. For explanations see Fig. 4

VELKÉ ZBOŽÍ BJ-17	Upper Cenomanian		Lower Turonian							
	W. archaeocretacea Zone		*Helvetoglobotruncana helvetica* Zone							
depth (m)	105.1	103.5	103.2	102.3	100.8	95. 1	90. 1	85. 0–85. 1	82. 0–82. 5	50.5
Gaudryina folium								x		x
Ataxophragmium depressum		x							x	x
Vaginulina robusta					x		x			x
Frondicularia verneuiliana				x	x	x				x
Gavelinella berthelini			x	x	○	●	○		○	○
Frondicularia fritschi										x
Frondicularia inversa						x				x
Gavelinella polessica			x		x	○	○	x		●
Gaudryina variabilis									x	x
Praebulimina crebra			x	x	x	x	●	○	○	●
Cassidella tegulata				x		○	●	●	x	○
Textularia foeda							x			x
Spiroplectammina sp.	x									
Gaudryina angustata				x				x	x	x
Arenobulimina preslii			x	x		○		x		○
Gaudryina praepyramidata						x		x	x	x
Vaginulina recta										x
Gaudryina trochus								x		x
Gavelinella belorussica			x	x	●	○				○
Lingulogavelinella pazdroae										x
Valvulineria lenticula			x	x	○	○	○	x	x	●
Gavelinella schloenbachi			x	x	x	○		x		x
Lingulogavelinella globosa			x	x			○			○
Gavelinella baltica			x	x				x		
Pseudotextularia cretosa	x									
Haplophragmoides sp.	x									
Whiteinella paradubia					x	x				x
Whiteinella brittonensis		x	x	x	○	x	x	x	x	○
Hedbergella planispira										x
Dicarinella imbricata			x					x		x
Helvetoglobotruncana helvetica						x		x	x	x
Heterohelix globulosa			x		○				x	○
Helvetoglobotruncana praehelvetica				x			○			x
Whiteinella archaeocretacea				x						
Heterohelix pulchra					x		x			
Praeglobotruncana delrioensis				x						
Ramulina globulifera						x			x	
Tappanina eouvigeriniformis			x	x						
Lenticulina sp.				x	x	x	x	x	x	x
Trochammina sp.	x								x	x
Dorothia turris					x	x				x
Quadrimorphina allomorphinoides								x	x	
Ammobaculites reophacoides										x
Hagenowina advena		x								
Dorothia oxycona								x	x	

Figure 6. Distribution of foraminiferal species in Velké Zboží BJ-17 borehole. For explanations see Fig. 4.

VELKÉ ZBOŽÍ BJ-18	Upper Cenomanian				Lower Turonian							
	Whiteinella archaeocretacea Zone							*Helvetoglobotruncana helvetica* Zone				
depth (m)	113.3–113.4	112.5	108.4	107.3	106.5	106.3	105.5	102.4	98.3–98.4	93.9–94.0	88.0–88.1	83.0–83.1
Gavelinella berthelini				x				x	○		x	○
Gyroidina nitida										x	x	○
Ataxophragmium depressum				x								x
Cassidella tegulata									x	○	○	x
Arenobulimina preslii				x						x	○	○
Nodosaria sp.												x
Lingulogavelinella globosa				x	x	○	●	●	○			x
Lenticulina sp.					x	x		x	x	x	x	x
Gaudryina folium												x
Gavelinella schloenbachi												x
Whiteinella brittonensis							x	○	○	x	x	x
Helvetoglobotrunc. helvetica								x	x		x	x
Vaginulina robusta							x	x	x		x	x
Gaudryina angustata										x	x	x
Gavelinella polessica							○		x			●
Dicarinella imbricata						x	x	○		x		x
Whiteinella paradubia						x	x	x		x	x	x
Frondicularia verneuilina						x					x	x
Frondicularia inversa							x	x		x		x
Lingulogavelinella pazdroae									x		x	x
Trochammina obliqua	x	x		x								x
Whiteinella baltica						x		○		x	x	x
Gavelinella baltica									x		x	x
Lenticulina comptoni						x	x		x			x
Frondicularia fritschi						x					x	x
Valvulineria lenticula						x	○	○		x		●
Hedbergella delrioensis					x			●		x		x
Ramulina globulifera						x						x
Gaudryina praepyramidata					x	x	x		x	x	x	
Gavelinella belorussica	x				x	○	x		x		x	
Textularia foeda										x	x	
Gaudryina trochus										x	x	
Gaudryina compressa ?										x	x	
Hedbergella planispira					x	x		x		x		
Marssonella oxycona				x				x		x		
Whiteinella aprica						x				x		
Praeglobotruncana oraviensis							x	x		x		
Helvetoglob. praehelvetica						○	x	○	○	x		
Praeglobotruncana delrioensis						x		x	x	x		
Dorothia filiformis				x		x	x	x	x			
Dorothia turris									x			
Whiteinella archaeocretacea				x				x	x			
Gavelinella cenomanica				x								
Ammodiscus cretaceus				x				x				
Vaginulina recta						x						
Haplophragmoides sp.				x								

Figure 7. Distribution of foraminiferal species in Velké Zboží BJ-18 borehole. For explanations see Fig. 4.

new types of angiosperm pollen appear: tetracolpate form aff. *Stephanocolpites*, and very small foveolate pollen aff. *Foveotetradites fistulosus* configured in tetrads (see Pl. VI). Non-marine sedimentation continues to the depth of 137.7 m (dark sandy mudstone), the percentage of pteridophyte spores increases while the amount of angiosperm pollen decreases. The diversification of angiosperm pollen remains high, among which the periporate species *Bohemiperiporis zaklinskae* appears. The first true marine influence occurs at a depth of 134.6 m (Peruc Member). Dinocysts (8 %) consist mainly of *Palaeohystrichophora infusorioides, Circulodinium, Cleistosphaeridium*, and *Spiniferites.* Chitinous foraminiferal linings (3 %) are also present. Pteridophyte spores prevail. Gymnosperm pollens are represented mainly by Taxodiaceae, with less-numerous inaperturate forms such as *Cycadopites fragilis, Eucommiidites minor*, and bisaccate pollen. An isolated record of *Ephedripites jansonii* and *Araucariacites australis* occurs. Angiosperm pollen is diverse and well preserved. Freshwater green zygnematacean algae *Chomotriletes minor* and *Ovoidites parvus* were identified. A similar marine content with an increasing amount of gymnosperm pollen (40 %) was recorded in dark grey clayey siltstone laminated with glauconite sandy claystone (131.9 m). Specimens of *Classopollis/Corollina*, together with bryophyte spores and pteridophyte spores dominate in the palynospectrum. Palynomorphs from the upper part of borehole HP-20 (119.5 m) are comparable to those from HP-19 (121.5 m). Pteridophyte spores prevail (45 %). *Classopollis classoides* and *Taxodiaceaepollenites hiatus* are the most common among gymnosperm pollen. Angiosperm pollen is rare. The percentage of marine microplankton increases (27 %), but the diversity remains low. The assemblage from borehole Velké Zboží OP-5 (122.3 m) is similar to that found in HP-19 (143.3 m), and it is characterized by the dominance of pteridophyte spores (93 %). Angiosperm pollen (4 %) consists of reticulate tricolpate and tricolporate forms. Changing conditions are recorded in the OP-5 borehole (112.4 m), where the marine influence is documented by the appearance of dinocysts (16 %) such as *Odontochitina, Xenascus, Palaeohystrichophora,* and *Circulodinium.* The percentage of pteridophyte spores decreases (36 %). Gymnosperm pollen (36 %) consists mainly of Taxodiaceae and *Classopollis/Corollina* pollen. Angiosperm pollen is rare, while Cenomanian species and the triporate pollen of *Complexiopollis* appear more commonly. The terrestrial content (spores, and gymnosperm and angiosperm pollen) and non-marine algae constitutes 96 % of the assemblage, with a minor marine contribution of dinocysts (*Epelidosphaeridia, Circulodinium*), foraminifers, and prasinophycean algae in the BJ-18 borehole (121.7 m). The palynomorph assemblage is well preserved and diversified. Pteridophyte spores prevail (49 %) (Gleicheniaceae, Schizaeaceae, Matoniaceae, Polypodiaceae). Bisaccate gymnosperm pollen including *Parvisaccites radiatus* and *Alisporites bilateralis* prevail, while *Ephedripites multicostatus* and *Sequoiapollenites* sp. rarely appear.

Lithological and paleoenvironmental interpretations

Depositional environment, facies assemblages, and bounding surfaces

Six facies assemblages were recognized in the Peruc-Korycany Formation: fluvial facies, estuarine bayhead delta, supratidal marsh facies, estuarine tidal flat and channel facies, estuarine and mouth sand facies, and inner marine facies. Open shelf facies include hemipelagic marlstones and limestones of the Bílá Hora Formation (Fig. 14).

Fluvial channel deposits (conglomerates and sandstones) and overbank deposits (siltstones, siltstones with coal seams and root zones) of an alluvial plain were recognized in boreholes HP-19 and HP-20, located in the axial position of the incised-valley fill (Fig. 14), and in borehole OP-5 situated on the slope of paleoelevation. These deposits are interpreted as part of the drainage system of a main paleovalley parallel to the present Jizera River (Klein et al. 1979, Uličný et al. 2003) (Fig. 1B). According to palynomorphs, the prevalence of pteridophyte spores and taxodiaceous pollen in the mudstones suggests swampy vegetation. The high percentage of angiosperm specimens in comparison with fern spores and gymnosperms only rarely occurs. This probably represents an alluvial plain assemblage consisting of shrubby and arboreal plants (Uličný et al. 1997a).

Estuarine bayhead delta facies were recognized in borehole HP-19. These facies comprise sand dominated upward-coarsening cycles of coarse-grained sandstones, occurring where the tributary entered the estuary. The occurrence of borings of marine bivalves indicates tidal influence. First marine influence in the environment is also documented by the appearance of acritarchs, chitinous foraminiferal linings, and mostly broken specimens of ceratioid and peridinioid dinocysts. Sometimes together with the marine plankton, non-marine elements occur. This bayhead delta facies disconformably overlies fluvial facies, as well as supratidal marsh facies and estuarine tidal flat and channel facies (Fig. 14).

Supratidal marsh facies are evident in borehole HP-20 as rooted mudstones with plant debris. The palynologic assemblage contains marine microplankton (8 %), foraminifers, spores, and pollen grains of Taxodiaceae (HP-20, sample 134.6 m in Figs 3, 12 and 13).

Finely laminated, dark grey mudstones with ripple-laminated, lenticular, fine-grained sandstones, and thin layers of coarse-grained sandstones scoured into the older sediments, are interpreted as estuarine tidal flat and channel facies. These facies sharply overlie supratidal marsh or fluvial strata, where the bayhead delta facies is not present (boreholes HP-20 and OP-5). It disconformably overlies Neoproterozoic rocks at a topographic paleoelevation (boreholes BJ-17 and BJ-18) (Fig. 14) where fluvial sediments are missing. Tidal influence in the heterolithic sediments is documented by glauconite admixture and by a palynologic assemblage comprised of marine microplankton (13 %), foraminifers, spores, and gymnosperms

HOŘÁTEV HP-19	Upper Cenomanian			Lower Turonian		
Standard nannofossil zones Sissingh (1977), Perch-Nielsen (1985)	CC10a				CC10b	
Upper Cretaceous nannofossil zones Burnett (1998)	UC5a		UC5b	UC5c	UC6b	
depth (m)	113.6	112.3	111.9	110.9	106.3	101.9
relative sample abundance	L	M	H	H	H	H
nannofossil preservation	M	M	VP	VP	P	VP
Axopodorhabdus albianus	C	F				
Biscutum ellipticum	F	A	F	A	C	F
Broinsonia enormis	C	F	F	F	F	F
Broinsonia matalosa	R	R		VR		VR
Broinsonia signata	A	A	R	F		
Bukrylithus ambiguus	R	VR	R	VR		
Eiffellithus turriseiffelii	A	C	C	C	C	C
Eprolithus floralis	F	F	F	F	R	F
Eprolithus cf. *moratus*	?					
Gartnerago cf. *theta*	R	R		r		
Haqius circumradiatus	R		VR		VR	
Helenea chiastia	R	F		VR		
Lithraphidites carniolensis	R	R	R	F	F	F
Manivitella pemmatoidea	R	R	VR	R	VR	F
Microrhabdulus decoratus	R			VR	VR	
Perissocyclus fenestratus	R	R			R	R
Placozygus cf. *fibuliformis*	R	F	R	VR		R
Prediscosphaera columnata	C	F	F	F	F	F
Prediscosphaera cretacea	F	F	C	F	C	C
Prediscosphaera ponticula	F	F	R	R		F
Prediscosphaera spinosa	R	R		R	VR	
Rhagodiscus asper	R	F	VR	VR		VR
Rhagodiscus splendens	F					VR
Retacapsa crenulata	R	F	F	R	F	R
Rotelapillus crenulatus	F	F	F	F	F	F
Scapholithus sp.	R					
Sollasites sp.	R	R	?			
Tegumentum stradneri	F	F	F	R	F	R
Tranolithus gabalus	R	F	R		VR	R
Watznaueria barnesae	VA	VA	VA	VA	VA	VA
Watznaueria britannica	R					
Zeugrhabdotus bicrescenticus	F	F	F	F	F	F
Zeugrhabdotus diplogrammus	C	C	C	C	A	A
Zeugrhabdotus erectus	R					
Zeugrhabdotus noeliae	F	F	C	C	F	F
Amphizygus brooksii		R		R	R	
Cretarhabdus conicus		F	R	R	R	F
Microrhabdulus belgicus		VR		VR	VR	
Stoverius achylosus		VR	VR	R	VR	F
Rhagodiscus angustus		R	R	F	VR	
Rhagodiscus plebeius		VR	VR			
Chiastozygus litterarius			F	VR		F
Gartnerago obliquum			R	R	F	R
Grantarhabdus coronadventis			F	F		R

HOŘÁTEV HP-19	Upper Cenomanian			Lower Turonian		
Standard nannofossil zones Sissingh (1977), Perch-Nielsen (1985)	CC10a				CC10b	
Upper Cretaceous nannofossil zones Burnett (1998)	UC5a		UC5b	UC5c	UC6b	
depth (m)	113.6	112.3	111.9	110.9	106.3	101.9
Helicolithus compactus			R	F		R
Helicolithus trabeculatus			F	F	F	R
Retacapsa angustiforata			R			
Watznaueria biporta			R		F	R
Watznaueria fossacincta			VR	VR		R
Zeugrhabdotus embergeri			R	R	VR	R
Cribrosphaerella ehrenbergii				R	F	
Eprolithus octopetalus				R		
Lucianorhabdus cf. *maleformis*				VR	R	VR
Quadrum intermedium (5 elements)				VR	VR	
Ahmuellerella octoradiata					R	F
Corollithion exiguum					R	
Corollithion signum					R	
Cyclagelosphaera rotaclypeata					VR	
Eprolithus moratus					F	R
Quadrum gartneri					R	
Quadrum intermedium (7 elements)					R	

Figure 8. Calcareous nannofossil distribution in the Hořátev HP-19 borehole. Abundance of nannofossil taxa: VA – very abundant (> 30 %), A – abundant (30–10 %), C – common (9–5 %), F – few (4–1 %), R – rare (< 1 %), VR – very rare (only 1–2 specimens observed in slide), r – reworked specimens. Estimates of the abundance of nannofossils in samples: H – high (> 50 specimens per field of view under the microscope), M – moderate (50–20 specimens), L – low (< 5 specimens). Preservation of nannofossils: M – moderate (overgrowth, etching or mechanical damage is apparent but majority of specimens are easily identifiable), P – poor (etching and mechanical damage is extensive, making identification of some specimens difficult), VP – very poor (some specimens cannot be identified).

(mainly halophyte and taxodiaceous pollen) (HP-20, samples 131.9 m and 131.55 m in Figs 3, 12 and 13).

Massive sandstones of the Korycany Member, which are well sorted, partly highly bioturbated, and glauconitic, are interpreted as intertidal estuarine and intertidal to subtidal mouth sand facies. The sandstones sharply overlie estuarine heterolithic sand and mud facies both in the estuary valley fill and on the paleoelevation area (Fig. 14). No macrofossils were found in these sandstones. Sand-filled burrows of *Thalassinoides*, *Ophiomorpha*, and *Diplocraterion* are common. In the upper part of these sandstones, intercalations and thin layers of heterolithic sediments occur similar in lithology and palynologic assemblage to the estuarine tidal flat and channels facies, but with higher dinocyst content. The gradual relative deepening of the sedimentological basin is indicated by higher dinoflagellate cyst diversification and by the appearance of gonyaulacoid forms, i.e. *Callaiosphaeridium asymmetricum*, *Florentinia mantelii*, *Surculosphaeridium* ?*longifurcatum* (see HP-19, sample 121.5 m, HP-20, sample 119.5 m, OP-5, sample 112.4 m in Figs 2, 3 and 14). Agglutinated foraminifers (e.g. *Trochamina, Bigenerina, Ammobaculoides and Ataxophragmium*) scarcely appear in these heterolithic sediments in boreholes HP-20 (121.9 m), BJ-18 (112.5 m and 113.4 m), and OP-5 (112.5 m and 113.4 m).

The inner shelf facies consisting of calcareous, clayey, glauconitic siltstones of the Pecínov Member are documented by a marine macrofauna, foraminifers, and calcareous nannofossils (see Figs 2, 3). Among the foraminifers, mostly agglutinated species and calcareous benthos with sporadic representatives of the planktonic genera *Hedbergella* and *Whiteinella* were found.

A major erosive surface and a transgressive lag separates the inner shelf facies from the underlying strata. On the paleohighs, the Pecínov Member transgressively overlies Neoproterozoic and early Paleozoic rocks with oyster accumulations at the base (e.g. in borehole OP-6, for location see Fig. 1C).

A highly diverse foraminifer and calcareous nannofossil assemblage in the marlstones and micritic limestones of the Bílá Hora Formation, and the abundance of planktonic species with the keeled type of tests and juvenile tests of calcareous foraminifers such as *Heterohelix*, indicate open sea conditions in the Lower Turonian. This facies is separated from the underlying inner shelf facies by a prominent erosive surface associated with stratigraphic condensation (glauconitic bed) at the base of the Bílá Hora Formation. This glauconitic key bed can be identified in the boreholes and in outcrops across almost the entire BCB.

NYMBURK HP-20	Upper Cenomanian			Lower Turonian		
Standard nannofossil zones Sissingh (1977), Perch-Nielsen (1985)	CC10a				CC10b	
Upper Cretaceous nannofossil zones Burnett 1998	UC3d–UC4b		UC5a	UC5c	UC6b	
depth (m)	117.8	117.0	116.7	116.4	113.5	111.4
relative sample abundance	L	M	M	H	H	M
nannofossil preservation	VP	M	M	M	P	P
Broinsonia signata	R	C	C	R	R	R
Eprolithus floralis	A	F	F	F	R	R
Manivitella pemmatoidea	C	R	R	VR	R	F
Prediscosphaera columnata	R	C	F	F	F	F
Watznaueria barnesae	VA	VA	VA	VA	VA	VA
Watznaueria britannica	VR		VR		R	R
Watznaueria fossacincta	F			R		
Zeugrhabdotus diplogrammus	R	C	F	A	A	A
Zeugrhabdotus scutula	R	R	R	F	R	
Zeugrhabdotus sp. (outer rim)	R					
Amphizygus brooksii		VR	VR	R	F	R
Axopodorhabdus albianus		C	F			
Biscutum ellipticum		C	F	F	R	R
Broinsonia enormis		F	F	F	C	F
Broinsonia matalosa		VR		R	R	R
Bukrylithus ambiguus		R	R	F	R	
Chiastozygus litterarius		VR		R	F	R
Corollithion kennedyi		R				
Cribrosphaerella ehrenbergii		R		R	R	F
Eiffellithus turriseiffelii		F	C	C	C	A
Gartnerago cf. *theta*		R	VR			
Helenea chiastia		R	R	VR		
Helicolithus trabeculatus		F	R	F	F	F
Lithraphidites acutus		VR				
Lithraphidites carniolensis		R	F	F	F	F
Nannoconus elongatus		VR				
Placozygus cf. *fibuliformis*		VR	R	F		
Prediscosphaera cretacea		C	C	F	C	A
Prediscosphaera ponticula		F	F	F	F	
Retacapsa angustiforata		VR		F	R	
Retacapsa crenulata		F	F	F	F	R
Rhagodiscus angustus		R	F	F	F	R
Rhagodiscus splendens		VR	R	R	R	
Rotelapillus crenulatus		F	F	F	F	
Sollasites sp.		R	R	R	VR	
Tegumentum stradneri		R	F	R	R	F
Thoracosphaera sp.		R				
Tranolithus gabalus		VR	VR	R		R
Watznaueria biporta		VR	R	F		VR
Zeugrhabdotus bicrescenticus		R	F	R	F	F
Zeugrhabdotus noeliae		R	F	F	F	F
Zeugrhabdotus trivectis		R	F			
Cretarhabdus conicus			R	R		R
Grantarhabdus coronadventis			VR	R	R	F

NYMBURK HP-20	Upper Cenomanian			Lower Turonian		
Standard nannofossil zones Sissingh (1977), Perch-Nielsen (1985)	CC10a				CC10b	
Upper Cretaceous nannofossil zones Burnett 1998	UC3d–UC4b		UC5a	UC5c	UC6b	
depth (m)	117.8	117.0	116.7	116.4	113.5	111.4
Ahmuellerella octoradiata				R		R
Corollithion exiguum				R		
Corollithion signum				VR		
Eprolithus octopetalus				VR		VR
Gartnerago obliquum				R	F	F
Helicolithus compactus				F	R	R
Microrhabdulus decoratus				R	R	
Stoverius achylosus				R	F	
Tranolithus orionatus				R	VR	
Zeugrhabdotus embergeri				F		F
Zeugrhabdotus erectus				R		
Braarudosphaera bigelowii					VR	
Eprolithus moratus					R	F
Lucianorhabdus cf. *maleformis*					R	
Haqius circumradiatus						VR
Eiffellithus turriseiffelii-eximius						VR
Isocrystallithus compactus						r
Prediscosphaera spinosa						VR

Figure 9. Calcareous nannofossil distribution in the Nymburk HP-20 borehole. For explanations see Fig. 8.

Biostratigraphy

In borehole BJ-16 Kouty (Fig. 1C), Hradecká et al. (1997) reported *Pseudoptera anomala*, *Chlamys robinaldina*, *Rastellum carinatum*, *Apiotrigonia sulcataria*, and *Neithea notabilis* from calcareous siltstones of the Pecínov Member. A similar assemblage was recognized in the same level in boreholes BJ-17, BJ-18, HP-19, and HP-20. This bivalve assemblage is typical of the Pecínov Member (formerly known in the BCB as the *Actinocamax plenus* Zone) of the central and southwestern part of the BCB (Soukup and Vodička 1967, Pražák 1989, Svoboda 1998, Uličný et. al. 1997b). In these cases, the calcareous siltstones contain *Metoicoceras geslinianum* and *Praeactinocamax plenus*, both of which characterize the Upper Cenomanian *Metoicoceras geslinianum* Zone. The bivalve *Neithea notabilis* is a typical fossil of the so-called Penrich Sandstone (*M. geslinianum* Zone) in Saxony (Häntzschel 1933). Nevertheless, based on the macrofaunal data, the Cenomanian-Turonian boundary cannot be precisely determined in the boreholes due to lack of any index species at the C-T boundary or its poor preservation.

The stratigraphically important foraminiferal species *Gavelinella cenomanica* Brotzen indicates a Cenomanian age for these samples. A relatively poor foraminiferal assemblage with rare occurrences of planktonic species of the genera *Whiteinella (W. archaeocretacea)* and *Hedbergella* make it possible to assign the strata to the planktonic *Whiteinella archaeocretacea* Interval and the Partial-range Zone (from the upper part of Upper Cenomanian to the lowermost part of the Lower Turonian) sensu Robaszynski and Caron (1995). A more diverse Early Turonian foraminiferal assemblage is represented by the *Helvetoglobotruncana helvetica* Zone (Robaszynski and Caron 1995) due to the occurrence of *H. helvetica*. The first occurrence of *H. helvetica* is correlated with the first occurrence of the calcareous nannofossil marker species *Eprolithus moratus* (Figs 2 and 3).

The last occurrence of the nannofossil species *Corollithion kennedyi* defines the UC3d-e Subzone boundary (lower Upper Cenomanian, Burnett 1998). The rare presence of this species in borehole Nymburk HP-20 is interpreted as having been reworked from the underlying strata. Conversely, *Lithraphidites acutus* may be interpreted as an autochthonous component. Its last occurrence defines the UC4-UC5 zone boundary, located within the stratigraphic interval of the Plenus Marls (*M. geslinianum* Zone, Burnett 1998). *Axopodorhabdus albianus* is a common component of Cenomanian nannofossil assemblages. Its last occurrence is a significant datum marking the UC5a-b Subzone boundary, located within the upper part of the Plenus Marls (*M. geslinianum* Zone, Burnett 1998, Paul et al. 1999).

The uppermost Cenomanian, the interval between the last occurrence of *Axopodorhabdus albianus* and the influx of Turonian nannoflora (probably equivalent to the *juddii* Zone), was identified only in the Hořátev HP-19 borehole

VELKÉ ZBOŽÍ BJ-17	Lower Turonian						
Standard nannofossil zones Sissingh (1977), Perch-Nielsen (1985)	CC10b				CC11		
Upper Cretaceous nannofossil zones Burnett (1998)	UC5c–UC6a			UC6b	UC7		
depth (m)	103.2	102.3	100.8	95.1	90.1	85.0	82.5
samle abundance	H	H	H	H	H	H	H
nannofossil preservation	M	M	M	M	M	M	M
Biscutum ellipticum	R	F	F	F	F	F	F
Broinsonia enormis	R	F	F	C	F	F	F
Broinsonia signata	R			F		F	F
Eiffellithus gorkae	F	R	F	F	F	F	
Eiffellithus turriseeiffelii	F	F	F	C	C	F	C
Eprolithus apertior	R						
Eprolithus floralis	F	F	F	F	F	F	F
Eprolithus octopetalus	R	R			F		
Gartnerago obliquum	F	F	F	F	R	F	F
Grantarhabdus coronadventis	F	R	R		R	F	F
Haqius circumradiatus	R		R	R			
?Helenea chiastia	R	R					R
Helicolithus compactus	R	R					
Helicolithus trabeculatus	F	F	F	F	F	F	F
Lithraphidites carniolensis	R		R	F	R	R	R
Manivitella pemmatoidea	F	R	F	R	R	F	F
Prediscosphaera columnata	C	F	F	F	R	R	R
Prediscosphaera cretacea	F	F	C	F	C	C	A
Prediscosphaera ponticula	F	F	C	F	F	R	F
Quadrum giganteum	R	R	R	F			
Quadrum intermedium (7 ray-like elements)	R		VR				VR
Retacapsa angustiforata	R		F	F	F	F	
Retacapsa crenulata	R				F	R	F
Rhagodiscus angustus	R	R		R	R	F	F
Tranolithus gabalus	R	F				R	R
Tranolithus orionatus	F	R	F	F	F		
Watznaueria barnesae	VA	VA	VA	VA	VA	VA	VA
Watznaueria biporta	R		R	R			
Zeugrhabdotus diplogrammus	C	C			R		
Zeugrhabdotus embergerii	F	R	C	C	C	C	A
Zeugrhabdotus noeliae	C	C	F				
Zeugrhabdotus trivectis	F	F	F	C	F	F	
Amphizygus brooksii		R	R	R	F		
Chiastozygus litterarius		R	F	F	F	F	
Cretarhabdus conicus		F	F	F	F		
Placozygus cf. *fibuliformis*		F	F	F	F	F	R
Prediscosphaera spinosa		R	R	R	R	R	R
Rhagodiscus splendens		R		F	F	R	F
Stoverius achylosus		R	R	R	F	F	F
Watznaueria fossacincta		R		VR	R	F	R
Loxolithus sp.		R	R				
Zeugrhabdotus bicrescenticus		R	F		F	R	F
Broinsonia matalosa			VR		VR		
Cribrosphaerella ehrenbergii			R	F	F	F	F

VELKÉ ZBOŽÍ BJ-17	Lower Turonian						
Standard nannofossil zones Sissingh (1977), Perch-Nielsen (1985)	CC10b				CC11		
Upper Cretaceous nannofossil zones Burnett (1998)	UC5c–UC6a			UC6b	UC7		
depth (m)	103.2	102.3	100.8	95.1	90.1	85.0	82.5
Lucianorhabdus cf. maleformis			R	R		F	
Rotelapillus crenulatus			F	R	F	F	F
Scapholithus fossilis			VR	VR			
Tranolithus minimus			VR				
Ahmuellerella octoradiata				F	F	F	F
Corollithion signum				R		F	R
Eprolitus moratus				F	F	F	F
Lapideacassis sp.				VR	R		
Quadrum gartneri				R	R		
Quadrum intermedium (5 ray-like elements)					VR		
Staurolithites laffittei					R		
Corollithion signum						VR	
Eprolithus rarus (6 elements)						VR	
Octolithus cf. *multiplus*						R	
?*Rhagodiscus plebeius*						F	
Sollasites horticus						VR	
Watznaueria britannica						R	R
Braarudosphaera bigelowii							R
Microrhabdulus belgicus							R

Figure 10. Calcareous nannofossil distribution in the Velké Zboží BJ-17 borehole. For explanations see Fig. 8.

(Fig. 2). Its short vertical range, or even its absence (Nymburk HP-20 borehole – see Fig. 3), may indicate an interruption of the otherwise continuous deposition, which is also suggested by a prominent marine erosion surface and a high content of glauconite and phosphates in the basal glauconitic bed of the Bílá Hora Formation (Figs 2, 3 and 15). In this interval, only agglutinated foraminifers appear. The foraminiferal assemblages are impoverished, and the calcareous tests of forams are decalcified.

The appropriate marker species to recognize the Turonian beds seems to be the nannofossil species *Eprolithus octopetalus,* the first occurrence of which is known from the lowermost Turonian (Burnett 1998). Nevertheless, the chronostratigraphic position of this datum remains obscure. Luciani and Cobianchi (1999) reported its occurrence in zone CC11, in the lower part of the *Helvetoglobotruncana helvetica* Zone. Burnett (1998) mentioned *E. octopetalus* at the base of subzone UC6b, and the range of zone CC11 approximately correlates with Zone UC7. The short interval between the first occurrences of *Eprolithus octopetalus* and *E. moratus* is regarded as a stratigraphically important datum comparable to the *Watinoceras devonense* ammonite Zone, the lowermost part of the Turonian (Burnett 1998). Inoceramids of *Mytiloides* ex gr. *labiatus* also occur at this level (Hořátev HP-19 borehole, 105.7 m).

Discussion

Fluvial, estuarine to shallow marine deposits were recorded from cores of the Peruc-Korycany Formation with palynomorph assemblages that correlate with the sedimentological interpretations. Similar palynomorph assemblages were found in the Pecínov quarry (Uličný et al. 1997a). In the lower part of the fluvial facies in borehole HP-20 (depth 150.3 m), a small percentage of acritarchs was found besides the typical continental palynologic assemblage that, as in the Pecínov quarry, indicates an influx of marine water upstream.

In the restricted marine facies assemblages, halophyte pollen of *Classopollis/Corollina* is a characteristic feature that indicates that their parent plants (derived from *Frenelopsis alata*, Cheirolepidicaeae, Hluštík and Konzalová 1976) were important components of the coastal marshes (Batten 1975). Batten (1982) found a direct correlation between increased numbers of cheirolepidiacean pollen and transgressive phases. A similar trend is evident through the fluvial to estuarine succession in borehole HP-20, associated with an increased number of dinocysts (Fig. 3). The diversity of dinocysts is usually low, and the association often consists of species tolerant of salinity changes, i.e. *Odontochitina operculata* or peridinioid type *Subtilisphaera perlucida.* Marine coastal to shallow shelf envi-

VELKÉ ZBOŽÍ BJ-18	Lower Turonian						
Standard nannoplankton zones Sissingh (1977), Perch-Nielsen (1985)	CC10b		CC11				
Upper Cretaceous nannofossil zones Burnett (1998)	UC5c–UC6a				UC7		
depth (m)	106.3	105.5	102.4	98.4	93.9	88.0	83.0
sample abudance	H	H	H	M	M	M	H
nannofossil preservation	M	M	M	P	P	P	M
Amphizygus brooksii	F	R	R	R		R	
Biscutum ellipticum	C	F	C	C	F	R	F
Bronsonia enormis	F	F	F	F	F	F	F
Chiastozygus litterarius	F	F	F	F	R	R	R
Cretarhabdus conicus	F	F	F	R	R	R	R
Eiffellithus turriseiffelii	F	F	C	C	C	F	C
Eprolithus floralis	R	F	F	R	R	R	F
Eprolithus octopetalus	F	R	F				
Gartnerago obliquum	R	F	F	R	F	F	F
Grantarhabdus coronadventis	R	R	F	F		R	R
?Helenea chiastia	VR						
Helicolithus compactus	R	R	F		R	R	F
Helicolithus trabeculatus	C	F	F	F	F	F	F
Lithraphidites carniolensis	R	R	R	R	R		R
Manivitella pemmatoidea	R	R	R	R	R	R	R
Prediscosphaera columnata	F	F	F	R	R	R	R
Prediscosphaera cretacea	C	C	C	F	C	C	C
Prediscosphaera ponticula	F	F	F	R	R	R	R
Quadrum intermedium (7 ray-like elements)	R			VR			
Retacapsa angustiforata	F	R	R	F	R	R	
Retacapsa ficula	VR		R		VR		
Rhagodiscus angustus	R	R	F	R	R	F	
Rhagodiscus asper	R			R		R	
Rotelapillus crenulatus	F	F	F	F	F	R	R
Tranolithus gabulus	F	R		R	R	F	R
Tranolithus orinatus	A	C	C	C	C	A	C
Watznaueria barnesae	VA	VA	VA	VA	VA	VA	VA
Watznaueria biporta	R	R			R	R	R
Watznaueria fossacincta	R				R	R	
Zeugrhabdotus bicrescenticus	R	F	R	R	R	F	F
Zeugrhabdotus diplogrammus	R	R	R	R	F		
Zeugrhabdotus noeliae	C	C	F	F		R	R
Zeugrhabdotus trivectis	F	F	R	F	R	R	
Corollithion signum		R	F		R		R
Cribrosphaerella ehrenbergii		R	R	F	R	R	R
Haqius circumradiatus		R		F			
Placozygus cf. *fibuliformis*		R	F	R	R	R	R
Retacapsa crenulata		F	R			R	R
Rhagodiscus splendens		R	R	R	R	R	R
Stoverius achylosus		F			R	R	R
Watznaueria britannica		R			R	R	
Ahmuellerella octoradiata			R	R	C	F	F
Broinsonia signata			R	F	F	F	
Eprolithus moratus			F	F	F	F	F

VELKÉ ZBOŽÍ BJ-18	Lower Turonian						
Standard nannoplankton zones Sissingh (1977), Perch-Nielsen (1985)	CC10b		CC11				
Upper Cretaceous nannofossil zones Burnett (1998)	UC5c–UC6a				UC7		
depth (m)	106.3	105.5	102.4	98.4	93.9	88.0	83.0
Lucianorhabdus cf. *maleformis*			R	R	R	F	R
Quadrum gartneri			R				
Sollasites horticus			VR				
Staurolithites laffittei			R	VR		R	
Tranolithus minimus			VR		VR		
Eprolithus apertior				VR			
Prediscosphaera spinosa				R		R	R
Braarudosphaera bigelowii					R		R
Lapideacassis sp.					R		
Octolithus ?multiplus					R		
Quadrum intermedium (5 ray-like elements)					VR	R	
Corollithion exiguum							VR
Octocyclus reinhardtii							R

Figure 11. Calcareous nannofossil distribution in the Velké Zboží BJ-18 borehole. For explanations see Fig. 8.

ronments yield dinocysts from the littoral group *Circulodinium,* the neritic group I – *Spiniferites,* and neritic group II – *Oligosphaeridium* and *Florentinia* (Wilpshaar and Leereveld 1994, Leereveld 1995). The relative abundance of ceratiacean (*Odontochitina*), peridiniacean (*Palaeohystrichophora*), and rare gonyaulacacean (*Oligosphaeridium*) groups indicate proximity to the shore, and are a useful salinity index. The increase of peridiniaceaen dinocysts indicates reduced salinity, whereas gonyaulacacean cysts are associated with offshore, open marine conditions (Davey 1970, Harland 1973, Batten 1979). Some studies (Wall 1965) have shown that acanthomorph acritarchs (i.e., *Micrhystridium*) are commonly associated with an inshore, restricted basinal environment. Many prasinophycean algae are considered to be euryhaline, and thus common in tidal pools and brackish water (Tappan 1980). Foraminiferal test-linings are useful environmental indicators because they are common in marine coastal to shallow shelf environments (Batten 1979). Miospores are also commonly more numerous than microplankton in near-shore deposits. The isolated record of gymnosperm pollen *Ephedripites* and *Araucariacites* is an indicator of arid/semiarid environments (Ibrahim and Schrank 1996). Ephedroid pollen characterises a Tethyan realm, while in the Boreal realm deposits are rarely encountered.

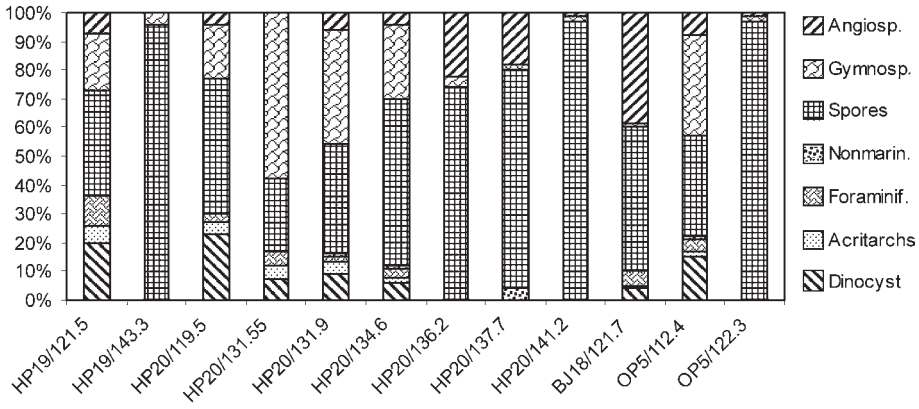

Figure 12. Distribution of dinocysts, acritarchs, non-marine plankton, spores, and pollen in productive samples of HP-19, HP-20, BJ-18 and OP-5 boreholes from the Poděbrady area.

The rare occurrences of agglutinated foraminifera species of *Trochammina, Bigenerina, Ammobaculoides*, and *Ataxophragmium* were recorded in non-calcareous heterolithic sediments from the Korycany Member. These foraminifers were probably able to tolerate the paralic environment with lower salinity (Koutsoukos and Hart 1990). Palynomorph assemblages from these beds (HP-20, sample 119.5 m) exhibit features similar to estuarine tidal flat and channel facies associations, but with a considerably higher content of dinocysts. It seems that the heterolithic intercalations in the Korycany sandstones were deposited in an intertidal to shallow subtidal environment, probably at the mouth of the estuary.

The dinocyst species *Epelidosphaeridia spinosa* (formerly regarded as Middle Cenomanian – the *E. spinosa* Subzone of Davey, 1970) occurs in some samples (HP-19: 121.5 m, HP-20: 119.5 m, BJ-18: 121.7 m, OP-5: 112.4 m). Robaszynski et al. (1988) and Paul et al. (1994) reported its occurrence also in the upper part of Lower Cenomanian (*Mantelliceras dixoni* Zone) and Middle Cenomanian (*Acanthoceras rhotomagense* Zone) in northwest Europe.

Boreholes No.	HP-19		HP-20									BJ-18	OP-5	
sample No./depth (m)	HP19/121.5	HP19/143.3	HP20/119.5	HP20/131.55	HP20/131.9	HP20/134.6	HP20/136.2	HP20/137.7	HP20/141.2	HP20/142.9	HP20/150.3	BJ18/121.7	OP5/122.3	OP5/112.4
Dinoflagellate cysts														
Achomosphaera ramulifera			x	x										
Callaiosphaeridium assymetricum														
Canningia sp.				x										
Cleistosphaeridium spp.	x				xx	x						xx		
Circulodinium distinctum	x		x		xx	xx						xx		xx
Epelidosphaeridia spinosa	xx		xx	x								xx		xx
Florentinia mantelii														x
Odontochitina operculata														x
Oligosphaeridium complex	x													
Palaeohystrichophora infusorioides			x			x								x
Pervosphaeridium pseudhystrichodinium						x								
Spiniferites ramosus	xx		xx		xx	x						x		xx
Surculosphaeridium ? longifurcatum	x													x
Xenascus ceratioides														x
Acritarcha and Prasinophyta														
Cymatiosphaera sp.	x					x		x				x		
Micrhystridium fragile					xx	xx								x
Micrhystridium spp.	xx		xx	x	x	xx								
Veryhachium hyalodermum				x										x
Non-marine algae Zygnemataceae														
Chomotriletes minor						x		xx	xx					
Ovoidites parvus					x	x		xx				xx		x
Paralecaniella sp.								xx				x		
Tetraporina sp.														x
Bryophyte and pteridophyte spores														
Biretisporites potoniei		x				x								
Calamospora sp.													x	
Camarozonosporites ambigens				xx	xx	xx	●					x		
Camarozonosporites insignis	xx		xx	xx	xx	xx		●						xx
Cicatricosisporites venustus	x	xx		x		xx						xx		
Cicatricosisporites sp.		xx						xx			x			
Cingutriletes clavus					xx			xx						
Clavifera triplex		x				x							xx	
Coronatispora sp.				xx				x						
Deltoidospora minor	xx	xx	x		x		xx		xx				xx	
Foveogleicheniidites confossus		xx					xx		x					
Foveotriletes subtriangularis						x								
Gleicheniidites carinatus							x	x					xx	
Gleicheniidites circiniidites												xx		
Gleicheniidites senonicus	●			xx		○	○	○	●	x	●	xx	●	●
Laevigatosporites ovatus					x	●	●	●	●			x		
Leptolepidites psarosus		xx			x								x	
Matonisporites sp.												x		
Microfoveolatosporites canaliculatus							x					x	x	
Ornamentifera echinata									x			x	xx	

Boreholes No.	HP-19		HP-20									BJ-18	OP-5	
sample No./depth (m)	HP19/121.5	HP19/143.3	HP20/119.5	HP20/131.55	HP20/131.9	HP20/134.6	HP20/136.2	HP20/137.7	HP20/141.2	HP20/142.9	HP20/150.3	BJ18/121.7	OP5/122.3	OP5/112.4
Plicatella spp.			xx						xx	x		xx		x
Reticulosporites sp.		x												
Retitriletes austroclavatidites			xx	xx	xx			x						xx
Sestrosporites pseudoalveolatus							x							
Stereisporites antiquasporites	xx		xx	xx	●		○		●			xx		xx
Stereisporites psilatus			xx				xx		xx					
Undulatisporites sp.						x								
Vadaszisporites urkuticus						x	x							
Gymnosperm pollen grains														
Alisporites bilateralis						xx						○		
Araucariacites cf. *australis*						x								
Classopollis classoides	●	x	xx	○	○	x								○
Cycadopites fragilis						xx			●					
Ephedripites jansonii						x								
Ephedripites multicostatus												x		
Eucommiidites minor						xx			xx					
Inaperturopollenites sp.		x			xx	x		x						
Parvisaccites radiatus	xx				x	●	xx		x		xx	○		xx
Phyllocladidites sp.						x								
Pinuspollenites sp.					xx	xx	x		x					
Sequoiapollenites sp.											x	x		
Taxodiaceaepollenites hiatus	xx		xx	xx	xx	○	xx	x	●		xx	○	x	○
Taxodiaceaepollenites vacuipites						xx			x					
Angiosperm pollen grains														
Bohemiperiporis zaklinskae					x		xx							
Brenneripollis peroreticulatus							xx	xx						
Clavatipollenites minutus					xx		xx	x						x
Complexiopollis sp.														x
aff. *Foveotetradites fistulosus*									xx					
Foveotricolpites sp.			x											x
Liliacidites sp. A						xx						x		x
Perucipollis minutus							●	xx	○				x	
Psilatricolpites parvulus	xx		x			xx	xx	xx					x	
Psilatricolporites sp.									xx					
Retitricolpites micromunus			xx				xx		●					
Retitricolpites němejci														
Retitricolpites virgeus									x					
Retitricolpites vulgaris			xx				xx							
Retitricolpites spp.					xx	xx	xx	xx	x	x		x		xx
Retitricolporites spp.	xx											x	xx	x
aff. *Stephanocolpites* sp.									x					
Tricolpites barrandei					x		xx		xx					
Tricolpites crassimurus								x						
Tricolpites cf. sagax						x								

Figure 13. Relative abundances of the main palynomorph groups through the HP-19, HP-20, BJ-18, OP-5 borehole sequences.
x – rare, xx – common (2–10 specimen), ● – abundant (11–25 specimen), ○ – frequent (more than 26 specimens)

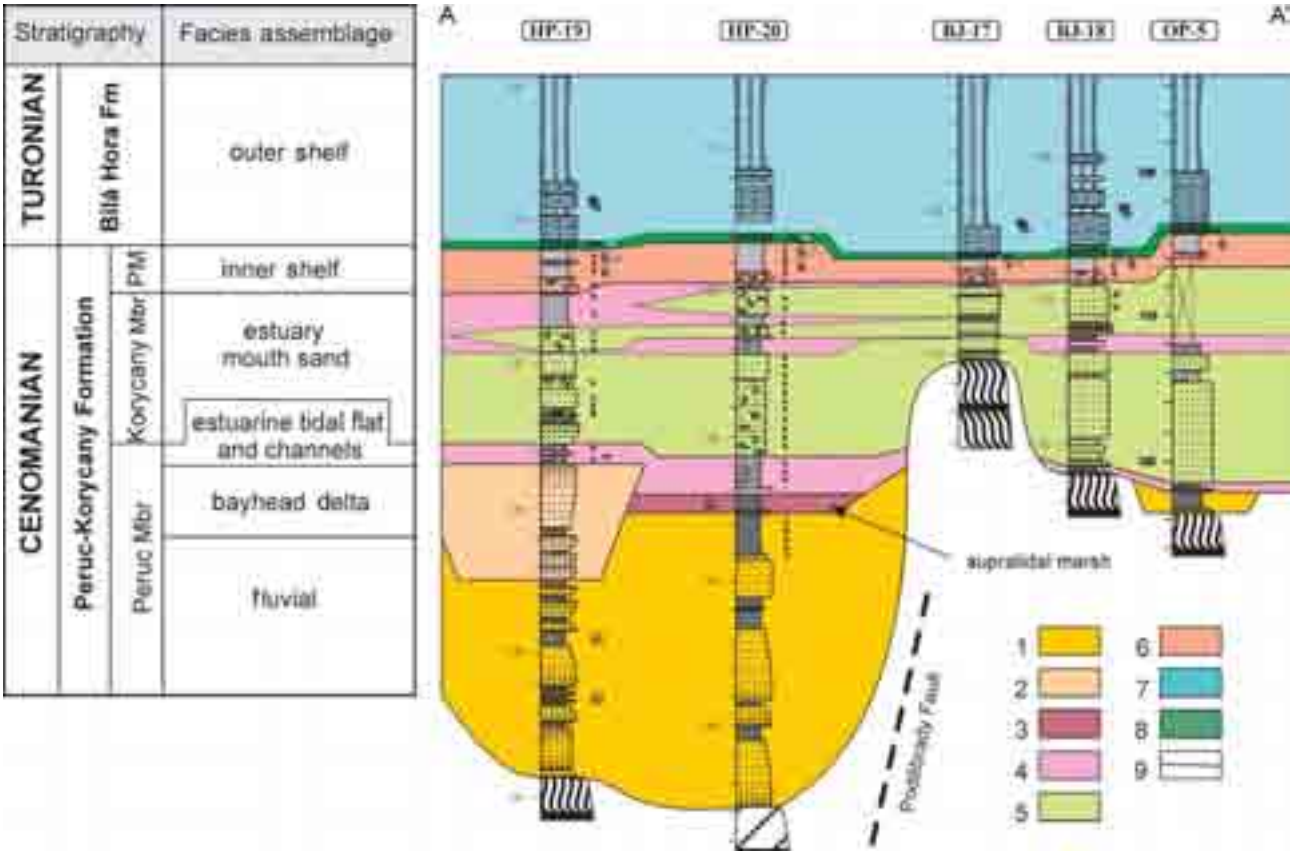

Figure 14. Stratigraphic cross section A–A´ of the Poděbrady area and facies assemblages, illustrating transgessive character of Cenomanian-Turonian sequence. Location of the cross section A–A´ is shown in Fig. 1C. Incised-valley fill and paleoelevation is shown. Heterolithic bed within Korycany Formation was chosen as key bed. For lithology see explanations on Fig. 2.
1 – fluvial facies, 2 – estuarine bayhead delta facies, 3 – supratidal marsh facies, 4 – estuarine tidal flat and channels facies, 5 – estuarine and mouth sand facies, 6 – inner shelf facies, 7 – open shelf facies, 8 – glauconitic bed, 9 – bounding surfaces, PM – Pecínov Member.

In Spain, *E. spinosa* was reported from the Upper Cenomanian above the first occurrence of planktonic foraminifers of *Helvetoglobotruncana praehelvetica*, and just below the first appearance of bivalve species *Mytiloides submytiloides* by Mao and Lamolda (1998). According to a recent study by Svobodová (unpublished), *E. spinosa* was found in the calcareous siltstones of the Pecínov Member in borehole Dolní Bousov DB-1, from the northern part of the BCB, together with *Praeactinocamax plenus* (Upper Cenomanians *M. geslinianum* Zone).

The biostratigraphically important angiosperm pollen *Complexiopollis* spp. from the Normapolles Group appears in sample OP-5 (from 112.4 m), and it may correspond with the upper part of the Korycany Member. According to Laing (1975), Durand and Louail (1976), Pacltová (1977), Louail et al. (1978), and Méon et al. (2004) the first primitive *Complexiopollis* pollen (three pores are often unclear) are found in the *jukes-brownei* Zone, Middle Cenomanian, but the earliest occurrence of true Normapolles, represented by the genera *Complexiopollis* and *Atlantopollis*, are known from the Upper Cenomanian (Solé de Porta 1978, Méon et al. 2004).

In the cores, stratigraphically important foraminifers and nannofossils were obtained only from calcareous siltstones of the uppermost part of the Cenomanian (Pecínov Member), and from the marlstones and micritic limestones of the Turonian Bílá Hora Formation.

The foraminiferal assemblage of the Pecínov Member consists mostly of agglutinated and calcareous benthos with the stratigraphically important *Gavelinella cenomanica*. The appearance of *Gavelinella cenomanica* in this region provides evidence for the local development of calcareous Cenomanian sediments, which are characteristic for the central part of the BCB between Mělník and Benátky n. J., where *G. cenomanica* is abundant (Hradecká 1993, Uličný et al. 1993).

The foraminiferal assemblage of the Upper Cenomanian Pecínov Member was set to the planktonic *Whiteinella archaeocretacea* Interval and Partial-range Zone sensu Robaszynski and Caron (1995). The presence of the planktonic *Rotalipora cushmani* Zone (the uppermost part of the Middle Cenomanian to the lower part of the Upper Cenomanian) was not recorded due to the very sporadic occurrence or absence of *Rotalipora cushmani* in the Cenomanian sediments of the BCB (see also discussion in Uličný et al. 1993).

In the literature, the Cenomanian-Turonian boundary is not clearly defined by the first occurrence of any nannofossil species. Some authors have mentioned the first occurrence of *Quadrum gartneri* in the lowermost Turonian (Lamolda et al. 1994, Luciani and Cobianchi 1999,

Paul et al. 1999, and others), though Burnett (1998) records its first occurrence in the upper part of the Lower Turonian. Polycycloliths of the genus *Quadrum*, having four large ray-like elements of equal size, and one to three small ray-like elements in each cycle of the wall, were also included as *Q. gartneri* up to 1992 when Varol (1992) described them as a new species, *Quadrum* intermedium. In the studied material, both *Quadrum gartneri* and *Q. intermedium* were observed in very low numbers in Turonian deposits, and they are suitable neither for the precise zonation nor for the determination of Cenomanian-Turonian boundary. For instance, species *Q. intermedium* (5 elements) was found in Hořátev HP-19 borehole at a depth of 110.9 m, in association with *Eprolithus octopetalus*. Nevertheless, rare *Q. intermedium* occurrences (introduced as *Q. gartneri* by Hradecká et al. 1997) were recorded from the uppermost Cenomanian of the nearby borehole Kouty BJ-16.

Figure 15. Core photo from borehole Sokoleč OP-3, core interval 63.1–63.25 m. Erosion surface at the base of green glauconitic sandy marlstone (base of Bílá Hora Fm.) with pebbles of quartz and phosphatic nodules. *Thallassinoides* burrows pipe glauconitic sediment down into the underlying dark grey siltstones of the Pecínov Member. Core is stored at CGS.

According to Roth and Krumbach (1986), the positive correlation of the C_{org} content of the sediment and the relative abundance of *Watznaueria barnesae* indicate carbonate dissolution caused by the release of carbon dioxide during the oxidation of organic matter. Assemblages with more than 40 % of *W. barnesae* are probably highly dissolved and secondarily enriched in this species. This phenomenon was observed especially in the Cenomanian, where low-diversity nannofossil assemblages are secondarily modified by carbonate dissolution. It is supported not only by higher percentage of *W. barnesae*, but also by the mode of coccolith preservation and by the absence of some "subtle" species of Stephanolithiaceae. In contrast, nannofossils in basal Turonian strata are well preserved, diversified, and small in size, though the abundance of *W. barnesae* is also high. Similar nannofossils, remarkably small in size but of a different age (Upper Turonian and Coniacian), were observed in the marine transgressive deposits of the Lower Gosau-Subgroup, Northern Calcareous Alps (Hradecká et al. 1999). In the overlying strata, the percentage of *W. barnesae* decreases slightly, while the sizes of nannofossils return to the standard form. The abundance and higher species diversity of the latter, along with the relatively common occurrence of "subtle" specimens of the family Stephanolithiaceae, may evince relatively settled marine depositional environments.

Conclusions

The following conclusions can be drawn from the foregoing discussion:

1. An incised valley filled by Cenomanian fluvial and estuarine sediments and paleoelevation was recognized in studying new and older boreholes. This paleovalley was a side tributary of the main Cenomanian depression in the central part of the BCB.
2. The sedimentary sequence of the Peruc-Korycany (Cenomanian) Formation shows an overall transgressive character from fluvial through estuarine, and up to inner shelf environment. The transgressive character of the sedimentary sequence was interpreted according to the succession of facies assemblages and the flora and fauna distribution in drill core samples.
3. The following depositional environments were recognized according to facies assemblages in the Peruc-Korycany Formation: fluvial facies, estuarine bayhead delta, supratidal marsh facies, estuarine tidal flat and channel facies, estuarine and mouth sand facies, and inner marine facies.
4. A transgressive succession from fluvial to supratidal marsh to estuarine tidal flat facies is well documented in Nymburk HP-20 borehole by the gradual increase of halophyte gymnosperm pollen and dinocysts that tolerate salinity changes, as well as by a decrease in the numbers of pteridophyte spores (Fig. 3).
5. In the general transgressive/regressive order through the Cenomanian–Turonian sequence, there are transgressive/regressive sequences of smaller orders, interrupted by major or prominent bounding surfaces associated with erosional surface and stratigraphic condensation of the uppermost Cenomanian strata. The gradual deepening into open shelf facies is documented by the increasing diversity of foraminifer and calcare-

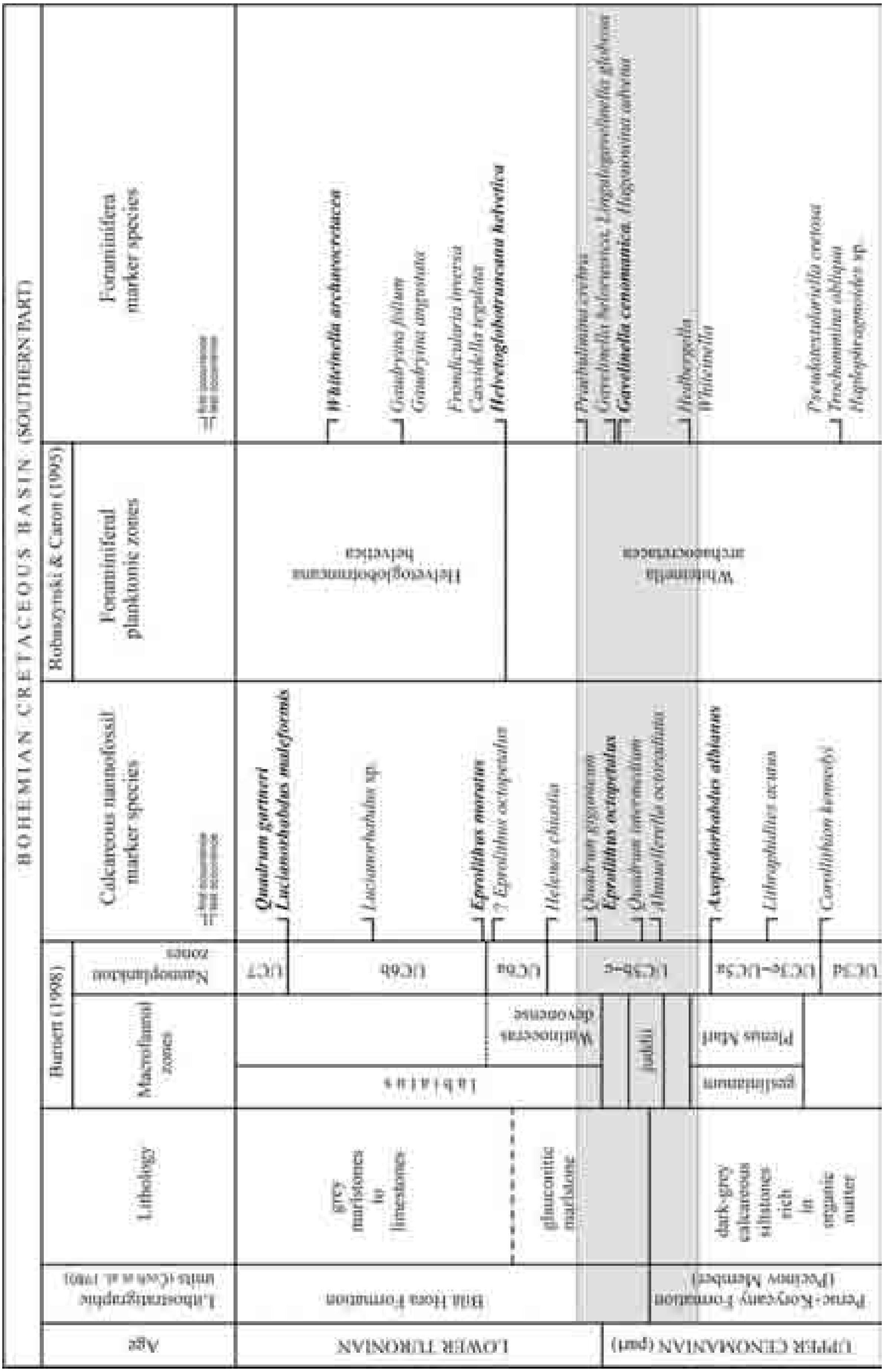

Figure 16. Correlation of foraminifers and calcareous nannofossils. Interval of stratigraphic condensation is marked in grey.

ous nannoplankton assemblages in the overlying hemipelagic sediments of Turonian age.

6. Based on the triporate angiosperm pollen Complexiopollis, the age of most of the studied samples from the Peruc and Korycany members correspond to the Middle to Upper Cenomanian. *Epelidosphaeridia spinosa* occurs from the Middle Cenomanian up to the Upper Cenomanian. In the BCB, this species was found also in siltstones yielding *Preactinocamax plenus* (*Metoicoceras geslinianum* Zone).
7. Biostratigraphically, the Upper Cenomanian marine strata can be subdivided into two parts according to the last occurrence of the nannofossil species *Axopodorhabdus albianus*. The lower part (zones ?UC4–UC5a) represented by calcareous siltstones of the Pecínov Member correlates approximately with the lower part of the Plenus Marl (*M. geslinianum* Zone). The upper part [zones UC5b–UC5c (lower part)] is represented by the glauconitic bed of the base of Bílá Hora Formation, and is separated from the lower part by a prominent erosion surface. This interval is correlated with the *Neocardioceras juddii* Zone, and probably with the uppermost part of the *M. geslinianum* Zone (Fig. 16).
8. The interval from the first occurrence of the nannofossil species *Eprolithus octopetalus* to the first occurrence of *Eprolithus moratus* (zones UC5c–UC6a) in the hemipelagic micritic limestones of the lower part of the Bílá Hora Formation coincides approximately with the *Watinoceras devonense* Zone, which is delineated within the lowermost part of Turonian.
9. The first occurrence of *Eprolithus octopetalus* falls into the *Whiteinella archaeocretacea* Interval and the Partial-range Zone. In lower part of the Bílá Hora Formation, the first occurrence of *Eprolithus moratus* coincides with the first appearance of foraminiferal planktonic species *Helvetoglobotruncana helvetica* (Fig. 16).

References

Batten D. J. (1975): Wealden palaecology from the distribution of plant fossils. Proc. Geol. Assoc. 85, 433–458.

Batten D. J. (1979): Miospores and other acid-resistant microfossils from the Aptian/Albian of Holes 400A and 402A, DSDP-IPOD Leg 48 Bay of Biscay. In: Initial Reports of the Deep Sea Drilling Project, 48. U.S. Government Printing Office, Washington, D. C., 579–587.

Batten D. J. (1982): Palynofacies and salinity in the Purbeck and Wealden of southern England. In: Banner F. T., Lord A. R. (eds) Aspects of micropalaeontology. London, 278–308.

Burnett J. A. (1998): Upper Cretaceous. In: Bown P. R. (ed.) Calcareous nannofossil biostratigraphy. Cambridge University Press, Cambridge, 132–199.

Čech S. (2004): Křídová výplň poděbradské zřídelní struktury. Zpr. geol. Výzk. v Roce 2003, 20–21 (in Czech with English abstract).

Čech S., Klein V., Kříž J., Valečka J. (1980): Revision of Upper Cretaceous Stratigraphy of the Bohemian Cretaceous Basin. Věst. Ústř. Úst. geol. 55, 277–296.

Davey R. J. (1970): Non-calcareous microplankton from the Cenomanian of England, northern France and North America. Part II. Bull. Br. Mus. (Nat. Hist.), Geol. 18, 33–397.

Durand S., Louail J. (1976): Intérét stratigraphique du sondage de Loudun (Vienne) pour l'étude du Cénomanien de l'ouest de la France. C. R. Hebd. Seances. Acad. Sci., Série D 283, 1719–1722.

Eliášová H. (1997): Coraux crétacé de Boheme (Cenomanien supérieur; Turonien inférieur–Coniacien inférieur), République tchèque. Bull. Czech Geol. Surv. 72, 3, 245–266.

Frejková L., Vajdík J. (1974): Příspěvek k paleogeografii a litologii cenomanských sedimentů v orlicko-žďárské faciální oblasti. Sbor. GPO 8, 5–28 (in Czech).

Häntzschel W. (1933): Das Cenoman und die Plenus-Zone der sudetischen Kreide. Abh. Peuss. Geol. Landesant., NF. 150, 1–161.

Harland R. (1973): Dinoflagellate cysts and acritarchs from the Bearpaw Formation (Upper Campanian) of southern Alberta, Canada. Paleontology 16, 665–706.

Hercogová J. (1968): Strukturní vrty OP-1 až OP-6 na Poděbradsku. Zpráva o mikrobiostratigrafickém vyhodnocení svrchní křídy. In: Hruška J., Kolářová M., Krásný J., Müller V., Vodička J. (eds) Podklady pro ochranná pásma lázní Poděbrad. Hydrogeologie Poděbradska a návrh ochrany lázní Poděbrad. Unpub. Czech Geological Survey – Geofond, Prague (in Czech).

Hluštík A., Konzalová M. (1976): Polliniferous cones of Frenelopsis alata (K. Feistm.) Knobloch from the Cenomanian of Czechoslovakia. Věst. Ústř. Úst. geol. 51, 37–45.

Hradecká L. (1993): Changes of foraminiferal assemblages and related events of the Late Cenomanian to Early turonian in the central part of the Bohemian Cretaceous Basin. Acta Univ. Carol., Geol. 3–4, 19–22.

Hradecká L., Lobitzer H., Ottner F., Sachsenhofer R. F., Siegl-Farkas A., Švábenická L., Zorn I. (1999): Biostratigraphy and Palaeoenvironment of the marly marine transgression of Weißenbachalm Lower Gosau-Subgroup (Upper Turonian-Lower Santonian Grabenbach-Formation, Northern Calcareous Alps, Styria). Abh. Geol. B.-A. 56, 2, 475–517.

Hradecká L., Pražák J., Švábenická L. (1997): Předběžné vyhodnocení vrtu Kouty BJ-16 (česká křídová pánev). Zpr. geol. Výzk. v Roce 1996, 113–115 (in Czech).

Hradecká L., Švábenická L. (1995): Foraminifera and Calcareous Nannoplankton assemblages from the Cenomanian-Turonian boundary interval of the Knovíz Section, Bohemian Cretaceous Basin. Geol. Carpath. 46, 5, 267–276.

Hruška J., Kolářová M., Krásný J., Müller V., Vodička J. (1968): Podklady pro ochranná pásma lázní Poděbrad. Hydrogeologie Poděbradska a návrh ochrany lázní Poděbrad. Unpub. Czech Geological Survey – Geofond, Prague (in Czech).

Ibrahim M., Schrank E. (1996): Palynological studies on the Jurassic-Early Cretaceous of the Kahraman-1 well, Northern Western desert, Egypt. Géologie de l'Afrique et de l'Atlantique Sud: Actes Colloques Angers 1994, 611–629.

Klein V. (1966): Stratigrafie a litologie svrchní křídy mezi Jizerou a Labem. Sbor. geol. Věd, Geol. 11, 49–75 (in Czech with German abstract).

Klein V., Hercogová J., Rejchrt M. (1982): Stratigraphie, Lithologie und Paläontologie der Kreide im Elbe-Faziesgebiet. Sbor. geol. Věd, Geol. 36, 27–92.

Klein V., Müller V., Valečka J. (1979): Lithofazielle und paläogeographische Entwicklung des Böhmischen Kreidebeckens. Aspekte der Kreide Europas. IUGS Series A 6, 425–446.

Koutsoukos E. A. M., Hart M. B. (1990): Cretaceous foraminiferal morphogroup distribution patterns, palaeocommunities and trophic structures: a case study from the Sergipe Basin, Brazil. Trans. R. Soc. Edinb.-Earth Sci. 81, 221–246.

Laing J. F. (1975): Mid-Cretaceous angiosperm pollen from Southern England and Northern France. Paleontology 18, 4, 775–808.

Lamolda M. A., Gorostidi A., Paul C. R. C. (1994): Quantitative estimates of calcareous nannofossil changes across the Plenus Marls (latest Cenomanian), Dover, England: implications for the generation of the Cenomanian-Turonian boundary event. Cretac. Res. 15, 143–164.

Leereveld H. (1995): Dinoflagellate cysts from the Lower Cretaceous Río Argos succession (SE Spain). Lab. Palaeobot. Palynol. Contr. Ser. 2, 1–175.

Louail J., Bellier J. P., Damotte R., Durand S. (1978): Stratigraphie du Cénomanien littoral de la marge Sud-Ouest du Bassin de Paris. L'example du sondage de Loudun. Géol. Méditer. 5, 1, 115–124.

Luciani V., Cobianchi M. (1999): The Bonarelli Level and other black shales in the Cenomanian-Turonian of the northeastern Dolomites (Italy): calcareous nannofossil and foraminifera data. Cretac. Res. 20, 135–167.

Mao S., Lamolda M. A. (1998): Quistes dinoflagelados del Ceno-

maniense superior y Turoniense inferior de Ganuza, Navara. I – Paleontología sistemática. Rev. Esp. Paleontol. 13, 2, 261–286.
Méon H., Guignard G., Pacltová B., Svobodová M. (2004): Normapolles. Comparaison entre l'Europe centrale et du Sud-Est pendant le Cénomanien et le Turonien: évolution de la biodiversité et paléoenvironnement. Bull. Soc. géol. Fr. 175, 6, 579–593.
Pacltová B. (1977): Cretaceous angiosperms of Bohemia – Central Europe. Bot. Rev. 43, 1, 128–142.
Pacltová B., Svobodová M. (1993): Facial characteristics from palynological point of view in the area of the Bohemian Cenomanian. Proc. Symposium Paleofloristic and Paleoclimatic changes during Cretaceous and Tertiary, September 1992 Bratislava, Konf., Symp., Semináre, Geol. úst. D. Štúra, 17–21.
Paul C. R. C., Lamolda M. A., Mitchell S. F., Vaziri M. R., Gorostidi A., Marshall J. D. (1999): The Cenomanian-Turonian boundary at Eastbourne (Sussex, UK): a proposed European reference section. Paleogeogr. Paleoclimatol. Paleoecol. 150, 83–121.
Paul C. R. C., Mitchell S. F., Marshall J. D., Leary P. N., Gale A. S., Duane A. M., Ditchfield P. W. (1994): Palaeoceanographic events in the Middle Cenomanian of Northwest Europe. Cretac. Res. 15, 707–738.
Perch-Nielsen K. (1985): Mesozoic calcareous nannofossils. In: Bolli H. M., Saunders J. B., Perch-Nielsen K. (eds) Plankton stratigraphy. Cambridge Univ. Press, Cambridge, 329–426.
Pražák J. (1989): Hranice cenoman–turon v centrální části české křídové pánve. Unpub. Czech Geological Survey, Prague (in Czech).
Robaszynski F., Alcaydé G., Amédro F., Badille G., Damotte R., Foucher J.-C., Jardiné S., Legoux O., Manivit H., Moncardini Ch., Sornay J. (1988): Le Turonien de la region-Type: Saumurois et Touraine, Stratigraphie, Biozonations, Sédimentologie. Bull. Centres Rech. Explor., Prod. El-Aquitaine 6, 1, 119–225.
Robaszynski F., Caron M. (1995): Foraminifčres planctoniques du Crétacé commentaire de la zonation Europe – Méditerranée. Bull. Soc. Géol. France 166, 6, 681–692.
Roth P. H., Krumbach K. P. (1986): Middle Cretaceous calcareous nannofossil biogeography and preservation in the Atlantic and Indian Oceans: Implications for paleoceanography. Mar. Micropaleontol. 10, 235–266.
Sissingh W. (1977): Biostratigraphy of Cretaceous calcareous nannoplankton. Geol. Mijnb. 56, 37–65.
Solé de Porta N. (1978): Palynology of two Cenomanian sections near Oviedo, Spain. Palinologia, Núm. Extraord. 1, 435–441.
Soukup J., Vodička J. (1967): Strukturní vrt do podloží křídy v Sobčicích u Jičína (KN-5). Zpr. geol. Výzk. v Roce 1967, 194–196 (in Czech).
Svoboda P. (1998): Transgrese svrchní křídy mezi Kralupy nad Vltavou a Korycany. Studie Okres. muz. Praha-východ 13, 129–154 (in Czech).
Svobodová M. (1990): Lower Turonian microflora at Skalka near Velim (Central Bohemia, CSFR). Bull. Czech Geol. Surv. 65, 5, 291–300.
Svobodová M., Méon H., Pacltová B. (1998): Characteristics of the Upper Cenomanian–Lower Turonian (anoxic facies) of the Bohemian and Vocontian Basins. Bull. Czech Geol. Surv. 73, 3, 229–251.
Štemproková-Jírová D. (1991): Biostratigraphy of planktic foraminifera from the Cenomanian and Turonian of the locality Velim (Bohemian Cretaceous Basin, Czechoslovakia). Acta Univ. Carol., Geol. 1–2, 103–125.
Švábenická L. (2004): Bohemian Cretaceous Basin – Cenomanian-Turonian boundary based on calcareous nannofossils. Zpr. geol. Výzk. v Roce 2003, 44–47 (in Czech with English abstract).
Tappan H. (1980): The paleobiology of plant protists. W. H. Freemann & Comp., San Francisco.
Uličný D. (1992): Low and high-frequency sea-level change and related events during the Cenomanian and across the Cenomanian-Turonian boundary, Bohemian Cretaceous Basin. Unpub. Thesis Charles Univ., Prague.
Uličný D. (1997): Sedimentation in a reactivated, intra-continental strike-slip fault zone: The Bohemian Cretaceous Basin, Central Europe. Gaea heidelbergensis, 3, Abstracts, 18th IAS Regional European Meeting, Heidelberg, 347.
Uličný D. (2001): Depositional systems and sequence stratigraphy of coarse-grained deltas in a shallow-marine, strike-slip setting: the Bohemian Cretaceous Basin, Czech Republic. Sedimentology 48, 599–628.
Uličný D., Hladíková J., Hradecká L. (1993): Record of sea level changes, oxygen depletion and the C anomaly across the Cenomanian – Turonian boundary, Bohemian Cretaceous Basin. Cretac. Res. 14, 211–234.
Uličný D., Kvaček J., Svobodová M., Špičáková L. (1997a): High frequency sea-level fluctuations and plant habitats in Cenomanian fluvial to estuarine succession: Pecínov quarry, Bohemia. Palaeogeogr., Palaeoclimatol., Palaeoecol. 136, 165–197.
Uličný D., Hladíková J., Attrep M., Čech S., Hradecká L., Svobodová M. (1997b): Sea-level changes and geochemical anomalies across the Cenomanian-Turonian boundary: Pecínov quarry, Bohemia. Paleogeogr. Paleoclimatol. Paleoecol., 132, 265–285.
Uličný D., Špičáková L., Čech S. (2003): Changes in depositional style of an intra-continental strike-slip basin in response to shifting activity of basement fault zones: Cenomanian of the Bohemian Cretaceous Basin. Geolines 16, 103–104.
Varol O. (1992): Taxonomic revision of the Polycyclolithaceae and its distribution to Cretaceous biostratighraphy. Newsl. Stratigr. 27, 3, 93–127.
Wall D. (1965): Microplankton, pollen, and spores from the Lower Jurassic in Britain. Micropaleontology 11, 2, 151–190.
Wilpshaar M., Leereveld H. (1994): Palaeoenvironmental change in the Early Cretaceous Vocontian Basin (SE France) reflected by dinoflagellate cysts. Rev. Palaeobot. Palynol. 84, 121–128.
Žítt J., Nekvasilová O., Bosák P., Svobodová M., Štemproková-Jírová D., Šťastný M. (1997a): Rocky coast facies of the Cenomanian-Turonian Boundary interval at Velim (Bohemian Cretaceous Basin, Czech Republic). First part. Bull. Czech Geol. Surv. 72, 1, 83–100.
Žítt J., Nekvasilová O., Bosák P., Svobodová M., Štemproková-Jírová D., Šťastný M. (1997b): Rocky coast facies of the Cenomanian-Turonian Boundary interval at Velim (Bohemian Cretaceous Basin, Czech Republic). Second part. Bull. Czech Geol. Surv. 72, 2, 141–155.

Appendix

Macrofauna taxa mentioned in the text

Cephalopoda
Praeactinocamax plenus (Blainville)

Bivalvia
Apiotrigonia sulcataria (Lamarck)
Chlamys robinaldina (D'Orbigny)
Neithea notabilis (Münster)
Perna cretacea Reuss
Pseudoptera anomala (Sowerby)
Rastellum carinatum (Lamarck)

Foraminiferal taxa mentioned in the text, in alphabetical order of genera epithets
Ammobaculites reophacoides Bertenstein
Ammobaculoides lepidus Hercogová
Ammodiscus cretaceus (Reuss)
Ammodiscus gaultinus Berthelin
Arenobulimina preslii (Reuss)
Ataxophragmium depressum (Perner)
Bigenerina selseyensis Heron-Allen-Earland
Cassidella tegulata (Reuss)
Dentalina sp.
Dicarinella imbricata (Mornod)
Dorothia filiformis (Berthelin)
Dorothia gradata (Berthelin)
Dorothia oxycona (Reuss)
Dorothia turris (d'Orbigny)
Frondicularia sp.
Frondicularia fritschi Perner
Frondicularia inversa Reuss
Frondicularia verneuiliana d'Orbigny
Gaudryina angustata Akimec
Gaudryina compressa Akimec
Gaudryina folium Akimec
Gaudryina praepyramidata Hercogová

Gaudryina trochus (d'Orbigny)
Gaudryina variabilis Mjatljuk
Gavelinella baltica Brotzen
Gavelinella belorussica (Akimec)
Gavelinella berthelini (Keller)
Gavelinella cenomanica (Brotzen)
Gavelinella polessica Akimec
Gavelinella schloenbachi (Reuss)
Gyroidina nitida (Reuss)
Hagenowina advena (Cushman)
Haplophragmoides sp.
Haplophragmoides nonioninoides (Reuss)
Haplophragmoides ovalis Jendrejáková
Haplophragmoides stelcki Hanzlíková
Hedbergella delrioensis (Carsey)
Hedbergella planispira (Tappan)
Hedbergella simplex (Morrow)
Helvetoglobotruncana helvetica (Bolli)
Helvetoglobotruncana praehelvetica (Trujillo)
Heterohelix globulosa (Ehrenberg)
Heterohelix pulchra Brotzen
Lenticulina sp.
Lenticulina comptoni (Sowerby)
Lingulogavelinella globosa (Brotzen)
Lingulogavelinella pazdroae Gawor-Biedowa
Lituotuba incerta Franke
Marginulina aequivoca Reuss
Marginulina robusta (Reuss)
Marssonella oxycona (Reuss)
Nodosaria sp.
Nodosaria bistegia (Olszewski)
Nodosaria obscura (Reuss)
Planularia complanata (Reuss)
Praebulimina crebra Štemproková
Praeglobotruncana delrioensis (Plummer)
Praeglobotruncana oraviensis Scheibnerová
Pseudotextularia cretosa (Cushman)
Quadrimorphina allomorphinoides (Reuss)
Ramulina globulifera Brady
Spiroplectammina sp.
Spiroplectammina scotti Cushman-Alexander
Tappannina eouvigeriniformis (Keller)
Textularia foeda Reuss
Trochammina sp.
Trochammina globosa Bolin
Trochammina obliqua Tappan
Vaginulina recta Reuss
Vaginulina robusta (Chapman)
Valvulineria lenticula (Reuss)
Whiteinella aprica (Loeblich & Tappan)
Whiteinella archaeocretacea Pessagno
Whiteinella baltica Douglas & Rankin
Whiteinella brittonensis (Loeblich & Tappan)
Whiteinella paradubia (Sigal)

Nannofossil taxa mentioned in the text, in alphabetical order of genera epithets
Ahmuellerella octoradiata (Górka) Reinhardt
Amphizygus brooksii Brooksii
Axopodorhabdus albianus (Black) Wind and Wise
Biscutum ellipticum (Górka) Grün
Braarudosphaera bigelowii (Gran and Braarud) Deflandre
Broinsonia enormis (Shumenko) Manivit
Broinsonia matalosa (Stover) Burnett
Broinsonia signata (Noël) Noël
Bukrylithus ambiguus Black
Chiastozygus litterarius (Górka) Manivit
Corollithion exiguum Stradner
Corollithion kennedyi Crux
Corollithion signum Stradner
Cretarhabdus conicus Bramlette and Martini
Cribrosphaerella ehrenbergii (Arkhangelsky) Deflandre
Cyclagelosphaera rotaclypeata Bukry
Eiffellithus turriseiffelii (Deflandre) Reinhardt
Eprolithus floralis (Stradner) Stover
Eprolithus moratus (Stover) Burnett
Eprolithus octopetalus Varol
Gartnerago obliquum (Stradner) Noël
Gartnerago theta (Black) Jakubowski
Grantarhabdus coronadventis (Reinhardt) Grün
Haqius circumradiatus (Stover) Roth
Helenea chiastia Worsley
Helicolithus compactus (Bukry) Varol and Girgis
Helicolithus trabeculatus (Górka) Verbeek
Isocrystallithus compactus Verbeek
Lithraphidites acutus Verbeek and Manivit
Lithraphidites carniolensis Deflandre
Lucianorhabdus maleformis Reinhardt
Manivitella pemmatoidea (Deflandre) Thierstein
Microrhabdulus belgicus Hay and Towe
Microrhabdulus decoratus Deflandre
Nannoconus elongatus Brönnimann
Perissocyclus fenestratus (Stover) Black
Placozygus fibuliformis (Reinhardt) Hoffmann
Prediscosphaera columnata (Stover) Perch-Nielsen
Prediscosphaera cretacea (Arkhangelsky) Gartner
Prediscosphaera ponticula (Bukry) Perch-Nielsen
Prediscosphaera spinosa (Bramlette and Martini) Gartner
Quadrum gartneri Prins and Perch-Nielsen
Quadrum intermedium Varol
Retacapsa angustiforata Black
Retacapsa crenulata (Bramlette and Martini) Grün
Rhagodiscus angustus (Stradner) Reinhardt
Rhagodiscus asper (Stradner) Reinhardt
Rhagodiscus plebeius Perch-Nielsen
Rhagodiscus splendens (Deflandre) Verbeek
Rotelapillus crenulatus (Stover) Perch-Nielsen
Stoverius achylosus (Stover) Perch-Nielsen
Tegumentum stradneri Thierstein
Tranolithus gabalus Stover
Tranolithus orionatus (Reinhardt) Reinhardt
Watznaueria barnesae (Black) Perch-Nielsen
Watznaueria biporta Bukry
Watznaueria britannica (Stradner) Reinhardt
Watznaueria fossacincta (Black) Bown
Zeugrhabdotus bicrescenticus (Stover) Burnett
Zeugrhabdotus diplogrammus (Deflandre) Burnett
Zeugrhabdotus embergeri (Noël) Perch-Nielsen
Zeugrhabdotus erectus (Deflandre) Reinhardt
Zeugrhabdotus noeliae Rood et al.
Zeugrhabdotus scutula (Bergen) Rutledge and Bown
Zeugrhabdotus trivectis Bergen
Zeugrhabdotus xenotus (Stover) Burnett

Palynomorph taxa mentioned in the text, in alphabetical order of genera epithets
Achomosphaera ramulifera (Deflandre) Evitt
Alisporites bilateralis Rouse
Araucariacites cf. *australis* Cookson
Biretisporites potoniei Delcourt & Sprumont
Bohemiperiporis zaklinskae Pacltová
Brenneriporis peroreticulatus (Brenner) Juhász & Góczán
Callaiosphaeridium asymmetricum (Deflandre & Courteville) Davey & Williams
Calamospora sp.
Camarozonosporites ambigens (Fradkina) Playford
Camarozonosporites insignis Norris
Canningia sp.
Chomotriletes minor Pocock
Cicatricosisporites venustus Deák
Cicatricosisporites sp.
Cingutriletes clavus (Balme) Dettmann
Circulodinium distinctum (Deflandre & Cookson) Jansonius
Classopollis /Corollina/ classoides (Pflug) Pocock & Jansonius
Clavatipollenites minutus Brenner
Clavifera triplex (Bolchovitina) Bolchovitina

Cleistosphaeridium sp.
Complexiopollis sp.
Coronatispora sp.
Cycadopites fragilis Singh
Cyclonephelium compactum Deflandre & Cookson
Cymatiosphaera sp.
Deltoidospora minor (Couper) Pocock
Dyadosporites ellipsus Clarke
Epelidosphaeridia spinosa Cookson & Hughes
Ephedripites jansonii (Pocock) Muller
Ephedripites multicostatus Brenner
Eucommiidites minor Couper
Florentinia mantelii (Davey & Williams) Davey & Verdier
Foveogleicheniidites confossus (Hedlund) Burger
aff. *Foveotetradites fistulosus* (Dettmann)
Foveotricolpites sp.
Foveotriletes subtriangularis Brenner
Gleicheniidites carinatus (Bolchovitina) Bolchovitina
Gleicheniidites circiniidites (Cookson) Dettmann
Gleicheniidites senonicus Ross
Inaperturopollenites sp.
Laevigatosporites ovatus Wilson & Webster
Leptolepidites psarosus Norris
Liliacidites sp. A
Matonisporites sp.
Microfoveolatosporites canaliculatus Dettmann
Micrhystridium fragile Deflandre
Micrhystridium spp.
Odontochitina operculata (O. Wetzel) Deflandre & Cookson
Oligosphaeridium complex (White) Davey & Williams
Ornamentifera echinata Bolchovitina
Ovoidites parvus (Cookson & Dettmann)
Palaeohystrichophora infusorioides Deflandre
Paralecaniella sp.
Parvisaccites radiatus Couper
Perucipollis minutus Pacltová
Pervosphaeridium pseudhystrichodinium (Deflandre) Yun
Phyllocladidites sp.
Pinuspollenietes spp.
Plicatella ethmos (Delcourt & Sprumont) Zhang
Plicatella sp.
Psilatricolpites parvulus (Groot & Penny) Norris
Psilatricolporites sp.
Reticulosporites sp.
Retitricolpites micromunus (Groot & Penny) Burger
Retitricolpites němejci (Pacltová) Laing
Retitricolpites virgeus (Groot, Penny & Groot) Brenner
Retitricolpites vulgaris Pirce
Retitricolpites spp.
Retitricolporites spp.
Retitriletes austroclavatidites (Cookson) Döring et al.
Sequoiapollenites sp.
Sestrosporites pseudoalveolatus (Cooper) Dettmann
Spiniferites ramosus (Ehrenberg) Loeblich & Loeblich ssp. *ramosus* aff.
Stephanocolpites sp.
Stereisporites antiquasporites (Wilson & Webster) Kremp
Stereisporites psilatus (Ross)
Surculosphaeridium ?longifurcatum (Firtion) Davey
Taxodiaceaepollenites hiatus (potonié) Kremp
Taxodiaceaepollenites vacuipites Kremp
Tetracolpites sp.
Tetraporina sp.
Tricolpites barrandei Pacltová
Tricolpites crassimurus (Groot & Penny) Singh
Tricolpites cf. *sagax* Norris
Undulatisporites sp.
Vadaszisporites urkuticus Juhász
Veryhachium hyalodermum (Cookson) Downie & Sarjeant
Xenascus ceratioides (Deflandre) Lentin & Williams

→

Plate I
1 — *Valvulineria lenticula* (Reuss), umbilical side, BJ-20, 113.5 m. 2 – *Helvetoglobotruncana helvetica* (Bolli), BJ-19, 110.9 m. 3 – *Valvulineria lenticula* (Reuss), spiral side, BJ-19, 110.9 m. 4 – *Gavelinella polessica* Akimec, BJ-20, 113.5 m. 5 – *Ramulina* sp., BJ-20, 113.5 m. 6 – *Gavelinella belorussica* (Akimec), BJ-19, 110.9 m. 7 – *Praebulimina crebra* Štemproková, BJ-20, 113.5 m. 8 – *Praebulimina crebra* Štemproková, BJ-19, 110.9 m. 9 – *Heterohelix pulchra* Brotzen, BJ-19, 110.9 m. 10 – *Gavelinella cenomanica* (Brotzen), Cenomanian, BJ-20, 116.7 m. 11 – *Gavelinella cenomanica* (Brotzen), Cenomanian, BJ-20, 116.7 m. 12 – *Ataxophragmium depressum* (Perner), BJ-20, 116.7 m.

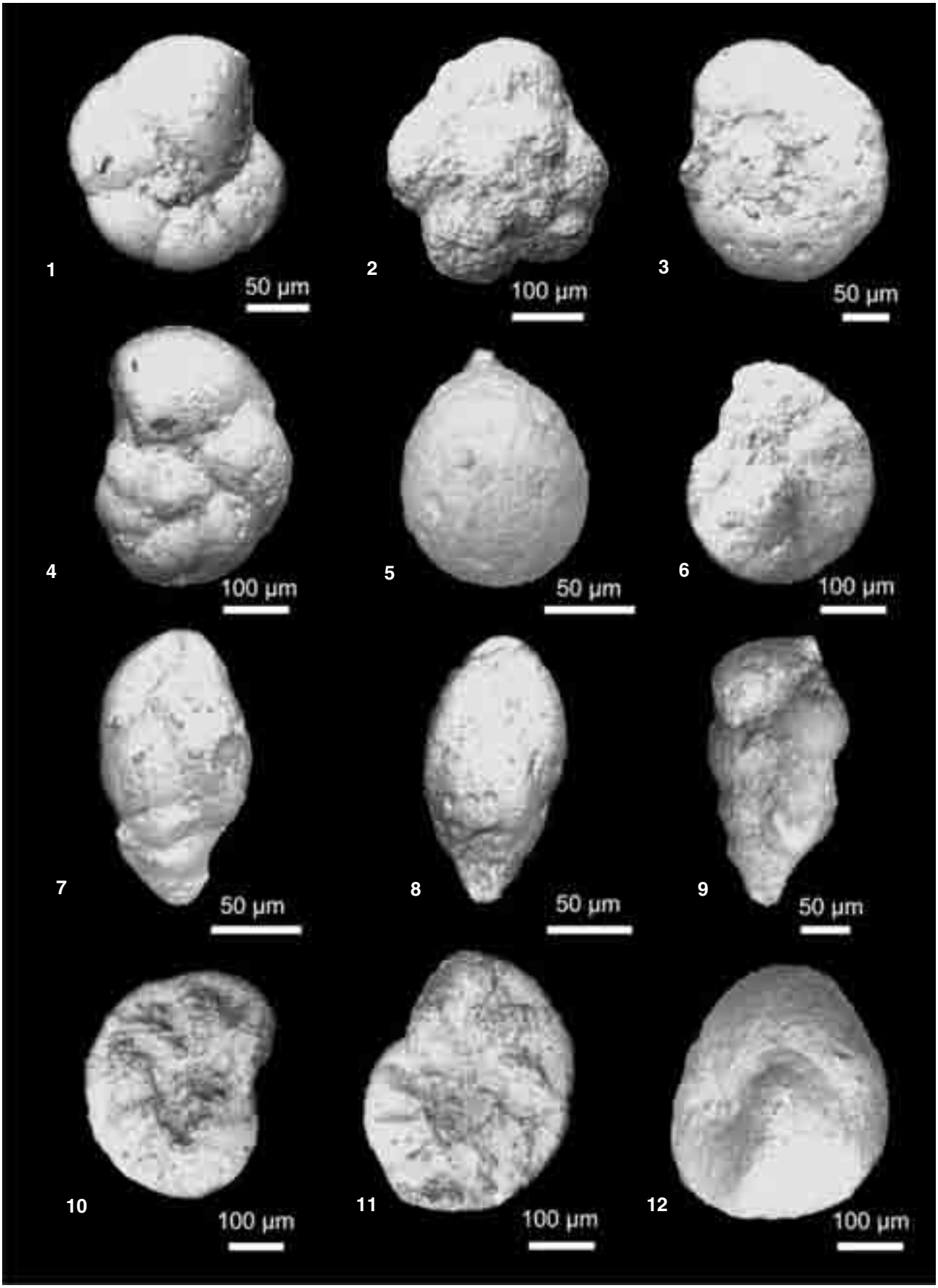
1
50 µm
2
100 µm
3
50 µm
4
100 µm
5
50 µm
6
100 µm
7
50 µm
8
50 µm
9
50 µm
10
100 µm
11
100 µm
12
100 µm

→

Plate II
1 – *Valvulineria lenticula* (Reuss), umbilical side, BJ-19, 110.9 m. 2 – *Lingulogavelinella globosa* (Brotzen), BJ-19, 110.9 m. 3 – *Gavelinella cenomanica* (Brotzen), BJ-20, 116.7 m. 4 – *Heterohelix pulchra* Brotzen, BJ-19, 110.9 m. 5 – *Haplophragmoides* sp., BJ-20, 116.7 m. 6 – *Trochammina obliqua* Tappan, BJ-20, 121.9 m. 7 – *Ammobaculites lepidus* Hercogová, BJ-20, 121.9 m. 8 – *Trochammina obliqua* Tappan, BJ-20, 121.9 m. 9 – *Praebulimna crebra* Štemproková, BJ-19, 110.9 m. 10 – *Cassidella tegulata* (Reuss), BJ-20, 113.5 m.

→→

Plate III
Calcareous nannofossils from the Cenomanian-Turonian boundary interval, Nymburk HP-20 borehole (if not otherwise indicated), Bohemian, Cretaceous Basin. PPL – plane-polarized light, XPL – cross-polarized light.
1, 2 – *Broinsonia enormis* (Shumenko) Manivit, Lower Turonian, 111.4 m, 1, PPL, 2, XPL. 3, 4 – *Broinsonia signata* (Noël) Noël, Upper Cenomanian, 117.0 m, 3, PPL, 4, XPL. 5, 6 – *Helicolithus trabeculatus* (Górka) Verbeek, Upper Cenomanian, 116.7 m, 5, PPL, 6, XPL. 7 – *Biscutum ellipticum* (Górka) Grün, Upper Cenomanian, 117.0 m, XPL. 8-10 – *Prediscosphaera columnata* (Stover) Perch-Nielsen, Upper Cenomanian, 117.0 m, 8,9, PPL, 10, XPL. 11, 12 – *Prediscosphaera spinosa* (Bramlette and Martini) Gartner, Lower Turonian, 111.4 m, 11, PPL, 12, XPL. 13–15 – *Prediscosphaera ponticula* (Bukry) Perch-Nielsen, Upper Cenomanian, 13, 14: 116.7 m, 13, PPL, 14, XPL, 15, 117.0 m, XPL. 16–18 – *Axopodorhabdus albianus* (Black) Wind and Wise, Upper Cenomanian, 16, 17: 116.7 m, 16, PPL, 17, XPL, 18, 117.0 m, XPL. 19–21 – *Eiffellithus turriseiffelii* (Deflandre) Reinhardt, Upper Cenomanian, 117.0 m, 19, PPL, 20, 21, XPL. 22, 23 – *Quadrum intermedium* Varol, Lower Turonian, Hořátev HP-19 borehole, 106.3 m, 22, PPL, 23, XPL. 24 – *Quadrum gartneri* Prins and Perch-Nielsen, Lower Turonian, Hořátev HP-19 borehole, 101.9 m, XPL. 25–28 – *Eprolithus floralis* (Stradner) Stover, Upper Cenomanian, 117.0 m, 25, 27, PPL, 26, 28, XPL. 29, 30 – *Eprolithus octopetalus* Varol, Lower Turonian, 116.4 m, 29, PPL, 30, XPL. 31–33 – *Eprolithus moratus* (Stover) Burnett; Lower Turonian, 111.4 m, 31, 32, PPL, 33, XPL. 34–36 – *Eprolithus* sp., lateral view; 34: Lower Turonian, 116.4 m, PPL, 35, 36: Upper Cenomanian, 117.4 m, 35, PPL, 36, XPL.

→→→

Plate IV
Calcareous nannofossils from the Cenomanian-Turonian boundary interval, Nymburk HP-20 borehole, Bohemian Cretaceous Basin. PPL – plane-polarized light, XPL – cross-polarized light.
1, 2 – *Corollithion kennedyi* Crux, Upper Cenomanian, 117.0 m, XPL. 3, 4 – *Stoverius achylosus* (Stover) Perch-Nielsen, Lower Turonian, 116.4 m, 3, PPL, 4, XPL. 5, 6 – *Zeugrhabdotus noeliae* Rood et al., Upper Cenomanian, 117.0 m, 5, PPL, 6, XPL. 7, 8 – *Gartnerago theta* (Black) Jakubowski, Upper Cenomanian, 117.0 m, 7, PPL, 8, XPL. 9 – *Gartnerago obliquum* (Stradner) Noël, Lower Turonian, 111.4 m, XPL. 10 – *Zeugrhabdotus trivectis* Bergen, Upper Cenomanian, 116.7 m, XPL. 11 – *Zeugrhabdotus bicrescenticus* (Stover) Burnett, Upper Cenomanian, 116.3 m, XPL. 12 – *Amphizygus brooksii* Bukry, Upper Cenomanian, 117.0 m, XPL. 13, 14 – *Tranolithus orionatus* (Reinhardt) Reinhardt, Upper Cenomanian, 117.0 m, 13, PPL, 14, XPL. 15, 16 – *Chiastozygus litterarius* (Górka) Manivit, Lower Turonian, 116.4 m, 15, PPL, 16, XPL. 17 – *Watznaueria britannica* (Stradner) Reinhardt, Upper Cenomanian, 117.0 m, XPL. 18 – *Watznaueria barnesae* (Black) Perch-Nielsen, Lower Turonian, 111.4 m, XPL. 19, 20 – *Retacapsa* sp.; Lower Turonian, 111.4 m, 19, PPL, 20, XPL. 21, 22 – *Retacapsa angustiforata* Black, Upper Cenomanian, 116.7 m, 21, PPL, 22, XPL. 23 – *Retacapsa crenulata* (Bramlette and Martini) Grün, Upper Cenomanian, 117.0 m, XPL. 24 – *Braarudosphaera bigelowii* (Gran and Braarud) Deflandre, Lower Turonian, 113.5 m, XPL. 25 – *Haqius circumradiatus* (Stover) Roth, Lower Turonian, 111.4 m, PPL. 26 – *Nannoconus elongatus* Brönnimann, Upper Cenomanian, 117.4 m, PPL. 27 – ?*Isocrystallithus compactus* Verbeek, Lower Turonian, probably reworked specimen from the underlying strata, 111.4 m, XPL. 28, 29 – *Lucianorhabdus maleformis* Reinhardt, Lower Turonian, 111.4 m, 28, PPL, 29, XPL. 30 – *Lucianorhabdus* cf. *L. maleformis* (sensu Burnett 1998), Lower Turonian, 111.4 m, XPL. 31, 32 – *Manivitella pemmatoidea* (Deflandre) Thierstein, Upper Cenomanian, 117.0 m, 31, PPL, 32, XPL. 33, 34 – *Lithraphidites acutus* Verbeek and Manivit, Upper Cenomanian, 117.0 m, 33, PPL, 34, XPL. 35, 36 – *Lithraphidites* cf. *L. acutus*, Upper Cenomanian, 117.0 m, 35, PPL, 36, XPL.

→→→→
Plate V
Palynomorphs from the Middle–Upper Cenomanian interval of the borehole Nymburk HP-20. Micrographs by M. Svobodová.
1 – *Perucipollis minutus* Pacltová, 134.60 m, 1243/2. 2 – *Bohemiperiporis zaklinskae* Pacltová, 136.20 m, 1244/2. 3 – *Tetracolpites* sp., 141.20 m, 1246/5. 4 – *Retitricolpites vulgaris* Pierce, 141.20 m, 1246/1. 5 – *Foveotetradites fistulosus* (Dettmann) Singh, tetrahedral tetrad, 141.20 m, 1246/3. 6 – *Retitricolporites* sp., 137.70 m, 1245/2. 7 – *Liliacidites* sp., 134.60 m, 1243/2. 8 – *Laevigatosporites ovatus* Wilson & Webster, 143.30 m, 1241/1. 9 – *Classopollis classoides* (Pflug) Pocock & Jansonius, 131.90 m, 1242/3. 10 – *Ephedripites jansonii* (Pocock) Muller, 137.70 m, 1245/1. 11 – *Tricolpites* cf. *sagax* Norris, 134.60 m, 1243/2. 12 – *Eucommiidites minor* Couper, 134.60 m, 1243/3. 13 – *Paralecaniella* sp., 137.70 m, 1245/1. 14 – *Chomotriletes minor* Pocock, 134.60 m, 1243/2. 15 – *Dyadosporites ellipsus* Clarke, 134.60 m, 1243/2. 16 – *Plicatella ethmos* (Delcourt & Sprumont) Zhang, 143.30 m, 1241/1. 17 – Foraminiferal linings, 134.60 m, 1243/2. 18 – *Cyclonephelium compactum* Deflandre & Cookson, 134.60 m, 1243/3.

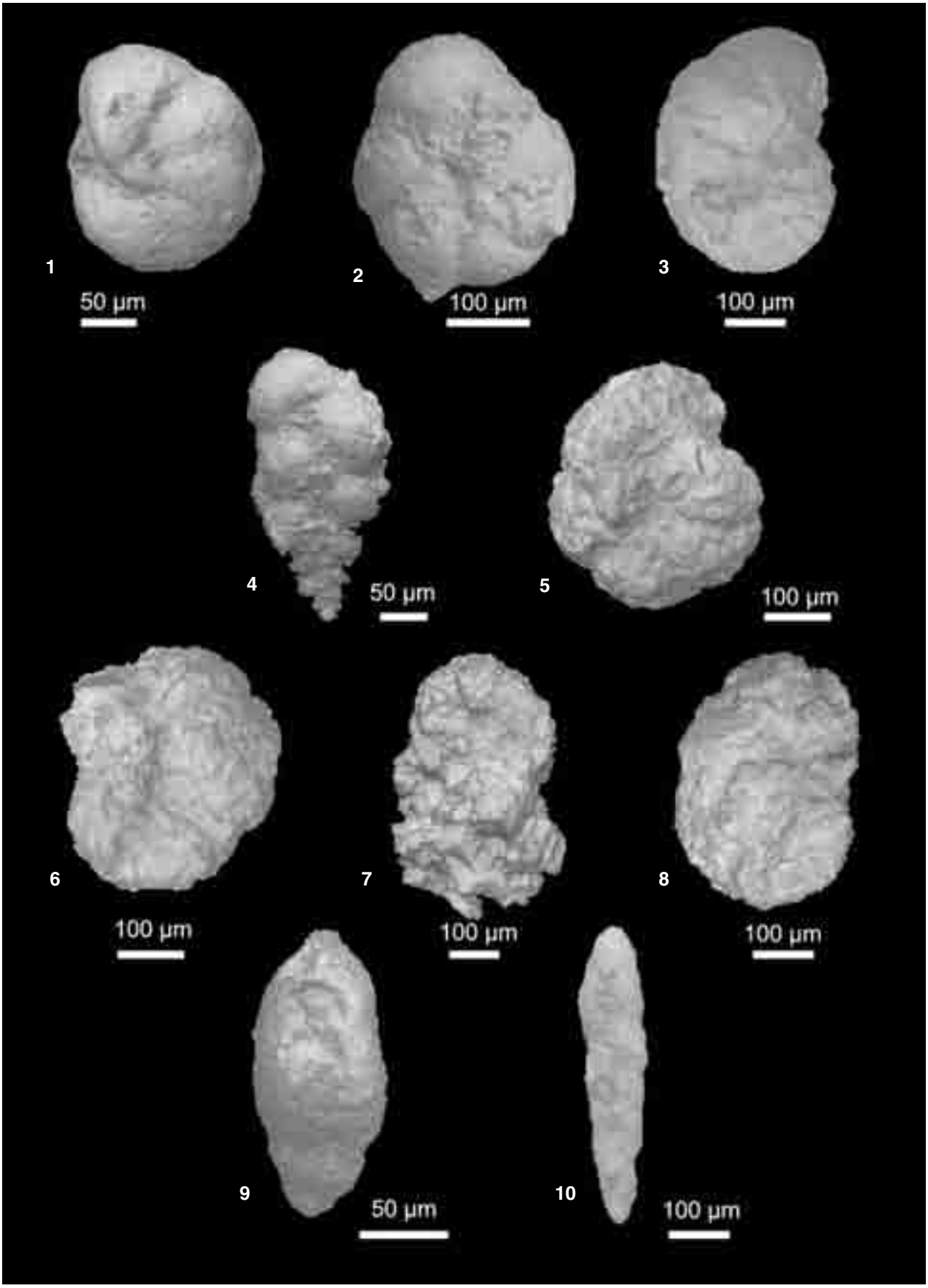
1
50 µm
2
100 µm
3
100 µm
4
50 µm
5
100 µm
6
100 µm
7
100 µm
8
100 µm
9
50 µm
10
100 µm

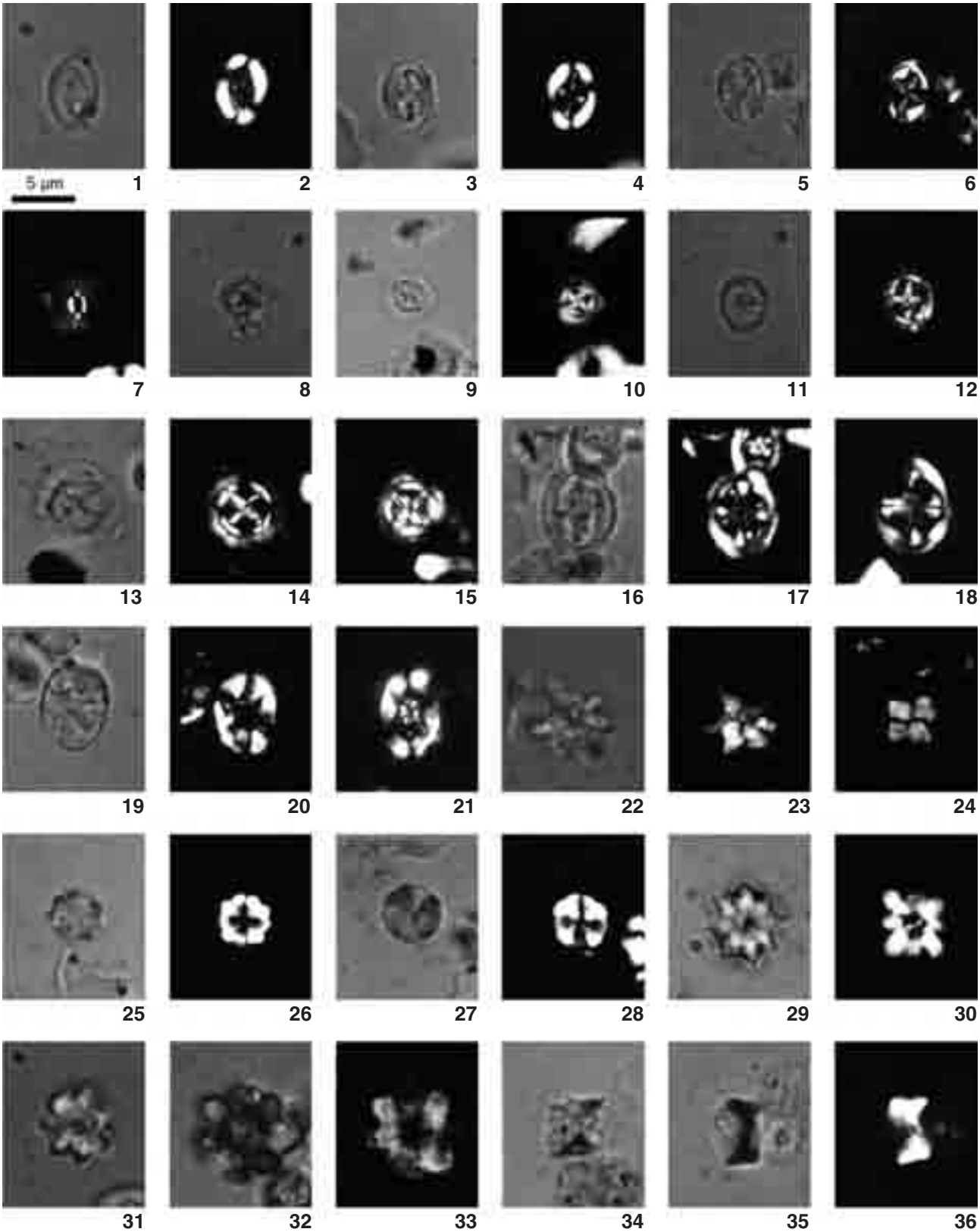
5 µm
1
2
3
4
5
6
7
8
9
10
11
12
13
14
15
16
17
18
19
20
21
22
23
24
25
26
27
28
29
30
31
32
33
34
35
36

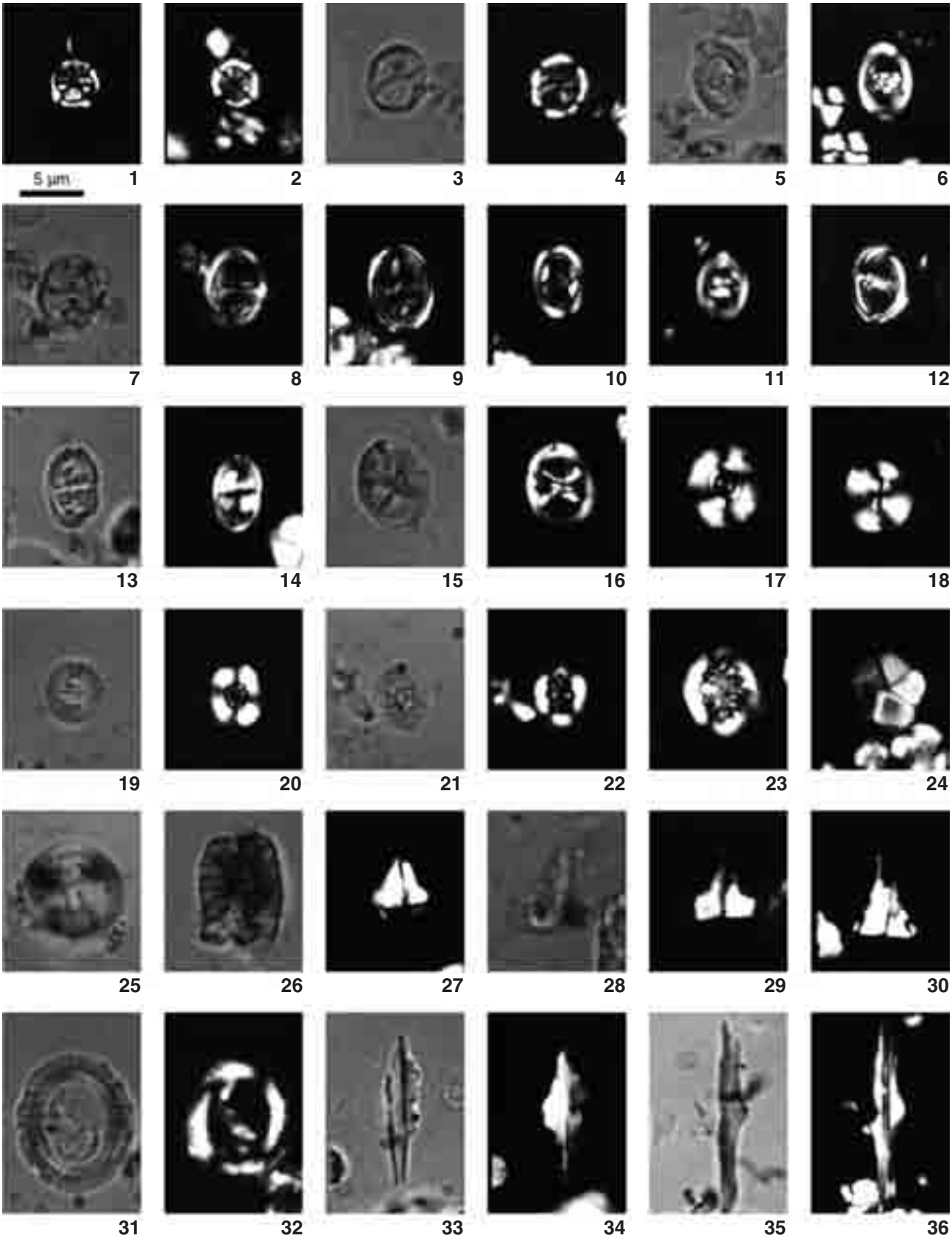
5 µm
1
2
3
4
5
6
7
8
9
10
11
12
13
14
15
16
17
18
19
20
21
22
23
24
25
26
27
28
29
30
31
32
33
34
35
36

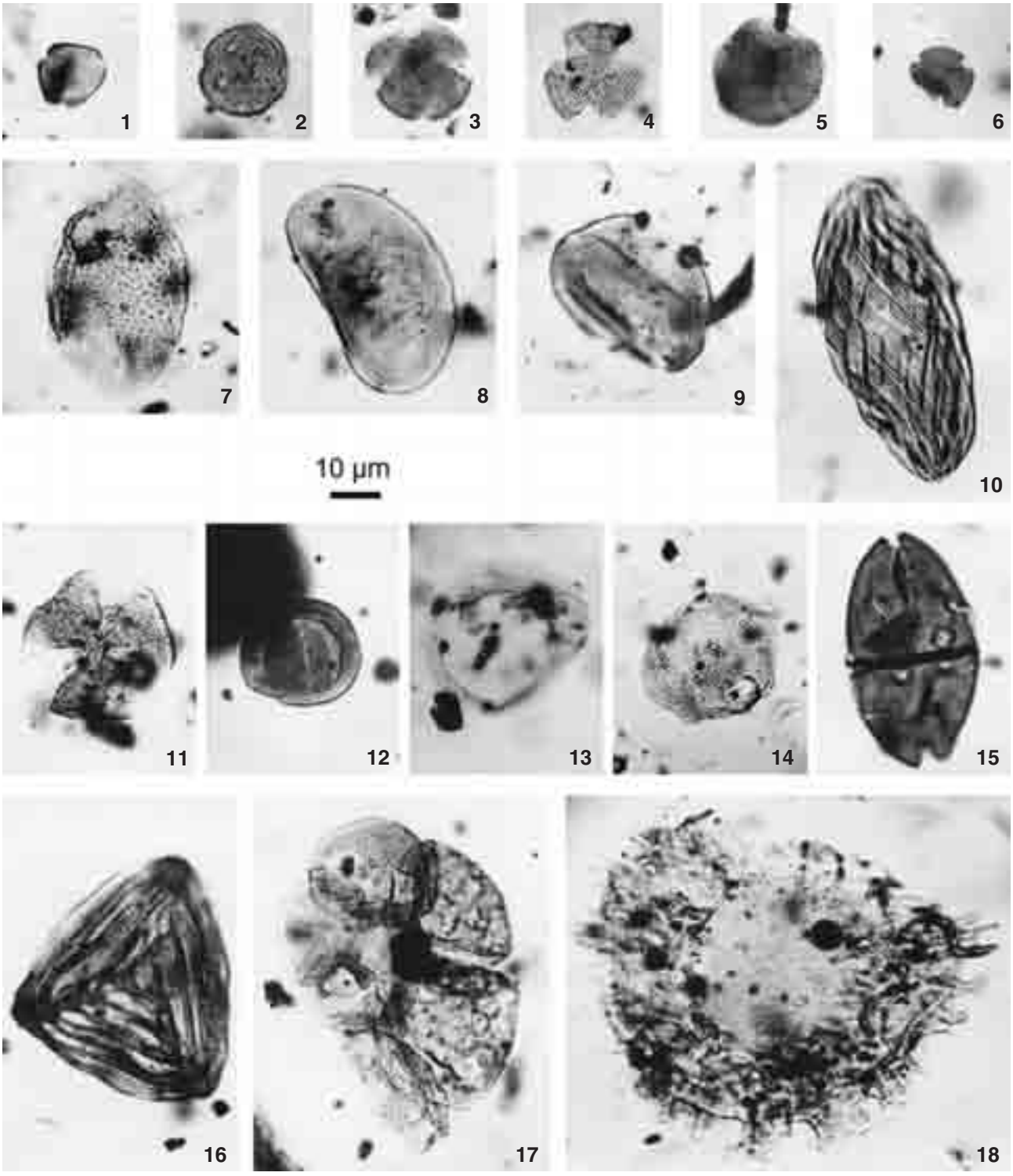
1
2
3
4
5
6
7
8
9
10
10 µm
11
12
13
14
15
16
17
18